Deciphering Tetraploid Tolerance

Andrew Crockford

University College London

and

Cancer Research UK London Research Institute

PhD Supervisor: Prof. Charles Swanton

A thesis submitted for the degree of

Doctor of Philosophy

University College London

September 2015

Declaration

I, Andrew Crockford, confirm that the work presented in this thesis is my own. Where information has been derived from other sources, I confirm that this has been indicated in the thesis.

Abstract

Chromosomal instability and aneuploidy are common features of human malignancies, which fuel genetic heterogeneity and can lead to inaccurate diagnosis and treatment failure. Tetraploidy has been shown as an intermediate of aneuploidy and, thus, understanding the molecular mechanisms governing tetraploid tolerance is of great importance. A frequent tolerance mechanism observed in experimental systems and human tumours is loss of *TP53,* highlighting its central role in the tetraploidy checkpoint. However, despite this association, more than half of genome-doubled tumours are *TP53* wild-type. The aim of this project was to understand how tetraploid cells could tolerate the polyploidy phenotype with a functional p53/p21 axis. Firstly, tetraploidy tolerance was investigated in an isogenic HCT-116 diploid and tetraploid system. The HCT-116 tetraploids showed functional p53, in response to DNA damage and segregation error induction, while also displayed elevated basal level of both proteins. Despite this, the tetraploid clones could proliferate and showed no evidence of cell cycle arrest, suggesting the p53/p21 tetraploidy checkpoint response had been overridden. Quantitative proteomics revealed cyclin D1 overexpression in the tetraploid clones. As cyclin D1 can sequester p21, their relationship was investigated and validated in the HCT-116 system. To further test if elevated cyclin D1 could affect tolerance, cytokinesis failure was pharmacologically induced in RPE cells, where cyclin D1 overexpression promoted tetraploidy tolerance across multiple assays. In addition, bioinformatics analysis revealed that D-type cyclins were overexpressed in *TP53, CDKN1A* and *RB1* wild-type, genome-doubled testicular germ cell tumours (TGCT). These findings indicate that D-type cyclin overexpression can provide tetraploidy tolerance *in vitro* and may be implicated in TGCT genome-doubling and pathogenesis.

Acknowledgement

Thank you to everyone in the TCT laboratory for all your guidance and friendship over the last few years. A special thank you to Panos and Sally for your advice and help with this project.

Thank you Charlie for all your support and enthusiasm and for taking me in when I was a bit of a lost sheep after my previous laboratory has closed. Thank you to all my friends who have helped me through and kept me smiling throughout my PhD. Dad and Amy, thank you so much for all your help support, you have been amazing.

Chan, you have been my rock, thank you so much for all your support, I love you dearly. Thank you to all my family for always supporting me.

I would like to dedicate this work to the memory of my mother Julie Crockford, who played a huge part in my academic success.

Publications

CROCKFORD, A., JAMAL-HANJANI, M., HICKS, J. & SWANTON, C. 2014. Implications of intratumour heterogeneity for treatment stratification. *J Pathol,* 232**,** 264-73.

FISHER, R., HORSWELL, S., ROWAN, A., SALM, M. P., DE BRUIN, E. C., GULATI, S., MCGRANAHAN, N., STARES, M., GERLINGER, M., VARELA, I., CROCKFORD, A., FAVERO, F., QUIDVILLE, V., ANDRE, F., NAVAS, C., GRONROOS, E., NICOL, D., HAZELL, S., HROUDA, D., O'BRIEN, T., MATTHEWS, N., PHILLIMORE, B., BEGUM, S., RABINOWITZ, A., BIGGS, J., BATES, P. A., MCDONALD, N. Q., STAMP, G., SPENCER-DENE, B., HSIEH, J. J., XU, J., PICKERING, L., GORE, M., LARKIN, J. & SWANTON, C. 2014. Development of synchronous VHL syndrome tumors reveals contingencies and constraints to tumor evolution. *Genome Biol,* 15**,** 433.

Table of Contents

Table of Figures

List of Tables

Abbreviations

2-DG	2-deoxy-glucose
2N	Diploid
4N	Tetraploid
5-FU	5-fluorouracil
6-AN	6-aminonicotinamide
APC	Adenomatous Polyposis Coli
Arg	Arginine
ATM	Ataxia telangiectasia mutated kinase
BSA	Bovine serum albumin
CAK	CDK activating enzyme
CBL	Chromosome bridging or lagging
CDK	Cyclin dependent kinases
CIN	Chromosomal instability
CRC	Colorectal cancer
DCB	Dihydocytochalasin B
DHEA	Dehydroepiandrosterone
DMEM	ulbecco's modified eagle medium
DMSO	Dimethyl sulfoxide
DNA	Deoxyribonucleic acid
DSB	Double strand break
DTT	Dithiothreitol
FBS	Foetal bovine serum
FI	Fluorescence intensity
FISH	Fluorescent in situ hybridization
fRMA	Frozen Robust Microarray
G1	Gap phase one
G2	Gap phase 2
G6PD	Glucose-6-phosphaste dehydrogenase
GFP	Green fluorescent protein
His	Histidine
HPLC	High performance liquid chromatography
HTS	High throughput screening

IC_{50}	Inhibition concentration 50
IDH1	Isocitrate Dehydrogenase
IMT	Isolated molecular target
IPTG	Isopropyl β-D-1-thiogalactopyranoside
IR	Ionising radiation
ITH	Intratumour heterogeneity
KDa	Kilo Dalton
m	Milli
M phase	Mitosis
MCF-7	Human breast adenocarcinoma cells
MN	Micronuclei
MS	Mass spectrometry
MSA	Multi stage activation
n	Nano
NADP	nicotinamide adenine dinucleotide phosphate
PPM	Parts per million
PPP	Pentose phosphate pathway
Pro	Proline
R5-P	Ribose-5-phosphate
RNA	Ribonucleic acid
RPE	Retinal pigment epithelium
RPM	Revolutions per minute
RPPA	Reverse phase protein array
RT	Room temperature
S phase	Synthesis phase
SAC	Spindle assembly checkpoint
SCNAs	Somatic copy number alterations
SDS	Sodium dodecyl sulphate
SEC	Size exclusion chromatography
Ser	Serine
SNP	Single nucleotide polymorphism
SSB	Single strand break
TCGA	The cancer genome atlas
TG	Giant trophoblast cell

Thr	threonine
TOF	Time of flight
TS	Trophoblast stem cells
wGII	Weighted genome insatiably index
μ	Micro

Chapter 1. Introduction

The diagnosis and treatment of many human cancers have improved significantly over the past twenty years, with an extensive armoury of therapeutics and clinical strategies available to clinical oncologists. Despite this advancement, patients with metastatic disease or tumours not emendable to surgical resection, remain incurable. Intratumour heterogeneity (ITH), which has been reported in many solid and haematological tumours, contributes significantly to this more than unsatisfactory outcome.

1.1 Chromosomal instability, aneuploidy and ITH

In 1976, Peter Nowell proposed the tumour clonal evolution model based on sequential selection (Nowell, 1976). The model predicts that tumours are derived from a single clone and, subsequently, genetic instability produces random intercellular aberrations that may be selected for, resulting accumulation of increasingly fit subclones. Nowell hypothesised this process occurred in a non-liner fashion, an idea that has been recently supported by studies haematological and solid malignancies (Gerlinger et al., 2012, Yap et al., 2012, Ding et al., 2012, Schuh et al., 2012, Nowell, 1976). Linear clonal evolution results in the selective genetic sweeps of the fittest clones, resulting in tumours with low genetic diversity (de Bruin et al., 2013). In contrast, non-linear branched evolutionary growth, allows the evolution of many independent subclones that can acquire a myriad of genetic lesions, producing extensive ITH.

Somatic mutations represent one mechanism involved in generating genetic aberrations required to drive tumour evolution. Another important pathogenic process that can produce an aberrant genome is chromosomal instability (CIN), which relates to a constantly elevated rate in karyotypic change through numerical and structural chromosomal defects (Gordon et al., 2012). CIN results in aneuploidy, which relates to a state of abnormal chromosome number and is frequently observed in solid and haematological malignancies (Gordon et al., 2012, Gerlinger et al., 2014, Greaves, 2009). However, aneuploidy is not synonymous

with CIN, as stable aneuploid tumours can exist (Kaneko and Knudson, 2000). Several studies have demonstrated that CIN and aneuploidy can provide the necessary genetic lesions that can increase metastatic potential and drug resistance. Yonkers *et al* demonstrated CIN in endocrine pancreatic tumours was an indicator of metastatic potential; highlighting that CIN can increase the frequency of metastatically viable subclones (Jonkers et al., 2005). Li *et al* showed that CIN and aneuploidy provide the basis for drug resistance in cancer cell lines (Li et al., 2005). CIN provided the high rates of spontaneous chromosome alterations required for the rate of the observed drug resistance and could also explain the acquisition of multi-drug resistance after single-agent treatment. These studies demonstrate that CIN can produce the intercellular genetic variation required to permit phenotypes, such as enhanced drug resistance and metastatic potential.

CIN can drive branched evolution to produce independent evolutionary trajectories, resulting in multiple subclones with differential karyotypes and phenotypes within a single lesion (Burrell et al., 2013b, Gerlinger et al., 2014). The emergence of spatially separated aneuploid subclones exacerbates the degree of heterogeneous somatic copy number alterations (SCNAs), resulting in genetic ITH. Branched tumour evolution, through CIN and aneuploidy, can therefore provide a diverse pool of clones with varying degrees of fitness under certain selection pressures. These clones can be selected for (e.g. drug resistant or metastatic clones), resulting in the poor survival outcomes and therapeutic responses observed in the clinical setting.

Our laboratory has shown that CIN-positive cell lines are more resistant to targeted and cytotoxic anticancer agents (Lee et al., 2011). The study concluded that an intrinsic CIN survival state may exist which enhances resistance, as opposed to selection and outgrowth of low frequency, resistant subclones. The genetic adaptions that permit continuous segregation errors may provide tolerance to drug treatment and enhanced survival, which may in turn support the selection and outgrowth of even more optimal clones, resulting in enhanced acquired therapeutic resistance. Paradoxically, CIN may be associated with cell death and improved patient outcome. Several studies have indicated that such thing as an ‘optimal level of CIN’ might exist and breaching a certain threshold becomes deleterious for the

cell (Birkbak et al., 2011, Kops et al., 2004). Kops *et al* demonstrated that mild suppression of the mitotic checkpoint is permissive for CIN and may enhance tumourigenesis, whereas further weakening or complete silencing of the checkpoint is lethal to cancer cells (Kops et al., 2004). In addition, our laboratory showed that oestrogen receptor-negative breast, ovarian, gastric and non-small cell lung cancers with extreme CIN associated with improved prognosis, compared to intermediate CIN (Birkbak et al., 2011). These studies indicate that CIN needs to be finely tuned in order to promote disease progression and can result in cytotoxicity, if pushed above a threshold.

Taken together, CIN results in aneuploidy and combined with branched tumour evolution can lead to the generation of multiple subclones within the same tumour, increasing the probability of drug resistance and metastasis by generating a large tumour gene pool to select from.

1.2 Maintenance of the diploid genome

In order to combat the harmful effects of CIN and aneuploidy, the cell has evolved to permit faithful replication and division of the genetic material, through a tightly regulated cell cycle.

1.2.1 The cell cycle

The cell cycle is comprised of four distinct and highly ordered phases, namely, gap phase one (G1), synthesis phase (S phase), gap phase two (G2) and mitosis (M phase)(Massague, 2004). S phase results in the replication of the genome, *via* semiconservative DNA synthesis from distinct regions, known as replication origins (Vermeulen et al., 2003). Newly formed chromatids are linked by cohesion in S phase, which is maintained through G2 phase, before entry into M phase. M phase is a complex process and is followed by cytokinesis (Nigg, 2001). In M-phase, sister chromatids undergo spindle attachment, before equatorial alignment, cohesion destruction and segregation to the spindle poles. After nuclear

membrane reformation, the actomyosin contractile ring promotes abcission in cytokinesis, splitting the cell into two daughter cells (Nigg, 2001).

1.2.2 The cell cycle control system

A series of biochemical switches exist to ensure ordered progression through the cell cycle. Cyclin dependent kinases (CDKs) control progression by phosphorylating their substrates to initiate specific phases of the cell cycle. CDK levels remain constant throughout the cell cycle and are instead governed by oscillations in cyclin concentration, a process regulated through transcription and degradation (Fung and Poon, 2005). Cyclin oscillations are coupled to specific cellular signals that ensure the correct CDK is activated at the relevant stage of the cell cycle, allowing ordered progression through the cell cycle. CDKs and cyclins can be grouped based on the cell cycle stage they regulate. In G1, cyclins D and E activate CDK4/6 and CDK2 respectively (Sherr and Roberts, 1999). During S phase, cyclin A is expressed and binds CDK2, whereas cyclin D is destroyed. Cyclin B regulates CDK1 to govern M phase (Nigg, 2001).

In addition to transcription and protein degradation, CDK-cyclin complexes can be regulated by cyclin kinase inhibitors (CKIs). There are two main families, the INK4 family (p16, p14, p15, p18, p19) and the CIP/KIP family (p21, p27, p57). The majority of the INK4 family inhibit CDK4/6 activity exclusively, whereas p14 can inhibit both G1 and G2/M kinases (Canepa et al., 2007). The CIP/KIP family is comprised of p21, p27 and p57 and have broader specificity and can bind multiple CDKs (Denicourt and Dowdy, 2004). CKIs inhibit the CDK by occupying the ATP-binding pocket, thus impairing substrate interaction (Hukkelhoven et al., 2012). Another level of regulation is provided by cell division cycle 25 (CDC25) phosphatases. Dephosphorylation of CDKs by the either CDC25A, B or C removes inhibitory phosphate groups in the CDK ATP-binding loop (Nilsson and Hoffmann, 2000). This activation step, combined with a phosphorylation event mediated by CDK-activating kinase (CAK) together with the binding of a relevant cyclin, permits transition through the cell cycle (Boutros et al., 2007).

1.2.3 Progression through the cell cycle: D-type cyclins and p21 in G1 phase

Mitogenic signalling through growth factor pathways, such as the RAS/ERK pathway, induce the transcription and stabilisation of D-type cyclins (Musgrove et al., 2011). D cyclins, mediated by p21, in turn assemble with CDK4/6 in the cytoplasm (LaBaer et al., 1997). Binding of p21 is required for complex formation, activity and nuclear localisation. CDK4-Cyclin D1-p21 complexes move to the nucleus in a timely manner, where CAK and dephosphorylation by CDC25C fully activate the complex, driving mono-phosphorylation of RB (Bockstaele et al., 2006a). The mechanistic relationship between of D-type cyclins and p21 in G1 are discussed in detail below.

1.2.3.1 D-type cyclins

There are three types of D-cyclin D1, D2 and D3. They can all interact with CDK4 or CDK6 and promote G1 progression. All three are closely related and cyclins D2 and D3 are 62% and 51%, respectively, identical to cyclin D1 (Musgrove et al., 2011). The cyclin box that binds the CDK and CKI is highly conserved between the there homologues, further suggesting they can preform similar functions.

1.2.3.2 p21 complexes with cyclin D1 and CDK4

The classical roles of p21 and other KIP/CIP CDK inhibitor family members are described in section 1.2.1. Paradoxically, a study by LaBaer *et al* provided strong evidence for the involvement of the KIP/CIP proteins p21, p27 and p57 in CDK4/6-Cyclin D complex formation and activation (LaBaer et al., 1997). The group noted that cyclin D1 and CDK4 could not be co-immunoprecipitated, in contrast to other CDK-Cyclin complexes. However, overexpression of p21, p27, or p57 enhanced CDK4 and D-type complex formation. Mutations in the either cyclin or CDK binding domains (CY domains) of p21 abolished complex formation, suggesting that p21 binds both the kinase and cyclin. In addition, other studies have shown that p21 and p27 can bind cyclins without CDKs, and can only interact with CDKs in presence of cyclin (Chen et al., 1996, Hall et al., 1995). *In vitro* biochemistry experiments showed low and intermediate levels of p21 aided complex formation and activity and correlated with p21 concentration. However, at high doses catalytic activity was inhibited. This observation possibly suggests that at low p21 levels a

1:1:1 binding relationship exits, however as ratios increase more than one p21 molecule can bind a single CDK4/6, resulting in kinase inhibition (LaBaer et al., 1997). This stoichiometric model of CDK4 inhibition was supported by a more recent study (Bockstaele et al., 2006b).

Kehn *et al* provided further evidence for p21 and cyclin D1 interaction (Kehn et al., 2004). The study demonstrated HTLV-1 tumour virus incudes p21 and cyclin D2, resulting in enhanced complex formation. In this study, purified cyclin D2, CDK4 and p21 formed catalytically active complexes in a dose-dependent manner at the same stoichiometric ratios as observed by LeBaer *et al*. Importantly, purified p21 could also inhibit CDK2 activity, clearly showing the CKI can inhibit CDK2, yet activate CDK4 at the same stoichiometry.

1.2.3.3 D-type cyclins can sequester and inhibit p21 to facilitate G1 progression

The above studies clearly show that p21 facilitates the formation and activation of CDK4-CyclinD1-p21 complexes. As p21 levels rise after mitogenic signalling, it is likely this mechanistic process is driver of G1 progression (Cheng et al., 1999, Sherr and Roberts, 1999). Another important consequence of this proteomic interaction is the titration of p21 and p27 from CDK2, coupling early and late G1 molecular events. Planas-Silva *et al* provide experimental evidence of p21 redistribution after oestrogen addition to tamoxifen-arrested breast cancer MCF-7 cells (Planas-Silva and Weinberg, 1997). Oestrogen addition resulted in a cyclin D1 increase combined with an elevation in CDK4 and CDK2 activity. The heightened CDK2 activity was not due to increased CDK2, Cyclin E1, CAK or changes in p21/p27 levels. The authors showed that the increase in cyclin D1 could titrate p21 from CDK2 after oestrogen-stimulated growth.

Khen *at a*l also showed CDK2 activity increased after cyclin D2 and p21 elevation after HTLV-1 virus infection, despite no change in cyclin E or CDK2 (Kehn et al., 2004). This observation further supports the notion that D-type cyclins can independently activate CDK2 by sequestering p21. Quintanilla-Martinez *et al*

showed cyclin D1 could sequester p27 in haematological malignancies. (Quintanilla-Martinez et al., 2003). The group noticed that in typical mantel cell lymphomas (MCL), p27 expression correlated with low ki67 staining. Paradoxically, more aggressive blastic MCL expressed high levels of p27 and commonly have t(11;14) translocations resulting in *CCND1* gene overexpression. The group hypothesised high cyclin D1 could buffer p27 and contribute to tumourigenesis. Sequential IPs in blastic MCL cell lines showed cyclin D1 was in excess, compared to p27, and sequestered the majority of the protein, thus buffering CDK2-cyclin E1 binding and inhibition.

In contrast to the above findings, some studies have suggested CKIs are not required for complex formation (Bagui et al., 2003, Bockstaele et al., 2006b, Gaben et al., 2004). Bagui *et al* showed $p21^{-/-}$ and $p27^{-/-}$ mouse embryonic fibroblasts (MEFs) had phosphorylated RB and when p27 was overexpressed kinase activity was reduced in a dose-dependent manner (Bagui et al., 2003). However, although re-addition of p27 inhibited kinase activity it aided CDK4-CyclinD-p27 complex formation. Therefore, the authors concluded that a small fraction of CDK4-cyclinD complex exists and contributes to kinase activity, whereas most complexes contain CKI and their primary role is sequestering p21 and p27 from CDK2.

1.2.3.4 Phosphorylation of p21/p27 and CDK redistribution

The enzymatic activating properties of CIP/KIP CKIs may not be exclusively dependent on D-type concentrations alone. One group noticed differential CKI phosphorylation in TGF-β sensitive cells compared to the phosphorylation profile of cycling TGF-β-resistant cells (Ciarallo et al., 2002).

James *et al* showed in arrested and cycling cells, CDK4 immunoprecipitates had similar amounts of p27 binding but in cycling cells the kinase was catalytically active, whereas in contact arrested cells no RB phosphorylation was observed (James et al., 2008). The group showed that p27's transition from a CDK4 inhibitor to activator was not concentration dependent but reliant on phosphorylation at the Y88 and Y89 residues. This phosphorylation by the kinase Abl, switched p27 into a

CDK4 activator, however the modification did not inhibit CDK2 binding unlike the findings from Kardinal *et al* (Kardinal et al., 2006). Larrea *et al* support these findings and suggest that phosphorylation of p27 at T157 and T198 may aid complex formation before Y88 and Y89 modification, which activates CDK4 (Larrea et al., 2008). Therefore, these studies suggest that the CDK4 activating activities of p27 require phosphorylation and similar mechanisms may regulate p21. Indeed, more recently, Hukkelhoven *et al* showed that phosphorylation of p21 at Y76, in a RCAS-PDGF-HA/nestin system, could contribute to enhanced tumour formation *in vivo* (Hukkelhoven et al., 2012). However, unphosphorylated p21 could still form complexes with CDK4-CyclinD.

Taken together the above studies suggest that p21 and p27 can aid CDK4-CyclinD complex formation and cyclin D1 plays a role in p21 sequestration, although it may not be essential. CKI phosphorylation likely plays a role in the activation and *in vitro* recombinant biochemistry assays suggest protein stoichiometry may also contribute (Figure 1.1). These findings add another layer of complexity to G1/S control.

1.2.3.5 D-type cyclin expression in cancer

CCND1 amplification occurs in breast, lung, skin and oral cancers and incidence rates range for 15-40% (Musgrove et al., 2011, Santarius et al., 2010). Focal amplifications of *CCND2* or *CCND3* are less commonly observed in tumours. 2% of gliomas harbour focal *CCND2* amplifications and is considered the only cancer type were *CCND2* involvement is classed as significant (Cancer Genome Atlas Research, 2008). Overexpression of cyclin D1 is more common and cannot be solely accounted by copy number gains, suggesting that deregulated growth factor signalling and protein stability networks are also responsible. Due to the high frequency of D-type cyclin overexpression in human tumours and correlation with enhanced proliferation in human tumours and as result a range of specific CDK4/6 specific inhibitors exist (Musgrove et al., 2011).

Aside from *CCND1* overexpression, D-type cyclins are frequently elevated in human tumours as result deregulated post-translational mechanisms (Alao, 2007,

Gong et al., 2014). In the normal cell cycle, cyclin D1 levels rise in early G1 until the G1/S boundary, where the protein is degraded to permit S phase, as cyclin D1 can inhibit PCNA (Fukami-Kobayashi and Mitsui, 1999). Cyclin D1 has a relatively short half-life of ~20 minutes, allowing rapid degradation upon mitogen withdrawal. Diehl *et al* showed phosphorylation of cyclin D1 at Thr286 resulted in ubiquitin mediated degradation. More recent studies have shown that *PARK2* and *FBXO4*, which form the PCF4 and PCF7 E3 ubiquitin ligase complexes cooperate to allow recognition of D and E-type cyclins (Gong et al., 2014, Bartek and Hodny, 2014, Lin et al., 2006). It was shown that focal deletions of PARK2 were frequent in human tumours (30%) and were mutually exclusive of *CCND1*, *CCNE1*, *CDK4* and *CDK2* amplification and loss of complex resulted increased cellular proliferation, CDK activity and RB phosphorylation.

For the PCF4 complex to recognise D-type cyclins, phosphorylation at Thr286 is required, as T286A mutations results in elevated cyclin D1 and stability (Gong et al., 2014). The kinase GSK3-β is thought to regulate this phosphorylation site and overexpression in mouse fibroblasts caused cyclin D1 cytoplasmic redistribution and reduced proteolytic turnover (Diehl et al., 1998, Diehl et al., 1997). The kinase is negatively regulated by RAS signalling and therefore links the growth pathway activation with cyclin D1 stabilisation, as well as *CCND1* induction. Yang *at al* also showed that cyclin D1-Thr286 phosphorylation was important for degradation during S phase (Yang et al., 2006a). However, during S phase there was no change in AKT, PI3K or GSK3-β activity, challenging the role of GSK3-β mediated phosphorylation. Nevertheless, these studies imply that D-type cyclin expression is tightly regulated by phosphorylation at Th286. They also provide evidence that a major mechanism contributing to cyclin D1 overexpression in human tumours results from enhanced protein stability.

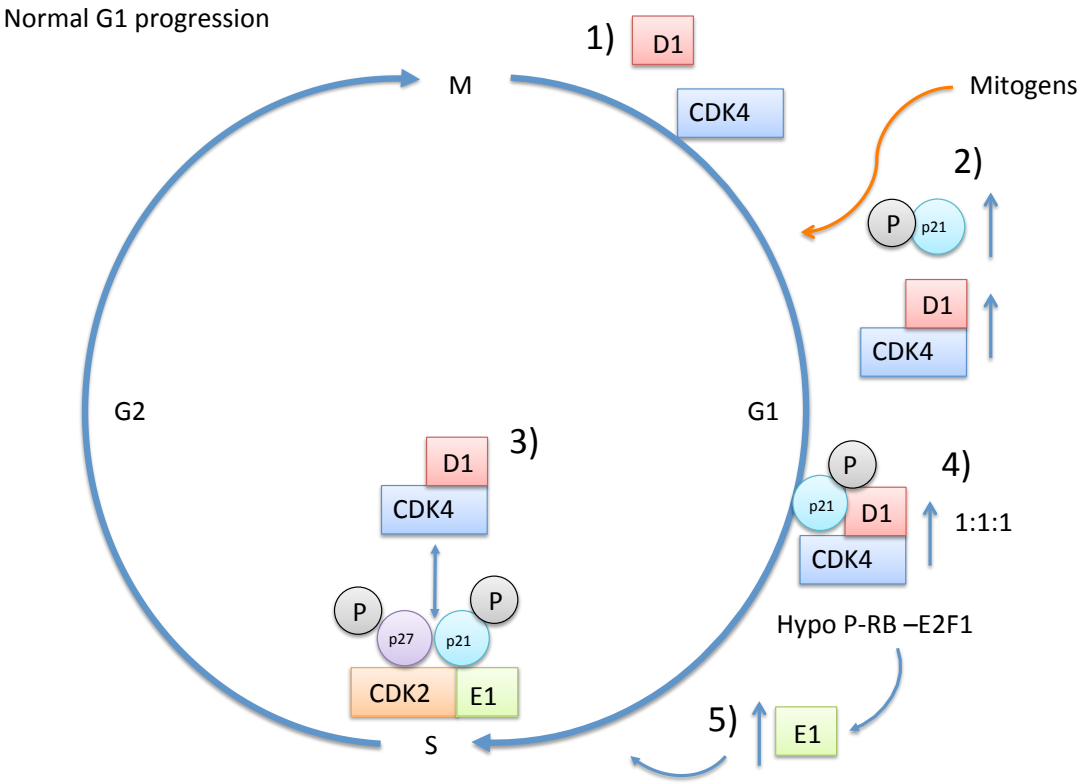

Figure 1.1 Interaction between cyclin D1 and p21 in G1/S control

1) In early G1 cyclin D and p21 are levels low. At this time, CDK2 is inhibited by p27 and p21 binding. 2) Mitogenic signalling induces p21 and cyclin D1 expression and complex formation occurs. 3) High levels of cyclin D titrate p21 and p27 from CDK2. p21 and p27 are constantly dissociating from CDK2. Therefore, high cyclin D1 levels will outcompete cyclin E1 for p21 binding. Mitogenic signalling also increases p21/p27 tyrosine phosphorylation. This disrupts p21/p27 Van Der Waal's forces and hydrogen bonding on the alpha helix responsible for obstructing the CDK ATP binding pocket. This switches p21 and p27 from an inhibitory confirmation to an active one. 4) Activated CDK4-CyclinD-p21/p27 complexes hypophosphorylate RB releasing E2F1. 5) E2F1 induces cyclin E1 transcription and results in CDK2 activity, further RB phosphorylation and E2F1 release and S phase progression.

1.2.4 Synthesis, G2 and mitotic cell cycle phases

Primary phosphorylation of RB by CDK4-cyclinD1-p21 complexes results in cyclin E transcription, CDK2 activation and hyperphosphorylation of RB, leading to E2F dependent gene transcription of S-phase initiation genes (Figure 1.1). Cells are now committed to division even in the absence of mitogenic stimuli and enter S phase, where DNA replication takes place (Foijer and Te Riele, 2006). The successful completion of S phase leaves the cell with two accurate copies of the genome that are segregated in M phase into daughter cells. The phases of mitosis are outlined in Figure 1.2. Before mitotic entry, the cell firstly pauses in G2, where CDK1-cyclin A levels are still maintained from the preceding S phase (Goldstone et al., 2001). During transition into M phase, cyclin A is degraded and cyclin B levels peak through transcription and protein stabilisation in G2 (Fung and Poon, 2005). Elevated levels of cyclin B result in more CAK activated CDK1-cyclin B complexes. However, the complex is still inhibited by Wee1 and Myt1-mediated phosphorylation, resulting in a pool of primed CDK1-cyclin B (Fung and Poon, 2005). In order to activate the system in a switch like fashion, CDC25 phosphatases are activated by polo kinase, which in turn leads to preliminary activation of CDK1. A positive feedback loop develops, whereby CDK1 inhibits Wee1 and activates CDC25 phosphatases resulting in rapid activation (Potapova et al., 2009). Activated CDK1 now initiates early events in mitosis, including nuclear envelope breakdown, chromosome condensation, bipolar mitotic spindle organisation and assembly (Enserink and Kolodner, 2010). After CDK1 has performed its early roles, the cell is prepared for the metaphase to anaphase transition. Activation of the anaphase-promoting complex (APC/C), a ubiquitin ligase, promotes the degradation of securin, which in turn frees separase to cleave the cohesion complex resulting in its rapid disruption and chromosome segregation takes place (Uhlmann, 2001). Emi1 inhibits APC/C activity in S and G2 phases, until CDK1-dependent phosphorylation and destruction (Margottin-Goguet et al., 2003).

Before the cell commits to chromosome segregation, the spindle assembly checkpoint (SAC) has to be satisfied. The SAC halts anaphase onset until every kinetochore (a protein complex localised to chromatid centromeres that permits

spindle attachment) is attached to the mitotic spindle, ensuring accurate chromosome segregation (Musacchio and Salmon, 2007). Inhibition of APC/C by the SAC prevents separase activation and cyclin B degradation, holding the cell in metaphase (Nigg, 2001). Kinetochore assembly in prophase recruits a complex of proteins including MAD1, MPS1, BUB1, BUB3, BUBR1 and CENPE. Kinetochores vacant of microtubule binding generate a diffusible inhibitory signal that is dependent on the assembly of all the aforementioned proteins (Musacchio and Salmon, 2007). Specifically, upon binding to the kinetochore complex, MAD2 is activated through a conformational change, before tightly binding to cdc20 (Yu, 2006). Cdc20 is an APC/C activator and its sequestration inhibits the system. Upon microtubule binding to the kinetochore, the MAD2 activation template is absent, relieving the SAC (Mapelli et al., 2007). Therefore, cdc20 is free to activate APC/C, inducing chromosome segregation. After segregation and nuclear membrane formation, cyclin B is destroyed by APC/C, which induces cytokinesis (Normand and King, 2010) .

Like mitosis, cytokinesis consists of a series of highly ordered stages (Normand and King, 2010). Firstly, the recruitment of RhoA to the cleavage site specifies the cleavage plane; problems in this phase will fail cytokinesis initiation (Normand and King, 2010). The second stage involves the cleavage furrow ingression through formation of the actomyosin ring and failure at this stage can result in a lack of furrow initiation or regression (Normand and King, 2010). As furrow regression completes, the two cells remain linked by the spindle midbody. Signalling at this stage safely promotes abscission and permanent separation the two daughter cells (Normand and King, 2010). Failure at any stage of cytokinesis can result in the formation of bi-nucleated tetraploid cells. After successful completion of cytokinesis, the two daughter cells enter G1 or G0 until mitogenic signalling instructs for another division.

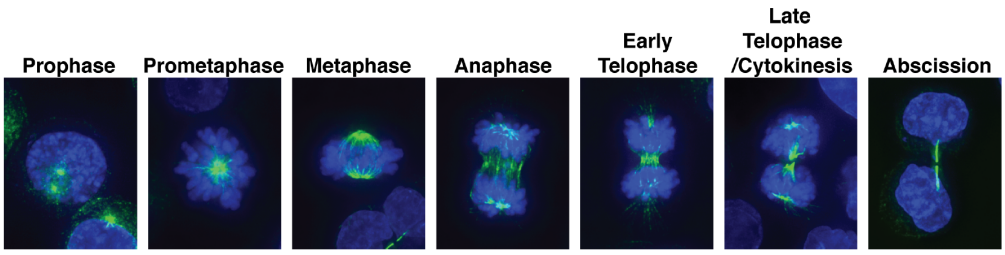

Figure 1.2 The phases of mitosis

Images of HCT-116 cells in the different stages of mitosis (DNA is stained with DAPI in blue and the mitotic spindle with anti-tubulin antibodies in green). The first mitotic stage is prophase, where chromosome condensation occurs and spindle fibres emerge from the centrosomes, before nuclear envelope breakdown. During prometaphase, kinetochores form at chromatid centromeres facilitating spindle attachment, centrosomes move to opposite poles and chromatids are aligned to the metaphase plate. The cell is now in metaphase with the mitotic spindle fully developed. The centrosomes are at opposite poles with each sister chromatid attached to a spindle fibre from each extremity. After satisfaction of the SAC, anaphase is initiated, resulting the in breakdown of cohesion proteins before chromosome segregation, whilst non-kinetochore spindle fibres lengthen and elongate the cell. During telophase, chromosomes are fully segregated to opposite poles, the mitotic spindle breaks down and the nuclear envelope re-forms. Finally, the formation of the cleavage furrow in cytokinesis occurs before abscission, resulting in the production of two genetically identical daughter cells. Images provided by Rebecca Burrell and Swanton laboratory.

1.2.5 Mitotic causes of chromosome missegregation and CIN

Deviation from the strict mitotic control, described above, can lead to chromosome missegregation. Unfaithful chromosome segregation contributes to CIN, resulting in divergent and unstable aneuploidy (Ganem et al., 2009). In order to achieve accurate segregation of the genome to the spindle poles and subsequent daughter cell generation, two pathways monitor fidelity in mitosis, the SAC and error correction. As discussed above, the SAC ensures all kinetochores are occupied by spindles through MAD2 inhibition of cdc20 and inactivation of APC/C. Once attachment is complete, chromosome segregation occurs. As the SAC has such a central role in regulating segregation it is easy to imagine that defects in system could lead to segregation errors (Kops et al., 2005).

Alternatively, segregation errors and CIN can arise though unresolved kinetochore–microtubule attachments. Incorrect attachments are problematic, as they can satisfy the SAC as all kinetochores are occupied and MAD2 signalling is supressed, leading to aberrant segregation, CIN and aneuploidy (Kops et al., 2005). The two types of aberrant spindle binding are known as syntelic and merotelic attachments. Syntelic attachment involves both kinetochores being attached to same spindle pole, and merotely occurs when one kinetochore is attached to spindle poles (Kops et al., 2005). Both occur frequently during mitosis and if unresolved, can lead to lagging chromosomes (Gregan et al., 2011).

If the frequencies of erroneous attachments are high, the system can become saturated, resulting in uncorrected errors and lagging chromosomes. Merotely is particularly dangerous, in that it can resist both error correction and the SAC, as both kinetochores are occupied and tension is present, resulting in anaphase initiation and chromosome (Gregan et al., 2011).

1.2.6 DNA damage response (DDR)

The cell employs DNA damage checkpoint pathways in order to sense errors and arrest the cell cycle in order to provide essential time and resources in repairing the damaged DNA (Kastan, 2008). DNA damage, resulting in single-strand and double-strand breaks, DSBs and SSBs, respectively, can lead to variety chromosomal abnormities, including fusions, translocations and acentric fragments that can lead to CIN in mitosis (Thompson and Compton, 2011). Pre-mitotic defects can lead to mitotic errors, such as anaphase bridges through the production of dicentric chromosomes, whilst acentric chromosomes can be lost or randomly segregated (Thompson and Compton, 2011). Therefore, pre-mitotic DNA damage can lead to copy number gains and losses through CIN. Indeed, our laboratory recently demonstrated replication stress in colorectal cancer (CRC) resulted in DNA damage that linked both structural and numerical CIN (Burrell et al., 2013a). The observation that pre-mitotic defects could result in numerical CIN may be a result of the DNA damage caused by structural CIN. The high frequency acentric and dicentric chromosomes observed after replication stress are likely to result in daughter cells with heightened DNA damage. Damaged chromosomes may be less likely to be replicated properly in S-phase and passed on to subsequent generations, and therefore may be lost resulting in numerical CIN. Loss of DNA repair proteins such as ATR and MRE11 result in high levels of CIN, as does low dose irradiation (IR), supporting a link between DNA damage and CIN (Deckbar et al., 2007, Brown and Baltimore, 2000, Buis et al., 2008). These studies show that defects in sensing and repair of DNA damage can lead to CIN and aneuploidy.

1.2.7 Aneuploidy tolerance

The aforementioned mechanisms demonstrate how cells can make segregation errors that can lead to CIN and aneuploidy. In mitosis, an aberrant SAC or problems in resolving kinetochore attachment can lead to lagging chromosomes resulting in loss or missegregation. In addition, pre-mitotic DNA damage can lead to structural and numerical CIN resulting in an unbalanced genome. However, cancer cells can have high rates of segregation errors and yet CIN and aneuploidy cannot be propagated (e.g. HCT-116). In order for CIN and aneuploidy to

propagate, chromosome missegregation must be coupled with a tolerance mechanism.

Thompson and Compton directly investigated the relationship between CIN and aneuploidy, by employing a system where LacGFP was integrated into a single chromosome in order to monitor its segregation (Thompson and Compton, 2010a). Elevating the rate of segregation errors in HCT-116 cells by washout treatment with monastrol, an inhibitor of the Eg5 kinesin that is critical for proper spindle formation (Kapoor et al., 2000), inhibited colony formation in cells that missegregated the labelled chromosome. The reduction in viability was p38, p53 and p21-dependent and did not elicit a DNA damage response.

Clonogenic assays showed treatment of *TP53*$^{-/-}$ cells with monastrol resulted in the formation of viable colonies, which showed deviation from the model chromosomal number, whereas p53 wild type colonies did not form. This suggests *TP53*$^{-/-}$ cells make segregation errors and proliferate, a hallmark of CIN (Thompson and Compton, 2010a). Intriguingly, *TP53*$^{-/-}$ cells not treated with monastrol maintained a stable diploid karyotype, suggesting that loss of a tolerance mechanism alone is insufficient to initiate CIN. The *TP53*$^{-/-}$ CIN-positive cells were then picked and subcloned, before karyotyping 50 cells from the resulting population. Karyotypes from these subclones often deviated from the model chromosome number, suggesting an elevated rate of karyotypic change (or CIN) in a previously stable diploid cell line (Thompson and Compton, 2010a). This result suggests the initial chromosomal imbalance, caused by monastrol, could maintain CIN, and gave rise to a diverse spectrum of aneuploid clones. A diverse pool of subclones within a population could be selected in the presence of a selection a pressure (e.g. drug treatment), highlighting the clinical importance of heterogeneous aneuploidy in tumours. Therefore, this study showed that elevating the segregation error rate in *TP53*$^{-/-}$ background leads to CIN and diverse aneuploidy, demonstrating that heightened rates of segregation errors in combination with a tolerance required for the maintenance of CIN.

A scenario that may promote elevated segregation error rates in combination with an aneuploidy tolerance mechanism is tetraploidy. Below tetraploidy is discussed in

detail, firstly examining routes to tetraploidization, before discussing tolerance and the ploidy states relationship with CIN and aneuploidy.

1.3 Tetraploidy

There are two different classes of polyploid cells, namely, allopollyploids and autopolyploids. Allopolyploids can be formed by fusion of diploid gametes, resulting from improper meiosis, from two hybrid organisms (Storchova and Pellman, 2004, Otto, 2007). Allopolyploidy is particularly important in evolution, as different genomes are combined and also undergo a degree of structural change and can contribute to the formation of new species (Storchova and Pellman, 2004). Autopolyploids are derived from a genome-doubling event of the same genome and can lead to whole organism polyploidy or can be confined to a population cells in euploid organism (Storchova and Pellman, 2004).

Tetraploidy is an autopolyploid state referring to the specific doubling of the diploid complement (2N), in contrast to aneuploidy which is not a 2N multiple. Polyploidy observed in normal mammalian tissue plays a beneficial role to the cell and organism (Davoli and de Lange, 2011a). However, polyploidy, and mainly tetraploidy, observed in tumours can lead to CIN aneuploidy and tumour evolution. Polyploid cells can be formed by three major mechanisms in animals; cell fusion, developmental endoreplication and mitotic errors (Storchova and Pellman, 2004). These processes are discussed in detail below in the context of normal development and disease.

1.3.1 Polyploidy and CIN in normal cellular physiology

Although polyploidy is well documented in plants, a wide variety of animal tissues are polyploid including the blood, liver, intestinal, brain, and skin, highlighting an important role in normal development (Davoli and de Lange, 2011a).

Cell fusion can create polyploid cells in normal development. Skeletal muscle fibres are formed though fusion of thousands of myoblasts. Initially, low numbers of myoblast fuse to form nascent myotubes, before further fusion events produce mature myotubes (Horsley and Pavlath, 2004). Macrophages also undergo cell fusion, although in contrast to myoblasts, it is a relatively rare event confined to specific instances such as chronic inflammation (Bruzzaniti and Baron, 2006). Fusion results in giant cells or osteoclasts that have an increased capacity to consume and degrade foreign bodies.

Endoreplication can be divided into two subcategories comprised of the endocycle and endomitosis (abortive mitosis). Endocycling involves the complete absence of mitosis, resulting in S phase and growth phase alternations with no division. Cells that undergo endomitosis, enter M phase but fail to complete the process and exit early from mitosis with either mono or bi-nucleate cells, depending on the point of exit (Fox and Duronio, 2013). They are both programmed, normal physiological mechanisms that generate polyploid cells and occur in a variety of mammalian tissues.

Differentiation of trophoblast stem cells (TS) to giant cells (TG) results in endocycling and polyploidization with ploidy profiles of up to 64N (Ullah et al., 2008). During differentiation, fibroblast growth factor 4 deprivation and increases in p57 expression attenuate cyclin B expression and CDK1 activity and blocks mitotic entry. This endocycling process is thought to benefit the cell by accelerating cellular growth, by shortening the cell cycle while increasing the chromosome complement. Megakaryocytes are thought to undergo endoreplication as repeat cycles can result in cells with ploidy profiles up to 128N. Many single cells would be required to produce the same number of platelets as a polyploid megakaryocyte. Increasing platelet production form a single cell is beneficial as less energy is required for membrane, due to lower surface area, synthesis and cell division. Therefore one polyploid megakaryocyte can produce and equivalent number of platelets at a reduced energy cost. (Ravid et al., 2002).

1.3.2 Pathogenic polyploidy in cancer

Polyploidy and CIN has been observed in normal tissues and is discussed in section 1.3.1. However, tetraploidy has also been shown to be an intermediate of aneuploidy, by promoting and supporting CIN and leading to tumour evolution and drug resistance (Dewhurst et al., 2014). Although the mechanisms that can produce normal or pathogenic polyploid cells are the same, there are some key differences between programmed and sporadic polyploidy.

Normal endoreplication is associated with permanent departure from the cell cycle and is synonymous with terminal differentiation (Fox and Duronio, 2013). Therefore, if the cell is not cycling, CIN and branched tumour evolution cannot occur. The liver is an interesting case, where proliferation and CIN are tolerated and rarely lead to cancer (Duncan et al., 2010). Even joint loss of *TP53* and *RB1* fail to produce tumours, suggesting that the liver has the capability to suppress tumour formation in the presence of CIN and aneuploidy (Fox and Duronio, 2013). Therefore, when polyploidy is programmed, it rarely leads to tumourigenesis as mechanisms are in place to prevent it. However, in tissues where non-programmed genome-doubling occurs, cell cycle re-entry is permitted and tetraploidy tolerance is provided, such that the resulting proliferating tetraploid cells can facilitate tumourigenesis and tumour evolution. Mechanisms involved in the formation of pathogenic tetraploid cells are described below.

1.3.2.1 Pathogenic cell fusion

Cell fusion can be a pathogenic event leading to fused cells with tumourigenic potential and CIN. Hu *et al* demonstrated the HPV16 virus E5 gene product acts as fusion protein (Hu et al., 2009). Microscopy and fusion assays demonstrated that viruses expressing the E5 protein could fuse human keratinocytes. The model proposed involves viral infection followed by a transient increase in E5 protein, permitting cell fusion before lowering expression. The fusion event will normally produce a p53 apoptotic response, however expression of E6 (p53 inactivation) and E7 (RB inactivation) suppress the response, resulting in a tetraploid cell with

deregulated DDR and cell cycle. This molecular phenotype may provide the background for CIN and carcinogenesis.

Another study showed fibroblasts over-expressing the *E1A* and *HRAS* oncogenes are fused by the MPMV^{E} virus, displayed high levels of CIN and aneuploidy, and has increased tumourigenic potential in murine models (Duelli et al., 2007). The study highlighted that it was specifically the fusion event that resulted in CIN, as non-fused diploid cells containing MPMV^{E} and oncogene over-expression did not display elevated CIN. Fusing cells at different cell cycle stages could be the cause of elevated CIN. For example, if an S phase cell was fused with a late G2 cell, incomplete replication could cause extensive DNA damage in M phase. Therefore, it is possible that cell fusion can cause CIN independently of any mutations.

1.3.2.2 Mitotic failure

Another common route to tetraploidy is characterised by the deregulated progression through mitosis and can be a result of two main events, namely, cytokinesis failure and mitotic slippage.

1.3.2.2.1 Cytokinesis failure

Failure in cytokinesis results in bi-nucleate cells that may enter S phase and a subsequent normal mitosis resulting in two mono-nucleated 4N daughter cells (Davoli and de Lange, 2011b). Emi1 and MAD2 have been implicated in cytokinesis failure (Sotillo et al., 2007, Margottin-Goguet et al., 2003, Lehman et al., 2006). Both proteins are negative regulators of the APC/C ubiquitin ligase (mitotic control discussed in section 1.2.2) and are both frequently overexpressed in human tumours. Fittingly, experimental overexpression of either of these two APC/C regulators can result in cytokinesis failure and the formation of bi-nucleate cells (Margottin-Goguet et al., 2003, Sotillo et al., 2007). Interestingly, prolonged overexpression of several APC/C inhibitors results in the stabilisation of downstream substrates, possibly hampering the correct coordination of cytokinesis (Meraldi et al., 2002, Mundt et al., 1997, Wheatley et al., 1997).

Shi and King estimated that 94% of bi-nucleate cells formed through furrow regression would show evidence of chromosome non-disjunction (Shi and King, 2005). Chromatin in the cleavage furrow may couple chromosome non-disjunction and cytokinesis failure. However, Shi and King *et a*l showed, chromosome bridging or lagging (CBL) occurred in only 53% of cells that become bi-nucleate by furrow regression, suggesting CBL couldn't fully account for the formation of all tetraploids (Shi and King, 2005). In addition, 15% of mono-nucleate cells completed cytokinesis even in the presence of CBL. Therefore, the presence of CBL is neither necessary nor sufficient to induce cytokinesis failure and bi-nucleation. In contrast to this study, others have found chromatin remaining in the spindle midzone can result in furrow regression and failed cytokinesis, for example, lagging or acentric fragments are present in the midzone (Mullins and Biesele, 1977, Davoli and de Lange, 2011a). In addition, the NoCut pathway in yeast can sense chromatin in the midzone and inhibit cytokinesis, which if unresolved, may lead to abscission failure and polyploidy (Norden et al., 2006). Interestingly, Aurora A kinase plays a fundamental role in the NoCut pathway, further highlighting overexpression can inhibit cytokinesis. There is clearly a debate on whether chromatin present in a cleavage furrow or a chromosome non-disjunction is a major mechanism for cytokinesis failure (Weaver et al., 2006). Nevertheless, cytokinesis failure can occur by a variety of mechanisms and result the formation of G1 tetraploid cells.

1.3.2.2.2 Mitotic slippage

Mitotic slippage is another mechanism that can result in the formation of G1 tetraploid cells (Aylon and Oren, 2011). The mechanism, again, involves APC/C inhibition, but in this case, the metaphase to anaphase transition fails and cells do not complete any further mitotic stages before entering G1. During prolonged SAC activation and inhibition of APC/C, cyclin B degradation can still occur *via* gradual proteasome-mediated degradation. As transcription is inhibited in mitosis, eventually cyclin B levels fall below a threshold, inactivating CDK1, and the cell "slips" out of mitosis (Blagosklonny, 2007). This route of tetraploidization produces mono-nucleate 4N cells, as chromosome segregation has not occurred.

Elhajouji *et al* showed that treatment with the spindle poison nocodazole, which causes SAC activation through spindle depolymerisation and thus constant MAD2 signalling, resulted in the formation of mono-nucleate tetraploid cells by mitotic slippage (Elhajouji et al., 1998). Rossio *et al* showed MAD2 overexpression in yeast resulted in mitotic slippage, with a concomitant reduction in cyclin B and securin (Rossio et al., 2010). Furthermore, the study conducted by Sotillo *et al* also noted MAD2 overexpression resulted in the formation of mono-nucleate in addition to bi-nucleate cells (Sotillo et al., 2007). This suggests that MAD2 overexpression can result in mitotic slippage, as well as cytokinesis failure. Loss of the Adenomatous Polyposis Coli (APC) that governs β-catenin and WNT signalling has been shown to associate with tetraploidization. Dikovskaya *et al* demonstrated that APC loss in cell lines resulted in increased spindle defects and a compromised SAC, thus, leading to mitotic slippage and tetraploid cell formation (Dikovskaya et al., 2007). Taken together, these studies show that aberrant expression of mitotic regulators can deregulate mitotic process resulting in slippage and cytokinesis failure and the formation of tetraploid cells.

1.3.2.3 DNA damage and pathogenic endocycling

A study by Davoli *et al* showed that a persistent DNA damage signal could result in the formation of viable tetraploid cells (Davoli et al., 2010). In early tumourigenesis and in the absence of p16 and p53, telomere shortening goes beyond the 'Hayflick limit', exacerbating shortening and induces massive CIN. During this time, short telomeres and shelterin dysfunction result in persistent activation of ATR/ATM and CHK1/2. These pathways inactivate CDK1-cyclin B activity, which inhibit entry into mitosis, and cause a prolonged G2 arrest. During this arrest, mitosis-independent destruction of geminin occurs, permitting the expression of cdt1, origin firing and genome duplication (Davoli et al., 2010). Post-crisis telomerase activation or telomere function restoration leads to the reduction of the DNA damage signal and the 8N cell can enter mitosis, producing two daughter tetraploids (Chin et al., 2004, Davoli et al., 2010).

Persistent DNA damage can also induce endocycling via other sources. Loss of the DNA damage processing and sensing proteins XRCC3, NBS1, Rad17 or overexpression of RPA result in endoreplication, supporting the hypothesis that persistent DNA damage can result in the formation of tetraploid cells (Reina-San-Martin et al., 2005, Yoshihara et al., 2004, Wang et al., 2003). Moreover, tumours lacking the homology-directed repair protein BRCA2 in p53-negative breast cancer are frequently polyploid, further supporting aberrant DNA damage pathways and polyploidy (Gretarsdottir et al., 1998). A final source of persistent DNA damage may arise from replication stress driven by oncogene overexpression, as shown by several studies, which results in induction of DNA damage and tetraploidization (Bartkova et al., 2005, Di Micco et al., 2006).

In the examples above, p53 loss was required to either permit the formation of a tetraploid after DNA damage-mediated endocycling, or to resist G1 arrest after cytokinesis failure. Therefore, loss of p53 plays an important role in the formation and survival of tetraploid cells. The role of p53 in supressing the proliferation of tetraploid cells after an aberrant mitosis is discussed below.

1.4 Tetraploid control systems

Mammalian cells have evolved systems to perturb the proliferation of tetraploid cells, formed through mitotic defects or cytokinesis failure (Aylon and Oren, 2011). As previously discussed, mitotic failure can result in the formation of G1 4N tetraploid cells. The observation of p53-dependent G1 arrest after tetraploidization has fuelled the idea of a tetraploidy checkpoint. The tetraploidy checkpoint may serve as final control mechanism to abort polyploid cells.

1.4.1 The tetraploidy checkpoint

Early evidence suggesting that cells could detect the formation of tetraploid cells was provided before the discovery of classical cell cycle checkpoints. In 1967, Smith *et al* purified lymphocytes from peripheral blood and showed cytochalasins, derived from moulds, could prevent cytokinesis and produce arrested bi-nucleated

cells (Smith et al., 1967). Thereafter, in 1972, Wright and Hayflick noted the same effect in lung fibroblasts (Wright and Hayflick, 1972). Transformation with SV40 and continuous cytochalasin treatment resulted in persistent nuclear division and lead to multi-nucleated cells. The authors concluded that “once a normal human diploid cell becomes bi-nucleate, intrinsic cell mechanisms come into play preventing further division – perhaps SV40 cells can escape this control” (Wright and Hayflick, 1972).

Subsequently, it was discovered that SV40 inactivates p53 and provided early evidence the transcription factor was central in the control of bi-nucleate cell survival (Ahuja et al., 2005). Further work in the 1990’s generated 4N cells by mitotic slippage after nocodazole treatment. In support of the earlier findings, this 4N G1 arrest was mediated by p53 and p21, resulting in decreased RB phosphorylation and was DNA damage-independent (Di Leonardo et al., 1997, Khan and Wahl, 1998). Andreasen *et al* attempted to investigate whether the G1 arrest after mitotic slippage was SAC-dependent or a more general “tetraploidy checkpoint” exists (Andreassen et al., 2001b). Treating REF-52 cells with dihydocytochalasin B (DCB) to promote cytokinesis failure, before drug washout, resulted in a permanent 4N G1 arrest, p53/p21 induction and decreased CDK2/RB, all indicative of a G1 arrest. In contrast, T-antigen transformed cells and REF-52 cells expressing a dominant negative form of p53 failed to arrest and progressed through the cell cycle. The authors obtained similar results with transient nocodazole treatment (Andreassen et al., 2001b). As tetraploid cells were formed by either mitotic slippage or cytokinesis failure, it was conclude that a general tetraploid checkpoint exists and was not dependent on specific signalling mechanisms in mitosis, such as SAC.

Conversely, two studies that shortly followed Andreasens’ work questioned such a checkpoint, while the presence of normal human tetraploid hepatocytes also complicates matters (Duncan et al., 2010, Wong and Stearns, 2005, Uetake and Sluder, 2004). A key weakness of the above studies is the pharmacological induction of tetraploidy, because the observed p53-driven G1 arrest of 4N cells may be a result of an off-target drug effect (e.g. DNA damage) rather than the formation of a tetraploid cell. Indeed, Lohez *et al* reported that lowering the dose of

DCB treatment was not sufficient to form tetraploid cells but still caused a diploid cell cycle arrest, suggesting the drug could cause cell cycle inhibition independently of tetraploidization (Lohez et al., 2003). In contrast, Uetake and Sluder showed that further lowering the DCB dose produces bi-nucleate tetraploid cells but they were able to proliferate, implying the absence of a tetraploid G1 arrest (Uetake and Sluder, 2004). Wong *et al* also suggested tetraploid cells created by cell fusion can cycle, and fusion of cytoplasts (enucleated cells) and diploid cells producing 2N cells with centrosomes could also proliferate (Wong and Stearns, 2005). These studies argue against the presence of a tetraploidy checkpoint that directly senses chromosome or centrosome number and arrest may be an off-target pharmacological effect.

Even so, Uetake and Sluder's study showed that bi-nucleate cells formed by the addition of DCB did arrest, whereas diploids did not. Furthermore, Shi and King's study showed that naturally occurring tetraploids, resulting from chromosome non-disjunction and subsequent cytokinesis failure, had differential fates depending on p53 status (Shi and King, 2005). Therefore, although in some systems tetraploid cells can proliferate, clearly tetraploids are more sensitive to G1 p53-dependent arrest, although it is unlikely that aberrant chromosome number is directly sensed.

1.4.2 Molecular mechanisms of the tetraploidy checkpoint

A possible trigger for the tetraploidy checkpoint is the tumour suppressor LATS2 kinase (Large Tumour Suppressor Kinase 2). Aylon et al showed that overexpression of LATS2 could reduce the ubiquitination of p53, by MDM2 inhibition (Aylon et al., 2006). In addition, treatment with nocodazole mediated LATS2 translocation to the nucleus, inhibiting MDM2 and stabilising p53. Consequently, p53 bound to the LATS2 promoter and induced p53 even further. Cell cycle analysis showed that p53 activation occurred during mitosis, before mitotic slippage, and gradually increased to an inhibitory threshold once the cell was in G1 (Aylon et al., 2006). This study provides evidence that microtubule damage and the ensuing SAC activation activate LATS2 to safeguard the cell in the event of a slippage event.

A recent study by Ganem *et al* showed that LATS2 was also implicated in activating p53 in response to a tetraploidization event (Ganem et al., 2014). Treatment of RPE cells with DCB-induced cytokinesis failure and p53/p21 expression, exclusively in the tetraploid cells. After DCB treatment, G1 tetraploid cells were sorted utilising the Fucci system (a system that allows identification of cell cycle phase) and screened in a siRNA library to identify genes that could promote survival. The screen identified that large tumour suppressor kinase 2 (LATS2) knockdown permitted the proliferation of tetraploid cells. It was discovered that centrosome amplification in the genome-doubled cells activated RAC kinase, which in turn inhibited RhoA, leading to LATS2 activation. As LATS2 is a negative regulator of MDM2, p53 was stabilised while YAP and TAZ transcription was reduced. This mechanism provides evidence for a tetraploidy checkpoint and can explain why DCB treatment under different conditions can yield different responses. Lowering the dose of the drug or growing cells on fibronectin shortens the length of G1. As the p53 response provided by this system is gradual, as also in the case of (Aylon et al., 2006), the threshold for inhibition may not be reached in these conditions, resulting in cell cycle progression of newly formed tetraploids. Moreover, tetraploid mouse hepatocytes also showed activation of LATS2, p53 and p21, whilst the response was absent in p53-null mice (Ganem et al., 2014). This finding provides strong evidence for hippo pathway activation *in vivo*. This discovery, in combination with fact that two different mechanisms of tetraploid induction using different compounds induced a p53-mediated G1 arrest (implying the arrest is due to tetraploidy and not alteration of a specific drug target), strongly suggests the presence of tetraploidy checkpoint and argues against the response being a pharmacological off-target effect.

In addition to cell cycle arrest, tetraploids may also have to resist apoptosis. Castedo *et al* showed that newly formed tetraploids undergo a p53/BAX dependent apoptosis (Castedo et al., 2006b). Expression arrays showed that newly formed tetraploids were characterised by a mild elevation in p53 target genes and underwent enhanced spontaneous apoptosis, which could be rescued by silencing PUMA or overexpressing BCL-2 (Castedo et al., 2006b). Therefore, apoptosis presents another hurdle for newly formed tetraploid to overcome.

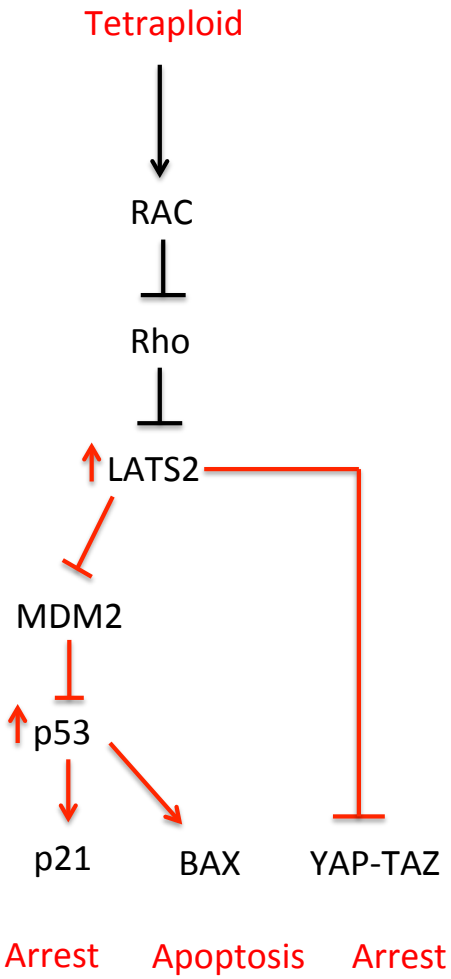

Figure 1.3 Tetraploid checkpoint pathway

After tetraploidization and centrosome amplification, a hyperactivation of the small G-protein RAC1 occurs. RAC1 antagonizes Rho, which is a negative regulator of the LATS2 kinase. The activation of LATS2 results in YAP cytoplasmic sequestration and TAZ degradation, inactivating the pro-proliferative Hippo pathway transcription factors, resulting in cell cycle arrest. In addition, LATS2 is negative regulator of MDM2 through protein degradation, leading stabilised p53, which induces p21 expression, resulting in a G1 arrest. p53 can also induce apoptosis through BAX expression.

1.5 Consequences of tetraploidy

If a newly formed tetraploid manages to overcome the tetraploidy checkpoint, the cell can continue to proliferate and divide. The consequences of overriding the tetraploidy checkpoint and continued proliferation are discussed below.

1.5.1 Tetraploidy and tumourigenesis

Fujiwara *et al* performed a series of experiments to investigate whether tetraploid cells can initiate tumourigenesis (Fujiwara et al., 2005). Treating *TP53*$^{+/+}$ or *TP53*$^{-/-}$ mammary mouse epithelial cells (MMECs) with DCB-generated generated bi-nucleate tetraploid cells. *TP53*$^{+/+}$ cells underwent one round of division but failed to propagate, whereas *TP53*$^{-/-}$ tetraploids proliferated and showed increased CIN compared to diploid cells. These data imply that MMECs do not have a G1 tetraploidy checkpoint but fail after the first division, possibly as result of enhanced CIN. When *TP53*$^{-/-}$ tetraploid cells were injected into mice, 25% of mice spontaneously formed tumours, whereas *TP53*$^{-/-}$ diploids did not form any tumours. Therefore, this study directly demonstrated that tetraploid cells could form tumours and this case, more frequently than diploids with the same genetic background.

In support of this seminal work, Sotillo *et al's* study showed that transient MAD2 overexpression which resulted in tetraploid cell formation *via* mitotic failure, also increased tumour formation (Sotillo et al., 2007). Importantly, this study demonstrated that transient MAD2 overexpression and subsequent tetraploidization can be the stimulus for tumourigenesis, as continued MAD2 overexpression was shown to not be required, unlike other oncogenes. Specifically, transient MAD2 overexpression could produce tetraploid cells, which facilitate tumour progression regardless of MAD2 expression. Duelli *et al* also noted the virally fused tetraploid cells formed tumours in mice, whereas infected diploids carrying the same oncogene overexpression did not (Duelli and Lazebnik, 2007).

Together, these studies provide evidence that a tetraploidization event can promote tumourigenesis, highlighting the importance of functional tetraploidy checkpoint.

1.5.2 Tetraploidy CIN and DNA damage

A substantial body of studies exists to suggest that tetraploid cells are intermediates of CIN and aneuploidy (Ganem et al., 2009, Dewhurst et al., 2014, Lv et al., 2012, Duelli and Lazebnik, 2007, Fujiwara et al., 2005). Therefore, it is expected that when a tetraploid cell evades the tetraploidy checkpoint and initiates tumourigenesis, the resulting tumour would be genetically complex.

Ganem *et al* investigated the mechanistic basis of elevated CIN in tetraploid cells (Ganem et al., 2009). Tetraploid cells, formed through cytokinesis failure or mitotic slippage, will have duplicated centrosomes and this can lead to multipolar chromosome segregation resulting in aneuploidy (Ganem et al., 2009). However, Ganem *et al* found that multipolar segregation was infrequent and highly toxic to cells, presumably due to massive CIN, and therefore could not explain elevated CIN and aneuploidy in tumours. On the contrary, the group showed that cells with extra centrosomes underwent bi-polar segregation as result of centrosome clustering. However, even though segregation was bi-polar, the frequency of lagging chromosomes was greater in cells with amplified centrosomes. It was shown that cells with amplified centrosomes pass through a multipolar spindle intermediate stage before clustering, which can lead to increased merotelic and syntelic attachment and lagging chromosomes (Ganem et al., 2009). Therefore, unique spindle geometry, as result of centrosome amplification, can result in relatively mild segregation errors resulting in non-catastrophic aneuploidy and CIN.

Janssen *et al* showed pharmacologically-induced whole chromosome segregation errors could lead to chromosomal damage during cytokinesis, resulting in DNA damage and activation of the p53-mediated DDR and cell cycle arrest (Janssen et al., 2011). The resulting DSBs lead to structural aberrations and chromosome translocations in daughter cells. Loss of p53 increased the frequency of structural chromosomal aberrations, highlighting its important role in maintaining genome stability. Crasta *et al* support the hypothesis that segregation errors can lead to DNA damage (Crasta et al., 2012). A proportion of lagging chromosomes induced by transient nocodazole treatment formed micronuclei (MN) and a reduction in helicase proteins caused replication stress and incomplete DNA replication upon

mitotic entry, which led to massive DNA damage and chromothripsis (extensive local structural chromosomal rearrangement) (Crasta et al., 2012). The resulting, translocations could persist as MN or upon nuclear envelope breakdown could be segregated and integrated into the nucleus.

Taken together these studies highlight how tetraploidy might lead to elevated CIN and DNA damage, resulting in aneuploid tumours. Centrosome amplification in tetraploids can lead to multipolar intermediates, leading to lagging chromosomes that can be incorporated in correctly into daughter cells (numerical CIN). A heightened rate of lagging chromosomes could also lead to increased chromosomal translocations through the generation of DSBs at cytokinesis, and the formation of MN the can result to massive genetic rearrangement by chromothripsis. Hence, tetraploid cells with extra centrosomes may be more prone to CIN and DNA damage then diploids and this can drive tumourigenesis and genetic evolution. As discussed previously, these mechanisms of CIN resulting in aneuploidy are dependent on a relevant tolerance mechanism, such as loss of p53, which may be provided by the tetraploid cell.

1.5.2.1 Tetraploidy is an aneuploidy intermediate

Building on these findings, direct evidence linking tetraploidy as an aneuploidy intermediate has been provided from *in vitro* and *in vivo* longitudinal studies. In addition to tumour formation, Fujiwara *et a*l noted mouse tetraploid tumours showed an array of abnormalities including extra centrosomes, non-reciprocal translocations, di-centric and double minute chromosomes. All tumours examined showed regional amplification of chromosome 9, a region overexpressed in human breast cancers (Fujiwara et al., 2005).

Further supporting this hypothesis, ovarian tumours are generally aneuploid and cancer risk increases with age and correlates with elevated tetraploid ovarian epithelial cells (Chuaire-Noack et al., 2010). Based on this observation, Lv *et al* investigated whether tetraploidy could act as a precursor to aneuploidy (Lv et al., 2012). The group created and continually passaged spontaneously immortalised

mouse ovarian cells and investigated ploidy at different passage numbers by flow cytometry. The majority of cells at passage 9 were diploid however, over time, genome-doubling occurred and at passage 36, cells were either tetraploid or aneuploid. Chromosome compositions, detected by fluorescent in situ hybridization (FISH), showed that early passage cells were exclusively diploid but became increasingly tetraploid, which correlated with an elevated fraction of aneuploid cells. Early and late passage cells were injected into mice and only the late genome-doubled aneuploid cells formed tumours. These data suggest that mouse ovarian diploid cells can give rise to tetraploids that become aneuploid and are more tumourigenic.

Finally, Davoli *et al* showed that tetraploid cells generated through telomere-induced endoreplication were more tumourigenic *in vitro* and *in vivo* (Davoli and de Lange, 2012). Tetraploid cells formed colonies more readily in soft ager assays and when these cells were injected into mice, they were more tumourigenic. Analysis of cell lines derived from tetraploid tumours revealed sub-tetraploid karyotypes, indicating chromosomal loss. In contrast diploid tumours remained stable and showed a near diploid karyotype. Therefore this study provides support for tetraploid cells being more tumourigenic and can act as an aneuploidy intermediate.

1.5.2.2 Connecting tetraploidy, CIN and aneuploidy

The above studies demonstrate tetraploidy can precede aneuploidy, possibly through CIN driving mechanisms such as proposed by Ganem *at al* (Ganem et al., 2009). However, these studies do not link CIN with tetraploidy and aneuploidy directly.

A recent study in our laboratory has linked tetraploidy as an intermediate of CIN and aneuploidy (Dewhurst et al., 2014). Chromosomally stable HCT-116 diploid and low frequency tetraploid cells were single-cell cloned and passaged for 18 months. Clonal FISH assays measured the cell-cell variation in chromosomal number (percentage of cells deviating from the colony mode) in order to investigate ploidy and numerical CIN.

Tetraploid colonies showed significantly greater chromosomal variation than diploids at both early and late passages. Although twice as many segregation errors were present in the tetraploids than the diploids, this simply reflected the DNA duplication, as the segregation error rate was the same, and could not solely explain the heightened cell-cell variation observed. When the colony modes (colony-colony variation) were investigated, all tetraploid clones produced aneuploid colonies, whereas only one aneuploid colony was found across all diploid clones. The high frequency of aneuploid colonies formed from tetraploid clones suggested that tetraploid cells can tolerate aneuploidy resulting in selection and outgrowth, producing modal chromosome numbers other than four. In contrast, all but one diploid clones had modal colony number of two, suggesting that although aneuploid cells are formed they are rarely viable, hindering aneuploid colony formation. Taken together, these data suggested that tetraploid cells could tolerate CIN and aneuploidy, whereas diploids could not. Direct proof of enhanced tetraploid tolerance to segregation errors was provided by live cell imaging experiments, which showed that after segregation errors, 58% of diploids died or arrested compared to just 16% of tetraploids (Dewhurst et al., 2014).

Importantly, the genetic complexity of the diploid and tetraploid clones was assessed at different time points over an 18-month period. The weighted genome insatiably index (wGII), which estimates the proportion of the genome with aberrant copy number compared with median ploidy weighted on per-chromosome basis, was used to asses CIN for *in vitro* clones and CRC tumours (TCGA public dataset). All diploid clones showed a low wGII similar to the early passage tetraploid clones but became increasing unstable and aneuploid overtime, recapitulating the genetic complexity in human CRC tumours.

In summary, this study demonstrated that in cancer cells that make segregation errors, tetraploid clones make twice as many, show elevated cell-cell variation, can form aneuploid colonies and tolerate segregation errors. Furthermore, tetraploid clones exhibited increasing levels of wGII in a longitudinal assay, which correlated with a reduction in ploidy, implying that the aneuploidy observed was a result of ongoing CIN. Other studies have suggested that in combination with a tolerance

mechanism, an increase in segregation error rate is required to promote CIN (Thompson and Compton, 2010a, Ganem et al., 2009). Although the rate per chromosome did not increase in this study, a doubling on a per cell basis from a basal rate of 19% was clearly sufficient. Therefore, this study directly links tetraploidy with elevated CIN, which may explain the presence of aneuploid CRC tumours.

1.5.2.3 Tetraploidy and aneuploidy in human tumours

Evidence that tetraploidy precedes aneuploidy has also been shown in human tumours (Maley et al., 2006, Olaharski, 2006, Galipeau et al., 1996, Dewhurst et al., 2014).

Galipeau *et al* followed a cohort of 90 patients with initially diploid Barretts oesophagus for at least twelve months (Galipeau et al., 1996). If tumours were still diploid at the first follow up, 11% of patients' tumours progressed to aneuploidy. However, in patients whose first follow-up biopsy was tetraploid, 73% progressed to aneuploidy, providing evidence that tetraploidy is an aneuploidy intermediate in human tumours. The study also found p53 loss proceeded tetraploidy, providing further evidence for a tetraploidy checkpoint. Providing further support, Olaharski *et al* showed in cervical cancer cells derived form 143 women that tetraploidy preceded aneuploidy (Olaharski, 2006). In CRC, the study by Dewhurst *et al* also showed that genome-doubling was a relatively early event, preceding the majority of copy-number losses and CIN and was predictor of poor outcome (Dewhurst et al., 2014).

The aforementioned studies clearly demonstrate that tetraploid cells form tumours and these tumours can be CIN and aneuploid and highlight the importance of the tetraploidy checkpoint in halting the proliferation of tetraploid cells. Failure to do so can result in tumour formation and progression, resulting in aneuploidy and ITH. A diverse pool of subclones increases the probability of clones able to metastasise and resist therapy, leading to poor survival rates.

1.5.3 Tetraploid drug resistance

The elevated rate of karyotypic change, caused by the tetraploidy-to-aneuploidy transition, can increase the probability of tumour subclones harbouring genetic alterations that can confer resistance to anti-cancer therapeutics (Jonkers et al., 2005, Li et al., 2005). It is, therefore, likely that progression from tetraploid intermediates to highly aneuploid cells contributes to the therapeutic failure observed in the clinical setting.

In addition to drug resistance generated through the aneuploidization of tetraploid precursors, tetraploid cells can be intrinsically drug resistant (Castedo et al., 2006b, Castedo et al., 2006a, Kuznetsova et al., 2015). Castedo *et al* generated tetraploid CRC HCT-116 and RKO cell lines and tested their drug sensitivity to a range of compounds. Tetraploids showed relative resistance to a panel of DNA damaging agents (cisplatin, camptothecin and oxaliplatin) compared to diploids, while also exhibiting a reduced apoptotic response (Castedo et al., 2006a). It was discovered that elevated levels of p53 in tetraploid cells enhanced transcription of the downstream target p53-ribonucleotide reductase (p53-R2), required for the conversion of ribonucleotides into deoxyribonucleotides and facilitates DNA repair (Castedo et al., 2006a). Therefore, p53-R2 overexpression in tetraploid cells, as result of constitutive p53 activation, could enhance DNA repair after treatment with DNA damaging agents, leading to therapeutic resistance (Castedo et al., 2006a). A more recent study by Kuznetsova *et al* also showed that tetraploid cells were more resistant to cytotoxic therapy than their diploid counterparts (Kuznetsova et al., 2015). However, in this study the mechanism of resistance was through cytoplasmic sequestration of p53.

In addition cytotoxic chemotherapeutic drug resistance, tetraploidy has been implicated in resistance to targeted therapies. Balsas *et al* cultured human multiple myeloma cells for 18 months whilst gradually increasing the dose of the proteasome inhibitor bortezomib, to create resistant cell lines (Balsas et al., 2012). The resulting cell lines were up to 6-fold more resistant to bortezomib whereas, unexpectedly, the cell lines did not display mutations in bortezomib's target PSMβ5, but rather overexpression of the proteasome subunit. Further analysis revealed that

resistant cells had undergone a genome-doubling event and this was the source of elevated PSMβ5. In agreement with a general up-regulation of proteins (through genome-doubling), resistant cell lines displayed cross-resistance to other chemically unrelated proteasome inhibitors (Balsas et al., 2012). This study demonstrated that genome-doubling can promote resistance to targeted therapies, by elevating the expression of the target proteins and leading to selection and outgrowth of the resistant tetraploid clone.

In summary, the aforementioned studies demonstrate that not only can tetraploidy lead to aneuploidy, which in turn elevates genetic diversity and a heightened probability of resistant subclones, but also that the tetraploid state can be inherently resistant to therapy.

1.5.4 Summary

The above studies show how tetraploidy can lead to CIN, aneuploidy and ITH. Polyploidization can be a normal event is some human tissues, such as the liver, providing a physiological benefit. However, these cells are either terminally differentiated or have mechanisms to suppress potentially oncogenic effects of polyploidy. In contrast, the tetraploidization of cells by failed mitosis, cytokinesis or induction of endocycling can give rise to highly malignant cells. A G1 arrest normally follows un-programmed tetraploidy, however this can be overridden by loss of tumour suppressors such as *TP53* and *CDKN1A*. Tetraploid cells can readily form tumours that become heterogeneously aneuploid through CIN. Tetraploidy *per se* and the resulting CIN and aneuploidy can lead to therapeutic resistance. Therefore, genome-doubling in human tumours contributes to the ITH observed in the clinic, impacting on patient survival by fuelling metastasis and anti-cancer drug resistance.

1.6 Study aims

This thesis describes the work undertaken to understand mechanisms of tetraploid tolerance.

Based on previous studies, it is of great importance to gain a greater understanding of how tetraploidy is tolerated. The isogenic HCT-116 tetraploid system, used by Dewhurst et al, would firstly be investigated. Uniquely, this system was not produced by pharmacological intervention and possessed non-coding mutations in *TP53* and *CDKN1A.* Understanding mechanisms of tetraploidy tolerance independent of p53 pathway mutations is important, as it could lead to the identification of novel targets and mechanisms amenable to therapeutic modulation. The primary aim of this thesis was to uncover tetraploidy tolerance mechanisms independent of p53/RB pathway mutations. This was addressed using global analytical techniques, such as quantitative proteomics, and molecular biology approaches.

Chapter 2. Materials & Methods

2.1 Materials

Table 2.1 Pharmacological agents

Agent	Supplier
5-Fluorouracil	Sigma-Aldrich
Oxaliplatin	Sigma-Aldrich
Epigenetic library	Selleckchem
Reversine	Sigma-Aldrich
Dihydrocytochalasin B	Sigma-Aldrich
Nocodazole	Sigma-Aldrich
Cycloheximide	Sigma-Aldrich

Table 2.2 Primary and secondary antibodies

Antibody	Species	Catalogue number	Supplier
His-tag	Mouse	ab18184	Abcam
p53	Mouse	sc-126	Santa Cruz
p-53 S15	Rabbit	9248	Cell Signalling
p21	Rabbit	2947	Cell Signalling
GAPDH	Rabbit	ab9385	Abcam
PARP	Rabbit	9542	Cell Signalling
Cleaved PARP	Rabbit	5625	Cell Signalling
RB	Mouse	9309	Cell Signalling
pRB 807/811	Rabbit	9308	Cell Signalling
PDCC6IP	Rabbit	2171	Cell Signalling
KIFC1	Rabbit	12313	Cell Signalling
Cyclin A1	Mouse	sc-271682	Santa Cruz

Antibody	Species	Catalogue number	Supplier
Cyclin B1	Rabbit	sc-752	Santa Cruz
Cyclin D1 (WB)	Mouse	556470	BD Biosciences
Cyclin E1	Mouse	sc-247	Santa Cruz
CDK4	Rabbit	sc-260	Santa Cruz
CDK2	Rabbit	sc-163	Santa Cruz
Cyclin D1 (IF)	Rabbit	ab16663	Abcam
Cyclin D1 Thr-286	Rabbit	3300	Cell Signalling
Actin	Mouse	ab49900	Abcam
ERK	Rabbit	9102	Cell Signalling
p-ERK (p44/42)	Rabbit	4370	Cell Signalling
Histone H2B	Goat	sc-8652	Santa Cruz

Table 2.3 siRNA Sequences

All siRNAs were ordered from Dharmacon and have the ON-target plus modification

Gene	Sequence	Catalogue number
Control-1	UGGUUUACAUGUCGACUAA	D-001810-01-05
Control-2	UGGUUUACAUGUUGUGUGA	D-001810-02-05
TP53-2	GUGCAGCUGUGGGUUGAUU	J-003329-15
CDKN1A	AGACCAGCAUGACAGAUUU	J-003471-12

Table 2.4 Q-PCR primer sequences

Gene	Forward sequence	Reverse sequence
TP53	TGACTGTACCACCATCCACTA	AAACACGCACCTCAAAGC
CDKN1A	CCATGTGGACCTGTCACTGT	GGCGTTTGGAGTGGTAGAAA
CCND1	TGTTTGTTCTCCTCCGCTC	GAGGAGCTGCTGCAAATGG
GAPDH	CTTCAACAGCGACACCCACT	GTGGTCCAGGGGTCTTACTC
ACTB	TGGATCAGCAAGCAGGAGTATG	GCATTTGCGGTGGACGAT

2.2 Methods

2.2.1 Cell culture

HCT-116 cells were obtained from the European Collection of Animal Cell Cultures (ECACC) by Cancer Research UK (CRUK). RPE-Fucci cells were kindly provided by Dr Laurent Sansregret (CRUK). These cell lines, as well as their diploid and tetraploid derivatives, were grown in Dulbecco's Modified Eagle Medium (DMEM) with 4.5g/L D-glucose, 1mM L-glutamine and 1mM sodium pyruvate (Gibco, Life Technologies), containing 10% foetal bovine serum (FBS) (LabTech) and 1X penicillin/streptomycin (Sigma-Aldrich) at 37°C in a 5% CO_2 atmosphere.

2.2.1.1 Clonogenic assays

Clonogenic assay were performed as described (Franken et al., 2006). Cells were seeded, after seeding density optimisation, at low densities in 6-well tissue culture plates or 100mm culture dishes (BD Biosciences). Cells were incubated for 16 hours to allow for cell attachment, before addition of test compounds. Cells were allowed to form colonies for a minimum of 10 days. Plates were washed with PBS, before staining with crystal violet (0.05% w/v) and methanol (20% v/v) for 30 minutes. Plates were then washed with 20% methanol and colonies were counted by image capture before calculating the surviving fraction with the Mathematica® software. For RPE clonogenic assays, cells were seeded at low density after the cell sorting process (section 2.2.17).

2.2.2 Short-term viability assay

Short-term 72 hours proliferation assays were performed using CellTitre-Blue®, according to manufacturer's instructions (Promega). Briefly, cells were seeded into 96-well tissue culture plates and incubated for 16 hours. Drug treatments were performed in a dose curve and incubated with cells for 72 hours. 20µl of Cell TitreBlue® was mixed with 100µl media and incubated for one hour, before fluorescence was measured in a Perkin Elmer Envision 2102 multi-label reader (Ex550/Em590). All fluorescence values were normalized to DMSO control.

2.2.3 Epigenetic screen

Two diploid and two tetraploid cell line pairs were screened using the Selleckchem epigenetics compound library, comprising of 51 epigenetic modulators. Cells were plated into 96-well culture plates before 16 hours incubation to allow cell attachment. The library was used on each clone, in triplicate, at 5μM for 72 hours. Sensitivity was assessed by the CellTitre-Blue® assay (see section 2.2.2). Response data was estimated as the value of each replicate divided by the mean of the control wells for each cell line. Diploid and tetraploid cell lines were compared using a Wilcoxon test, a non-parametric statistical test that does not assume normality and is used to compare two sets of scores that come from the same participants.

2.2.4 siRNA transfections

The final concentration of siRNA used for all experiments was 40nM. For a single 6-well tissue culture plate transfection, 3μl of 20μM siRNA was mixed with 197μl of Opti-MEM (Gibco) in a 1.5ml microtube. At the same time, 4μl of transfection reagent (RNAiMax Thermo Fisher) was incubated with 196μl Opti-MEM for five minutes. After this period, both solutions were mixed and incubated for a further 30 minutes at room temperature. During this time, cells were plated at density of $1.1x10^6$ cells in 1,100μl of DMEM media. 400μl transfection was then added dropwise to each well.

For 96-well plates, 10μl of 400μM siRNA diluted in DMEM was added to each well. RNAiMax was diluted to concentration of 0.15μl/10μl of Opti-MEM and 10μl of mix was added per well and incubated for 30 minutes at room temperature. Cells were seeded at a density of 5,000/80μl to each well, to achieve a final volume of 100μl.

2.2.5 Western blotting

Cells were grown until 60-80% confluent, before being washed in PBS and trypsinised (Trypsin-EDTA 0.25%, phenol red; GIBCO). Trypsin was inactivated with FCS-containing media before cells were pelleted by centrifugation at 1,000rpm for five minutes. Cells were washed with PBS and pelleted before being resuspended in cell lysis buffer (Abcam ab152163; constituents: 0.216% Beta glycerophosphate, 0.19% sodium orthovanadate, 0.001% leupeptin, 0.38% EGTA, 10% Triton-X-100, 3.15% Tris-HCl, 8.8% sodium chloride, 0.29% sodium EDTA, 1.12% sodium pyrophosphate decahydrate). Lysates were quantified for protein content by Bradford assay (Bradford, 1976). Equal amounts of protein were mixed with loading buffer (BioRad) and loaded into 10 or 15-well NuPAGE® Novex® 4-12% Bis-Tris Gels (Invitrogen NP0321BOX), before subjected to electrophoresis at 200V for 45 minutes with MOPS running buffer (Invitrogen). Gels were transferred to poly-vinylidene (PVDF; GE Healthcare) membranes before semi-dry transfer in 20% methanol-containing transfer buffer (Invitrogen) at 125mA for one hour. Membranes were blocked in blocking buffer consisting of 5% non-fat milk TBS-T (Tris-Buffered-Saline-Tween: 50mM Tris-Cl, pH 7.5. 150mM NaCl, 0.1% tween). Membranes were incubated with primary antibodies for 16 hours at 4^{o}C in 5% BSA (bovine serum albumin) in TBS-T. Membranes were washed three times in TBS-T before incubation with the appropriate HRP-conjugated secondary antibody (Dako) for one hour in blocking buffer at room temperature. Membranes were washed a further three times in TBS-T before detection with Immobilon Chemiluminescent HRP substrate (Merck Millipore).

2.2.6 Indirect immunofluorescence

Cells were grown on 22/22mm glass coverslips pre-treated with poly-lysine to enhance cell attachment. After the desired incubation time, cells were washed with PBS before fixing and permeabilisation using PTMEF (4% formaldehyde, 20mM PIPES, 10mM EGTA, 1mM $MgCl_2$) for 10 minutes. Coverslips were then PBS-washed before blocking in 3% BSA in PBS at room temperature for one hour. Next, coverslips were incubated with 150µl of primary antibody optimally diluted in blocking buffer for 1.5 hours at room temperature. Coverslips were then washed

three times before addition of 150µl of secondary antibodies (goat anti-rabbit AF594, Molecular Probes) diluted at 1/500 in blocking buffer, protected from light for one hour. Finally, coverslips were washed three times and mounted on glass slides with Vectashield mounting medium (Vecta H-1000) and sealed with clear nail varnish. Images were acquired on an Olympus Delta Vision RT microscope (Applied Precision) equipped with a CoolSnap HQ camera. Images were deconvolved using conservative settings for 8 cycles. Images were analysed using softWoRX Explorer (Applied Precision LLC).

2.2.7 Quantitative PCR

RNA was extracted from cells using the RNeasy Qiagen kit, according to the manufacturer's instructions. RNA concentrations were quantified on a NanoDrop instrument (Thermo Scientfic) and adjusted to 10ng/µl before cDNA synthesis using the first-strand cDNA synthesis kit (GE healthcare), according to the manufacturer's instructions. Real-time quantitative polymerase chain reaction (qPCR) primers were designed using Primer-BLAST (Ye et al., 2012). Multiple qPCR primers were ordered for genes of interest and primers that produced a single product in the melt curve were deemed acceptable for use. QPCR was performed using SYBR® GreenER with premixed ROX (Invitrogen) according to the ΔΔCT method, namely, values were firstly normalised to GAPDH or β-actin, before secondary normalisation to parental HCT-116 values. Three replicates were performed per clone on an Applied Biosystems 7900 real time PCR machine using 96-well plates.

2.2.8 Protein Immunoprecipitation

Cell pellets were lysed on ice in KLB lysis buffer (50mM Tris pH 7.4, 150mM NaCl, 0.1% Triton X-100, 0.1% Nonidet P-40, 4mM EDTA, 50mM sodium fluoride, 0.1mM sodium orthovanadate, 1mM dithiothreitol. Lysates were centrifuged at 13,000rpm for 15 minutes at 4^{o}C before quantitation by Bradford assay. Sample concentrations were adjusted so all samples were of equal concentrations in 250µl of lysis buffer and 30µl were removed for inputs. 1µg of primary antibody was

added before incubation at 4^{o}C for 16 hours, with rotation. 30µl of protein G beads (Sigma-Aldrich) were added and incubated at 4^{o}C for one hour, with rotation. Protein G beads were washed three times in lysis buffer before dissociation with sample buffer. Equal volumes were subjected to western blotting to identify protein interactions.

2.2.9 *In vitro* kinase assays

Any procedures that involved handling of ^{32}P were carried out by Dr Emanuela Maria Cuomo (UCL). Endogenous CDK4 and CDK2 were immunoprecipitated, as described in section 2.2.8. No EDTA was present in buffers as the compound is a magnesium chelator and can inhibit the reaction. After incubation of protein G beads in antibody-bound lysates, samples were washed three times in KLB lysis buffer. After washing, beads were re-suspended in kinase buffer before incubation with ^{32}P labelled ATP and full length GST-RB, which served as the substrate for the kinase activity, for 30 minutes. After this time, the reaction was terminated by addition of 4x Laemmli buffer (BioRad) before separation by SDS-PAGE and radiography.

2.2.10 Apoptosis array

The apoptosis array was carried out according to the manufacturer's instructions. The array is a Reverse Phase Protein Array (RPPA), consisting of a nitrocellulose membrane spotted with antibodies against 35 human apoptosis markers. Cells were lysed and incubated before expression was detected by chemiluminescence. After quantification by densitometry the fold change between conditions was calculated.

2.2.11 Cycloheximide assay

2x10^{5} diploid and 1.7x10^{5} tetraploid cells were seeded into 6-well tissue culture dishes and incubated for 16 hours. Media was removed before addition of fresh media containing 50µg/ml cycloheximide for the desired time-course. After the indicated time of incubation, media was aspirated before immediate lysis in KLB

lysis buffer at 4°C. Lysates were analysed by western blotting. Cyclin D1 stability was calculated by normalising cyclin D1 protein levels to GADPH loading control. Normalised values were then expressed as a percentage of untreated control.

2.2.12 ERK assay

$2x10^5$ diploid and $1.7x10^5$ tetraploid cells were seeded into 6-well tissue culture dishes and incubated for 16 hours. Media was removed before addition of fresh media containing no serum for 24 hours. Serum-free media was removed before addition of fresh media containing 10% serum and was incubated for the desired length of time. Finally, media was aspirated before immediate lysis in KLB lysis buffer, at 4°C.

2.2.13 Nocodazole trap assay

Cells were seeded into 10cm dishes and treated with nocodazole (1μM), for 16 hours. After this period, cells were harvested and washed with PBS before fixing with 70% ethanol and stored at 4°C for 24 hours. Fixed cells were then prepared for DNA profile analysis.

2.2.14 Flow cytometry

2.2.14.1 DNA profiles

Cells were trypsinised and washed with PBS before fixing with 70% ethanol and stored at 4°C for 24 hours. Cells were washed before staining with propidium iodide (Sigma-Aldrich) and RNA digestion with RNase (Life Technologies). DNA profiles were obtained after setting laser voltages for untreated diploid HCT-116 cells.

2.2.14.2 Antibody-based FACS

Cycling cells were trypsinised, washed and pelleted before fixation with 2% formaldehyde and incubated at 4°C. Cells were washed twice in 0.1% BSA before

blocking in the same solution for one hour at room temperature. After this time, cells were washed with blocking buffer and 0.5% Triton X-100 (Sigma-Aldrich) to permeabilise the cell nuclei, before a final wash in blocking buffer. At this time, cell pellets were divided into fresh tubes. One set was stored at 4^{o}C whereas the other set, 100µl of blocking buffer containing primary antibody at the appropriate concentration was then incubated at 4^{o}C for 16 hours. Next, pellets were washed twice in blocking buffer. Both sets of pellets (untreated and primary antibody treated) were then resuspended in 100µl of buffer containing DAPI (1µg/ml) and the corresponding fluorescent secondary antibody (1/500) and incubation for one hour at room temperature protected from light. This procedure results in primary, secondary and DAPI versus secondary and DAPI treated replicates. After this period, stained cell pellets were washed twice before resuspension in PBS. Samples were analysed on a Fortessa flow cytometer (BD Biosciences), before analysis with FlowJo software.

2.2.15 Subcellular fractionation

Cells were grown into 10cm tissue culture dishes until 70-80% confluent, before being washed in PBS and pelleted by centrifugation at 1,000rpm for five minutes and transferred to 1.5ml microtubes. Pellets were then lysed in buffer A (10mM HEPES pH 7.9, 10mM KCL, 0.1mM EDTA, 0.1mM EGTA, 1mM dithiothreitol [DTT]) supplemented with protease and phosphatase inhibitors on ice for 15 minutes. After this time, Tergitol-type NP-40 (NP-40) was added to the solution to achieve a final concentration of 0.6%. Lysates were centrifuged at 1,000rpm for five minutes, before the cytoplasmic supernatant was removed and stored in fresh microtubes on ice. The remaining pellet was then resuspended in buffer C (20mM HEPES pH 7.9, 400mM NaCl, 0.1mM EDTA, 0.1mM EGTA, 1mM DTT) supplemented with protease and phosphatase inhibitors (1 tablet per 10ml; Roche Complete Protease inhibitors and Roche PhosStop), before shaking at 1,100rpm (4^{o}C) for 15 minutes. After this time, the nuclear supernatant was removed and stored in fresh microtubes.

2.2.16 Viral CCND1 overexpression in HCT-116 and RPE-Fucci

Any procedures that involved handling of virus were performed by Sally Dewhurst (CRUK), who prepared the CCND1 and control lentivirus. 293FT cells were cultured in standard DMEM supplemented with 1mM sodium pyruvate. Cells were plated at a density of $6x10^6$ and cultured for a further 16 hours in antibiotic-free media. The transfection mix (10µg CCND1 DEST vector, 7µg psPAX2 [packaging vector], 3 µg pMD.2G (envelope vector), 0.5ml Opti-MEM + lipofectamine 2000) was then added to the cells and media was replenished after 24 hours. Another 24-28 hours later, viral supernatants were harvested before filtering through a 0.45µm HV filter (Millipore). For infection, 2ml of fresh media containing 8µg/ml polybrene (infection reagent) was added to cells cultured in a 6-well tissue culture plate. Next, 50-200µl of viral supernatant was added to each well and incubated for 3 days, before puromycin selection.

2.2.17 Cytokinesis failure - DCB assay

On day 0, RPE-Fucci, RRE-Fucci Control and RPE-Fucci CCND1 cells were seeded into separate 15cm tissue cultures dishes. After 24 hours, cells were treated with dihydrocytochalasin-B (DCB, Sigma-Aldrich) for 16 hours. After this period, cells were washed for five minutes, five times, before trypsinisation and DNA staining with 10µg/ml Hoescht for one hour at 37^oC. Samples were then washed in PBS before aliquoted into sorting tubes after being strained to ensure single-cell suspensions. Samples were sorted using an Influx BD cell sorter (BD Biosciences). The Fucci markers were excited were excited at 561 (emission 610/20 mCherry), 488 (emission 530/40 Venus) and 405 (Hoescht emission 460/50). $mCherry^{+ve}/Venus^{-ve}$ G1 tetraploid cells were sorted and kept on ice before washing, counting and seeding at a density of 4,000 cells/well. The 96-well plates were pre-loaded with siRNA and transfection reagent for desired gene silencing (method described in section 2.2.4). For clonogenic assays, cells were seeded at low density in 6-well plates (method described in section 2.2.1.1). After incubation for the desired timeframe, the 96-well assays were treated with S-Trityl-L cysteine (STLC) for 12 hours. STLC inhibits Eg5 and arrests cells in prophase (Skoufias et al., 2006). In this assay, to determine if cells have progressed though

the G1/S boundary and overcome arrest, cells in G2/M are scored as proliferating. In the absence of STLC, cycling cells will be in G2/M, but some may also have progressed through the cycle, back to G1, and would not be counted as proliferating competent. Therefore, pre-treatment with STLC before analysis will arrest all cycling cells in M-phase and allow more reliable detection of proliferating cells. After 72 hours (total for the whole assay), plates were fixed with 4% paraformaldehyde (PFA) and stored at 4^{o}C, until required. Next, plates were washed with PBS and stained with DAPI (1µg/ml) and permeabilised with 0.5% Triton X-100 for five minutes at room temperature. Plates were imaged using the Cellomics Arrayscan Vti machine with a 10x numerical aperture objective. The percentage of G2/M cells was calculated using the Target Activation Cellomics Bioapplication (TACB) and was then compared to RPE-Fucci and relative fold-change values were calculated.

2.2.18 Microarray profiling

RNA was extracted using the RNeasy extraction kit following the manufacturer's instructions, before RNA quality testing by Qubit (Life technologies). Purified RNA was sent to the Cancer Research UK Manchester institute for analysis using Affymetrix Human Gene 1.0 ST arrays. Probir Chakravarty, Dr Tejal Joshi, Dr Nicolai Birkbak and Nicholas McGranahan performed the data analysis.

Data was normalised using the frozen Robust Microarray (fRMA) method (McCall et al., 2010), summarising probes sets at gene level. Genes that showed differential expression between diploids and tetraploids were identified using the Student's t-test with a significance threshold of $p<0.05$. Significant genes were further filtered by selecting those that showed a ≥ 2-fold change.

2.2.19 SILAC

SILAC was performed in collaboration with the CRICK proteomic facility with Dr Bram Snijders and Dr Vesela Encheva. The facility staff performed proline incorporation checks and subsequent methods.

2.2.19.1 SILAC isotopes

Unlabelled, hydrochloride forms of L-arginine and L-lysine (R0K0) obtained from Sigma-Aldrich (light isotopes). Hydrochloride forms of L-arginine [13C6, 15N4] and L-lysine [13C6, 15N2] (R10K8) were obtained from CK Isotopes (Heavy isotopes).

2.2.19.2 Labelling of cells

DC14 and TC13 (passage five and 42) were cultured in DMEM supplemented with light or heavy isotopes. Each clone at both early and late passages was cultured in 'heavy' or 'light' media, as replicate experiments that could be inversely correlated after analysis. DMEM media supplemented with 150mg/L L-Proline (Sigma-Aldrich). Cells were passaged for a minimum of eight population doublings in T175 tissue cultures flasks. After this time, cells were trypsinised and counted. $3x10^6$ cells were aliquoted into 1.5ml microtubes, before lysis with 300µl 8M urea/Tris pH 8.5 on ice. Samples were then sonicated for 10 seconds and cooled on ice, before mixing at a 1:1 ratio. Next lysates were quantified by Bradford assay before separation by SDS-PAGE. Gels were stained with EZ blue (Sigma), before de-staining and storage in water.

2.2.19.3 In-gel digestion (for protein quantitation)

Polyacrylamide gel slices were prepared for mass spectrometric analysis using the Janus liquid handling system (Perkin-Elmer). Briefly, the excised protein gel pieces were placed in individual wells of 96-well microtiter plates and destained with 50% acetonitrile, 50mM ammonium bicarbonate, reduced with 10mM DTT, and alkylated with 55mM iodoacetamide (all reagents from Sigma-Aldrich). After alkylation, the proteins were digested with 6ng/µl trypsin overnight at 37°C. The resulting peptides were extracted in 2% formic acid, 1% acetonitrile.

2.2.19.4 In-solution digestion (for phosphoproteomics)

Cells were lysed in 9M urea, 20mM HEPES, pH 7.8, supplemented with 100 units/ml of benzonase and sonicated to reduce viscosity (3mm probe, 50%

amplitude, three 15 second bursts, on ice). Between 4-5mg of protein per sample were used as estimated by Bradford protein assay. Lysates were reduced with 10mM DTT for 30 minutes at room temperature, followed by alkylation with 20mM iodoacetamide (Sigma-Aldrich) for 30 minutes at room temperature in the dark. Lysates were digested initially with LysC (Promega) for 2 hours at 37^{o}C. The lysates were then diluted with 100mM ammonium bicarbonate, 5% acetonitrile to a final urea concentration of less than 2M. The samples were digested 1:100 enzyme to protein ratio (w/w) with trypsin (Promega) overnight at 37^{o}C. The next day, two additional aliquots of trypsin were added and incubated at 37^{o}C four hours each. After the digestion, the samples were acidified with TFA (Thermo Fisher Scientific) to final concentration of 1% (v/v). All insoluble material was removed by centrifugation and the supernatant was desalted with Sep-Pak C18 cartridges (Waters) and lyophilized for 2 days.

2.2.19.5 SCX fractionation of phosphopeptides

Peptides were resuspended in 90µl of 10mM ammonium formate pH 2.9 and 25% acetonitrile, sonicated and all insoluble material was removed by centrifugation. Separation was performed using Agilent 1200 (Agilent) HPLC at a flow rate of 1ml/min. The peptides were loaded on 20cm Polysulfoethyl-Asp SCX column (4.6mm inner diameter, 5µm particle size, PolyLC). Solvent A was 10mM ammonium formate pH=2.9, 25% acetonitrile, and the solvent B was 500mM ammonium formate pH=6.8, 25% acetonitrile. The samples were run on a linear gradient 0-80% B in 10 minutes. The total run time including column conditioning was 30 minutes. A total of six fractions were collected every two minutes between 1-13 minutes after injection (one fraction=2ml). The collected fractions were vacuum dried and used for phosphopeptide enrichment.

2.2.19.6 TiO2 enrichment of phosphopeptides

Dried fractions were solubilised in 1ml of loading buffer (80% acetonitrile, 5% TFA, 1M glycolic acid), sonicated and mixed with 5mg of TiO2 beads (Titansphere, 5µm GL Sciences Japan). Samples were incubated for 10 minutes with agitation

followed by a one minute 2,000 × g spin to pellet the beads. The supernatant was removed and the beads were washed with 150µl of loading buffer. This was followed by two wash steps, first with 150µl 80% acetonitrile, 1% TFA and second with identical volume of 10% acetonitrile, 0.2% TFA. After each wash beads were pelleted by centrifugation (one minute at 2,000 × g) and the supernatant discarded. The remaining solution and beads were dried in a vacuum centrifuge for 30 minutes followed by two elution steps at high pH. For the first elution step, the beads were mixed with 100µl of 1% ammonium hydroxide (v/v), incubated for 10 minutes with agitation and pelleted at 2,000 × g for one minute. For the second elution step the beads were mixed with 100µl of 5% ammonium hydroxide (v/v), incubated for 10 minutes with agitation and pelleted at 2,000 × g for one minute. The two elutions were combined, vacuum dried and desalted using C18 Stage Tips (Rappsilber et al., 2007). Briefly, each Stage Tip was packed with one C18 Empore™ high performance extraction disk and conditioned with 100µl of 100% methanol, followed by 200µl of 1% TFA. The sample was loaded on the conditioned Stage Tip, washed six times with 200µl of 1% TFA and eluted with 50µl of 80% acetonitrile, 5% TFA. The desalted peptides were vacuum dried in preparation for LC-MS/MS analysis.

2.2.19.7 LC-MS/MS

For MS analysis, peptides were resuspended in 0.1 %TFA and loaded on 50-cm Easy Spray PepMap column (75µm inner diameter, 2µm particle size, Thermo Fisher Scientific) equipped with an integrated electrospray emitter. Reverse phase chromatography was performed using the RSLC nano U3000 (Thermo Fisher Scientific) with a binary buffer system at a flow rate of 250nl/min. Solvent A was 0.1% formic acid, 5% DMSO, and solvent B was 80% acetonitrile, 0.1% formic acid, 5% DMSO. The diGly enriched samples and the in-gel digested samples (RNA polymerase IP, CSB IP and chromatin proteome) were run on a linear gradient of solvent B (2- 40%) in 150 minutes, total run time of 180 minutes including column conditioning. The phospho-enriched samples were run on a linear gradient of 2-35% B in 150 minutes, total run time of 186 minutes. The nanoLC was coupled to a

Q Exactive mass spectrometer using an EasySpray nano source (Thermo Fisher Scientific).

The Q Exactive was operated in data-dependent mode acquiring HCD MS/MS scans (R=17,500) after an MS1 scan (R=70,000) on the ten most abundant ions using MS1 target of 1×10^6 ions, and MS2 target of 5×10^4 ions. The maximum ion injection time utilized for MS2 scans was 120 milliseconds, the HCD normalized collision energy was set at 28, the dynamic exclusion was set at 10 seconds, and the peptide match and isotope exclusion functions were enabled.

The phospho-enriched samples were also analysed using a LTQ Orbitrap Velos (Thermo Fisher Scientific), where the HPLC conditions were as described above. CID and Multi Stage Activation (MSA) fragmentation were used in separate runs to increase the total number of identified phosphopeptides. The LTQ Orbitrap Velos was operated in data-dependent mode acquiring 10 CID or MSA MS2 scans (R=17,500) after an MS1 scan (R=60, 000). MS1 target was set at 1×10^6 ions, and MS2 target at 3×10^4 ions. The CID normalized collision energy was set at 35 with 10 millisecond activation time and a maximum ion injection time for MS2 scans at 50 milliseconds. The dynamic exclusion was set at 20 seconds and singly charged peptides and peptides with unassigned charge states were excluded from fragmentation.

2.2.19.8 Quantification of incorporation and L-arginine ->L-proline conversion

The percentage of incorporation of the heavy (R10K8) amino acids was assessed after the cells have doubled six times in the heavy medium. The cells were lysed and separated on SDS-PAGE and analysed by LC-MS/MS, as described previously. The data was searched using MaxQuant/Andromeda, but an additional label for heavy L-proline was established to assess the percentage of conversion of heavy L-arginine to heavy L-proline. Ratios of MaxQuant-derived intensities for peptides containing R10K8 versus R0K0 peptides were used to determine the percentage of incorporation (R10K8/ R0K0). The same strategy was used to calculate the level of L-arginine->L-proline conversion (R10K8P6/R10K8P0).

2.2.19.9 Data processing and analysis

Raw data files were analysed with MaxQuant software (version 1.3.0.5), as described previously (Cox et al., 2009). Parent ion and tandem mass spectra were searched against UniprotKB Homo sapiens database (August 2012). A list of 247 common laboratory contaminants provided by MaxQuant was also added to the database. For the search, the enzyme specificity was set to 'trypsin' with maximum of two missed cleavages. The precursor mass tolerance was set to 20 parts per million (ppm) for the first search (used for mass re-calibration) and to 6ppm for the main search. Carbamidomethylation of cysteines was specified as fixed modification, oxidized methionine and N-terminal protein acetylation were searched as variable modifications. Phosphorylated serine, threonine and tyrosine were added to the list of variable modifications when samples enriched for phosphorylated peptides were searched. The datasets were filtered on posterior error probability to achieve 1% false discovery rate on protein, peptide and site level.

2.2.20 Bioinformatics

Dr. Nicolai Birkbak performed all bioinformatics analyses.

2.2.20.1 Copy number analysis

Raw TCGA SNP data for testicular germ cell tumours (TGCT) and matched normal samples was downloaded from the TCGA on 2015-08-04, and processed, as described (Birkbak et al., 2012). Briefly, Affymetrix SNP data was pre-processed using the CRMAv2, CalMaTe and TumorBoost algorithms within the AROMA framework (Bengtsson et al., 2009, Bengtsson et al., 2010, Ortiz-Estevez et al., 2012). Allele-specific copy number was determined using ASCAT v2.3 (Van Loo et al., 2010).

2.2.20.2 Expression analysis

Pre-processed RNA-seq data, normalized using the RSEM method and summarized to gene level, was downloaded from the TCGA. RNA-seq data was log2 transformed, and expression levels of *CCND1*, *CCND2*, *CCND3* and *CDKN1A* was compared using Pearson's correlation.

2.2.20.3 Genome-doubling algorithm

A modification of the genome-doubling algorithm used by Carter *et al* was used to assess the likelihood of genome doubling in the TCGA TGCT samples (Carter et al., 2012). A *P*-value threshold of 0.001 was used for samples with ploidy ≤3, but for samples with a ploidy of 4, $P \leq 0.05$ was used, and all samples where ploidy exceeded 5 were classified as genome doubled.

Briefly, the rationale behind the analysis was based on the notion that if genome-doubling occurs then homologous chromosomes must have two copies across the genome. If subsequent loss of genetic material occurs from one chromosome then the copy number will be odd (i.e. one), this being the minor allele. The copy number of the other allele (major) will still be even (i.e. two). Therefore, if the majority of the major allele is even, this implies the tumour would have undergone a genome-doubling event as all chromosomes would have doubled at the same time. This is in contrast to tumours that may have increased their ploidy by specific gains of chromosomes. In this context, the major allele will not necessarily be even across the majority of the genome, as the major allele will be odd (one) and only fraction (the minor) even. Using this principle the algorithm calculated the probability of genome-doubling from TCGA SNP comparative genome hybridisation CGH data.

2.2.20.4 Whole exome sequencing DNA sample preparation

DNA extraction was carried out using the Qiagen DNeasy Blood and Tissue extraction kit, following the manufacturer's instructions. DNA quality was assessed using a QuBit instrument (Life Technologies). DNA preparation and sequencing was carried out by the Advanced Sequencing Facility at Cancer Research UK

London Research Institute. Paired-end sequencing was carried out as described (Gerlinger et al., 2012). Briefly, DNA was fragmented into 250-300bp (base pairs) fragments, before adaptors were ligated to each end. Adaptor-ligated templates were purified with Agencourt AMPure SPRI beads (Beckman Coulter), and amplified by ligation mediated PCR. DNA was then hybridised to SureSelect Biotinylated RNA library (BAITS) and bound to streptavidin beads. Each sample was loaded into an Illumina Genome Analyser II, and paired-end sequencing was performed to at least 30X coverage. Raw image files were processed with HCS1.4.8 software using default parameters to call bases.

2.2.20.5 WES alignment and variant calling analysis

Alignment and variant calling was carried out by Harshil Patel (Bioinformatics and Biostatistics, London Research Institute). Raw reads were aligned to the human hg19 genome assembly using BWA 0.5.9 (Li and Durbin, 2009), with a maximum mismatch threshold of 4 within 101bp; all other parameters were left as default. Alignments were post-processed to remove reads that mapped to multiple genomic loci and those that could have arisen from PCR duplication (using Picard tools 1.81, (Picard). The Genome Analysis ToolKit (version 2.3-9-ge5ebf34, (DePristo et al., 2011) was used to perform indel realignment and indel left alignment. After filtering, a median exome coverage of 76X was observed per sample. Base-level nucleotide counts were obtained using the deepSNV package (Gerstung et al., 2012), with a minimum base quality threshold of 20, and subsequent variant calling was performed across all samples simultaneously using scripts written in Python. Variants with a minimum nucleotide count of 5 and an allele frequency less than 0.1 were excluded from further analysis. Variant annotation was performed with ANNOVAR release 2012Oct23 (Wang et al., 2010).

2.2.20.6 WES downstream filtering

All variant calls in all samples were filtered as follows: The number of times a variant appeared in diploid and tetraploid samples was added as a filter. Mutations occurring in any diploid sample were removed. Unique tetraploid mutations were

then filtered for the number of samples they occurred in. Different amino acid substitutions in the same gene, occurring in the same tetraploid sample, were not counted as two different samples. The predicted consequence of each mutation was assessed using the tools SIFT-predictor, PolyPhen-predictor and Mutation-taster contained in the ANNOVAR variant calling package (Wang et al., 2010).

2.3 Statistics

Western blotting densitometry was quantified using ImageJ software. For grouped diploid versus tetraploid comparisons mean values were compared and tested for significance using the unpaired student's t-test in Prism software, unless otherwise stated in the text.

Chapter 3. Investigating the molecular basis of tetraploidy tolerance

3.1 Introduction

Cell cycle checkpoints maintain the integrity of the diploid genome and protect against the oncogenic effects of CIN and aneuploidy (Davoli and de Lange, 2011a). Classic examples of these pathways are the SAC and DNA damage checkpoints.

The SAC senses unattached chromosomes in anaphase, resulting in APC/C inhibition and mitotic arrest until all chromosomes have been properly attached. Loss of SAC can result in segregation errors and an unbalanced genome (Musacchio and Salmon, 2007). DNA damage checkpoints act as safeguards against damaged DNA progressing through the S and M phases of the cycle, to ensure errors are not duplicated and that proper segregation is achieved (Davoli and de Lange, 2011a). Progression past these checkpoints can result in CIN, cytokinesis failure and tetraploidy (Hayashi and Karlseder, 2013).

The tetraploidy checkpoint has been proposed as the 'last resort' checkpoint and is deigned to clear polyploid cells, contributing to the maintenance of the diploid genome. Studies have shown newly formed tetraploid cells to undergo a p53-dependent G1 arrest and termed this phenotype the 'tetraploidy checkpoint' (Andreassen et al., 2001a, Andreassen et al., 2001b). The stimulus for p53 activation is not fully understood but, despite conflicting studies, it is generally accepted that tetraploid cells are susceptible to p53-dependent arrest, although the response is not likely to directly sense the polyploid genome (Ganem and Pellman, 2007, Uetake and Sluder, 2004). Combined with studies showing correlation between tetraploid tumour cells and p53 mutations, a strong case for the role of p53 in the regulation of polyploid cell survival is emerging (Ramel et al., 1995, Galipeau et al., 1996). This chapter is aimed at understanding the status and dynamics of p53, as well as drug resistance, in the isogenic HCT-116 diploid/tetraploid system (Figure 3.1).

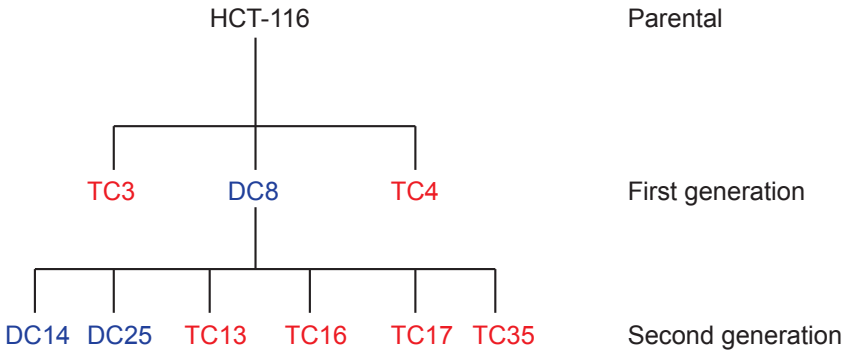

Figure 3.1 Tetraploid isogenic system

To generate the isogenic tetraploid system, parental HCT-116 cells were stained with DAPI and analysed by flow cytometry. Cells were selected based on ploidy status (2N or 8N), before being subjected to cell sorting and single-cell cloning. This produced diploid clone (DC) DC8 and tetraploid clones (TC) TC3 and TC4. The same procedure was performed on DC8 after 37 weeks (p37) to produce a second generation of clones. This is an important step, as it shows that tetraploid cells can spontaneously arise from a single diploid precursor *in vitro* within the 37-week time frame.

3.2 p53/p21 response in tetraploids

TP53 mutations have been shown to correlate with polyploidy in murine and human tumours and a likely reason for this observation is its integral role in the tetraploidy checkpoint (Galipeau et al., 1996, Ramel et al., 1995, Aylon and Oren, 2011). Mutations in *TP53* are likely to allow newly formed tetraploid cells to bypass the G1 checkpoint, permitting proliferation and survival and, therefore resulting in CIN and aneuploidy (Andreassen et al., 2001b, Dewhurst et al., 2014). Previous work on the *TP53* and *CDKN1A* status of the tetraploid clones revealed no coding mutations, suggesting that the tetraploid clones overcome the tetraploidy checkpoint in a p53-independent manner (Dewhurst et al., 2014). To investigate the status of the p53 and p21 pathway, multiple components of this pathway were investigated by mutational analysis, functional assays of the p53 response and cell cycle analysis.

3.2.1 Mutational analysis by WES

Whole exome sequencing (WES) was performed on all diploid and tetraploid clones at early (p5) and late (p50) passages (Figure 3.2A). Whole genome sequencing (WGS) was not employed in this study, as the primary aim was to identify coding DNA alterations that disrupt protein function. Early and late passage clones were analysed to investigate if specific mutations were selected over time. WES revealed no mutations were shared exclusively in the tetraploid clones, compared to the diploids, suggesting that tolerance to tetraploidy, in this system, is not provided by a single ubiquitous somatic event. Hierarchical clustering was performed to analyse the profile of non-synonymous mutations in the diploid and tetraploid clones (Figure 3.2A). The analysis showed diploid and tetraploid clones did not cluster, implying that the two ploidy states cannot be separated based on their mutational profiles. The clones also failed to cluster specifically in relation to passage number.

Exome sequencing confirmed previous findings, showing no mutations in *TP53* or *CDKN1A*. The sequencing data also demonstrated the absence of *RB1* mutations; another gene commonly mutated in tetraploid cells, as it renders the G1 checkpoint inactive and permits the survival of tetraploid cells (Davoli and de Lange, 2011a). In

addition, a further 15 genes known to be associated with the G1/S checkpoint were specifically analysed (Figure 3.2B). Only *MYC* and *PCNA* mutations were exclusively present in the tetraploid clones, although *MYC* was only mutated in TC16 (p5 and p50), with *PCNA* only mutated in late passage TC35 cells (p50). This mutational pattern implies lack of mutations converging on different parts of the tetraploidy checkpoint.

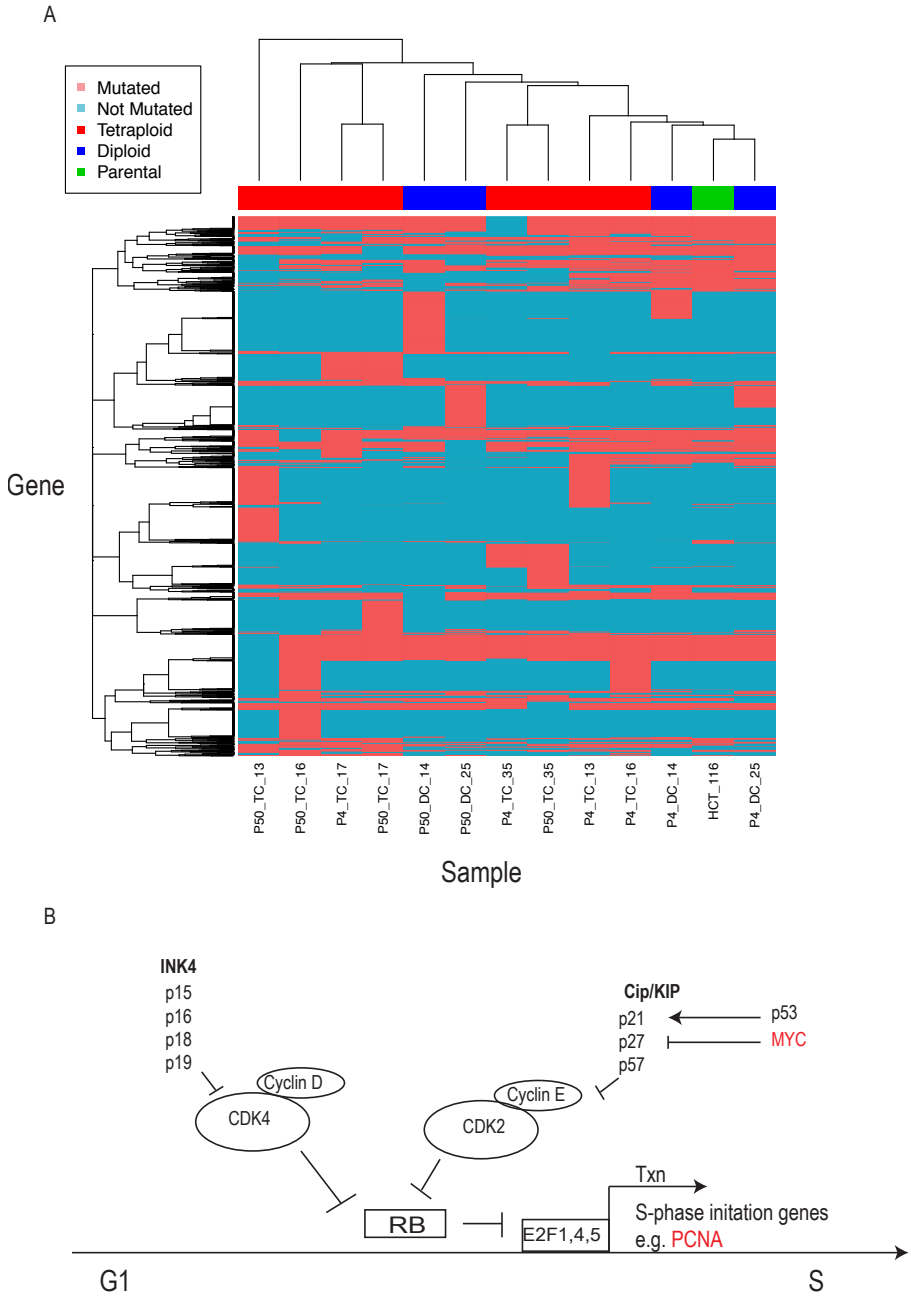

Figure 3.2 Mutational analysis by WES

Intronic and synonymous mutations were removed from the total number of mutations, resulting in 4,138 non-synonymous SNVs. These mutations were observed in 3,287 genes. Mutated genes present in HCT-116 parental cells alone or present in all clones were removed, leaving 2,360 genes. Genes were subjected to hierarchical clustering, with genes on the Y-axis and samples on the X-axis. (B) G1/S pathway. Gene products in black were not mutated in the diploid and tetraploid clones. Gene products in red were mutated specifically in the tetraploid clones (not all tetraploid clones).

3.2.2 DDR in tetraploids

Even though *TP53* and *CDKN1A* were not mutated, the axis could still be repressed by genetic, epigenetic, transcriptomic or post-translational abnormalities in other components of the pathway and provide tolerance to the tetraploid phenotype.

To test whether the p53 and p21 pathways were fully functional in our tetraploid clones, cells were treated with 5-FU, a member of the fluoropyrimidine family of compounds. Fluoropyrimidine were first developed in the 1950's, based on the observation that rat hepatomas metabolised uracil more readily than normal tissue, indicating that enhanced pyrimidine synthesis may be semi-selective target for cancer therapy (Longley et al., 2003a). 5-FU is a common anti-cancer agent used in treatment of breast, head and neck and CRC (Longley et al., 2003a). Specifically, 5-FU is an analogue of uracil with a fluorine atom substitute in place of hydrogen at the C-5 position (Figure 3.3A). In the clinical setting, response rates to single-agent therapy with 5-FU in advanced CRC are approximately 10-15%, however this can be improved to 40-50% if combined with oxaliplatin or irinotecan (Longley et al., 2003b). There are three major mechanisms of action of 5-FU, all of which cause severe cellular toxicity, which is induced at lower doses in cancer cells in comparison to normal cells due to the former's greater requirement for RNA synthesis, DNA synthesis and DNA repair (Longley et al., 2003a). In practice, this confers a degree of cancer cytotoxic selectivity.

3.2.2.1 5-FU treatment induces tetraploid p53 and p21

The DNA and RNA damage caused by 5-FU activates p53 and p21, causing arrest and apoptosis (Longley et al., 2003a). 5-FU treatment for sixteen hours, before harvesting and analysis by western blot, induced p21, p53 and p53 Ser-15 phosphorylation. Induction of p53 protein levels and phosphorylation, as well as the up-regulation of p53 target genes are indicative of a fully functional transcriptional response (Figure 3.3B). Untreated tetraploid p53 and p21 levels were generally elevated in the tetraploid clones. This observation suggests that the tetraploid cells have constitutively high levels of p53 and p21, perhaps indicating a persistent level of cellular stress. The lack of p53-Ser15 phosphorylation under non-treated conditions, despite corresponding elevated total protein levels, suggests the mechanism of increased p53 up-regulation is not due to the DNA damage response. Tetraploid clones TC16, TC17 and TC35 displayed reduced p53-Ser15 phosphorylation, which may indicate a dampened DDR and resistance to 5-FU exposure.

3.2.2.2 Tetraploid clones show enhanced resistance to 5-FU

Previous research has suggested that tetraploid cells are more resistant to cytotoxic chemotherapeutics and IR (Castedo et al., 2006a, Castedo et al., 2006b, Sharma et al., 2013, Balsas et al., 2012). To investigate whether our tetraploid clones displayed drug resistance, cells were treated with a range of 5-FU doses for 72 hours, before viability was quantified. A three-day proliferation assay showed that diploids and tetraploids were generally equally sensitive to short-term 5-FU exposure, further validating an active DDR (Figure 3.3C). To investigate if there was a difference in cytotoxic drug sensitivity over a prolonged period of time, diploid and tetraploid clones (early and late passages) were exposed to 5-FU for 12-16 days.

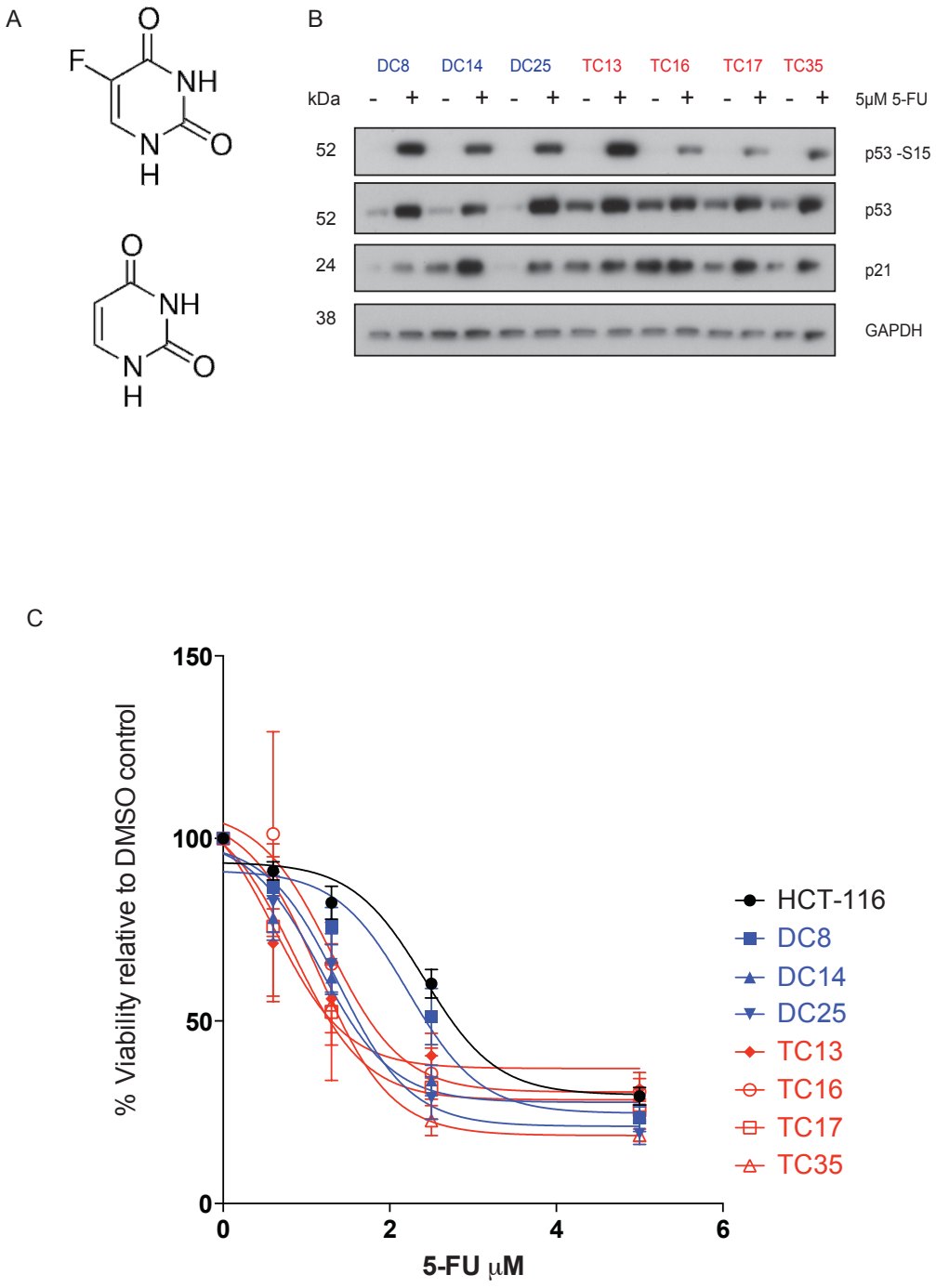

Figure 3.3 Response to drug treatments

(A) Chemical structure of 5-FU (B) Western blot analysis shows activation of the p53/p21 pathway after 5-FU treatment. Cells were treated with 5μM 5-FU for 16 hours. (C) Clones were treated with a range of 5-FU doses (0-10μM) for 72 hours before being assessed for cell viability. Error bars represent standard deviations of 3 replicates.

Firstly, early passage clones (p14-16) were tested over a dose range, revealing a difference in sensitivity at the 5μM dose. After quantification and normalisation of colonies, it was clear that the tetraploids were more resistant than diploid clones (Figure 3.4A & Figure 3.5A). TC13 was the most resistant, with a surviving fraction of 37%, while the other tetraploid clones ranged from 1.9%-9.6%. In contrast, DC14 and DC25 showed no colony formation and the surviving fraction of DC8 was only 0.6%. These data suggest even at an early passage (p10-14), the tetraploid clones are more resistant to 5-FU.

The tetraploid clones can tolerate chromosomal segregation errors and, as a result, become genetically diverse over time (Dewhurst et al., 2014). This event recapitulates the genetic complexity observed in CRC tumours, which may result in drug resistance. To test if late passage clones were more drug resistant than early clones, possibly as a result of CIN tolerance, late passage diploid and tetraploid clone were exposed to 5μM 5-FU for 16 days and allowed to form colonies. The control colonies were slightly too large and in some cases single colonies could not be accurately counted, however the overexposure allows the easy visualisation of 5-FU resistant tetraploid clones (Figure 3.4B). In order to increase the accuracy of colony counting, cells were seeded at lower densities of 150 and 200 cells per well and incubated for 12 days and these conditions produced smaller colonies that could be reliably counted (Appendix).

Quantification showed that, in general, the late passage tetraploids were more resistant to 5-FU treatment. Three tetraploid clones (TC13, TC17 and TC35) were extensively more resistant to 5-FU than diploids, however TC16 was more sensitive than DC14 and DC25 but similar to DC8 (Figure 3.5B). All diploid and tetraploid clones showed a greater level of resistance in the late passage experiment. A possible explanation for this observation could be that HCT-116 cells are microsatellite unstable (MIN), thus the cumulative acquisition of mutations in the diploid clones could explain the elevated resistance in the late clones. These data suggest that tetraploid cells are intrinsically more resistant to 5-FU and the effect seen in the late passage clones could be the combined effect of MIN and the inherent resistance.

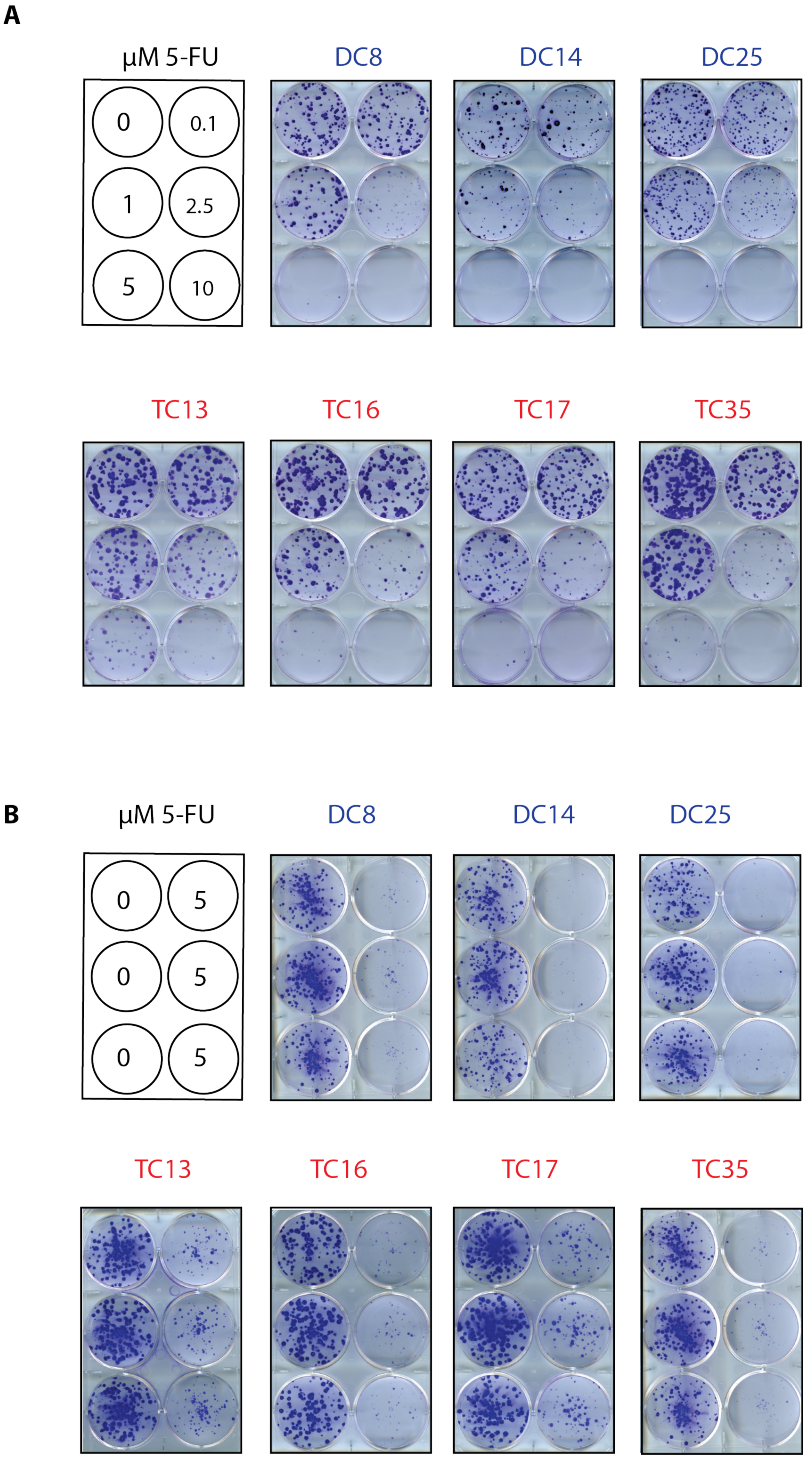

Figure 3.4 Long term 5-FU treatment of early and late passage clones

(A) Clones were seeded at 250 cells per well and incubated for 14 days with the indicated concentration of 5-FU. Colonies were stained with crystal violet, before counting and quantification. (B) Clones were seeded at 300 cells/well and incubated for 16 days with the indicated concentration of 5-FU. Colonies were stained with crystal violet and before counting and quantification.

Oxaliplatin is commonly used in combination with 5-FU and can increase response rates. Oxaliplatin is a derivative of cisplatin and has a similar mechanism of action (Graham et al., 2004). After IV administration of oxaliplatin, the drug is activated by displacement of oxalate ligand giving rise to OH- groups that can form adducts with DNA and create intra- and interstrand cross-links. These cross-links interfere with DNA replication and transcriptional machinery, resulting in cell death by apoptosis. To test if the tetraploid clones were resistant to oxaliplatin, late passage diploids were treated with the drug in a ten-day clonogenic assay at doses ranging from 5-0.3μM (Figure 3.5C). Treatment of diploids and tetraploids with oxaliplatin revealed no differential sensitivity at any dose.

In summary, although short term proliferation assays in this CRC cell line model did not exhibit a difference in sensitivity to 5-FU, longer term clonogenic assays revealed elevated resistance to 5-FU in early and late tetraploid clones, suggesting that tetraploidy in CRC might contribute to clinical drug resistance and therapy failure, or perhaps select for tetraploid, genome-doubled recurrences. The finding that tetraploids and diploids are equally sensitive to oxaliplatin may explain why combination of 5-FU and oxaliplatin is more effective in the clinical setting and implies that single-agent oxaliplatin therapy might be more effective at clearing resistant tetraploid clones.

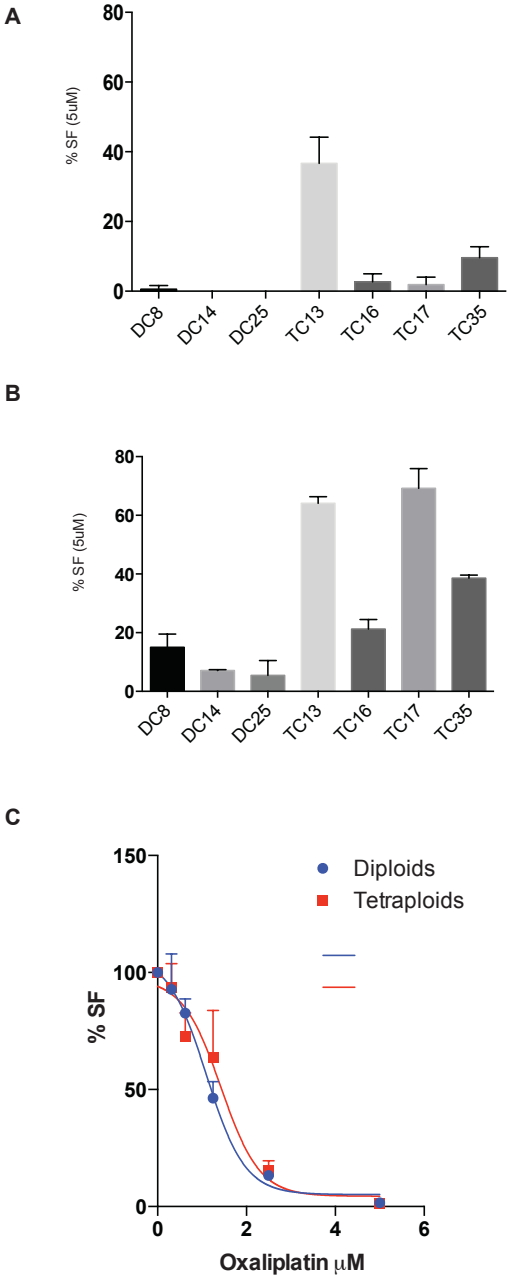

Figure 3.5 Quantification of clonogenic assays

(A) Early passage; three replicates from one experiment. Error bars represent standard deviation (SD) of three replicates (B) Late passage; colonies from three replicates were counted and the surviving fraction (SF) was calculated (SF = treated colonies/cells seeded x plating efficiency [PE]). Quantification was performed by automated Wolfram Mathematica software. Error bars represent SD. (C) Diploid clones (DC8, DC14 and DC25) and tetraploid clones (TC13, TC16, TC17 and TC35) were treated with oxaliplatin in a clonogenic assay for 10 days. Diploid and tetraploid clones were grouped. Results from three independent experiments are shown. Error bars represent SD.

3.2.3 p53 response to segregation errors

The observed elevated basal p53 and p21 levels in (Figure 3.3B) are not likely to be a result of the DDR, as no p53-Ser15 phosphorylation was observed, suggesting other routes of p53 activation could be contributing to increase protein levels. Previous work has shown that the tetraploid clones make twice as many segregation errors relative to the diploids (a function of genome-doubling) and are more resistant to cell cycle arrest and death (Dewhurst et al., 2014). As no mutations were found in p53, it was hypothesised that the increased segregation error rate may contribute to elevated p53 and p21 and resistance to apoptosis is provided downstream of p53.

3.2.3.1 Reversine induced segregation errors elevate tetraploid p53 and p21

To test whether p53 and p21 could be induced by segregation errors in the isogenic system, the MPS1 kinase inhibitor, reversine, was used to inhibit the SAC and promote whole chromosome mis-segregation (Figure 3.6A) (Lan and Cleveland, 2010). MPS1 is required to recruit SAC proteins to unattached kinetochores and thus contributes to SAC activation and APC/C inhibition. Therefore the absence of MPS1 can result in chromatid segregation before microtubule attachment and cause lagging chromosomes. Indeed, loss of MPS1 has been shown to cause rapid aneuploidy and cell death (Janssen et al., 2009). Reversine is a potent inhibitor of MPS1 (IC_{50} 3nM) and, therefore, provides a useful chemical tool to pharmacologically induce segregation errors and investigate the p53 response to segregation errors and aneuploidy (Santaguida et al., 2010).

Reversine treatment induced p53 and p21 in the tetraploids and PARP cleavage in all clones (Figure 3.6B). Although there was clonal variation in p53 and p21 induction, there was no specific strong down-regulation of both tumour suppressors in the tetraploid clones (Figure 3.6B). In contrast, there was a consistent reduction of PARP cleavage exclusively in the tetraploid clones.

These results demonstrate that p53 and p21 can be induced by segregation errors in both the diploids and tetraploids, however PARP cleavage is suppressed,

suggesting reduced apoptosis only in the tetraploids after reversine treatment. These findings support the aforementioned hypothesis, suggesting that the doubling in segregation error rate might partly explain the elevated p53 and p21 protein levels in tetraploids and resistance to apoptosis might occur downstream of p53.

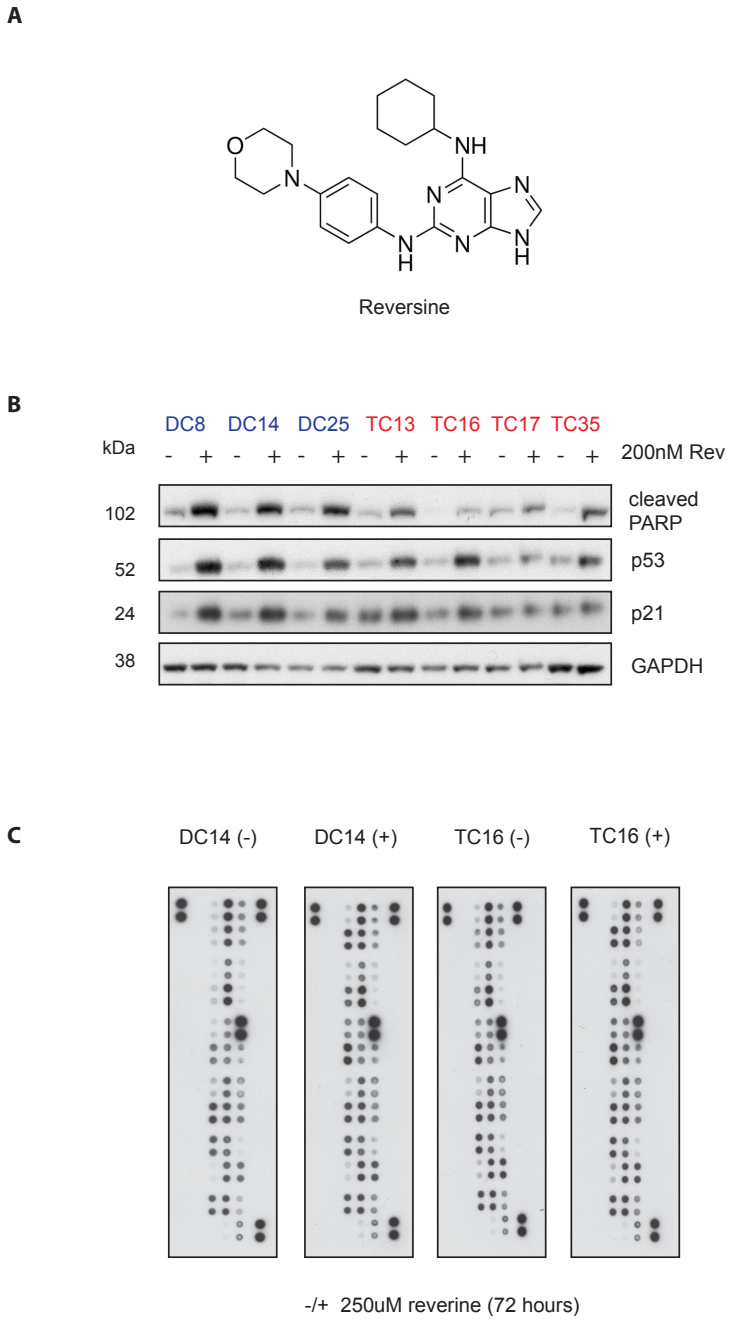

Figure 3.6 p53/p21 response to reversine and apoptosis array

(A) Reversine chemical structure. (B) Western blot analysis of p53/p21 response in all clones after 200nM reversine treatment for 72 hours. (C) Modified western blot analysis of apoptosis array. Cells were treated with 250nM for 72 hours. Dots represent a range of proteins involved in apoptosis (for protein names and quantification see Figure 3.7).

3.2.3.2 Reversine apoptosis array

The decrease in tetraploid PARP cleavage post-reversine treatment, despite the elevated p53 and p21 levels, suggests that the mechanisms that provide tolerance to segregation errors are located downstream of p53. It is possible that tetraploids exhibit reduced PARP cleavage because of overexpression of anti-apoptotic proteins or defects in the apoptotic pathway. To test this, an apoptosis array was performed on DC14 and TC16, as these clones showed a substantial difference in post-reversine PARP cleavage.

The array consists of a nitrocellulose membrane spotted with antibodies against 35 apoptosis human cell markers (Figure 3.6C). Cells were lysed and incubated, before expression was detected by chemiluminescence. After quantification by densitometry the fold change between conditions was calculated. The basal levels of p53, p27 and p21 were all greater in the tetraploid clones, consistent with earlier findings (Figure 3.3B & Figure 3.7A). However, the analysis revealed increases in multiple forms of phosphorylated p53, in contrast to previous results (Figure 3.3B). This is likely due to non-specific binding, possibly un-phosphorylated p53, as the increase was also seen in the reversine-treated samples and previous data in this chapter has shown the compound does not induce the DDR (p53-Ser15) (Figure 3.4A). However, in the cases of p53-Ser46 and p53-Ser392, basal activation cannot be ruled out. The analysis also revealed up-regulation of the anti-apoptotic proteins cLAP-1 and livin and also the tumour necrosis factor receptor (TNFR), however these ratios were likely artefacts of extremely low expression compromising reliable quantification (raw data in Appendix). Reversine treatment induced p21, p27, p53 and cleaved caspase-3 in DC14 (Figure 3.7B), however caspase cleavage was absent in TC16, supporting the hypothesis of a supressed apoptotic response in the tetraploids (Figure 3.7C). Induction of p53, p27 and p21 in TC16 was subtle and this probably reflects higher basal levels of these stress proteins. There was no reduction in expression of anti-apoptotic or overexpression of pro-apoptotic proteins in the tetraploid clones, implying that apoptotic resistance to segregation errors after p53 induction may be attributed to other mechanisms.

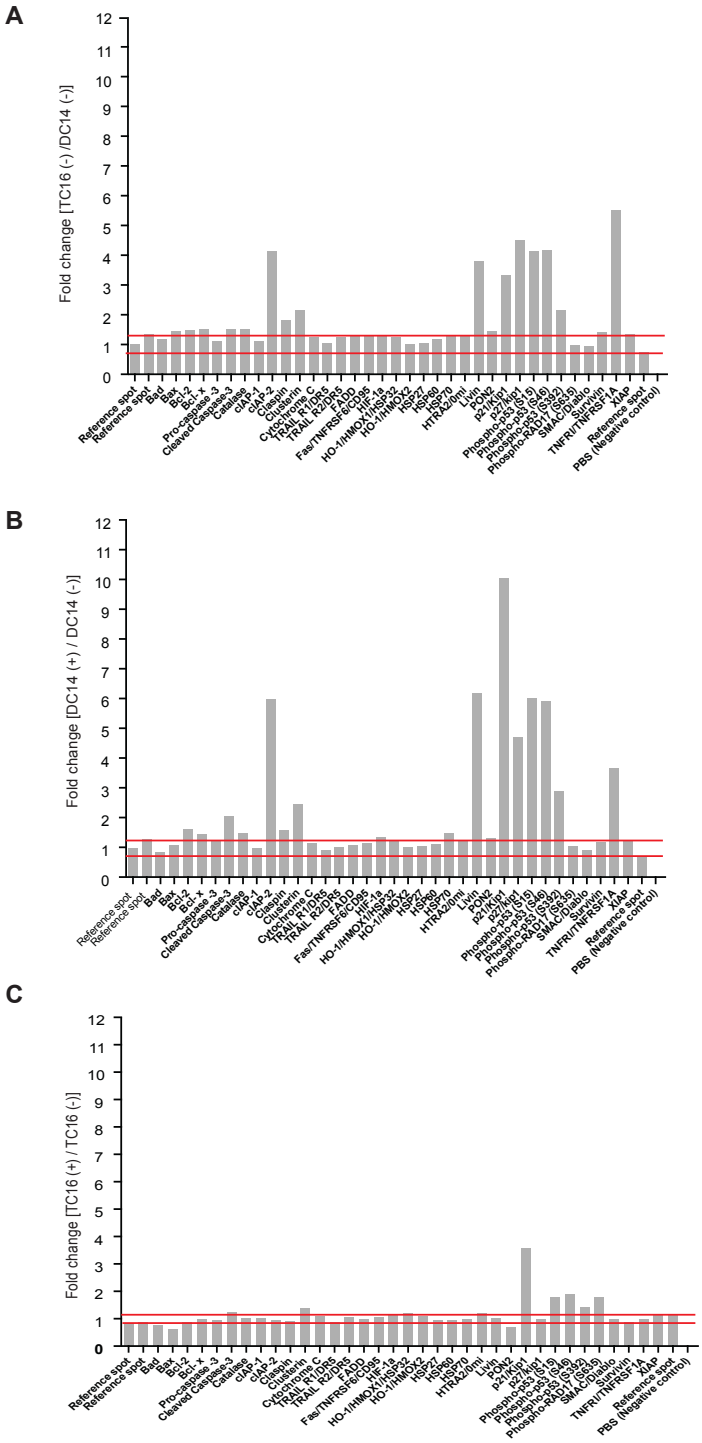

Figure 3.7 Quantification of apoptosis arrays

Duplicate apoptosis array protein spots were quantified by densitometry and ratios between samples were calculated. (A) Fold change in TC16 untreated apoptotic protein expression relative to DC14. (B) Fold change in DC14 apoptotic protein expression relative after reversine treatment relative to untreated. (C) Fold change in TC16 apoptotic protein expression relative after reversine treatment relative to untreated. Red lines indicate expression threshold based on control spot variance.

Taken together, these data suggest that the tetraploid clones have substantially higher basal p53 and p21 levels and importantly the pathway is active. The axis can be activated by DNA damage, although this route is unlikely to be contributing to the basal elevation, as no p53-Ser15 was observed. Reversine-induced p53 and p21 were apparent in the all clones, providing evidence that segregation errors can activate the pathway. These results suggest that the heightened rate of segregation errors in the untreated tetraploid clones, compared to the diploids, might contribute to the enhanced p53/p21 levels. The p53/p21 response could not induce PARP cleavage as effectively in the tetraploids, providing a potential mechanism that might explain the increased frequency of cell survival after an endogenous segregation error (Dewhurst et al., 2014). The apoptosis array demonstrated an induction of p53 and cell cycle inhibitor proteins and a reduced apoptotic response in the tetraploid clones, as represented by reduced PARP cleavage, although the mechanism contributing to decreased tetraploid apoptosis could not be determined in the assay.

Although, collectively, the data suggest that the tetraploid clones are tolerating segregation errors by a dampened apoptotic response, the cells still have enhanced levels of p21. Increased segregation errors and other tetraploidy associated cellular stressors are likely to be contributing to elevated p21. Heightened levels of p21, comparable to diploid levels after 5-FU and reversine treatment would be expected to cause cell cycle arrest (Kaeser et al., 2004). Therefore, it is tempting to speculate that the tetraploids may have developed a mechanism to cycle in the presence of elevated p21 which, combined with a decreased apoptotic response, produces a molecular network able to circumvent a hyper-activated p53/p21 axis.

3.3 Cell cycle characterisation of tetraploids

Although the tetraploid clones proliferate slightly slower (Dewhurst et al., 2014), how they cycle with an activated tetraploidy checkpoint is an important question and will give further clues on how they tolerate tetraploidy. As the tetraploidy checkpoint induces p21, the mechanism that allows continued proliferation in presence of the cell cycle inhibitor is likely to be the mechanism that permitted the initial override of the checkpoint. To confirm the tetraploids were cycling in the presence of high p21, RB phosphorylation status and cell cycle dynamics were assessed.

3.3.1 Basal p53 and p21 expression is elevated in the tetraploid clones

The basal levels of p53 and p21 were validated and quantified by western blotting (Figure 3.8A). The analysis confirmed a 2.3 ($p = \leq 0.01$) and 3.5 -fold ($p = \leq 0.001$) increase in the tetraploids compared to diploids in p53 and p21, respectively (Figure 3.8B and C). There is a relative p53 and p21 increase compared to GAPDH in the tetraploids, suggesting specific protein overexpression.

Of technical note, quantification of total tetraploid protein on a per cell basis by Bradford assay also showed a near doubling (1.98-fold; $p \leq 0.001$), compared to diploids (Appendix). All proteins in this study were analysed against proteins that show no relative difference between the diploid and tetraploid clones. Therefore, tetraploid loading controls take protein doubling into account and, therefore, any further increase relates to specific protein overexpression.

mRNA levels determined by quantitative PCR (Q-PCR) revealed no difference in TP53 levels between the diploid and tetraploid clones (Figure 3.8D and E). This finding is consistent with the post-translational regulation of p53 (Dai and Gu, 2010) and suggests up-regulation in the tetraploid clones is a result of protein stabilisation. In contrast, CDKN1A levels were generally elevated in the tetraploid clones (Figure 3.8F). When all the diploids were compared to the tetraploids, there was an average 1.7-fold increase in CDKN1A mRNA (Figure 3.8G). The *CDKN1A* gene is a transcriptional target of p53 (Mirza et al., 2003). To investigate the extent of p53-

mediated induction of p21, siRNA was used to silence p53, before analysis of p21 protein expression by western blot (Figure 3.8H). Loss of p53 completely abolished p21 expression in the tetraploids and diploids, suggesting that the elevated p21 levels observed were exclusively p53-driven. Taken together these data suggest in tetraploid clones p53 is stabilised resulting in increased p21 transcription and protein expression.

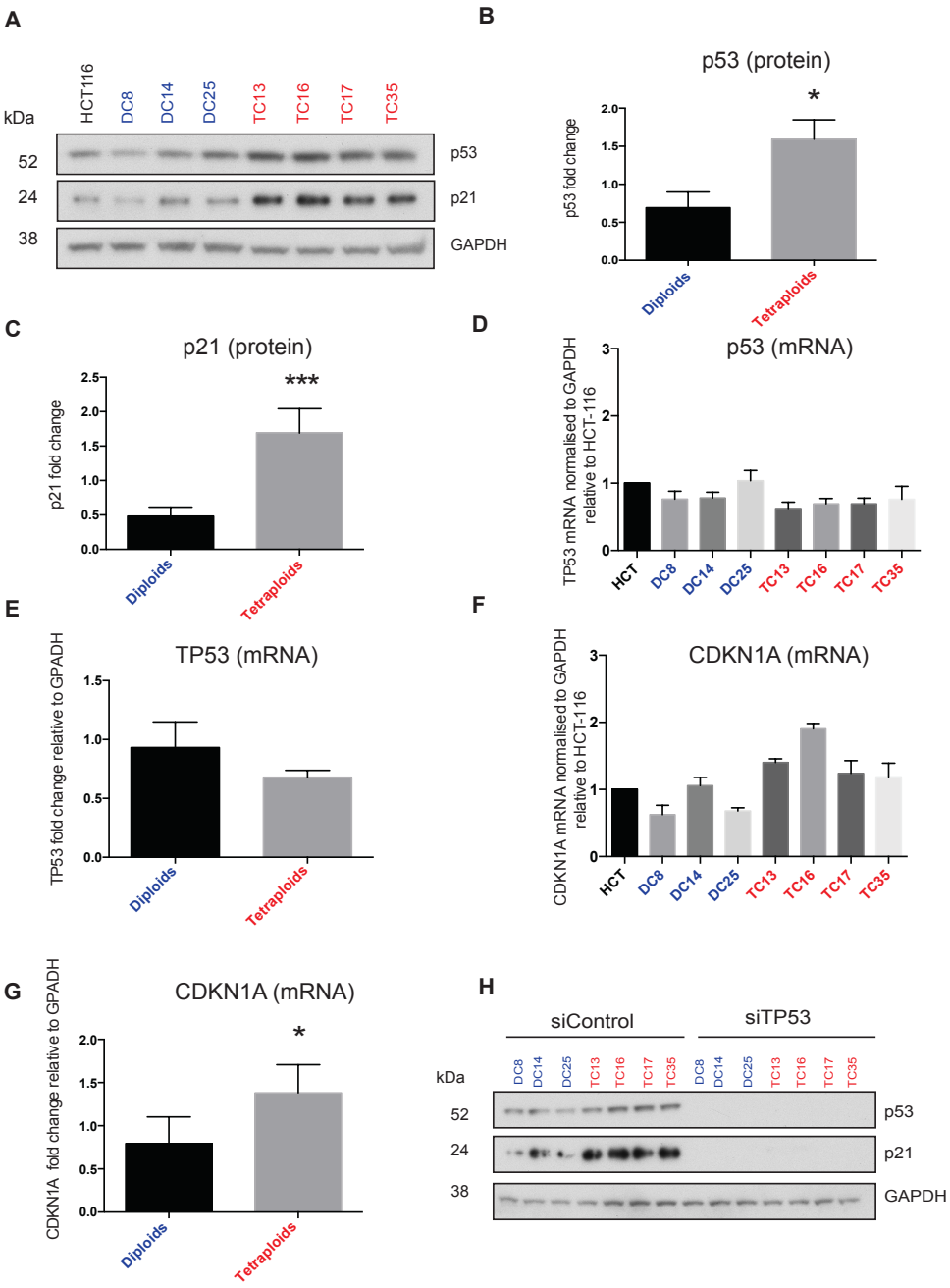

Figure 3.8 Validation and quantification of p53 and p21 protein and mRNA levels

(A) Basal p53 and p21 levels in diploid and tetraploid clones analysed by western blotting with densitometry quantification (B and C). Representative example of three independent experiments. (D) TP53 mRNA measured by Q-PCR. N=3 (E) Combined comparison of diploids and tetraploids. (F) CDKN1A mRNA measured by Q-PCR. N=3. (G) Combined comparison of diploids and tetraploids. (H) siRNA knockdown of p53 in all clones. Lysates were analysed by western blotting and probed for p53 and p21; GAPDH was used as a loading control. Error bars = SD. Unpaired student's-t-test * = ≤ 0.01 ** = ≤ 0.001.

3.3.2 Tetraploid p21 is elevated in both cytoplasmic and nuclear subcellular locations

Phosphorylation of p21 at Thr145 in the cytoplasm by AKT signalling results in p21 cytoplasmic sequestration and is considered oncogenic, as p21 can no longer inhibit CDK2. This event is also permissive for an anti-apoptotic function, by inhibiting cytoplasmic pro-apoptotic regulators (Abbas and Dutta, 2009).

To investigate if the elevated tetraploid p21 was being sequestered in the cytoplasm, cell fractionations were performed (Figure 3.9). Consistent with previous data, p21 was elevated in the tetraploid clones. However, there was no specific enrichment in the cytoplasm, demonstrating that p21 was not being sequestered in the cytoplasm and thus permitting CDK2 activity and cell cycle progression. Analysis of p53 revealed that the transcription factor was predominantly nuclear, in agreement with p21 gene induction. This result also suggests that apoptosis is not supressed by cytoplasmic sequestration of p53.

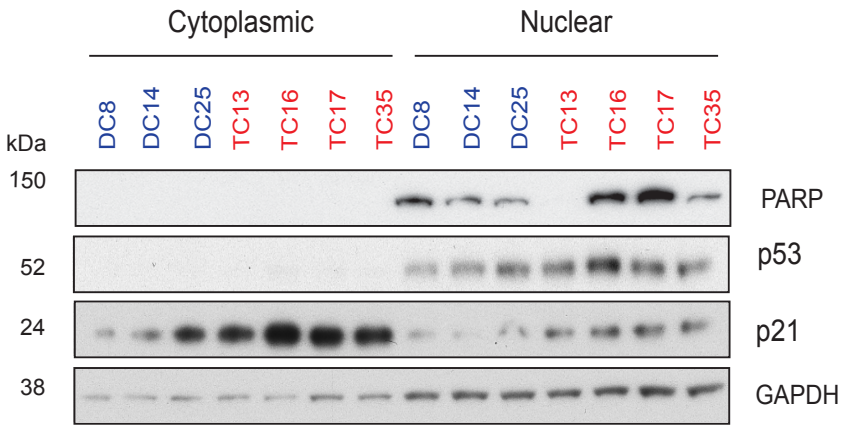

Figure 3.9 p21 and p53 subcellular localisation

Cycling cells were fractionated into nuclear and cytoplasmic fractions. This was achieved by different lysis buffers optimised to rupture cell or nuclear membranes specifically. Fractionated lysates were separated by SDS-PAGE before immuno-blotting. PARP was used as a purity control, GAPDH as a loading control. Representative example of three independent experiments.

3.3.3 Phospho-RB status is similar between diploid and tetraploid clones

To determine whether the tetraploid clones had a similar proliferation profile compared to the diploids and were cycling without arrest in the presence of high p21/p53, RB-pSer807/811 was analysed by western blotting (Figure 3.10). Phosphorylation of RB at pSer807/811 is considered a marker of progression from G1 to S phase of the cell cycle and cellular proliferation status (Elangovan et al., 2008). The amount of total RB protein was shown to be elevated in the tetraploid clones. However, when RB-pSer807/811 was normalised to the steady state levels of the protein, RB-pSer807/811 was in fact slightly reduced in the tetraploid cells, although this was not statistically significant and could be attributed to clonal variation (Figure 3.10C). These data suggest there is no major difference in RB-pSer807/811, indicating tetraploid clones are cycling in presence of elevated p21.

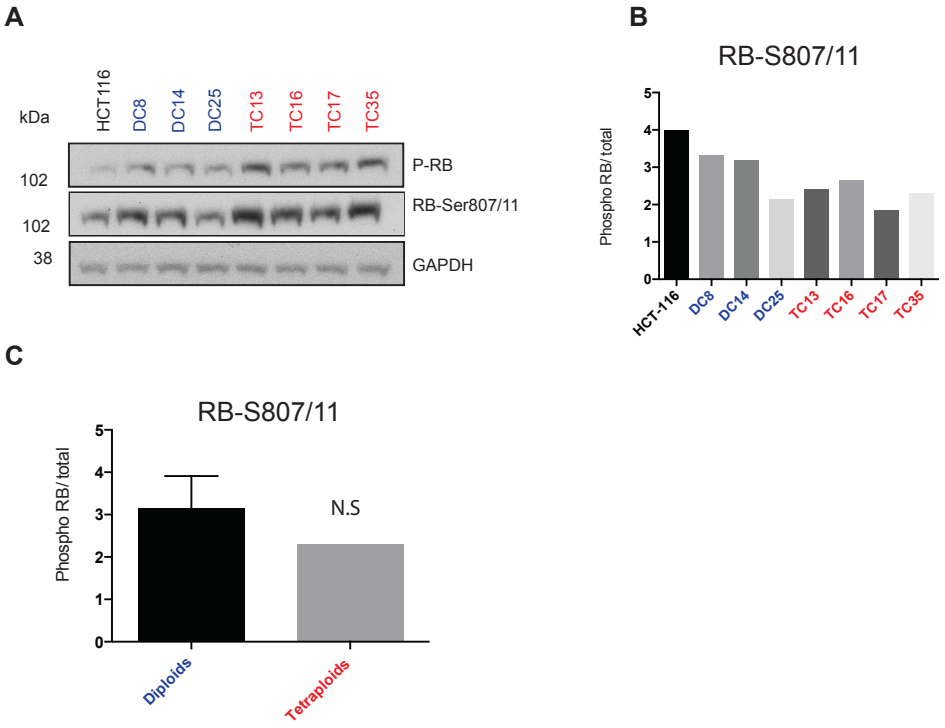

Figure 3.10 Phospho-RB status

(A) RB-Ser807/881 and steady state RB levels analysed by western blot; GAPDH was used as a loading control. (B) RB levels in individual clones and (C) Pooled clones were quantified by densitometry. Error bars represent SD. Representative example of two independent experiments.

3.3.4 Tetraploid clones do not display elevated G1 arrest despite raised p21 levels

In order to expand on previous findings and further investigate the cellular proliferation and absence of G1 arrest in a p53/p21-high background, a nocodazole trap assay was carried out (Figure 3.11). Nocodazole is a spindle poison that prevents microtubule polymerisation and spindle attachment resulting in SAC activation and mitotic arrest (Kallas et al., 2011, Matson and Stukenberg, 2011). Cells can be 'trapped' in mitosis by treatment with nocodazole for 16 hours, before analysis by flow cytometry, which should reveal a single G2/M peak. If a G1 arrest is occurring, the G2/M phase peak will decrease, as a fraction of cells will be represented in the arrested G1 peak. The diploid and tetraploid clones were subjected to the mitotic trap assay and only a minor G1 arrest was detectable (Figure 3.11A and B). There was no significant difference ($p= 0.0676$) between the average percentage of diploids remaining in G1 (2.6%) and tetraploids (3.4%) after treatment. These data provide additional evidence for tetraploid proliferation in the presence of elevated p21 and p53.

A

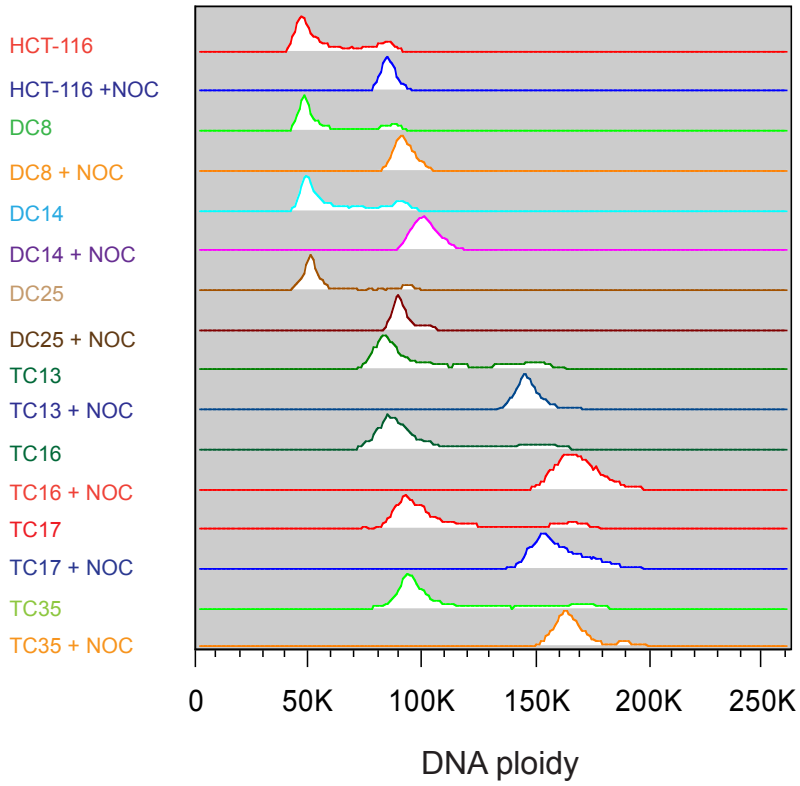

B

% G1 cells

Clone	Untreated	Nocodazole
HCT-116	65.5	2.62
DC 8	65.8	2.91
DC-14	58	2.44
DC-25	68.6	2.62
TC-13	63.1	3.69
TC-16	68.7	2.88
TC-17	60.3	4.39
TC-35	62.1	2.93

Figure 3.11 Analysis of G1 arrest

(A) DNA content profiles of the diploid and tetraploid clones after treatment with nocodazole for 16 hours before PI staining and analysis by flow cytometry. (B) Table showing percentage of cells in G1 -/+ nocodazole treatment. Representative example of two independent experiments.

3.4 Population based p21 expression analysis

The levels of p21 protein appear to be elevated in the tetraploid clones as confirmed by western blot (Figure 3.10A). However, this approach could not distinguish between all cells expressing equal levels of p21 or distinct subpopulations differentially expressing p21. In order to confirm this, as well as to investigate the distribution of p21 within the population and throughout the cell cycle, p21 immunodetection coupled with flow cytometry was performed. Representative examples of the analysis are displayed in Figure 3.12. Analysis of individual clones TC16, TC17 and TC35 showed consistently greater 'p21 high' populations, whereas TC13 displayed a p21-positive fraction similar to the diploid clones (Figure 3.13A). A grouped comparison revealed no significant difference (p= 0.0989) in the percentage of cells that express p21 between the diploid (48%) and tetraploid clones (60%) (Figure 3.13B). The relative intensity of p21 per cell was calculated by measuring the median p21 intensity value of all gated cells. The average fold change of p21 intensity was 2.3 times greater in the tetraploid cells (p= <0.0001) (Figure 3.13C, D). These data support the western blot analysis, confirming p21 up-regulation in the tetraploid clones. This implies that the same number of cells express p21 in diploid and tetraploid clones, but on average there was more protein per cell in tetraploids, as there is no clear indication of an 'extra high' p21 subpopulation.

DNA staining with DAPI was combined with p21 immunodetection, to allow determination of the distribution of p21 throughout the cell cycle. In order to analyse p21 in relation to cell cycle phase, the total percentages of all cell cycle phases were summed and defined as 100%. G1, S and G2/M fractions were then expressed relative to this total, ensuring a defined comparison of cell cycle phases. Cell cycle fractions were not expressed as percentages relative to the whole cell count, as a proportion of cells existed outside the gated areas, meaning the gated cells would not equal 100% and skew the analysis. There were fewer G1 p21-positive cells in the diploid clones compared to the tetraploids, although this was not statistically significant (p = 0.2815) (Figure 3.13E, F). This result may suggest that tetraploid clones cycle slightly slower through G1, however the nocodazole

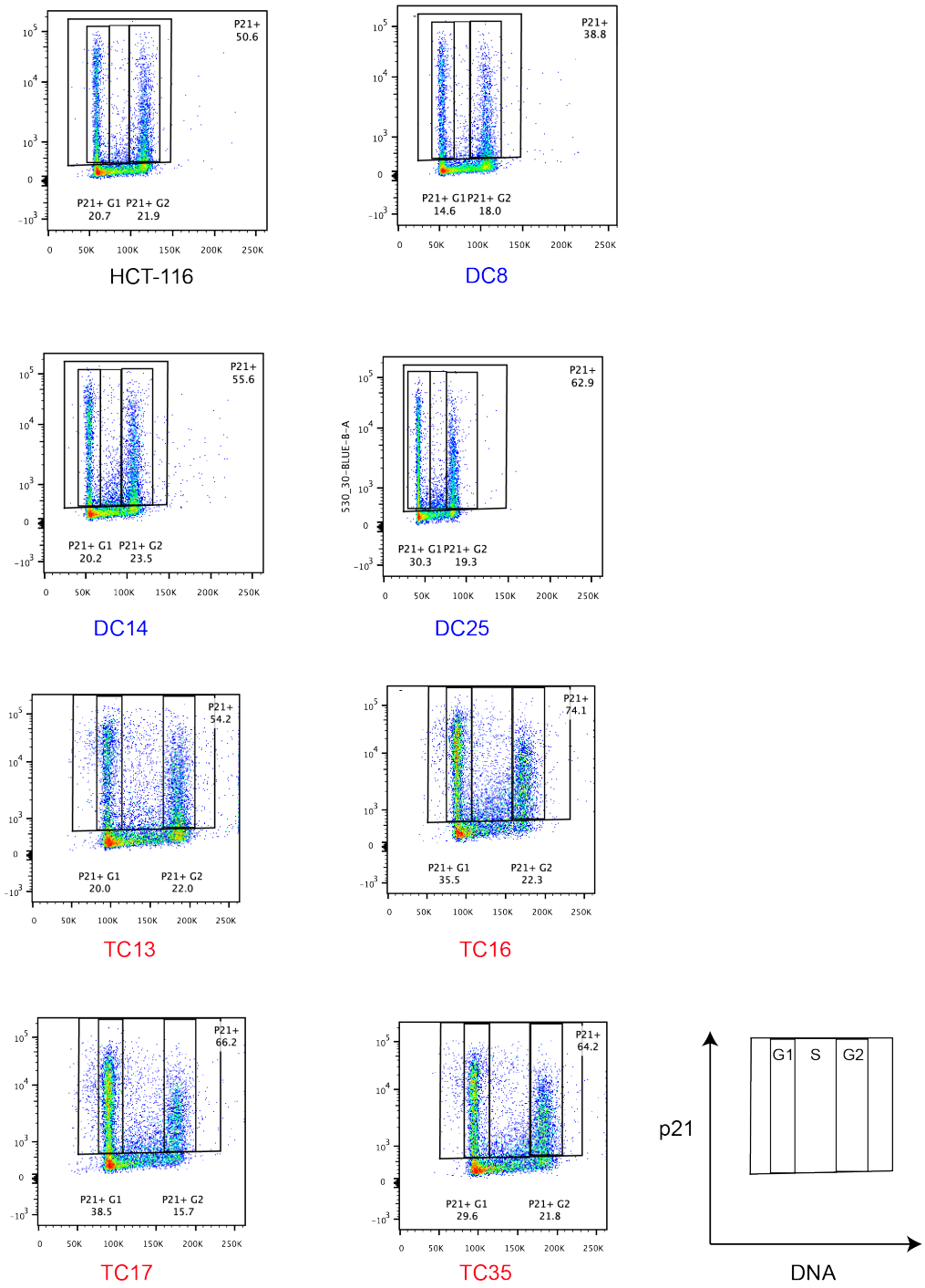

Figure 3.12 p21 expression analysis

p21 expression was investigated in the diploid and tetraploid clones. Cells were incubated with a p21 primary antibody followed by a FITC-conjugated anti-p21 secondary antibodies. Stained cells were subjected to flow cytometry and p21 intensity was quantified. Shown are the population density plots. The gated area represents p21-positive cells. The p21-positive threshold was set at intensities above the signal produced the secondary antibody alone. Representative example of two independent experiments.

trap experiment excludes a significant G1 arrest (Figure 3.11). Tetraploid cells expressed more p21 in the G1 phase of the cell cycle. The percentage of cells in S phase was significantly greater (1.8-fold, $p \leq 0.01$) in the tetraploid clones (7.5% and 13.7% for diploids and tetraploid respectively), possibly suggesting a longer synthesis phase (Figure 3.13 E and F). As a result of the elevated percentage of p21 positive tetraploids in G1 and S phase, the G2 fraction was significantly smaller ($p \leq 0.05$) in the tetraploids (30.2%) compared to the diploids (42.7%) (Figure 3.13, E and F). These data support a slower progression through the cell cycle in agreement with previous proliferation curves (Dewhurst et al., 2014).

The p21 median intensity was also calculated for each phase of the cell cycle. Interestingly, the tetraploid clones showed greater p21 intensity in all phases of the cell cycle (Figure 3.13G). The greatest difference was evident in G1, with tetraploid clones expressing 2.2 times more p21 ($p \leq 0.01$). Importantly, elevated p21 was also observed in the S and G2/M phases with a significant 1.8-fold change ($p \leq 0.01$ and ≤ 0.001 respectively) (Figure 3.13G). Collectively, these data support the previous finding of elevated p21 in the tetraploid clones and also implies they can progress from G1 through to G2/M despite increased p21.

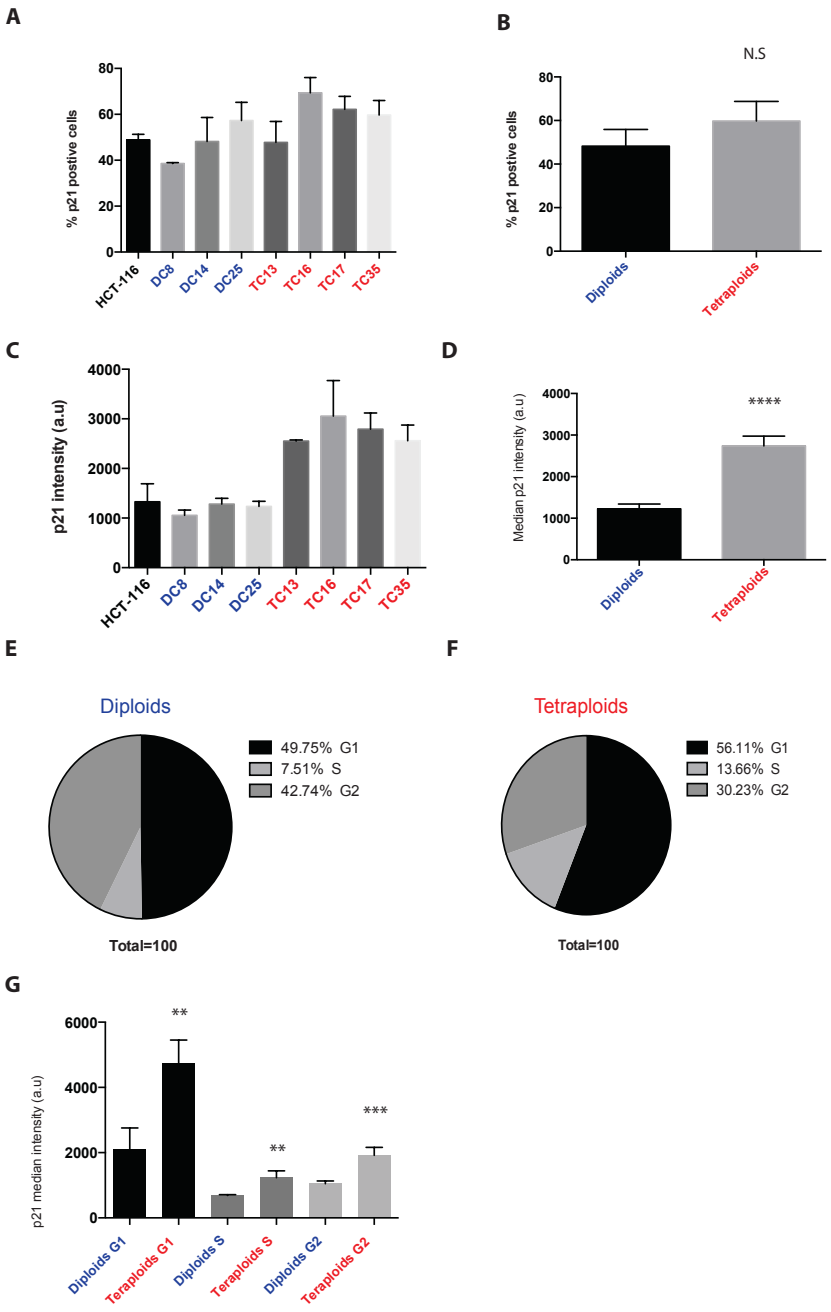

Figure 3.13 Cell cycle quantification of p21 flow cytometry analysis

(A) The percentage of p21-positive cells across all cell cycle phases. (B) Diploid and tetraploid group comparison of percentage of positive p21 cells. (C) Median intensity of p21-positive cells across all cell cycle phases. (D) Grouped median p21 intensity across all phases of the cell cycle. (E,F) Percentage of diploids and tetraploids in all phase of the cell cycle. (G) p21 median intensity in all phases of the cell cycle. Data displayed, N=2. Error bars indicate the SD of two independent experiments. Unpaired student's-t-tests * = p<0.05, ** p= <0.01 *** p=0 <.001 **** p= <0.0001, NS:non-significant.

3.5 Discussion and Conclusions

The primary aim of this chapter was to investigate the p53 and p21 status in the tetraploid clones, as they are both important components of the tetraploidy checkpoint. Drug treatments inducing DNA damage and segregation errors revealed the p53 and p21 axis to be active in the tetraploid clones. The basal levels of p53 and p21 in the tetraploid clones were substantially elevated, suggesting the tetraploid clones are cycling with high levels of both proteins that would normally induce cell cycle arrest and death in diploids. Therefore, these data provide evidence the tetraploid clones can activate the tetraploidy checkpoint response, as evidenced by the up-regulation of p21 expression, while a mechanism bypassing the inhibitory effects p53 and p21 must be in place to provide continuous and initial tetraploidy tolerance. In addition, the tetraploid clones were more resistant to 5-FU, a finding that may help explain drug resistance in the clinic.

The HCT-116 cell system was used, as it is chromosomally stable which allowed the effects of tetraploidy on CIN and aneuploidy to be studied. However, HCT-116 cells are MSI, which means there is a high mutational burden and clones can drift genetically by somatic mutation. This can cause issues when trying to understand molecular phenotypes as they may change simply as a function of genetic drift. The high mutational burden also challenges the initial identification of relevant mutations from NGS data.

Exome sequencing failed to identify common mutations present in the tetraploid clones including *TP53*, *CDKN1A* or *RB1*, suggesting a tolerance mechanism independent of inactivating mutations in G1/S control components. Activation of p53 and p21 could be achieved by DNA damage and segregation error induction and protein levels in tetraploid clones were high. This result supports the sequencing data, confirming the expression of a wild-type p53 and not an inactive mutant. As exogenously induced segregation errors by reversine could elevate p53 and p21 protein expression, the previously observed increased rate of endogenous segregation errors in the tetraploid clones (Dewhurst et al., 2014), might partly explain elevated levels of p21 and p53. This observation is in agreement with Thompson and Compton, who showed that induction of segregation errors in HCT-

116 cells induced a p53 response (Thompson and Compton, 2010b). Despite this experimental association, further work is required to conclusively show endogenous segregation errors are responsible for p53 induction. A possible strategy to address this question involves reducing the tetraploid segregation error rate, and investigating if p53 levels fall.

In addition, it is likely that other tetraploidy associated mechanisms are also contributing to elevated p53 and p21 levels. Ganem *et al* recently proposed that Hippo signalling was responsible for a graded p53 response after tetraploidization, where LATS2 activation inhibits MDM2, thus stabilising p53 (Ganem et al., 2014). Therefore as extension of the current work, it would be of great interest to analyse components of the Hippo pathway in the HCT-116 tetraploidy system, in order to determine whether the pathway contributes to the observed elevations of p21 and p53. If Hippo signalling were responsible for p53 and p21 elevation, this would suggest the HCT-116 tetraploids are proliferating with a constitutively activated tetraploidy checkpoint.

In addition, Thompson and Compton also demonstrated p38 activation after segregation error induction in HCT-116 cells, possibly suggesting that the response to aneuploidy is triggered by ROS (Bragado et al., 2007, Thompson and Compton, 2010b). Therefore, an intriguing extension to this study would involve analysis of p38 and ROS levels in the tetraploid clones. A more extensive DNA damage analysis could also be performed in the tetraploids, by investigating the DNA damage pathway activation after a segregation error induction (e.g. ATM, CHK1/2). The combination of these studies with the analysis of Hippo signalling and segregation errors outputs, could clarify further which pathways and processes are active upstream the of p53 and p21 pathway in the tetraploid clones.

Castedo *et al* showed that tetraploid cells undergo apoptosis after tetraploidization in a BAX dependent manner, highlighting another obstacle newly formed tetraploids have to overcome (Castedo et al., 2006b). The HCT-166 tetraploid clones in this study were less sensitive to reversine-induced apoptosis suggesting that one possible mechanism of tolerance may be a dampened apoptotic response

downstream of p53, although the mediator of this phenotype was not detected in an apoptosis array.

However, although tetraploids exhibited a compromised apoptotic response, they still possessed high levels of p53 and the cell cycle inhibitor p21. TP53 mRNA levels were similar between all clones, suggesting post-translational modification of p53 is responsible for the heightened protein expression. In agreement with *CDKN1A* being a transcriptional target of p53, p21 mRNA levels were significantly elevated in the tetraploid clones. In addition, knockdown of p53 resulted in the complete loss of p21 protein expression, suggesting p21 expression is exclusively driven by p53-dependent CDKN1A induction.

Another mechanism that can suppress the inhibitory effect of p21 is cytoplasmic sequestration. Phosphorylation of p21-Thr145 inhibits translocation to nucleus. Due to the absence of a satisfactory p21-Thr145 antibody, the cellular localisation of p21 was assessed by compartment fractionation experiments. There was no cytoplasmic enrichment of p21 in the tetraploid clones, compared to the diploids, as p21 was greater in both the nucleus and cytoplasm. Of note, p53 was predominantly nuclear, also ruling out cytoplasmic sequestration of the transcription factor. These data show that p53 and p21 are elevated in the nucleus of the tetraploid clones, which would result in cell cycle arrest in normal cells. In contrast, a recent study showed CIN positive HCT-116 and RPE tetraploid cells sequestered p53 in the cytoplasm (Kuznetsova et al., 2015).

Analysis of cell cycle progression by RB-Ser807/811 phosphorylation status, nocodazole trap experiments and flow cytometry revealed the tetraploids could progress through the cell cycle without G1 arrest, despite expressing high p21 in all cycle phases. A possible explanation for the variability seen in the RB-Ser807/11 analysis was the use of unsynchronised cells. Populations of cells within the different clones may have been at different cell cycle phases at the time of lysis, which may explain the relatively variable result. To address this issue, cells could be synchronised in M phase and released, before phospho-RB analyses at different G1/S time points, permitting a more reliable comparison between clones. RB can be phosphorylated at many sites and a more extensive RB-phosphorylation

panel, such as Ser795, Ser608/612 and Ser780, could be used to further investigate tetraploid G1/S progression (Rubin, 2013). Nevertheless, these data combined with the confirmation of an active p53 pathway and high basal protein levels, suggest that tetraploidy-associated stress is promoting constitutive p53/p21 pathway activation and the tetraploid clones are resisting G1 arrest and apoptosis.

Taken together, the data presented in this chapter, show that tetraploidy tolerance in the HCT-116 isogenic system is not provided by mutating a member of the p53/p21/RB pathway, and implies the involvement of a more complex mechanism. This molecular phenotype provides a unique opportunity to study novel tetraploidy tolerance mechanisms bypassing a functional p53/p21 axis. Consistent with this, a pan-cancer analysis of nine tumour subtypes revealed 43% of *TP53 wild-type* tumours were genome-doubled compared to 58% in *TP53* mutant tumours (McGranahan et al., 2015). In addition, the analysis showed that although there is a significant co-occurrence between mutant *TP53* and genome-doubling, 65% of all genome-doubled tumours were *TP53 wild-type*. This suggests that other mechanisms of tolerance do exist in the clinical setting and understanding their molecular basis is important, as it may provide opportunities for therapeutic intervention together with an understanding of how chromosome segregation errors are propagated and how intercellular heterogeneity and cancer evolution is accelerated.

Tetraploid cells treated with 5-FU were found to be more drug resistant. Similarly, Castedo *et al* showed that their tetraploid HCT-116 clones were more resistant to cisplatin, oxaliplatin and camptothecin, through up regulation of p53R2, a protein that facilities DNA repair (Castedo et al., 2006a, Castedo et al., 2006b). In addition, Kuznetsova *et al* showed elevated drug resistance to a wide range of cytotoxic anticancer agents in tetraploid HCT-116 and RPE cells (including 5-FU), although differences were small. In this study, although early diploids and tetraploid clones were equally sensitive at lower doses, tetraploid clones treated with 5μM and 10μM 5-FU, specifically TC13, were more resistant than diploids. This may suggest that in the tetraploid clones there are more highly resistant 5-FU subclones, compared to diploid cultures. These subclones may require higher drug doses to completely clear them and prevent outgrowth during treatment, resulting in greater tetraploid

surviving fractions. This provides evidence for the intriguing concept that 5-FU treatment might select for the reoccurrence of tetraploid tumours as a result of elevated resistance. As tetraploid cells can support CIN and aneuploidy, this could result in further drug resistance and more aggressive disease.

When late passage clones were tested, although the tetraploid clones also demonstrated elevated resistance, the diploid clones were also more resistant. This may suggest the possibility that tetraploid clones are inherently more resistant to 5-FU and elevation seen in the late passage diploid and tetraploids are a function of MIN and the accumulation of somatic mutations during clonal evolution. To improve this part of the study, dose response curves could be constructed ranging from 1-5μM to demonstrate a dose-dependent relationship and completely rule out the possibility of an off-target effect at higher doses. As there was no differential sensitivity to oxaliplatin and the drug completely cleared diploid and tetraploid clones at the same dose (5μM), this might explain why combination with 5-FU is more active than single-agent therapy (Longley et al., 2003a).

Understanding the molecular of basis of resistance may explain why tetraploid resistance is only observed after 5-FU treatment. It is possible that tetraploids have a greater nucleotide pool and are therefore less sensitive to depletion of RNA and DNA precursors, such as 5-FU, but are equally sensitive to DNA damage by oxaliplatin. To investigate this hypothesis, other antimetabolite drugs that deplete nucleotide pools could be tested (e.g. gemcitabine) in order to investigate if a similar phenotype is observed. Additionally, resistant 5-FU colonies could be expanded, before survival analysis by clonogenic assay and oxaliplatin treatment to confirm class specific drug resistance.

Although the apoptosis array did not highlight any major pathway aberrations, all the clones should be analysed, as there may be mechanistic clonal variation. Apoptotic pathway aberrations may converge at different points, promoting resistance to cell death after segregation errors in the tetraploid clones (Taylor et al., 2008). For example, some tetraploid clones could overexpress BCL-2, whilst others may underexpress BAD, resulting in compromised apoptotic pathways (Taylor et al., 2008). Reversine treatment failed to induce BAX or BAD, suggesting

that caspase-3 cleavage might be induced by an alternative pathway or perhaps the current assay is not sensitive enough. The integration of fluorescent secondary antibodies would allow a more sensitive and reliable detection and quantification. Thorough western blot analysis and other apoptosis assays could also be used to further dissect the apoptosis pathway downstream of p53.

This chapter provides evidence that tetraploids have an elevated and functional checkpoint, which suggests that they should be undergoing a G1 arrest. Several lines of investigation show that there is no tetraploid G1 arrest and future work is needed to address how the tetraploid clones are overriding high p21 levels. Global analysis of the transcriptome and proteome may highlight molecular mechanisms capable of overriding the activated p53/p21 pathway.

Chapter 4. Quantitative proteomics of diploid and tetraploid cells

4.1 Introduction

The previous chapter has shown that p21 levels are elevated in the tetraploid clones and yet despite this they are still proliferating. In an attempt to understand how this may be occurring and to unearth further clues as to how the tetraploidy tolerance is provided in our system, RNA expression analysis and quantitative proteomics were performed. These powerful techniques allow the quantification and detection of differences in mRNA and protein expression.

These techniques have been previously combined to investigate differences in expression in aneuploid cells (Pavelka et al., 2010, Stingele et al., 2012). Pavelka *et al* showed that protein expression in yeast correlated with increased copy number and that aneuploidy could produce phenotypic variation, in comparison to isogenic euploid cells (Pavelka et al., 2010). Stingele *et al* generated human aneuploid trisomic and tetrasomic cell lines and quantitatively determined changes in DNA copy number, mRNA and protein expression (Stingele et al., 2012). mRNA levels reflected DNA copy number, however, proteins were reduced towards diploid levels. This was particularly apparent for protein complex subunits and kinases. This suggests that protein subunits were regulated at the protein level to maintain the correct stoichiometric ratios, while kinases were post-translationally regulated to maintain diploid kinase signalling. The group also noted down-regulation of DNA and RNA metabolism pathways and up-regulation of metabolic and autophagy pathways (Stingele et al., 2012). Furthermore, the group expanded these findings and showed that tetraploid cells generated from HCT-116 cells, *via* cytokinesis failure, resulted in aneuploidy and the transcription profile elicited the same changes as trisomic cells, suggesting aneuploidy produces uniform response (Durrbaum et al., 2014).

Taken together these studies suggest that, in aneuploid cells, a large proportion of regulation to permit survival is achieved at the protein level. This chapter aimed to

apply RNA profiling and quantitative proteomics to identify potential differences in mRNA and protein levels between diploid and tetraploid clones. This may provide important information on how cells manage tetraploidy and increased CIN. Three proteomic experiments were performed, comparing diploid and tetraploid clones, at both early and late passage time points. The global phosphoproteome was also compared in in the early clone pair.

4.2 mRNA expression analysis

Firstly, RNA was extracted from exponentially growing diploid and tetraploid clones and analysed using Affymetrix Human Gene 1.0 ST arrays. Surprisingly, only a limited number of transcriptional differences were identified between the diploid and tetraploid clones (Figure 4.1A). As there were no striking differences between clones and differences were not exclusive to ploidy state, these genes were not followed up. Therefore in the genome-doubled tetraploid system, mRNA expression may have scaled directly with DNA content, producing no detectable gene expression differences and regulation of expression as at the protein level. This would be consistent with the approximate doubling of total protein content (Appendix). This finding is in agreement with previous studies, which suggest that mRNA levels scale with DNA content and regulation is at the protein level (Stingele et al., 2012). Therefore SILAC was conducted to compare the proteome of diploid and tetraploid cells.

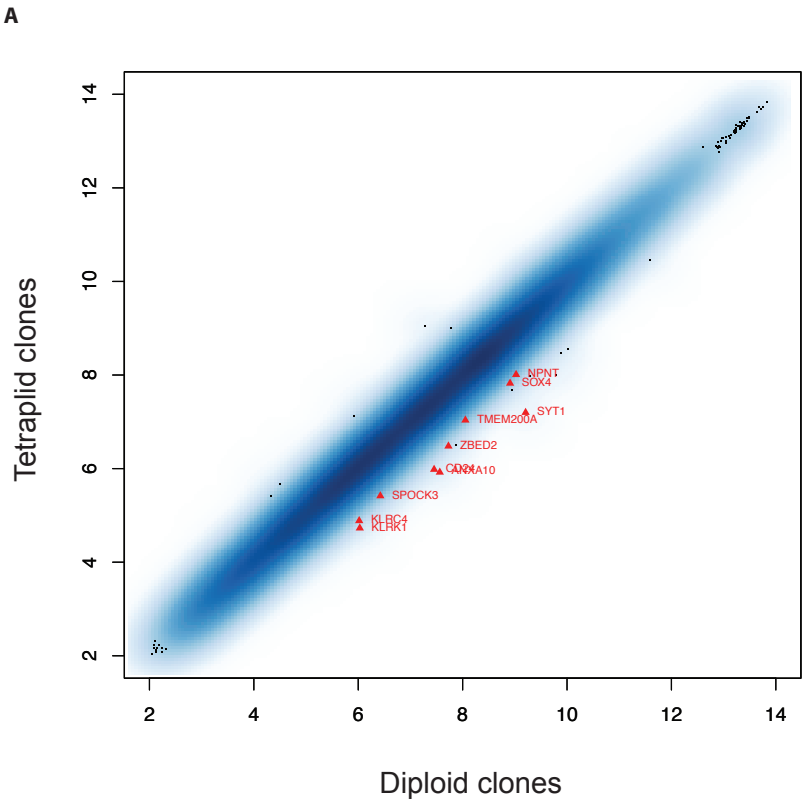

Figure 4.1 Diploid versus tetraploid mRNA expression analysis

(A) Combined expression analysis of all diploid and tetraploid clones, early and late passage. Genes labelled in red show significant expression changes by 'hypothesis testing'. For genes to score as a 'hit', the difference in expression should be >2-fold at p≤0.01.

4.3 Stable Isotope Labelling of Amino acids in Cell culture (SILAC)

To investigate whether the gene expression was regulated at the proteome level, Stable Isotope Labeling of Amino acids in Cell culture (SILAC) was performed. It was hypothesised that proteomic regulatory mechanisms may result in differential protein expression, which could provide tetraploidy tolerance and permit proliferation in the presence of high p21. Two experiments were carried out comparing diploid and tetraploid clones, at both early and late passage. Proteomic differences at both early and late time points may indicate proteins that are required for survival, whereas investigating differences at specific timepoints may also provide information on transient changes and evolved adaptations.

4.3.1 SILAC principle

SILAC is a relatively new technique, first published in 2002 (Ong et al., 2002, Blagoev et al., 2003). The principle allows quantitative proteomic comparisons between multiple samples, as opposed to standard mass spectrometry. Populations of cells are grown in 'heavy' and 'light' tissue culture media that provides the basis for comparison. The 'light' condition is a normal growth medium with standard amino acids present, whilst the 'heavy' media contains arginine and lysine with ^{2}H, ^{13}C and ^{15}N isotopes. Cells are grown in 'light' or 'heavy' media for a minimum of five population doublings, allowing incorporation of the isotopes into the proteome. This results only in a change of proteome mass and no other chemical changes (Mann, 2006). After five population doublings, fully labelled populations of 'heavy' and 'light' cells exist and are mixed 1:1, before separation by SDS-PAGE. The proteins in the SDS-PAGE gel are digested by trypsin, which cleaves proteins on the carboxy-terminal of arginine and lysine, producing a peptide mixture (Ong et al., 2002). Peptides are further separated by high performance liquid chromatography (HPLC) and eluted in order of hydrophobicity, before electrospray ionisation in the mass spectrometer ionisation chamber. In this study, a 'time of flight' (TOF) analyser was used to separate peptides by their mass.

before peptide sequencing. The mass to charge (m/z) ratio is plotted on the chromatogram, as this corrects for the effect of ionisation on the peptide. At this point the relative abundances of the ‘light’ and ‘heavy’ samples are calculated. The ‘heavy’ peptides in the sample have slightly greater m/z ratio than the ‘light’ species on the mass spectrum, permitting relative quantification between the two samples (Figure 4.2). The peptides are identified by another MS analysis known as ‘tandem MS’ or MS/MS. The peptide, known as the precursor ion, is fragmented to product ions by cleavage of amide bonds. The mass of the product ions (single amino acids) is then determined and matched to a database that reveals the peptide sequence and thus identifies the protein (Steen and Mann, 2004).

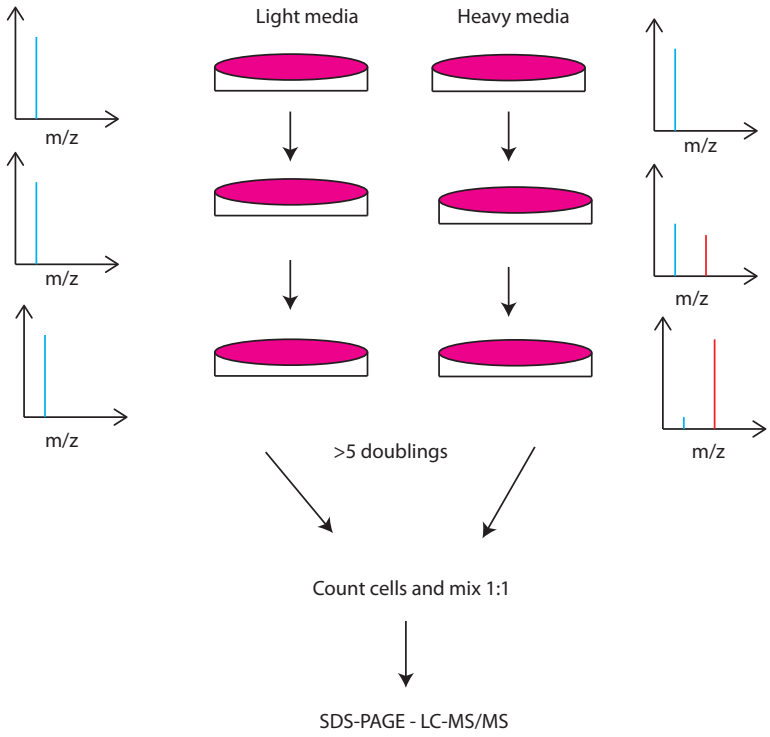

Figure 4.2 Principle of the SILAC labelling strategy

Cells are cultured in 'light' or 'heavy' media for a minimum of five population doublings. In the 'heavy' condition the mass spectrums show how a peptide species becomes labelled. At first the entire fraction is 'light'. Midway through the labelling process the fraction of 'heavy' and 'light' peptides is equal and after 5> doublings 99% of proteins should be a 'heavy' species. This allows for sensitive and valid quantification of relative protein abundances between the two samples. After labelling cells are mixed at 1:1 ratio and separated by SDS-PAGE, before HPLC, mass spectrometry, peptide ratio calculations and peptide identification. m/z, mass/charge ratio.

4.4 SILAC analysis of DC14 vs TC13

For technical reasons it was not practical to analyse the whole isogenic system by SILAC. Therefore, a representative diploid-tetraploid pair was selected and any differences discovered were validated across all clones. After labelling, 'heavy' labelled cells were checked for lysine and arginine incorporation (**Figure 4.3**). It immediately became apparent that there was a problem with the 'heavy' labelled cells. Although lysine and arginine labelling was sufficient, secondary 'heavy' proline peaks were apparent on the mass spectrum (**Figure 4.3**). The 'heavy' isotope incorporation checks revealed high Arg→Pro conversion rates of approximately 28-30%, causing problems for data analysis. 'Heavy' labelled proline will produce a fraction of peptides that contain 'heavy' arginine, lysine and proline producing three peaks for a single peptide on the mass spectrum ('Light' + 'Heavy'-arg-lys + 'Heavy' arg-lys-pro; Figure 4.4). Abundance of 'heavy' labelled peaks will be underestimated as the proline satellite peaks will contain a proportion of the overall peptide, which cannot be factored into the quantification process (Figure 4.4).

This problem is relatively common (Van Hoof et al., 2007), however conversion of ~30% is very high and a solution to reduce this level was required in order to progress. One option involves changing the labelling system so the need for metabolic incorporation is bypassed, for example, isotope affinity tags (ICAT). At the time, this would require specialist technical assistance and further prolonged assay development and so was not deemed viable. Van hoof *et al* suggest the use of isotope 'trickery' to compensate for peak reduction. Applying isotopically labelled $^{15}N_4$-$^{13}C_6$ -Arginine to 'light' media would fuel conversion to 'heavy' proline in the 'light' condition controlling for conversion, resulting in comparable peaks (Van Hoof et al., 2007). However, this method assumes conversion will be a constant between cell lines and can complicate analysis.

A

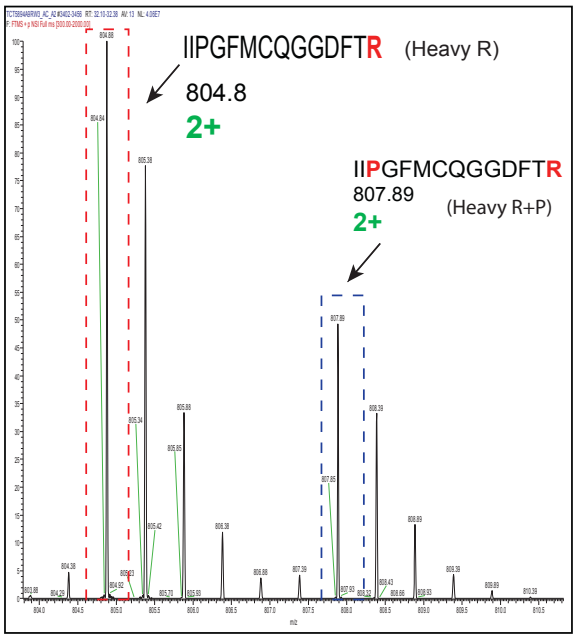

TC16 p6

B

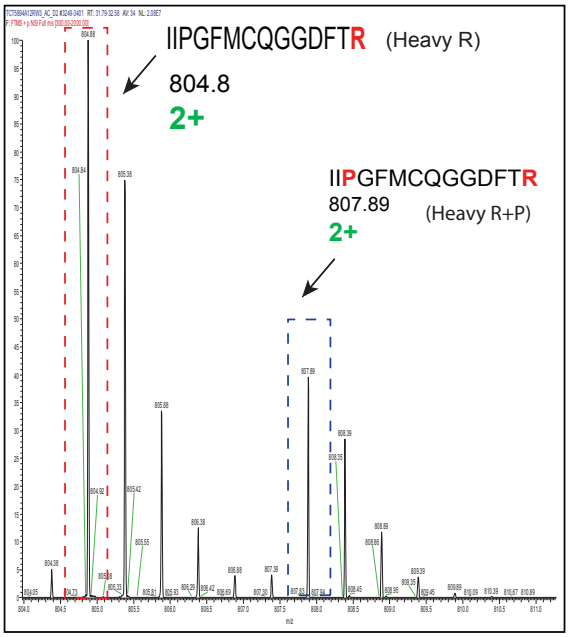

TC16 p52

Figure 4.3 Examples of proline conversion satellite peaks
(A and B) Isotope incorporation check mass spectrum (MS1 spectra) demonstrating the presence of 'heavy' proline satellite peaks. Samples analysed were heavy samples only, i.e. not mixed with light samples. Peaks outlined in red on the left are the expected monoisotopic peaks containing 'heavy' arginine only (**R**), whereas peptides containing 'heavy' arginine and proline (**R**+**P**) are shifted to the right, outlined in blue.

Simpler methods involve reducing the 'heavy' arginine content to lower the conversion of arginine to proline, or increase the amount of proline in the media to shift the reversible reaction in the favour of arginine production. A slight reduction in arginine concentration may not have been effective in this study due to the high conversion rates calculated. However, Bendall *et al* demonstrated that the addition of exogenous proline to SILAC media reduced 'heavy' proline monoisotopic peaks in a dose-dependent manner and completely abolished conversion when cells were treated with >100mg/L (Bendall et al., 2008).

The Bendall method was therefore adopted in an attempt to overcome the high proline conversion rate in the isogenic HCT-116 cell lines (Figure 4.4C). 'Heavy' SILAC media was supplemented with multiple doses of exogenous L-proline and used to culture diploid parental HCT-116 cells. After five doublings, cells were lysed and separated by SDS-PAGE before proline incorporation checks. Scatter plots displayed in Figure 4.5 show the ratio of peptides containing 'heavy' arginine and lysine versus 'heavy' arginine-lysine-proline peptides. The median ratio of peptides containing a single proline was used to calculate the conversion rate, as peptides with multiple proline residues have greater ratios due to signal dispersion. The analysis was expected to reveal negative ratios (Log2 scale), as 'heavy' proline peptides are usually a small fraction of the total.

Addition of exogenous proline at a range of doses appeared to supress the proline conversion observed. Untreated HCT-116 cells had a conversion rate of 20-30%, consistent with earlier checks for DC14 and TC13. However, addition of 100mg/L of proline reduced conversion to <1% and 400mg/L almost entirely abolished conversion. The scatter plots in Figure 4.5 clearly show that as the proline concentration is increased, the conversion rate falls and the number of 'heavy' containing peptides is decreased to almost undetectable levels. From these data it was decided that 150mg/L would be used for future SILAC experiments to abolish proline satellite peaks, permitting accurate quantification of peptides.

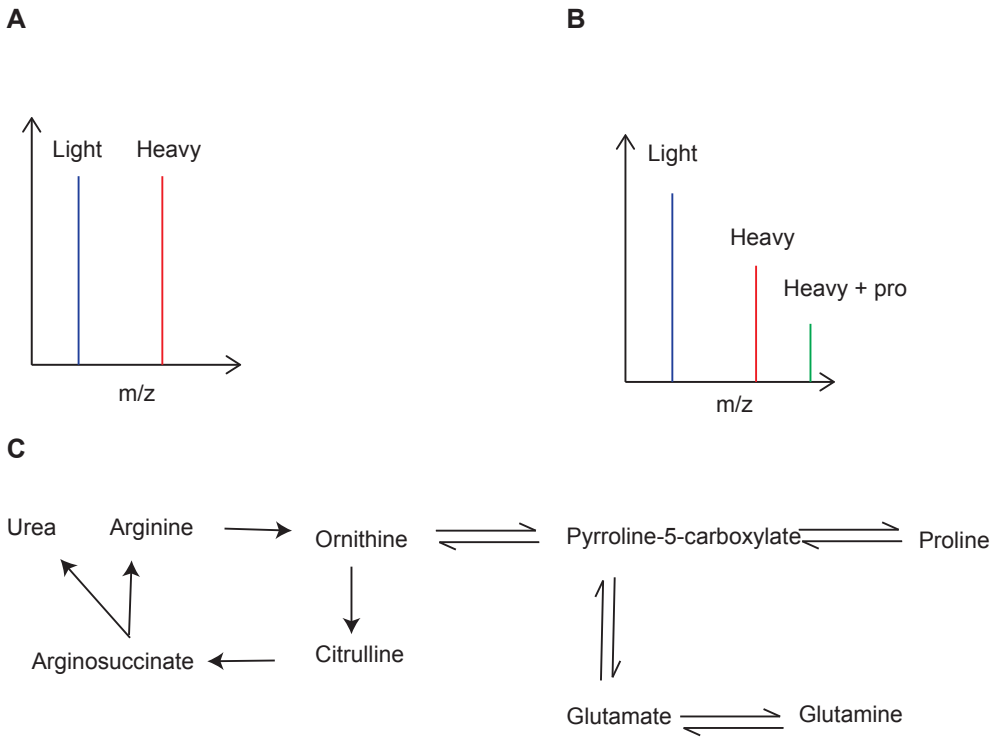

Figure 4.4 Proline satellite peaks and arginine metabolism

'Heavy' arginine conversion to 'heavy' proline can hinder a reliable comparison between 'heavy' and 'light' samples. The chromatogram in (A) shows the abundances of a peptide in a 'heavy' and 'light' sample are equal. If a fraction of 'heavy' proline exists and is incorporated into the peptide, three species of peptide will be detected as opposed to the expected two. (B) This hinders reliable detection, as the 'heavy' monoisotopic peak used to calculate a ratio relative to the 'light' condition is underrepresented, as a fraction of the peptide is now present in the third 'heavy' lysine, arginine and proline peak. (C) Addition of exogenous proline solves this problem, by reducing the synthesis of proline from 'heavy' arginine and favouring the reverse reaction.

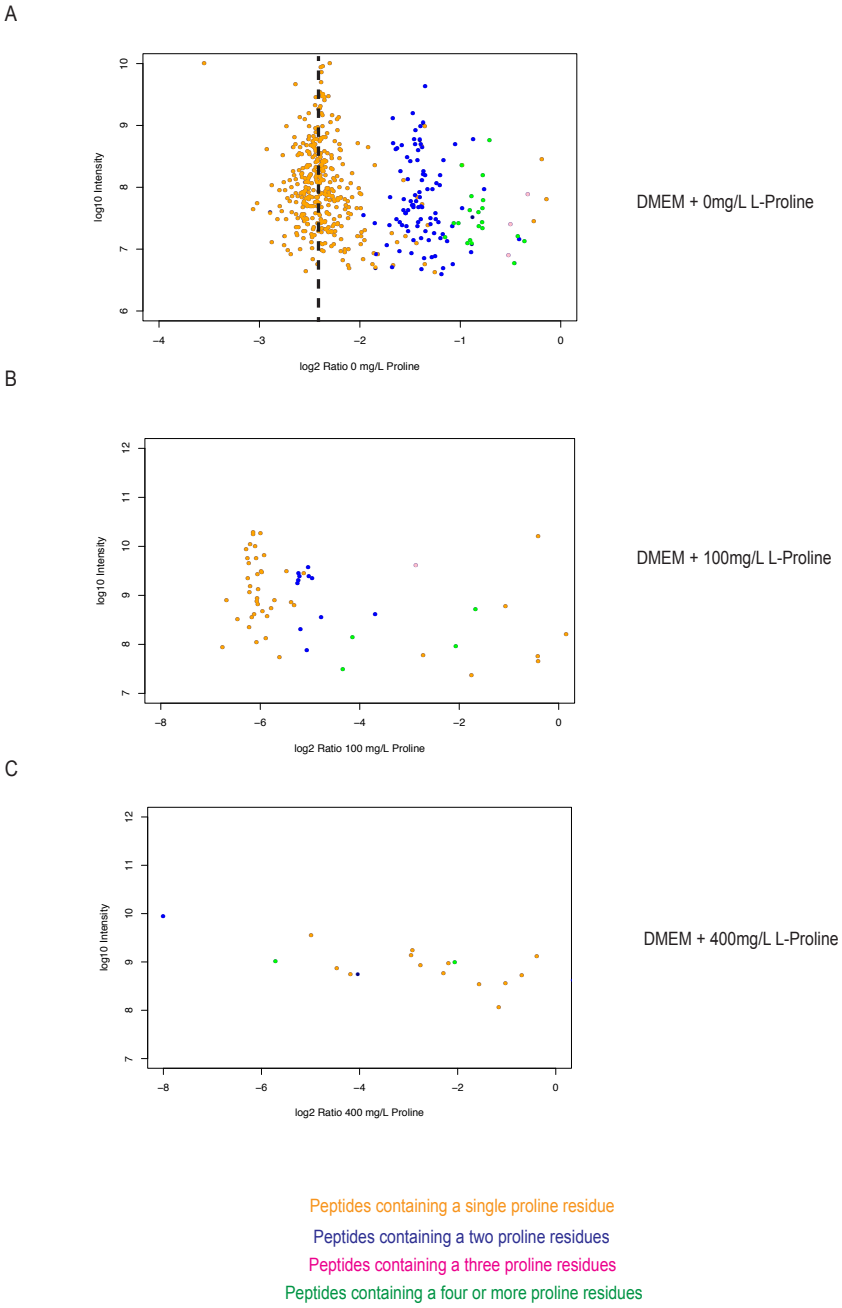

Figure 4.5 Addition of exogenous L-proline & 'heavy' prolinecontaining peptides

Standard DMEM media was supplemented with increasing concentrations of L-proline. After five population doublings, cells were lysed and separated by SDS-PAGE, before trypsin digestion and analysis by mass spectrometry. Ratios of 'heavy' Lys-Arg/Lys-Arg-Pro peptides were calculated and plotted. The median conversion ratio of single proline containing peptides (the most abundant and reliable species) was used to calculate the overall proline conversion and was expressed as a percentage. Dashed line: median conversion ratio of single proline peptides.

4.4.1 Analysis of DC14 and TC13

With the issue of proline conversion solved, the SILAC procedure was repeated under the optimised conditions. After culturing for more than five population doublings, cells were harvested, counted and mixed at a ratio of 1:1, in different combinations (Table 4.1). Mixes were lysed with 8M urea before quantification and separation by SDS-PAGE. All the mixes resulted in good separation and defined protein bands with minimal smearing, suggestive of protein quality adequate for MS.

4.4.2 Control for experimental variation

The first pair selected for analysis was mix 1 that contained DC14p5 labelled ‘heavy’ and ‘light’ (Figure 4.6A). This analysis allowed the detection of intrinsic variance within the experimental process. In theory, all proteins would ideally return to a ratio of Log2=0 (1:1), as the same samples have been compared. In reality, some variation would be present due to quantification errors and slight differentials in expression between samples. Figure 4.6A shows the scatter plot for mix 1 and demonstrates a tight distribution and a limited spread. When the ratio distributions were compared between all samples, it was clear that the control had a much tighter distribution, implying intrinsic variance to be satisfactory (Figure 4.6B). This provided confidence that the changes seen in the experimental samples were a result of differential expression and not artificially induced by the technique or ‘heavy’ and ‘light’ medias.

		'Heavy' Media			
		DC14p5	DC14p42	TC13p5	TC13p42
'Light' Media	DC14p5	Mix 1	2	Mix 3	4
	DC14p42	5	6	7	Mix 8
	TC13p5	Mix 9	10	11	12
	TC13p42	13	Mix 14	15	16

Table 4.1 SILAC mixing combinations

Components of each clone mix, with mix 1 acting as the control. Mixes 3 and 9 are reverse labelling repeats of early clones. Mixes 8 and 14 are late reverse repeats. Yellow box: control mix. Green boxes: experimental comparisons.

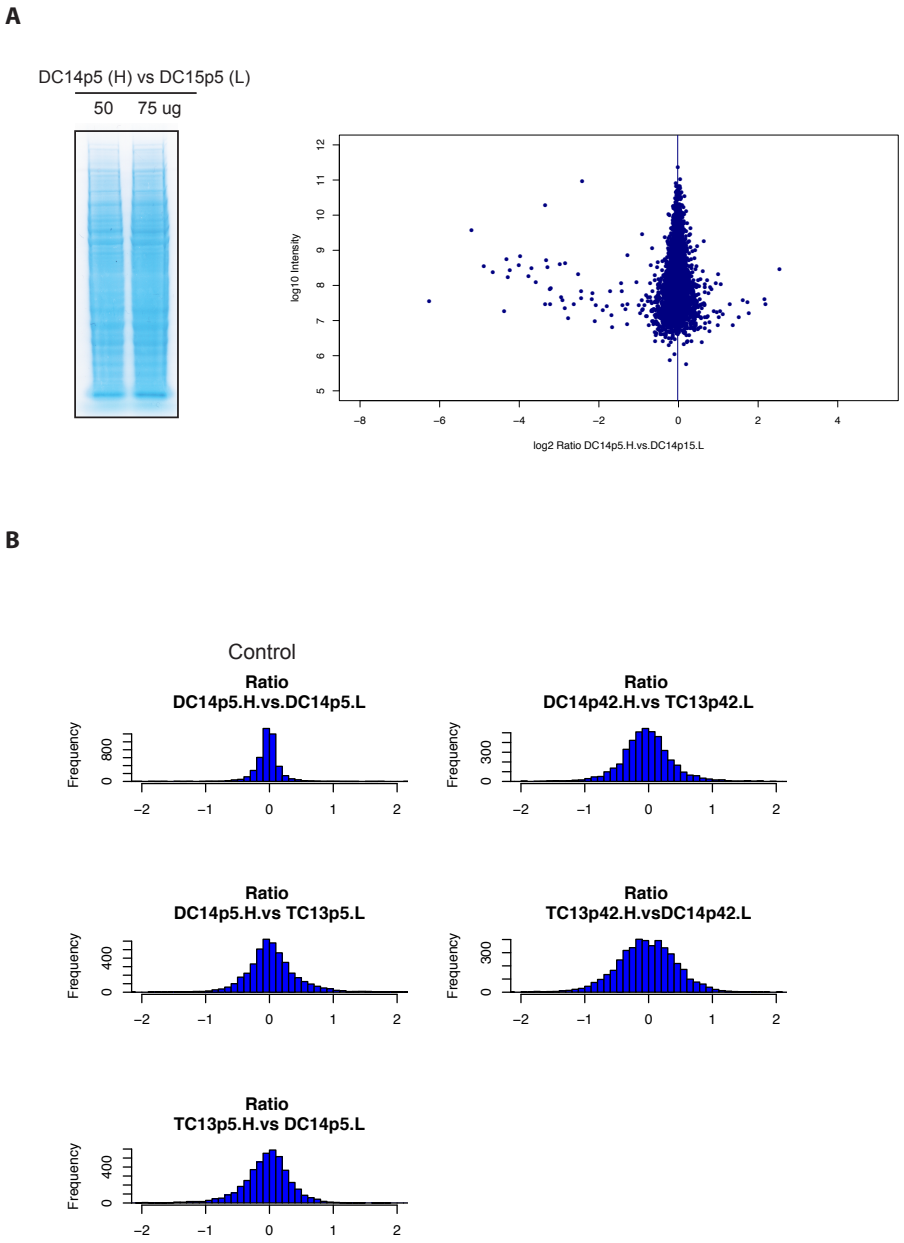

Figure 4.6 Control mix and ratio distributions across all mixes

(A) SDS-PAGE separation of mix 1 stained with Coomassie blue to check protein quality. The gel was processed for mass spectrometry analysis and sample ratios plotted in a scatter plot. The raw 'heavy'/'light' ratios were normalised to the median ratio and plotted on a Log2 scale. (B) Distributions of ratios for all mixes. Mix 1 demonstrated a tighter distribution than the experimental mixes as it served as control for experimental variation. (H) Heavy, (L) Light.

4.4.3 Sample correlation analysis

Each mix was performed in duplicate and each replicate was labelled in the reverse combination, for example, mix 3 (DC14p5 [L] + TC13p5 [H]) versus mix 9 (DC14 [H] +TC13p5 [L]). This was carried out to ensure reproducibility and that 'light' and 'heavy' media had no effect in protein expression. Figure 4.7A shows the correlations between mix 3 and 9 (early samples) and Pearson correlation coefficient of -0.25 was calculated. Figure 4.7B shows the correlation of mixes 8 and 14 (late samples) and possessed a Pearson correlation coefficient of 0.44. Therefore, the reverse experiments showed a satisfactory negative correlation, which implied that the experiment was successful and the replicates had similar peptide ratios.

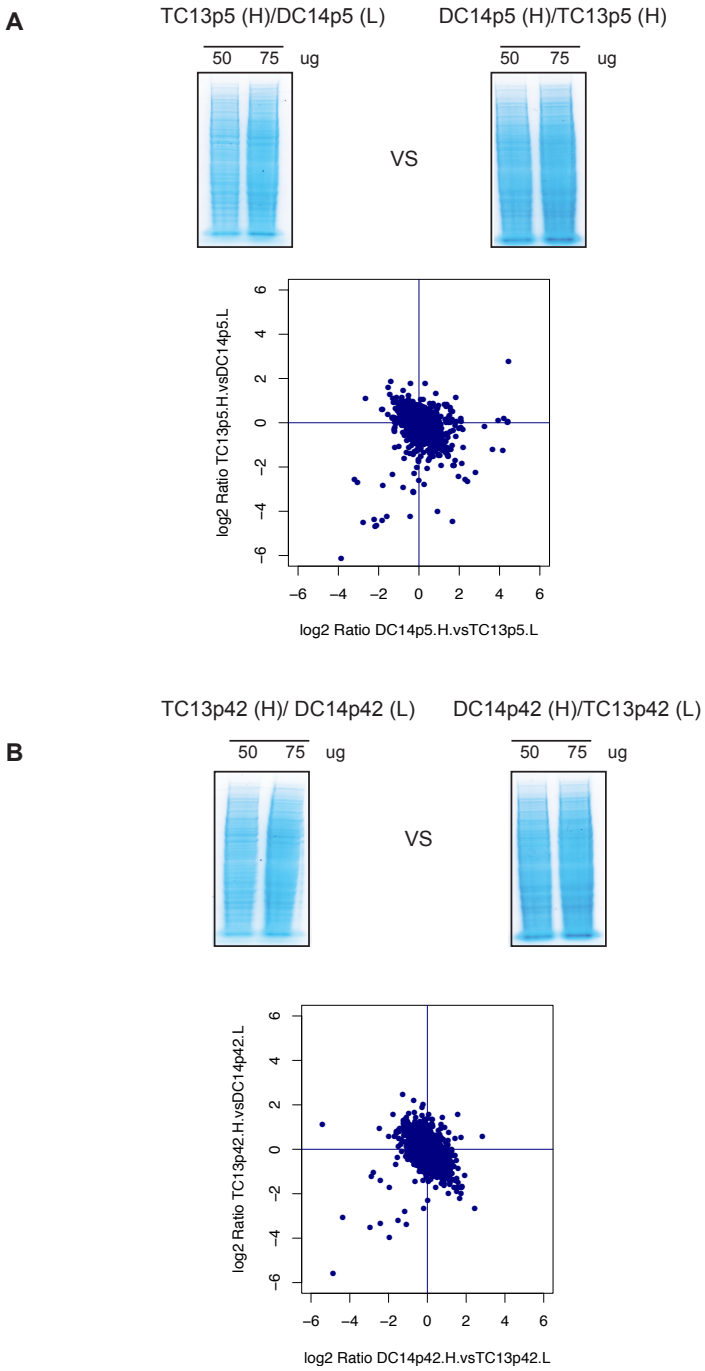

Figure 4.7 Mix correlation plots and protein gels

(A) Correlation between early diploid and tetraploid repeat experiments. Labelling was reversed for each repeat to ensure differential media formulations did not affect the result. (B) Correlation between late diploid and tetraploid samples. (H) Heavy, (L) Light.

4.4.4 Comparison of protein groups between diploids and tetraploids

As the experimental controls gave the expected results, the data could be analysed to find proteomic differences between the diploid and tetraploid samples. The data was first analysed to identify classes of proteins that showed differential expression levels. Figure 4.8 shows a scatter plot comparing protein groups from mix 8 and 14 (late clones) and demonstrated a strong expected negative correlation between them. Late clones were analysed as they provided a stronger negative correlation between repeats than early samples. Protein groups depleted in the tetraploid cell line appeared to be related to ribosomal subunits and associated proteins, possibly suggesting down-regulation of protein translation. These data also showed that the tetraploid clones had enrichment of chromatin components and nuclear proteins. As tetraploid cells with a 4N DNA content were predicted to have elevated levels of the majority of these proteins, this protein enrichment suggested that the technique has been successful and that valid biological differences were being detected. Interestingly, histone methyltransferase complex components, including histone-lysine N-methyltransferase (MML) and chromobox protein homolog 5 (CBX5), showed enrichment in the tetraploid cell line. This finding may be suggestive of an increased demand for epigenetic regulators as a result of genome-doubling.

To test this hypothesis, the diploid and tetraploid pair analysed by SILAC and two others (DC8, DC14, TC13, TC16) were screened in an epigenetic inhibitor library (Figure 4.9). Clones were subjected to library containing 51 epigenetic modulators for 72 hours at 5μM dose. The screen revealed tetraploids were significantly sensitive ($p \leq 0.01$) to two histone deacetylase inhibitors, PCI-34051 and valproic sodium salt. In addition, tetraploids showed significant resistance to 2-methoxyestradiol. However, although these differences in sensitivity were significant, the actual differences were minor and in the case of valproic sodium salt, survival was above 80% in all samples. TC13 was generally more resistant to all treatments, consistent with earlier experiments investigating 5-FU.

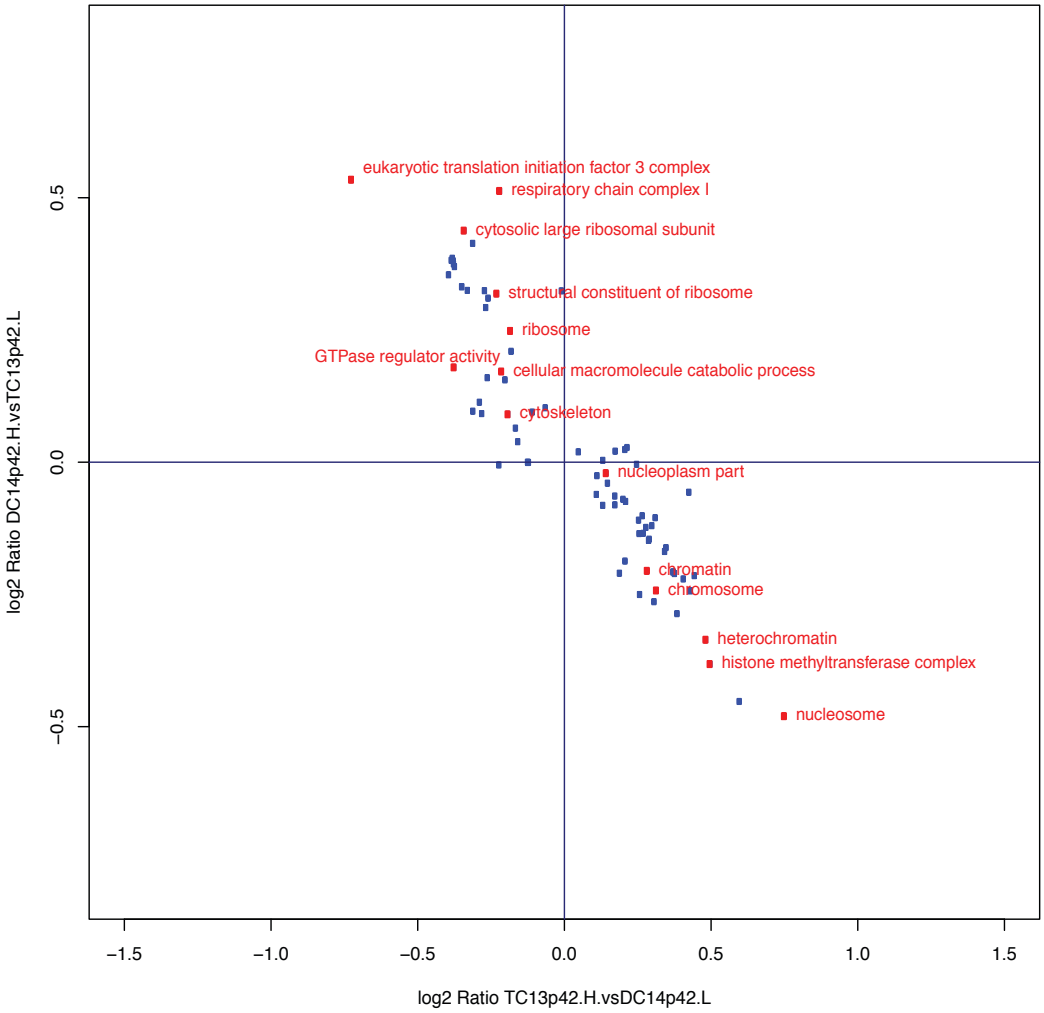

Figure 4.8 Late clone protein group 2D analysis

Scatter plot displaying classes of proteins that differ between late DC14 and TC13 produced by Perseus software. The 2D analysis function is an algorithm that quantifies relative up and down-regulation of cellular pathways. Red dots and text represent pathways of interest that show differential regulation between diploids and tetraploids.

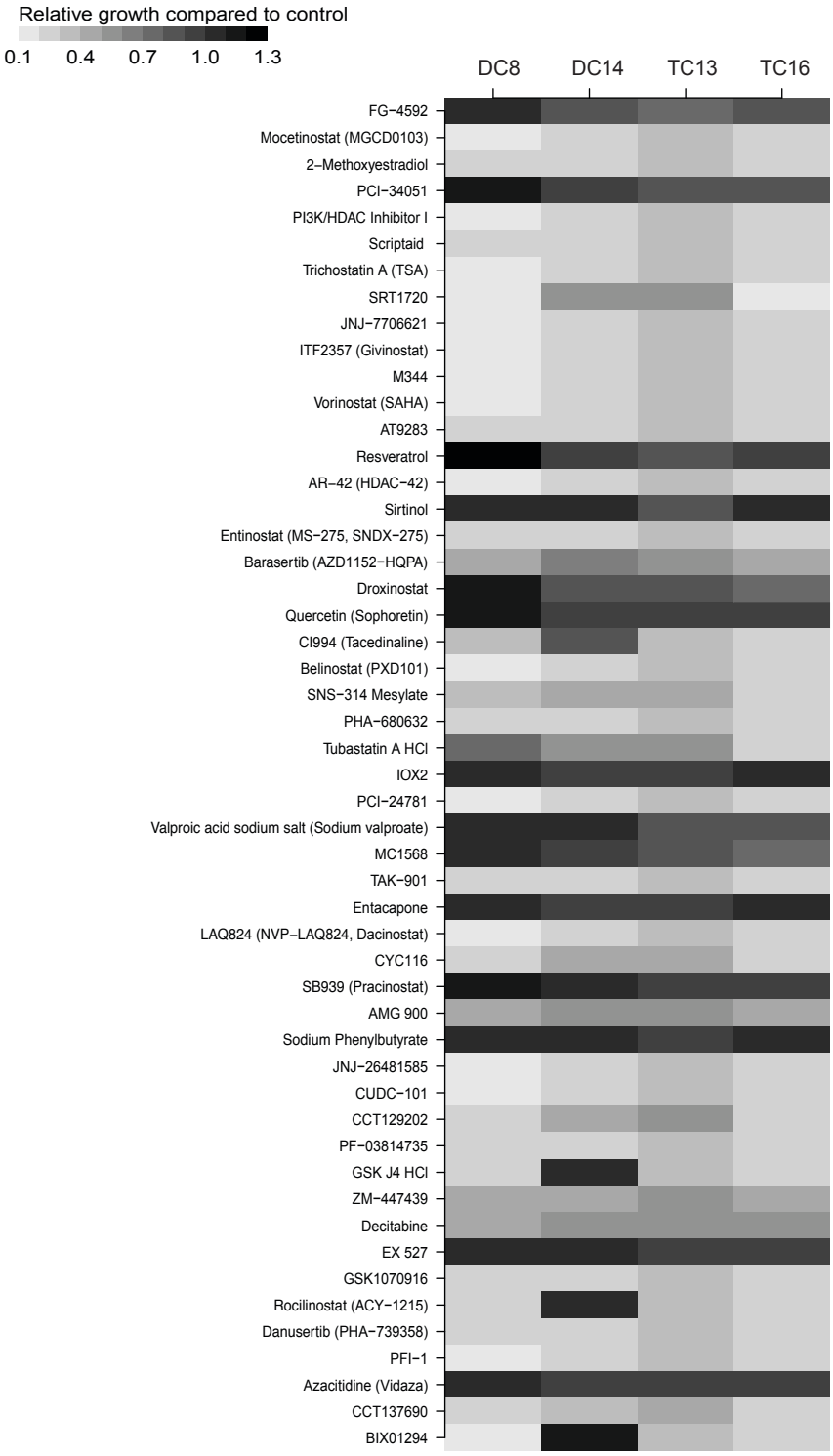

Figure 4.9 Epigenetic drug screen

Diploid and tetraploid clones were seeded into 96-well assay plates containing 5μM of compound. Cells were incubated in the presence of drug for 72 hours, before measurement of metabolic activity by cell titre blue. Treated samples were normalised to DMSO control.

4.4.5 List of differentially abundant proteins in diploids and tetraploids

Profile plots were generated in order to obtain a list of proteins that were differentially expressed between diploid and tetraploid samples (Figure 4.10). Profile plots were chosen as the best way to analyse the MS data, as they display data clearly across all samples analysed. Tetraploid enrichment ratios were manually set at approximately Log2=2 for 'heavy' labelled tetraploid samples, and approximately Log2=-2 for mixes with 'light' labelled tetraploids. As the ratio calculation is always 'heavy'/'light', this setting would identify proteins enriched in tetraploids (Figure 4.10A). The opposite settings were applied to find depleted proteins in the tetraploids (Figure 4.10B). Proteins displaying expression ratios that exceed these settings were likely to be impurities. Ratios for mix 1 were set at zero in order to ensure that the proteins selected did not show variation in the control condition, increasing the likelihood that hits were a result of biological differences and not induced artificially. These filters were applied and the software identified a manually set number of proteins that most closely followed the set ratio profiles. The MS data were interrogated for a total of 50 proteins enriched or depleted in tetraploid cells (early and late). A selection greater than 50 was not useful, as many proteins whose ratios fall within the box plots would start to be included and would, therefore, not be significantly deregulated. Proteins present in both early and late passage clones were taken forward, as de-regulation at both time points enhances the probability of the aberrations contributing to chronic tolerance, as opposed to proteins only aberrant at a specific time-point.

A

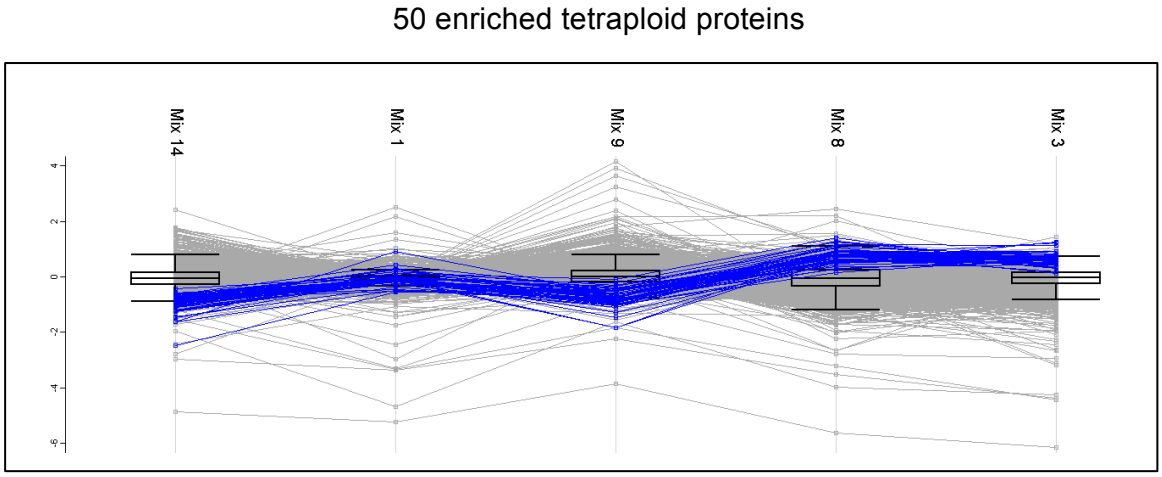

B

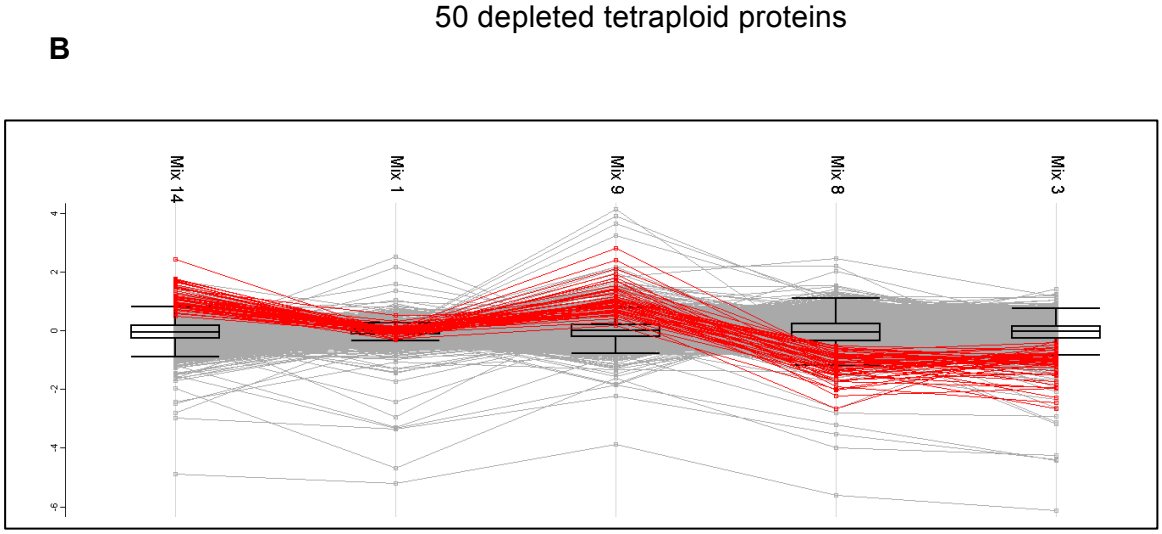

Figure 4.10 Profile plots for top 50 enriched or depleted proteins

(A and B) Profile plots displaying 50 proteins that are enriched or depleted across all samples. Peptides must have been detected at least twice in all samples in order to be considered. The y-axis represents fold change and the samples (mixes) are plotted on the x-axis. Ratio values set are displayed in tables below plots and were set manually. Enrichment and depletion ratios set at approximately log2 2 or –2. This degree of expression change is considered relevant and is common setting used for this type of analysis.

Proteins that were identified as enriched or depleted in the early and late tetraploid cells are listed in Table 4.2. Firstly, the enriched protein list was analysed against the gene ontology database, grouping proteins according to their function, and a degree of overlap was observed (Table 4.3). The analysis revealed fourteen biological processes that could be enriched in the tetraploid cells relative to their diploid counterparts. Although a degree of overlap was observed, due to nature of the gene ontology phylogenetic structure, mitotic control, cell cycle, chromatin regulation and DNA packaging all emerged as plausible differences that could aid the tetraploid phenotype. Validation of these findings across all the clones in the isogenic system is required, to ensure that the differences are not a result of intrinsic clonal variation. Down-regulated proteins were also analysed by the GO database and only a small overlap was observed Table 4.4.

Proteins enriched in tetraploids	Proteins depleted in tetraploids
ABCF1	AGL
ABCF2	ALDH16A1
ACAA1	ALDH1A3
AP1M1	ARPC5
ATG9A	ASPH
ATL3	BDH1
B2RBA9	BPNT1
CDCA5	CAMK2D
CDCA8	CARS2
CHAF1B	CLIC4
CNN2	CPS1
CRABP2	DPP4
DNAJC1	DUT
EPHA2	EBF2
GART	ECH1
GTSF1	EIF3J
GUSB	EIF4A2
H1F0	FAM114A1
HACL1	FAM203B
HEBP1	FAM49B
HELLS	FBXO2
HINT3	IRS1
HNRNPK	ITGA3
IGF2R	KIAA0391
INCENP	KPNA6
KIAA1524	LGALS3BP
KIF20A	MAOB
KIF22	MGST2
KIF4A	MOV10
MSH2	NDRG1
MSH6	NQO1
MYADM	NSUN4
NAGK	PALLD
NCAPD3	PFKP
PBK	PFN2
PDCD6IP	PKM2
PDLIM1	PTK2
PEX3	RAC2
PKP2	SERPINB1
PLP2	SERPINB5
RBPJ	SH3KBP1
RRP9	SLC16A1
SCAMP4	SORD
SLC29A1	STK39
STOM	TNIK
STX3	TRIM72
TPX2	TUBB3
TSFM	TUBB6
UBE2S	TWF2
VAMP8	UBR4

Table 4.2 List of genes identified by the mass spec profile plots

50 proteins identified from the enrichment or depletion profile plots. Enrichment and depletion ratios were set at log2 of 2 and -2.

Gene/Gene Set Overlap Matrix	Organelle organisation and biogenesis	Establishment of localisation	DNA packaging	Chromosome organisation and biogenesis	Transport	Mitosis	M phase of mitotic cell cycle	Chromatin assembly	Base excision repair	M phase	Chromatin assembly or disassembly	Establishment of cellular localisation	Mitotic cell cycle	Chromosome segregation	Cellular localisation	Cell cycle phase	Cell cycle process
Gene Symbol																	
CDCA5	■	■	■	■		■	■			■		■	■	■	■	■	■
PEX3	■	■			■							■			■		
KIF4A	■	■			■							■			■		
HELLS	■	■	■	■				■			■						
CHAF1B	■	■	■	■				■			■						
MSH2	■	■		■					■								
CNN2	■	■															
ATG9A	■	■															
SLC29A1		■			■												
IGF2R		■			■												
KIF20A		■			■												
PLP2		■			■												
ABCF2		■			■												
DNAJC1		■										■			■		
TPX2						■	■			■			■			■	■
KIF22						■	■			■			■			■	■
MSH6									■								
INCENP														■			

Table 4.3 Gene ontology analysis from top 50 enriched tetraploid proteins

The 50 enriched tetraploid proteins detected by SILAC were entered into the gene ontology database. Proteins that showed pathway convergence are displayed. Blue shaded squares indicate pathway involvement.

Gene/Gene Set Overlap Matrix	Oxidation-reduction processes	Response to metal ion
Gene Symbol		
MGST2		
PFKP		
NQO1		
ALDH1A3		
SORD		
CPS1		
BDH1		
ALDH16A1		
AGL		
ASPH		
ECH1		
MAOB		
CAM2KD		
CPS1		
ASPH		
NDRG1		
CLIC4		

Table 4.4 Gene ontology analysis from top 50 depleted tetraploid proteins

The 50 depleted tetraploid proteins detected by SILAC were entered into the gene ontology database. Proteins that showed pathway convergence are displayed. Red shaded squares indicate pathway involvement.

4.4.6 Investigation and validation of SILAC 'hits'

The 50 enriched or depleted proteins identified by the profile analysis were manually reviewed by checking protein function, *via* the human gene compendium database. Proteins, with functions that could provide benefit to the tetraploid clones, were checked for correlation in the two repeat experiments to confirm validity of the profile plot results. Peptide detection coverage was also considered when following up 'hits', as this relates to confidence in protein identification and quantification.

4.4.6.1 ALIX (PDCD6IP)

Programmed cell death interacting protein (PDCD6IP/ALIX) was identified as being enriched in early and late tetraploid cells by approximately 2-fold (Figure 4.11). ALIX is a mammalian protein with many cytosolic roles, such as endocytosis. The protein was first identified as the binding partner of the Ca^{2+} regulator ALG-2, which is required for induction of apoptosis (Odorizzi, 2006). Studies have shown that ALIX cooperates with ALG-2 to activate apoptosis and overexpression of ALIX results in cell death. Conversely, the mutated form of ALIX acts an anti-apoptotic regulator (Odorizzi, 2006). Overexpression in the tetraploid system may be a result of an ALIX-dependent stress response. All members of the isogenic cell system were analysed for ALIX expression by western blot. Western blotting in Figure 4.11 clearly shows more ALIX protein in TC13, validating the SILAC result. Encouragingly, GAPDH showed no variation across all samples in the SILAC result, and western blot analysis confirmed no relative variation between ploidy states and clones (Figure 4.11B). However, rather than an up-regulation in the tetraploid clone, there is down-regulation only in DC14 and all other clones showed expression similar to the tetraploids, suggesting DC14 has abnormal expression and the difference is probably due to clonal variance (Figure 4.11C). As this was not a general phenotype of all diploids, the ALIX protein was not investigated any further.

A

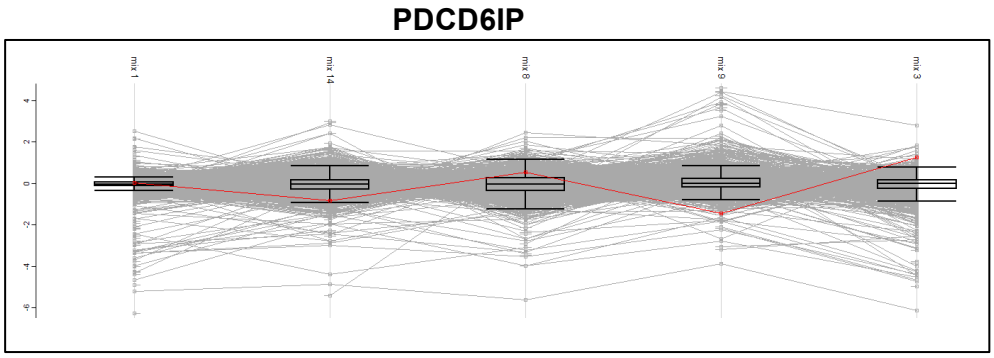

B

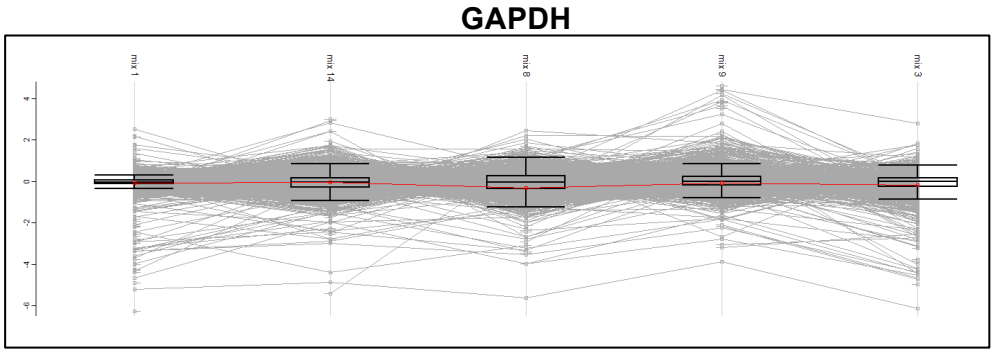

C

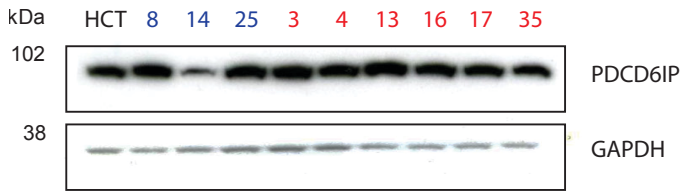

Figure 4.11 PDCD6IP (ALIX) and GAPDH plots and validation

Profile plots for displaying protein ratios each SILAC sample. (A) PDCD6IP and (B) GAPDH. (C) Western blot validation of PDCD6IP for all clones. GAPDH loading control.

4.4.6.2 NDRG1

The tumour suppressor N-myc downstream-regulated gene 1 (NDRG1) was found to have reduced expression in early and late tetraploid cells by approximately 3-fold relative to DC14 (Figure 4.12). NDRG1 is an α/β hydrolase and has been implicated in suppression of metastasis in colon, prostate and breast cancer (Bae et al., 2013). Elevated NDRG1 expression has been shown to be predictive of cellular stress and the protein can be induced by p53 (Bae et al., 2013). Experiments in human DLD-1 colorectal cancer cell lines have demonstrated NDRG1 is required for p53-dependent apoptosis (Bae et al., 2013). The SILAC result indicated lower expression of NDRG1 in the tetraploid cell line, which may support the tetraploid phenotype by suppression of the p53 response (Figure 4.12A). Western blot analysis of all clones suggested that the SILAC technique had quantified the abundances correctly in DC14 and TC13 (Figure 4.12B). Western blotting revealed that NDRG1 may be depleted in TC13, however again the depletion was likely due to clonal variation and not ploidy specific.

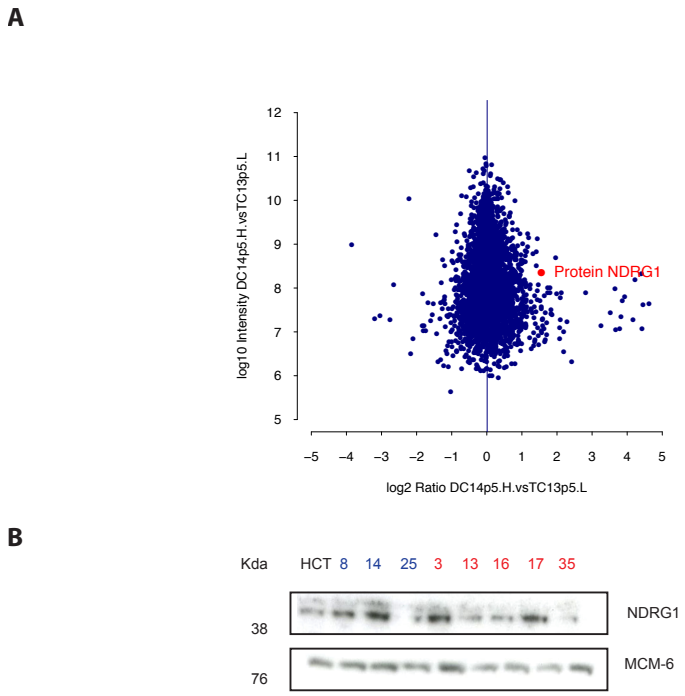

Figure 4.12 NDRG1 scatter plots and validation

A) SILAC scatter plot displaying NDRG1 expression ratio. B) NDRG1 western blot validation for all isogenic system members. MCM-6 acts as the loading control.

4.4.6.3 Kinesins

The kinesins KIF4A, KIF20A and KIF22 were present in the enrichment list for the tetraploid cell line and a manual review of the SILAC data revealed KIFC1 to be also enriched by approximately 50%, suggesting kinesins may provide an important role in tetraploid cells (Table 4.2 and Figure 4.13A.)

KIFC1 has been described to participate in an important role in centrosome clustering (Kwon et al., 2008). The kinesin has been shown to be an essential factor for centrosome clustering in tetraploid cells with abnormal numbers, but is dispensable in normal diploid cell lines (Kwon et al., 2008). This rendered KIFC1 into an attractive therapeutic target, as inhibition of KIFC1 should selectively kill cancer cells with amplified centrosomes and spare normal diploid cells, reducing toxicity. It has been shown by Sally Dewhurst that tetraploids have supernumerary centrosomes, compared to diploids (Appendix). Therefore overexpression might facilitate centrosome clustering, permitting survival. The SILAC data showed that KIFC1 is upregulated in the tetraploid cell line (Figure 4.13B). However, western blot analysis of all clones showed that the SILAC result did not validate and expression was similar between clones.

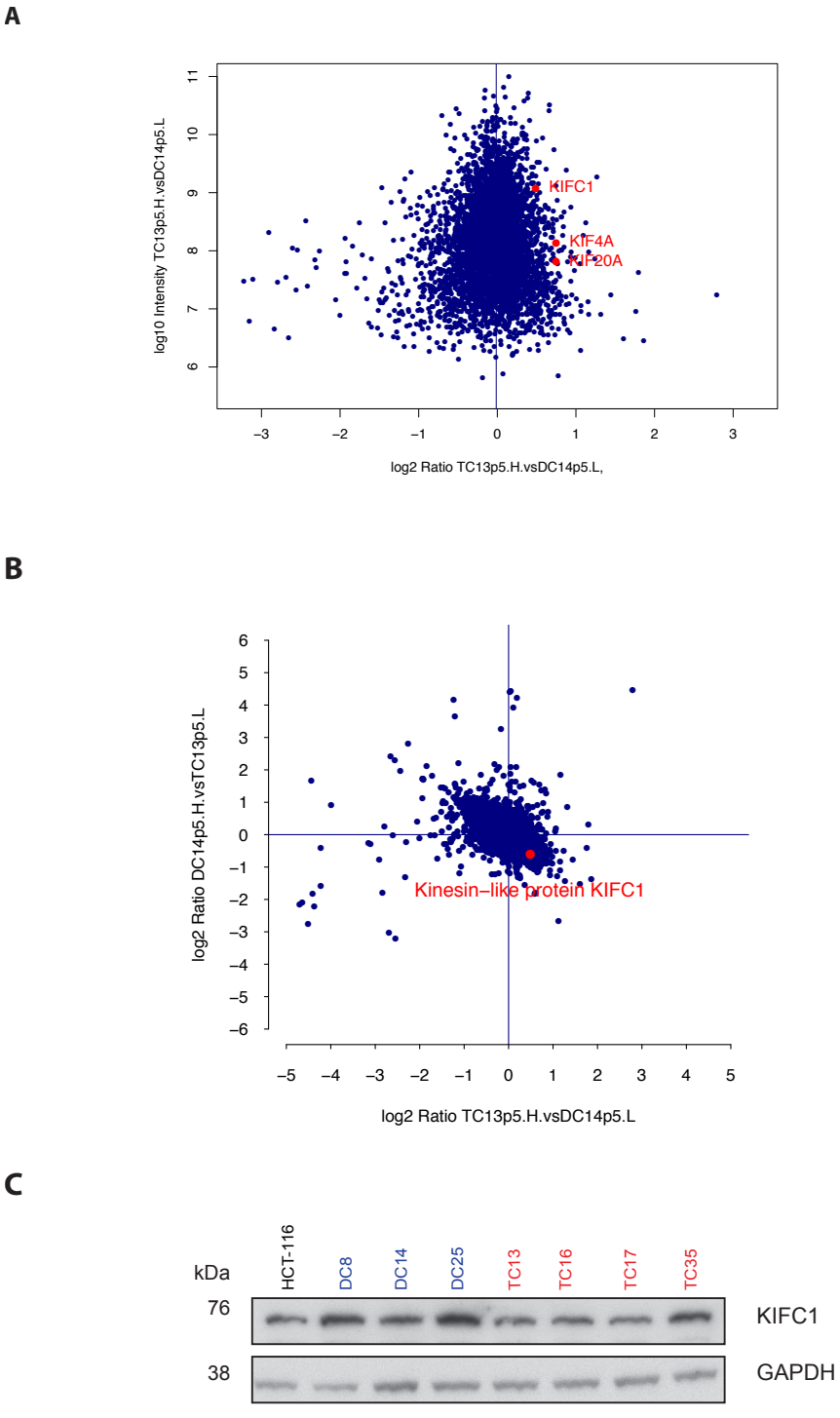

Figure 4.13 Kinesin scatter plots and validation

(A) Scatter plot for mix 3 showing enriched kinesins. (B) Correlation plot for mix 3 versus mix 9 displaying KIFC1 enrichment in both samples. (C) Western blot analysis of KIFC1 protein in all clones.

4.4.6.4 Cyclin D1

Manual analysis of the data, investigating proteins that showed good inter-replicate experiment correlations, revealed cyclin D1 could be elevated in the tetraploid samples. In ‘mix 3’ versus ‘mix 9’ cyclin D1 was approximately 2-fold greater in TC13 relative to DC14 (Figure 4.14A, B). In the later passage samples, cyclin D1 showed slight increase in ‘mix 14’ but was not detected in the duplicate control experiment. Western blot analysis of all clones in the isogenic system revealed cyclin D1 was elevated in four out of six clones (Figure 4.14). Quantification by densitometry and comparison of the diploid and tetraploid averages revealed a 4.9-fold increase in tetraploid cyclin D1 protein expression. Although cyclin D1 was detected by SILAC, the signal intensity was low which can hinder quantification and may explain the discrepancy between the two techniques.

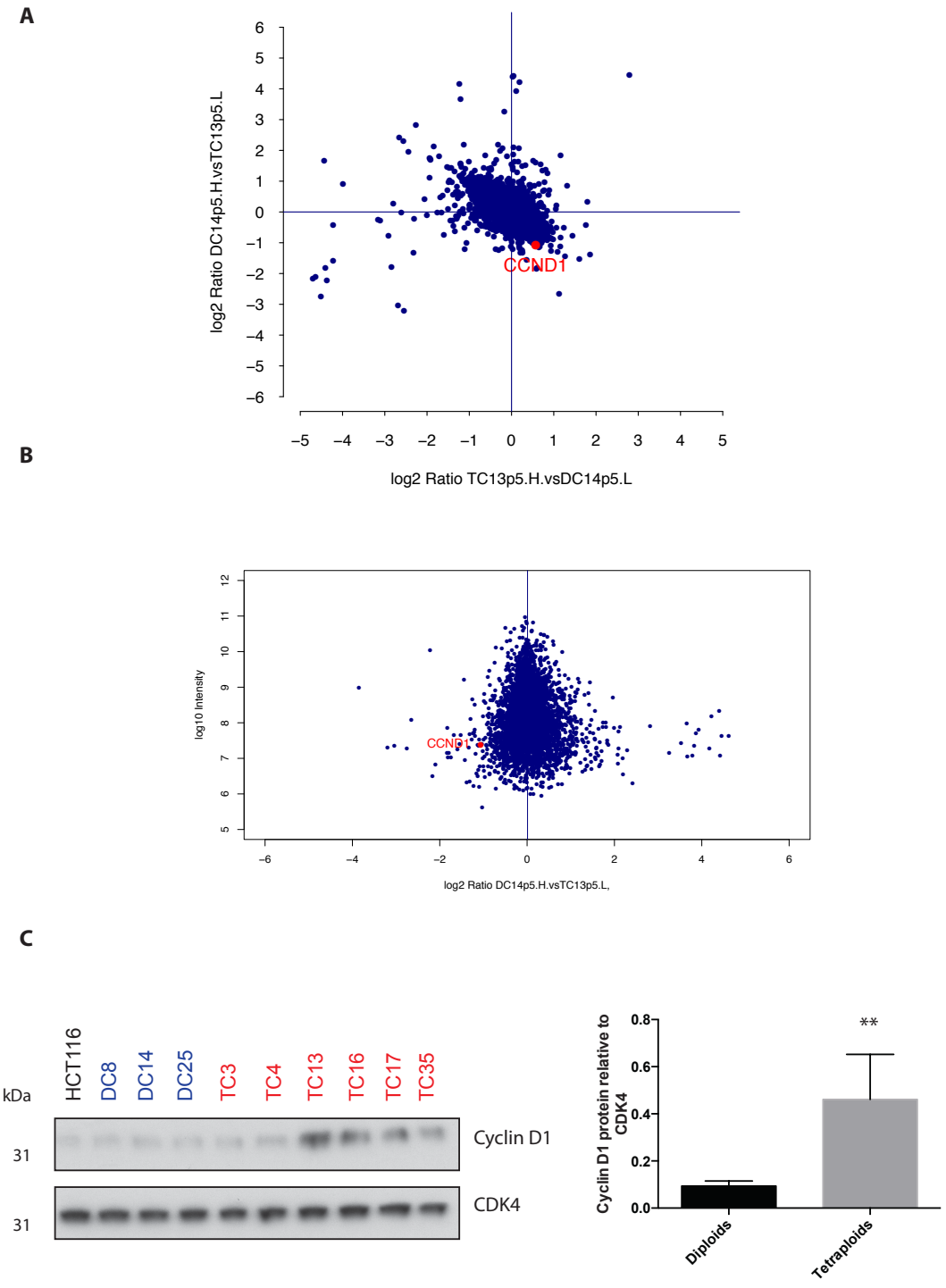

Figure 4.14 Cyclin D1 scatter plots and validation

(A) Correlation scatter plot displaying protein abundance. The X-axis represents the tetraploid/diploid protein ratios with the Y representing the inverse (diploid/tetraploid), and reveals tetraploid enrichment of cyclin D1. (B) Raito of protein abundance (tetraploid/diploid), relative to signal intensity displaying cyclin D1 enrichment. (C) Western blot validation and quantification of cyclin D1 in all early clones (p8-10); CDK1 was used a loading control.

4.5 Phosphoproteomics

The SILAC experiments have attempted to quantify total protein differences between a diploid and tetraploid cell line pair. The total protein global differences between DC14 and TC13 were apparent but not extreme, and it was possible there would be a greater difference in the phosphoproteome (proportion of total protein phosphorylated) of the diploid and tetraploid cells. Phosphorylation is an immensely important process that regulates many biological systems and global quantitative phosphoproteomics is a powerful tool that allows the quantification and identification of current and novel phosphorylation sites between multiple samples.

4.5.1 Principle of quantitative phosphoproteomics

As the phosphopeptides present in the sample represent only a fraction of the total protein, they needed to be separated from the sample to produce an enriched phosphopeptide fraction that can be analysed by MS/MS (Macek et al., 2009). This approach involved use of a combination of strong cation exchange (SCX) chromatography and titanium dioxide (TiO_2) enrichment. SCX is a form of ion exchange chromatography that utilises differences in molecular charge for separation. At pH 2.7, un-phosphorylated peptides have a charge of +2 due to protonation of the N-terminus amino group and the C-terminus arginine or lysine (Macek et al., 2009). If the peptide gains a negatively charged phosphate, the charge of the overall peptide charge will fall to +1. The phosphopeptide can then be eluted independently of the non-phosphorylated form by a salt gradient, as the phosphorylated species will be bound with less affinity (Macek et al., 2009). Further enrichment is achieved by mixing the separated phosphopeptides with TiO_2 spherical porous particles, which absorb organic phosphopeptides in acidic conditions and can then be de-absorbed in alkaline conditions (Macek et al., 2009). This combination of techniques provides a powerful phosphopeptide enrichment process permitting analysis of the phosphoproteome by mass spectrometry and peptide sequencing.

4.5.2 Phosphoproteomic analysis of DC14 and TC13

DC14 and TC13 cell lines, previously labelled with ‘heavy’ and ‘light’ lysine and arginine isotopes for conventional SILAC, were lysed, digested and their phosphopeptides enriched before relative quantification between the two samples (Figure 4.15). The analysis revealed that six TNIK phosphopeptides, implicated in WNT-pathway signalling were depleted in the tetraploid cell line. However, TNIK total protein levels were also depleted, suggesting the decrease in phosphorylation is a result of protein reduction rather that altered phosphorylation status. The experiment did not reveal any changes in phosphorylation that were not a result of differential protein expression and suggests the phosphoproteome was relatively similar between the two samples.

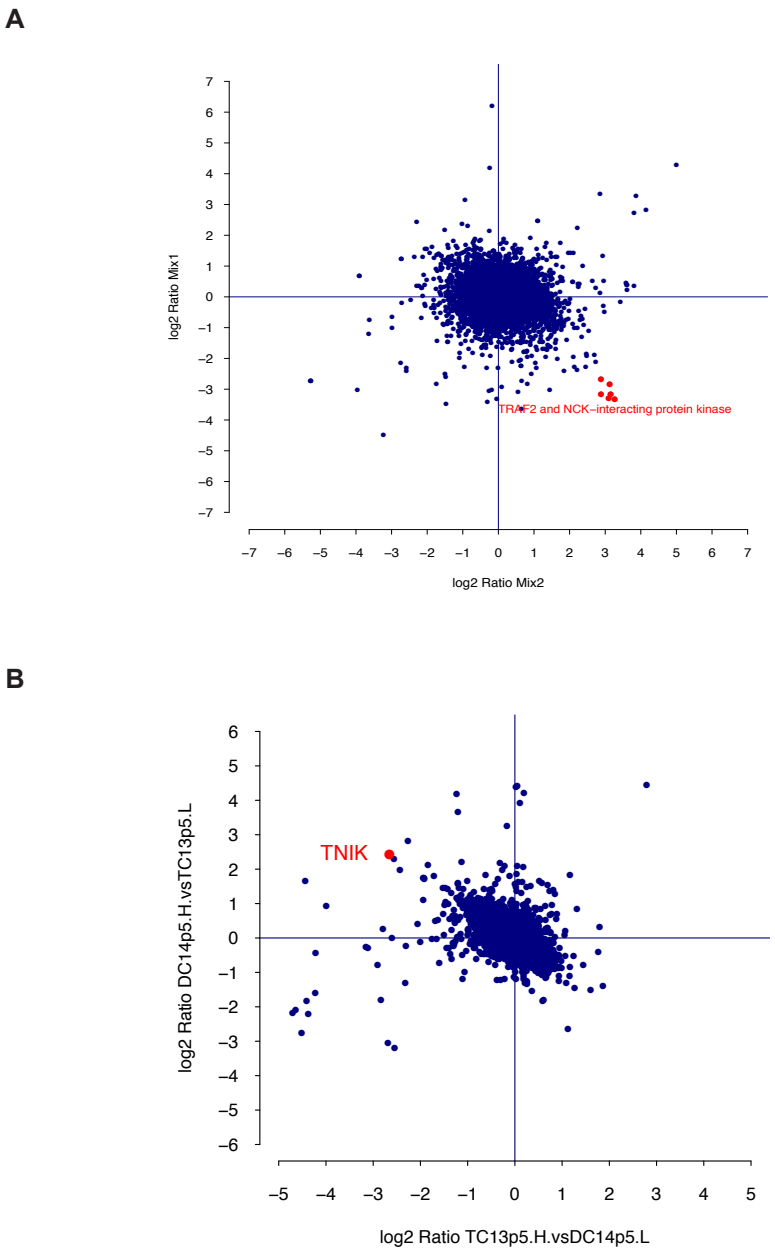

Figure 4.15 Phospho-TNIK detection and total protein comparison

(A) Phosphoproteomics revealed depleted phosphorylation of six TNIK peptides in TC13. (B) Total protein SILAC showed elevated protein amount in tetraploids is responsible for result.

4.6 Discussion and Conclusions

The primary aim of this of the study presented in this chapter was to utilise quantitative proteomics to explore differences in the proteome between diploid and tetraploid clones that may provide tetraploidy tolerance. The principle finding was cyclin D1 overexpression, which was validated by western blot and will be discussed in great detail in the following chapter.

The SILAC assay performed well and good correlations were achieved between replicate experiments. The number of proteins covered in replicate experiments was 3,896 and although satisfactory, a greater depth would allow detection of less abundant proteins that may be contributing to tetraploidy tolerance.

Although 'hit' validation was successful in all but one proteins investigated, demonstrating the sensitivity of the SILAC approach, in most cases the result only validated in the clones analysed and not other family members. In order for a 'hit' to fully validate, the enrichment or depletion was required to be specific to the tetraploids and in more than two individual clones. In order to reduce the probability of following up proteins that only show differences in expression between the diploid and tetraploid clones, as a result of clonal variation and not a specific ploidy effect, the whole isogenic family had to be analysed.

This would have allowed the detection of proteins specifically up-regulated in multiple tetraploid clones and increase the likelihood of discovering proteins involved in tetraploidy tolerance. Importantly, this would also permit a diploid/diploid comparison, which would demonstrate the proteomic variability of two cloned diploids, providing a control for the diploid/tetraploid analysis. If the diploid/diploid comparison was similar to that of the diploid/tetraploid, this would suggest that most of the proteomic differences were due to clonal variation and not ploidy status.

One possibility would be to compare all clones to a reference clone (e.g. DC8) and analyse in paired format through multiple independent SILAC runs. This analysis is possible, however to achieve a satisfactory proteome coverage for 8-10 clones would be immensely time-consuming, due to the low throughput nature of SILAC.

Tandem Mass Tag (TMT) technology can address this problem and has very recently become available to our laboratory. In contrast to SILAC metabolic labelling, TMTs are used to label peptides after cell lysis, with up to 10 samples labelled with different TMTs before multiplexing. The TMT with a known mass dissociates from the peptides of each sample after collision induced dissociation (CID) detection. This provides a unique reporter low m/z peak for each sample that is relative to peptide abundance in each sample and, thus, comparative abundances can be calculated. This technology therefore allows accurate quantification of global proteomic changes in multiple samples in a single mass spectrometry experiment. This new technique would allow analysis of all ten members of the isogenic system and would provide a more thorough and detailed analysis.

Phosphoproteomics revealed no significant changes in protein phosphorylation between DC14 and TC13, however based on the degree of clonal variability observed it would be wise to compare all clones. Although phosphorylation sites were enriched in the analysis, this was a result of increased total protein as opposed to a relative increase in phosphorylation. Differences in growth pathway signalling may have been overlooked by this analysis due to pathway saturation. High serum and growth factor levels may mask the activities of signalling pathways due to an excess of receptor stimulation (Gerlinger et al., 2012). A possible strategy that may be more effective at identifying differences in growth factor signalling involves starving the cells before analysis. After starvation for a defined period of time, cells could be stimulated with serum before analysis of phosphorylation status. This would yield information on the activity and strength of growth factor pathways in the two cell lines.

Pathway analysis was performed using the SILAC hits an attempt to identify more global changes. Previous research has shown that protein levels generally scale with gene copy number in aneuploid cells (Stingele et al., 2012, Pavelka et al., 2010). The SILAC data presented in this chapter supports this observation, as the tetraploid median expression value for all proteins detected was 2-fold grater than diploid values. In addition, the total protein amount on a per cell basis shows a near doubling of protein in tetraploid clones.

Gene ontology analysis of the 50 most enriched and most depleted proteins revealed several changes in biological processes and molecular pathway between the diploid and tetraploid clones. Pathways or processes commonly up-regulated in the tetraploid clones included organelle organisation and biogenesis, protein localisation, mitosis, chromatin and chromosome organisation and DNA packaging. These findings are in contrast to Stingele *et al*, who showed that similar pathways are down-regulated in trisomic and tetrasomic cell lines (Stingele et al., 2012). On the other hand, Stingele *et al* showed up-regulation in pathways implicated in endoplasmic reticulum regulation, carbon metabolism, mitochondrial metabolism, Golgi vesicles and lysomes. One similarity between the two investigations was the up-regulation of biosynthetic pathways in aneuploid and tetraploid cells. Stingele *et al* showed elevations in lipid membrane biogenesis, while the proteomics analysis identified elevations in tetraploid organelle synthesis.

Pathway analysis for depleted proteins in the tetraploid clones revealed convergence on two biological systems involving oxidative-reduction processes and response to metal ions. These data might be suggestive of a suppression of metabolic pathways in tetraploids, in contrast to Stingele *et al.* The likely reason for this is that in the present study tetraploid cells were compared to diploids, whereas Stingele *et al* compared aneuploid cells possessing one extra chromosome to diploids. The global imbalances caused by a single chromosome defect may be different to those caused by tetraploidy, resulting in discrepancies between the two studies. However, as the late tetraploids are likely to be aneuploid, they may show are more aneuploid-like profile. Indeed, a study investigating aneuploid cells after a tetraploid intermediate, showed mRNA profiles were highly similar to trisomic cell lines (Durrbaum et al., 2014). The present study was designed to identify proteomic irregularities that could provide essential tetraploidy tolerance, which would be required in both early and late passages. Therefore, ‘hit’ calling parameters were set to identify protein differences in both sets of clones. This strategy may have excluded aneuploid specific differences in late clones. It is possible that some of the traits identified by Stingele *et al* are exclusively present in late tetraploids and therefore would not have been considered a hit. Nevertheless, many of the deregulated pathways in early and late tetraploids presented in this chapter were

the complete opposite compared to Stingele *et al,* suggesting there are fundamental differences between the studies. Therefore, in addition to analysis of more clones, a more detailed analysis of enrichment and depletion profiles at multiple passages would be beneficial. This could provide insight as to how the proteome changes over time with increasing CIN and emerging aneuploidy.

The most significant finding in this chapter was cyclin D1 overexpression in the tetraploid early clones. Validation of cyclin D1 revealed an elevation in the second generation clones only. These clones were derived from DC8 and the result might suggest that the second-generation tetraploid clones were derived from a subclonal population with high cyclin D1 expression. A low frequency subclonal cyclin D1 tetraploid population in the DC8 cell line was unlikely to be detected by western blotting given the total tetraploid fraction is only 0.5%. Alternatively, as the age of TC3 and TC4 are unknown, they may have acutely expressed cyclin D1 before more efficient tolerance mechanisms were initiated (Figure 3.1). As cyclin D1 expression reproducibly validated by western blot and has been implicated in p21 sequestration (LaBaer et al., 1997), it was taken forward as the lead 'hit' and chapter 6 explores its role in tetraploidy tolerance *in vitro* and in human tumours.

Chapter 5. Cyclin D1 overexpression and tetraploidy tolerance

5.1 Introduction

Quantitative proteomics detected cyclin D1 overexpression in the early tetraploid clones. The aim of this chapter was to investigate if elevated cyclin D1 expression could provide tetraploid tolerance. Based on the previously discussed findings, (section 1.2.3.3), it was hypothesised that the observed elevations in tetraploid p21 could be inhibited by high cyclin D1 expression in HCT-116 tetraploid clones. An elevation in Cyclin D1-CDK4 complexes could sequester heightened p21 protein levels, limiting CDK2-Cyclin E1 binding. Evidence for overexpression of cyclin D1 being able to promote tetraploidy was provided by Casimiro *et al*, who showed that cyclin D1 overexpression in MEFs enriched the number of 8N polyploid cells from approximately 5% to 15% within 3 divisions (Casimiro et al., 2012). .

The primary objective of this chapter was to investigate how cyclin D1 is elevated and whether the expression corresponds spatially and temporally to p21 expression in HCT-116 isogenic system. The binding of p21 to CDK4 and CDK2 and the effect on the catalytic activity of the latter was also assessed. In addition, cyclin D1 overexpression was performed in RPE cells, which have an unperturbed G1/S control, to investigate if cyclin D1 could permit tetraploid tolerance. Furthermore, D-type cyclin expression was also explored in genome-doubled p53 wild-type tumours.

5.2 Cyclin D1 characterisation in the isogenic HCT-116 system

In order to investigate the role of cyclin D1 in the HCT-116 isogenic system, the protein was analysed by a variety of techniques. Expression, stability, localisation and complex formation were all analysed, before overexpression in parental HCT-116 cells.

5.2.1 Cyclin D1 expression is elevated relative to other cyclin members

Quantitative proteomics revealed an elevation of cyclin D1 (Chapter 4) in the tetraploid clones and may provide tolerance by counteracting high p21 levels by sequestration. To investigate whether increased expression of cyclin D1 was specific, relative to other cyclins, the diploid and tetraploid clones were analysed by western blot for the expression of cyclin A1, B1, D1 and E1. The analysis clearly showed that only cyclin D1 was elevated in the tetraploids, indicating a specific deregulation that suggests that cyclin D1 might be implicated in the tetraploid tolerance phenotype (Figure 5.1A).

5.2.2 Elevated p53 and p21 are not directly responsible for elevated cyclin D1 levels in tetraploid clones

It is possible that the observed tetraploid increase in p53 and p21 is responsible for increased cyclin D1 levels, as p21 can stabilise cyclin D1 (LaBaer et al., 1997). To investigate the relationship between p53, p21 and cyclin D1 overexpression, *TP53* mRNA was silenced by siRNA (Figure 5.1B). As observed in previous experiments, p21 expression was solely p53-dependent (Figure 3.8H). It was also clear that a reduction in p53 or p21 resulted in a partial reduction of cyclin D1 (Figure 5.1B). This was obvious in the diploids and the tetraploids and most likely reflects the loss of p21-CDK4-Cyclin D1 complexes, although a role for p53-dependent regulation cannot be ruled out. Although cyclin D1 levels were reduced in all clones after p53 and p21 loss, there was still an elevation in the tetraploid clones (Figure 5.1B). Therefore, the increased levels of p53 and p21 cannot be directly responsible for increased cyclin D1 expression in the tetraploid clones, suggesting other mechanisms are contributing.

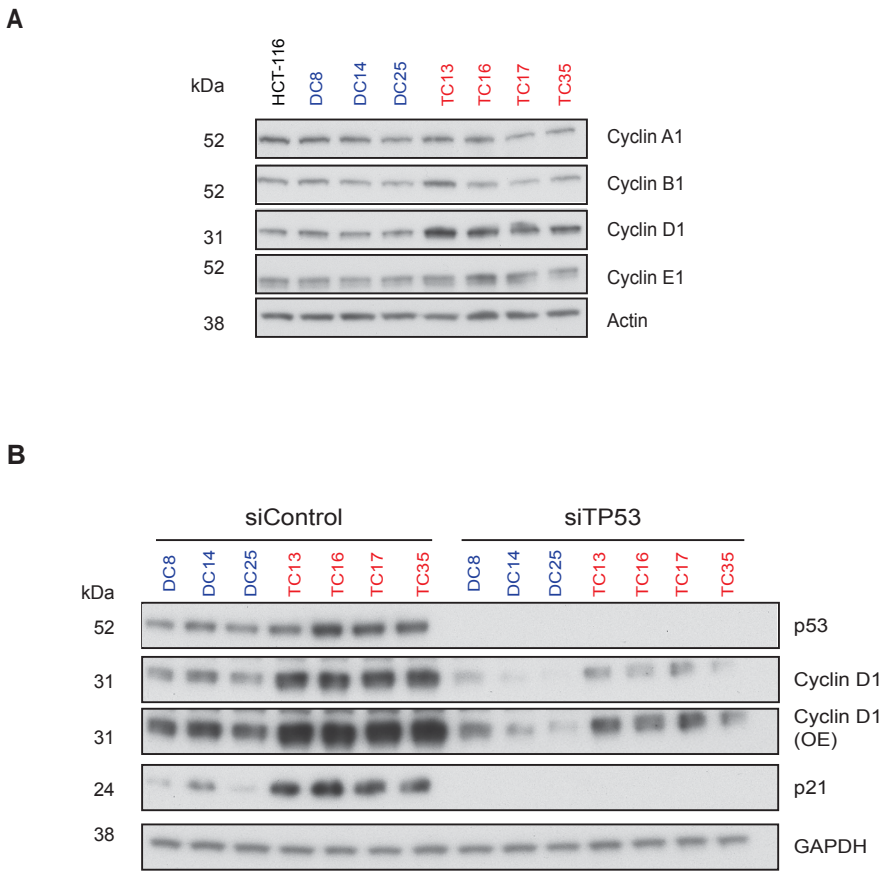

Figure 5.1 Cyclin expression levels and p53 knockdown

(A) Comparison of all major cyclins in the diploid and tetraploid clones. Representative of two independent experiments (B) Western blot analysis after *TP53* knockdown in clones. siTP53 oligos were incubated with cells for 72 hours before western blotting. GAPDH and actin were used as a loading control. (OE): overexposure. Representative of three independent experiments.

5.2.3 Tetraploid clones have elevated cyclin D1 mRNA expression and enhanced ERK pathway signalling

The heightened levels of cyclin D1, observed in the tetraploid clones, could be explained by a corresponding increase in RNA levels. CCND1 mRNA was quantified by Q-PCR, which revealed an increase in the transcript levels. All tetraploid clones had elevated CCND1 mRNA and TC13 showed the greatest change of just over 2-fold (Figure 5.2). On average, the tetraploid clones had 1.64-fold more CCND1 mRNA than the diploid clones ($p = 0.0062$; Figure 5.2B). As CCND1 was elevated, relative to GADPH, it is unlikely that the increase in the transcript was a function of genome-doubling. *CCND1* amplifications are common in human tumours and result in cyclin D1 overexpression (Musgrove et al., 2011). Previous studies in our lab investigating chromosome copy number showed that tetraploids had no gain of chromosome 11q (Dewhurst et al., 2014), suggesting other mechanisms are responsible for mRNA induction.

CCND1 is a transcriptional target of many growth-signalling pathways, like RAS/ERK (Musgrove et al., 2011). To investigate whether the tetraploid clones had elevated ERK signalling, cells were serum-starved for 24 hours, before re-addition over a defined time-course. The activation of the pathway was determined by western blot analysis of total and phospho-ERK (Figure 5.2C). Three of the four tetraploid clones displayed enhanced signalling, compared to a diploid counterpart. This experiment was performed in diploid *versus* tetraploid-paired format (by random pair assignment), which allowed multiple time points to be analysed. All diploid clones showed an activation of the ERK pathway after serum addition, which was delayed when compared to tetraploids. Of note, clones TC13 and TC16 still showed ERK signalling at time 0, 24 hours after serum starvation and addition of serum did not enhance the activity of the pathway any further. This suggests that under serum deprivation, the tetraploids can maintain a greater basal level of ERK pathway activation and an increase upon serum is not observed, as the pathway is already saturated. However, although TC17 had a similar basal level of signalling, serum addition produced a stronger response compared to DC8 clone. In contrast, TC35 showed no activation of the pathway compared to DC25. Together these

results provide evidence that ERK signalling may be enhanced in the tetraploid clones, which could account for the elevated CCND1 mRNA expression.

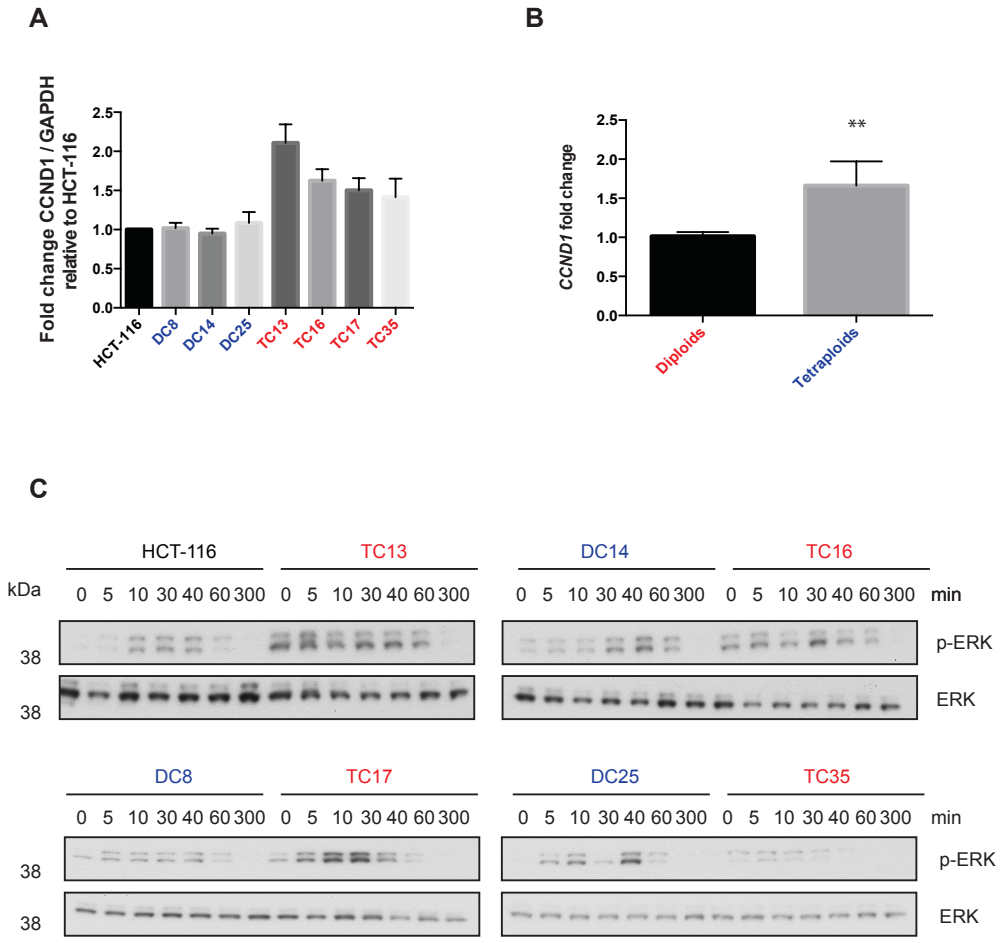

Figure 5.2 Cyclin expresion levels and ERK signaling

(A, B) CCND1 mRNA quantification. Error bars represent SD (B) Quantification of CCND1 mRNA pooled in diploids and tetraploids. (C) ERK pathway activation. Cells were serum starved for 24 hours before 10% serum addition. Cells were lysed, before immunoblotting for total and p-ERK. Upper band ERK1 (p44), lower band ERK2 (p42). Representative of two independent experiments.

5.2.4 Cyclin D1 protein stability is enhanced in tetraploid clones

The 1.6-fold elevation in CCND1 transcript does fully explain the 4.9-fold increase in protein measured in Figure 4.14 and suggests other mechanisms may be contributing to the overexpression. Given the importance of cyclin D1 overexpression, resulting from stabilisation by post-translational mechanisms (Alao, 2007), cyclin D1 stability was assessed in the diploid and tetraploid clones. I was hypothesised that increased protein stability in combination with enhanced mRNA expression might be accounting for the observed cyclin D1 elevation. Therefore, cells were treated with cycloheximide (CHX) and harvested at different time points, before western blotting for cyclin D1 (Figure 5.3).

In all cases, cyclin D1 was more stable in the tetraploid clones. For technical reasons, analysis was performed in a paired format (diploid versus tetraploid). Comparison of DC8 vs TC13 and DC14 vs TC16 revealed that the greatest difference in protein stability was at 30 and 20 minutes respectively, with a rapid decline in diploid cyclin D1 in both cases. HCT-116 vs TC17 and DC25 vs TC35 showed a more subtle difference, although cyclin D1 was consistently more stable in the tetraploid clones, with the greatest difference at 40 minutes. These findings suggest, in addition to an increase CCND1 mRNA, that cyclin D1 is stabilised at the protein level, resulting in elevated expression. A sharp increase in cyclin D1 is observed in three out of four diploid versus tetraploid comparisons after approximately 20 minutes of CHX-mediated inhibition of translation. One possible explanation for this observation is the activity of other regulatory mechanisms that were not investigated, as the primary objective was to assess cyclin D1 stability.

The experiment was repeated analysing p53 stability (Appendix). The spike observed for cyclin D1 was not observed in the p53 analysis, suggesting this quality is specific to cyclin D1 regulation and not a technical artefact of the experiment. These data suggest the cyclin D1 is stabilised and may be a contributing factor fuelling the elevation in cyclin D1 that could counteract and sequester elevated p21.

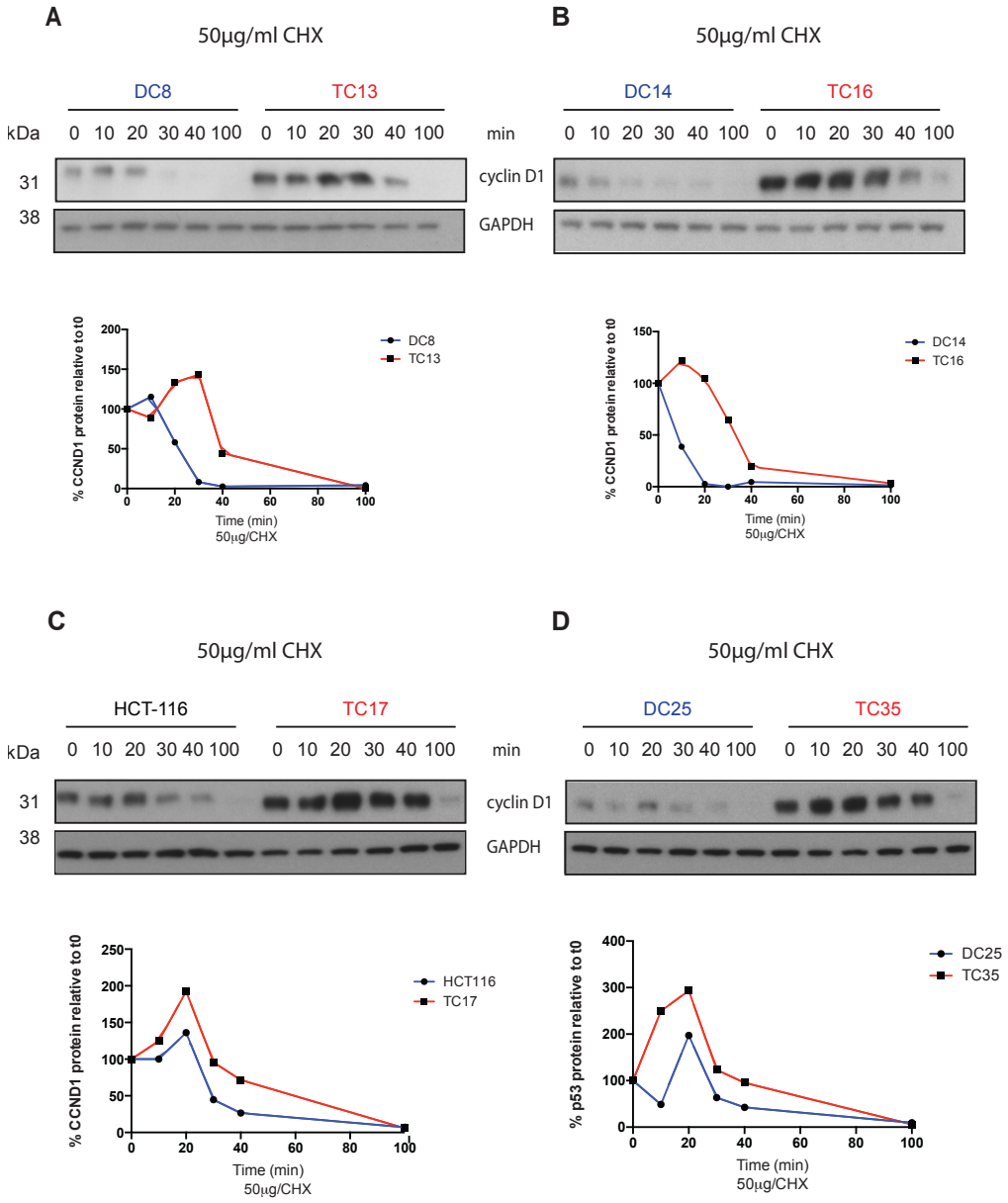

Figure 5.3 Cyclin D1 protein stability

(A—D) A comparison of cyclin D1 protein stability between diploid and tetraploid clones. Cells were treated with 50µg/ml cycloheximide and incubated at 37°C for the indicated times. Cells were lysed, before immunoblotting and western blotting for cyclin D1. For quantification, cyclin D1 protein was normalised to GADPH before expression as percentage relative to 0 minutes. Representative of two independent experiments.

5.2.5 Tetraploid clones display heightened cyclin D1 phosphorylation

As previously discussed, in section 1.2.3.1, phosphorylation of cyclin D1 at Thr286 by GSK3-β results in its nuclear export and its subsequent ubiquitin-mediated degradation by the PCF4 complex. Therefore, a possible mechanism of cyclin D1 protein stabilisation might be mediated through reduced Thr286 phosphorylation and nuclear retention, or inactivation of the PCF4 complex. Analysis of the exome sequencing data revealed no mutations in members of the PCF4 complex (mechanism discussed in section 1.2.3.1), suggesting that the protein would be ubiquitinated efficiently. Phosphorylation of cyclin D1-Thr286 was significantly elevated (1.6-fold; $p \leq 0.05$) in the tetraploid clones, implying increased nuclear export, as opposed to nuclear retention by hypo-phosphorylation in the tetraploid clones (Figure 5.4A and B). This result implies stabilisation is maintained through another mechanism.

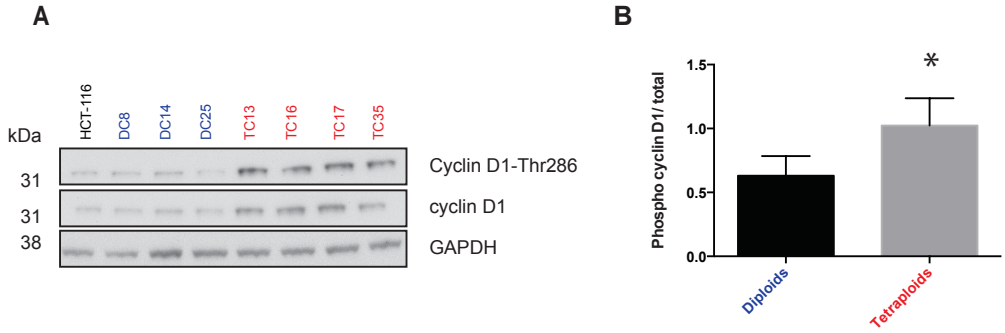

Figure 5.4 Cyclin D1-Thr286 phosphorylation

(A) Levels of cyclin D1 phospho-Thr286 in the diploid and tetraploid clones. (B) Quantification of the phosphorylated Thr 286 cyclin D1 fraction by densitometry. Error bars represent SD. Representative of two independent experiments. * p= <0.05.

5.2.6 Tetraploid cyclin D1 expression is elevated in all cell cycle phases and co-localises with raised p21 in the cytoplasm and nucleus

The increase in cyclin D1-Thr286 phosphorylation, observed in Figure 5.4, might result in more cytoplasmic cyclin D1. Increased cytoplasmic cyclin D1 tetraploids would challenge the hypothesis that elevated cyclin D1 is sequestering p21 from CDK2. Alternatively, the elevation could be a result if an increased S phase (Figure 3.13). Cyclin D1-Thr286 phosphorylation occurs during S phase, rapidly reducing cyclin D1, as expression in this phase inhibits replication. Prolonged S phase may result in further tetraploid cyclin D1 reduction, compared to diploids. Low S phase cyclin D1 could free p21 and cause S phase arrest in tetraploids (Zhu et al., 2004).

The distribution of cyclin D1 throughout the cell cycle was investigated by flow cytometry in the diploid and tetraploid clones. The analysis revealed an elevation of tetraploid cyclin D1 in all phases of the cell cycle (Figure 5.5A). The average fold change of tetraploid cyclin D1, relative to diploids, was 1.4 in G1, 1.6 in S and 1.4 in G2/M (Figure 5.5B). Cyclin D1 levels were reduced in S phase, in both diploids and tetraploids by 32% and 19% respectively, relative to G1. This is a small but significant ($p \leq 0.05$) difference, suggesting that cyclin D1 export and degradation in the tetraploids is less efficient and elevated cyclin D1 transcends the cell cycle.

To explore cyclin D1 subcellular distribution, cytoplasmic and nuclear fractionations were carried out in the diploid and tetraploid clones (Figure 5.5C). Purity of the distinct fractions was determined by mutual exclusivity of the nuclear protein histone H2B (Kanda et al., 1998). The levels of p21 were greater in both the nucleus and cytoplasm in tetraploid clones (Figure 5.5C), consistent with earlier experiments (Figure 3.9). In addition, p53 levels were higher in the tetraploid clones and again were exclusively nuclear (Figure 5.5B). Importantly, cyclin D1 levels were high in the nucleus and cytoplasm, suggesting that elevated p21 levels may be actively sequestered in the cytoplasm and nucleus.

Taken together, these two experiments indicate that elevated nuclear p21 levels are accompanied by elevated cyclin D1 and despite an increased S phase, which

likely results in elevated cyclin D1-Thr286, nuclear cyclin D1 levels are still higher in tetraploid clones and expression is higher in all other cell cycle phases.

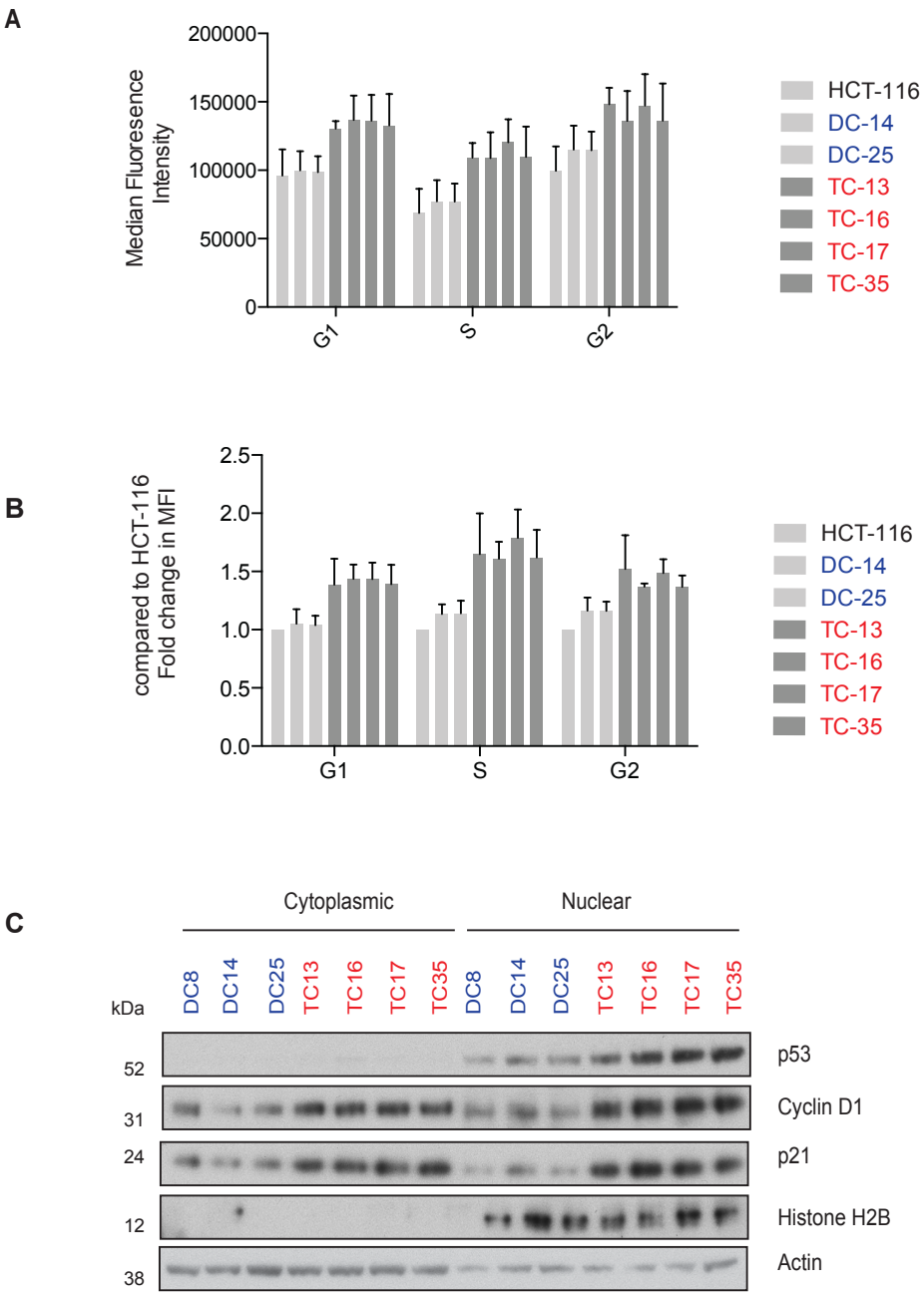

Figure 5.5 Flow cytometry analysis and cyclin D1 localisation

(A) All clones were stained for cyclin D1 analysed by flow cytometry. The median fluorescence intensity was calculated and plotted for each cell cycle phase.(B) Fold change in cyclin D1 median fluoresce intensity (MFI) relative to HCT-116 for all clones. Error bars represent SD, N=3. (C) Cellular fraction of the diploid and tetraploid clones. Actin served as loading control and histone H2B as a fractionation control. Representative of three independent experiments.

5.2.7 Preliminary immunoprecipitations reveal elevated tetraploid p21-CDK4-cyclinD1 complexes

The previous data suggest that cyclin D1 is elevated in tetraploid clones and may sequester high p21 levels. To investigate the status of CDK4 and CDK2 complexes, in relation to cyclin D1 and p21 binding, immunoprecipitations (IPs) were performed. The rationale behind these experiments was that the presence of high CDK4-Cyclin D1-p21 complexes and low CDK2-Cyclin E1-p21 binding in the tetraploids, relative to the diploids, would provide evidence for p21 sequestration by cyclin D1.

As expected, CDK4 IPs in the tetraploids showed equal protein levels (Figure 5.6A). CDK4-bound cyclin D1 was variable between clones and not specifically increased in the tetraploids as expected. The level of p21 binding was far greater in the tetraploids, although was also marginally detectable in diploid clones. This observation suggests that the high tetraploid p21 is in complex with CDK4. The same principle was applied for CDK2 (Figure 5.6B). Again, cyclin E1 was highly variable between all clones and not tetraploid-specific. The level of CDK2-CyclinE1-p21 binding was elevated in the tetraploids, possibly suggesting inhibition of the kinase and disagrees with the aforementioned hypothesis. However the diploid clones also showed p21 binding to CDK2. This is in agreement with the hypothesis that most CDK2 is p21-bound and only a small, unbound fraction is required for proliferation (Planas-Silva and Weinberg, 1997).

The activities of CDK4 and CDK2 were tested by kinase assays (Figure 5.6C). Endogenous CDK4 and CDK2 was immunoprecipitated from cycling cells incubated with ^{32}P-labelled ATP and kinase activity on RB monitored. The CDK4 assay in Figure 5.6C shows variability and no specific difference between the clones. DC8 and TC17 possessed the highest activity, whereas DC14 had the lowest. CDK2 activity was also variable but, as with CDK4, all clones showed more activity than the mock, suggesting activation. Again, DC8 showed the greatest activity, with TC35 also exhibiting high levels. These results clearly demonstrate the degree of clonal variability in the isogenic system. Nevertheless, the kinase assays provided evidence for CDK4 and CDK2 activity in the tetraploids, despite

elevated p21 binding and support the hypothesis that p21-CDK association is non-inhibitory in the tetraploids, possibly as a result of elevated cyclin D1.

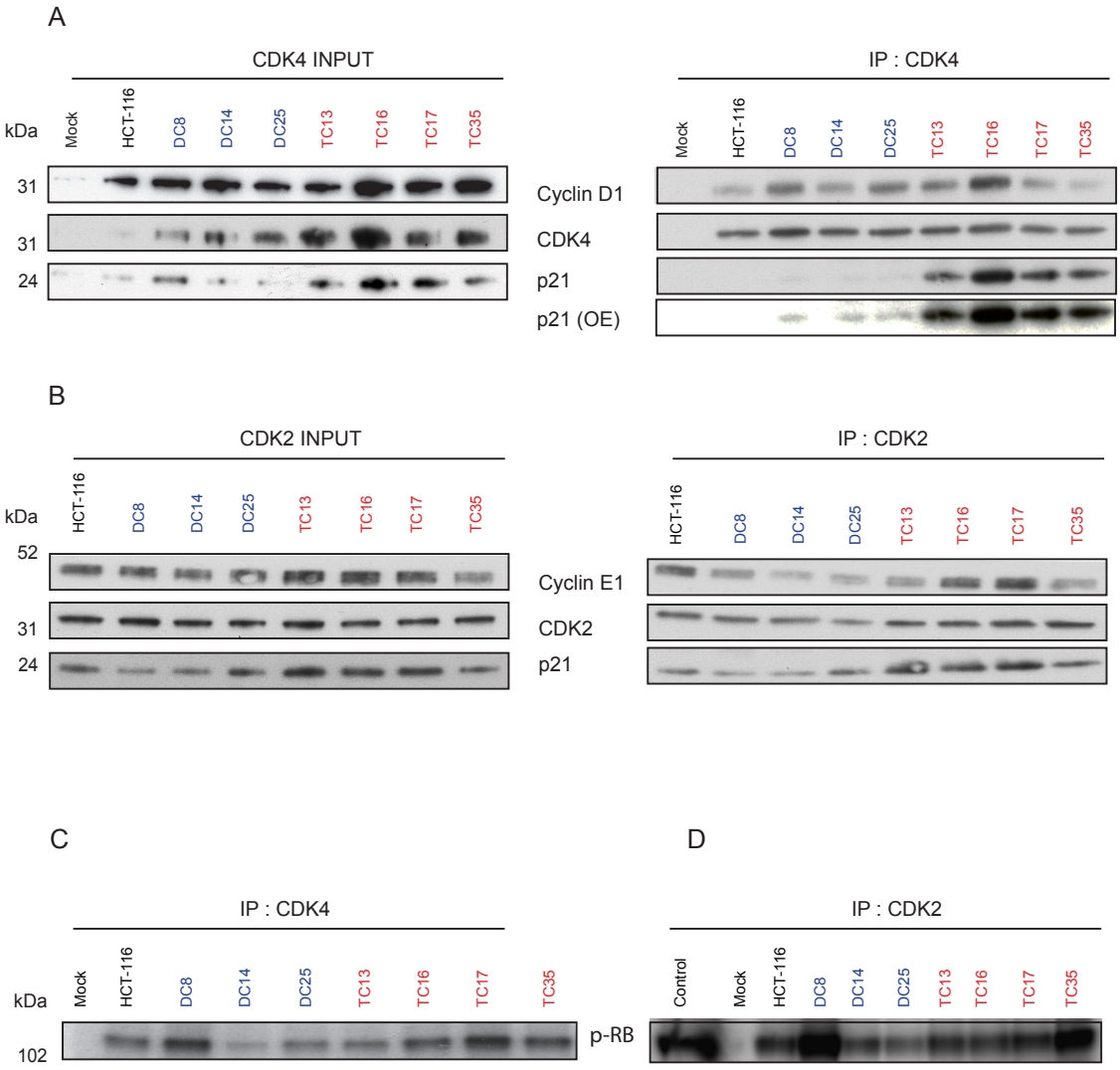

Figure 5.6 Preliminary CDK4 and CDK2 immunoprecipitations and kinase assays

(A) CDK4 input and CDK4 IP. All clones were lysed and Immunoprecipitated of CDK4. Lysates were separated by SDS-PAGE before immunoblotting. Representative of three independent experiments. (B) CDK2 input and CDK2 IP. All clones were lysed and Immunoprecipitated of CDK4. Lysates were separated by SDS-PAGE before immunoblotting. Representative of two independent experiments. (C) CDK4 kinase assay. Endogenous CDK4 was immunoprecipitated as above. CDK4 pull downs were incubated with radiolabeled 32P ATP substrate and full length RB. Signal was measured by radiography. (D) Kinase assay repeated for endogenous CDK2. Both kinase assays representative of two independent experiments.

5.2.8 Cyclin D1 overexpression in parental HCT-116 cells does not increase the basal tetraploid population

Results in this chapter have indicated that cyclin D1 overexpression in tetraploid cells might inhibit the activity of p53-induced expression of p21. In addition, the elevated p21 expression, in the presence of increased cyclin D1 protein, appears to support increased CDK4-cyclin D1-p21 formation, which appears to maintain RB phosphorylation at critical residues required for G1/S transition, possibly by sheltering CDK2 from p21 inhibition. Conceivably, therefore, elevated Cyclin D1 expression may provide insight into the tetraploidy tolerance mechanism. Consistent with this hypothesis, previous studies have shown that overexpression of cyclin D1 in MEFs results in an enhanced 8N tetraploid fraction, suggesting cyclin D1 can promote or at least be permissive for tetraploidization (Casimiro et al., 2012).

In order to investigate whether cyclin D1 could increase the fraction of newly generated tetraploids, the *CCND1* gene was overexpressed by viral infection in the parental HCT-116 cells (Figure 5.7A), after which cells were allowed to expand, before propidium iodide staining and flow cytometry analysis (Figure 5.7B). The HCT-116 vector control cells displayed an average 8N fraction of 0.18% compared to 0.21% ($p = 0.5626$) of CCND1 overexpressing cells, showing no significant increase in the spontaneous formation of tetraploid cells (Figure 5.7C). Therefore, this indicates that HCT-116 cells do not behave the same way as MEFs. This could be due to the fact that MEFs are prone to genomic instability when successively passaged in culture, in contrast to HCT-116 cells. Therefore it is possible in MEFs CCND1 overexpression facilitates an already inherent mechanism. The degree of sensitivity in the current assay may also be unsatisfactory, and this topic is discussed in section 5.5.

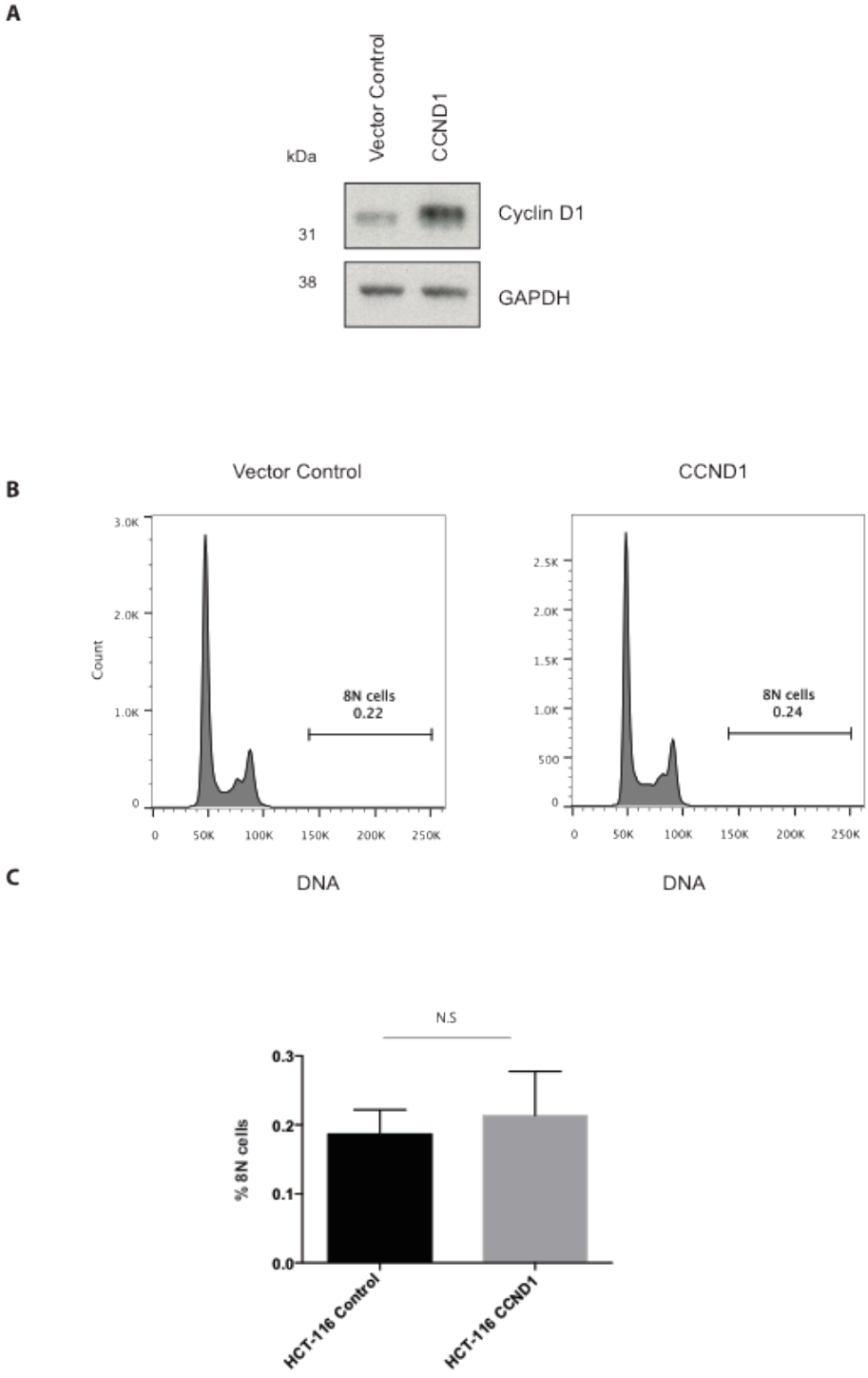

Figure 5.7 CCND1 overexpression in HCT-116 cells

(A) Western blot analysis displaying the level of CCND1 overexpression. (B) Representative DNA ploidy plots for HCT-116 vector control and *CCND1* overexpression. Un-synchronised cells harvested in the exponential growth phase before staining with PI and analysis by flow cytometry. (C) Percentage of 8N tetraploid control and *CCND1* cells. Error bars represent SD, N=3.

5.3 Cyclin D1 overexpression in RPE pharmacologically-induced tetraploids

The work in the isogenic HCT-116 tetraploid system has revealed cyclin D1 as a protein possibly implicated in tetraploid tolerance within a $p53^{+/+}/p21^{+/+}$ background. However, due to the variable nature of the clones and their high mutational frequency, driven by the MSI of this cell line, definitively showing that cyclin D1 is providing a survival advantage has been challenging in this system (*see section 5.5)*. However, this work in combination with the defined role of cyclin D1 in p21 regulation hints at the possible ability of the protein overriding the p53/p21-dependent tetraploidy checkpoint.

5.3.1 Generation of tetraploid RPEs

In order to generate a more controlled system, the retinal pigment epithelial cell (RPE) line was used. RPEs are stable diploid cells, have a normal p53 response and undergo G1 arrest upon chemical induction of tetraploidy (Ganem et al., 2014). Therefore, inducing tetraploidy in RPE cells allows the investigation of mechanisms that can override the p53-dependent G1 tetraploidy checkpoint.

To induce tetraploidy, cells were treated with 2μM dihydrocytochalasin B (DCB), a drug that inhibits actin polymerisation and contractile ring formation, inducing cytokinesis failure and formation of tetraploid (Fujiwara et al., 2005). DCB treatment results in a mixed population of diploid and tetraploid cells and distinguishing between them presents a technical challenge. A solution to this problem is to utilise the Fucci reporter system (Newman and Zhang, 2008). The Fucci reporter system expresses hCdt1-Cherry (cdt1) and hGem-green (geminin). Cdt1 is a member of the pre-recognition complex involved in origin licensing and is rapidly degraded and inhibited in S and G2/M phases by ubiquitination by geminin, a protein exclusively expressed in late S-G2/M (Newman and Zhang, 2008). Flow based cell-sorting analysis allows sorting of G1 (red) tetraploids from G2 (green) diploids and thus provides an elegant method to distinguish between different phases of the cell

cycle. Distinct populations of cells can be sorted before seeding and assessment of cell survival or other downstream assays (Figure 5.8).

To investigate whether cyclin D1 overexpression can permit the survival of newly formed $p53^{+/+}$/ $p21^{+/+}$/ $RB1^{+/+}$ RPE-Fucci tetraploid cells, cyclin D1 was stably overexpressed by viral infection and the stable cell lines were characterised (Figure 5.8). Western blot analysis and immunofluorescence confirmed cyclin D1 overexpression in the RPE cells (Figure 5.8A, B) and proliferation kinetics were investigated by construction of a growth curve (Figure 5.8C). All three conditions were in the lag phase until 12 hours. After this, cyclin D1 cells entered the exponential phase, although the controls remained in the lag phase for a further 12 hours. The exponential doubling times between RPE-Fucci (15.03h), RPE-Control (14.86h) and CCND1 cells (16.25h) revealed no overwhelming difference. Therefore, cyclin D1 overexpression reduces the lag phase, resulting in an initial increase in cell number. As the control cells enter the exponential phase and proliferate at the same rate, the increase of cyclin D1-cells remains constant at ~1.7-fold.

In order to see if cyclin D1 overexpression increased the basal tetraploid fraction in the RPE-Fucci, RPE-Control and RPE-CCND1 cell lines, ploidy was determined by flow cytometry (Figure 5.9). RPE-Fucci had a basal >6N faction of 0.015% compared to 0.020% in the CCND1-overexpressing cells. This finding suggests that tetraploidy is rare or poorly tolerated in the RPE cell line. This makes the model a good system to investigate if cyclin D1 overexpression can provide tetraploid tolerance after pharmacological induction, due to a low number of endogenous polyploid cells, which would only enhance the detection of viable DCB-induced tetraploid cells.

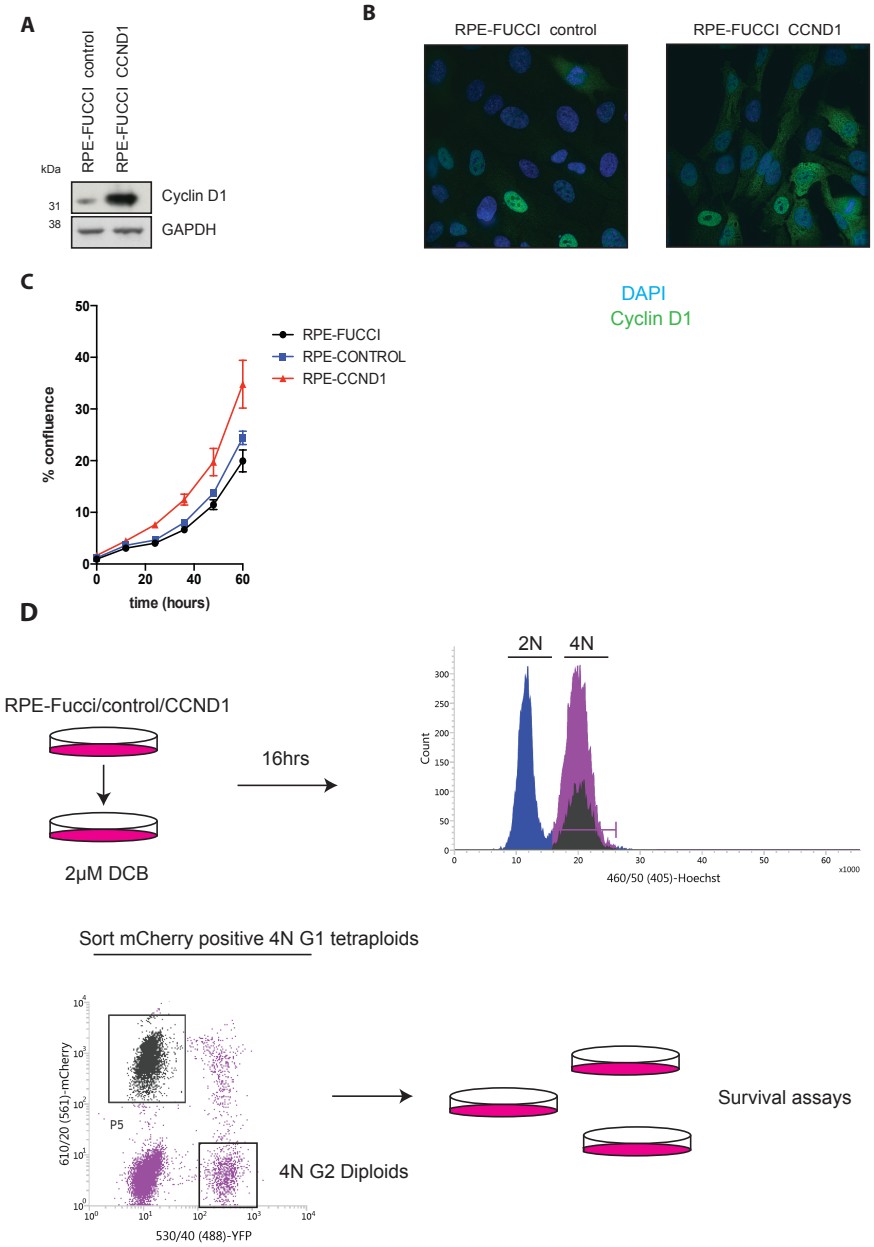

Figure 5.8 Cyclin D1 overexpression and experimental strategy in RPE-Fucci

(A) Western blot validation of CCND1 overexpression RPE-Fucci cells. (B) CCND1 expression tests by immunofluorescence. (C) Growth curves for RPE-Fucci, control and CCND1 cells. Cells were plated and cell surface area coverage was calculated. Error bars represent SD (D) Experimental procedure used to isolate tetraploid cells. Cells were seeded before treatment with 2μM DCB to induce cytokinesis failure and tetraploidy. Cells were analysed by flow cytometry to determine ploidy, and the 4N peak containing cycling G2 diploids (black peak) and DCB induced G1 tetraploids (purple peak), was sorted to isolate the G1 tetraploids. This was achieved by selecting G1 mCherry positive 4N cells, before plating for downstream assays.

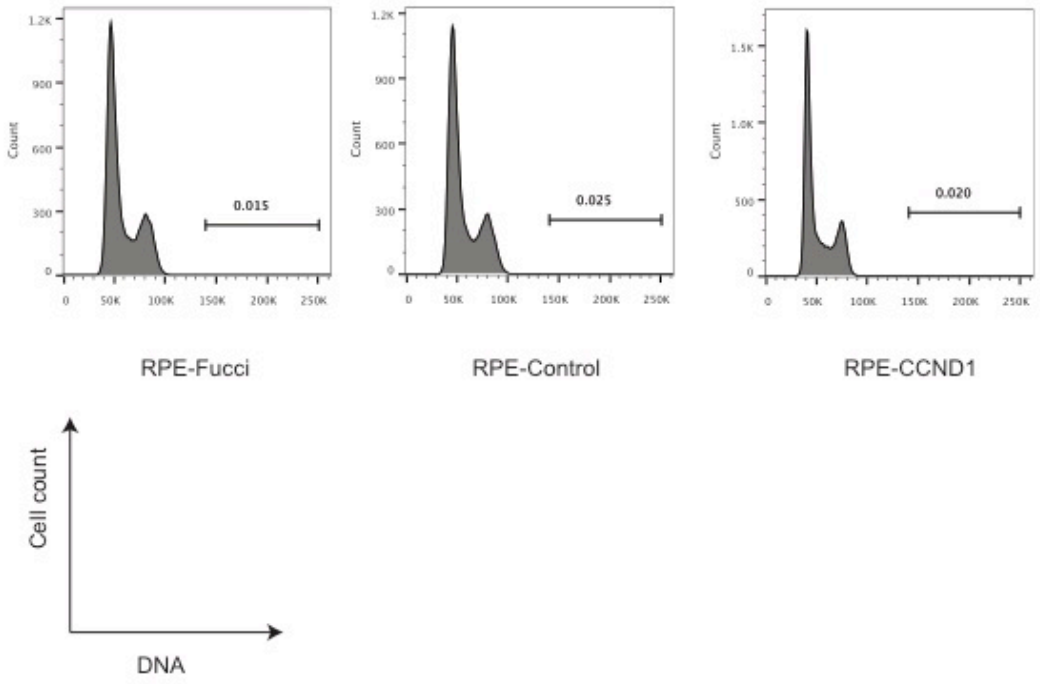

Figure 5.9 RPE baseline 8N fraction

DNA ploidy plots for RPE-Fucci, RPE-Control and RPE-CCND.1 Un-synchronised cells were harvested in the exponential growth phase before stained with PI and subjected to ploidy analysis by flow cytometry. Representative of two independent experiments.

5.3.2 Cyclin D1 overexpression in DCB induced tetraploids promotes the bypass of G1 arrest and entry into G2 phase

Induction of tetraploidy by DCB results in a 4N population of cells arrested at G1 and this can be observed in the DNA ploidy plots which correspond to the sorted populations. DCB treatment produced a 4N G1 arrest in approximately 50% of cells, represented by an increased G2/M peak (Figure 5.8D). The percentage of cycling tetraploid cells can be determined by calculating the fraction of 8N cells within the total population (Figure 5.10A). An 8N population represents tetraploid cells that have passed through the G1 tetraploidy checkpoint, replicated their DNA and entered the G2/M phases of the cell cycle. The RPE-Fucci and RPE-control cells had an average 8N fraction of 2.4% and 2.6% respectively ($p = 0.8303$) (Figure 5.10B). In contrast, the RPE-cyclin D1 cells possessed an average 8N of 13.8%, indicating a respective 5.7 ($p= 0.0013$) and 5.3 ($p=0.0021$) fold increase, compared to RPE-Fucci and RPE-control cells (Figure 5.10B). These data provide evidence that tetraploid cyclin D1-overexpressing cells are able to override the tetraploidy-induced G1 arrest and enter the G2/M phases of the cell cycle more efficiently.

These data also suggest that the difference is not simply due the shortened lag phase or elevated proliferation rate of CCND1 cells. The percentage of RPE-FUCCI-CCND1 8N cells increases post DCB tetraploidization. Therefore, even if the RPE-FUCCI-CCND1 cells are cycling faster, and thus would result in more G1 tetraploids being generated compared to controls, there is a relative increase in the 8N fraction above the expected background. Therefore, the findings of this experiment are directly comparable and are not simply a function of differential growth kinetics.

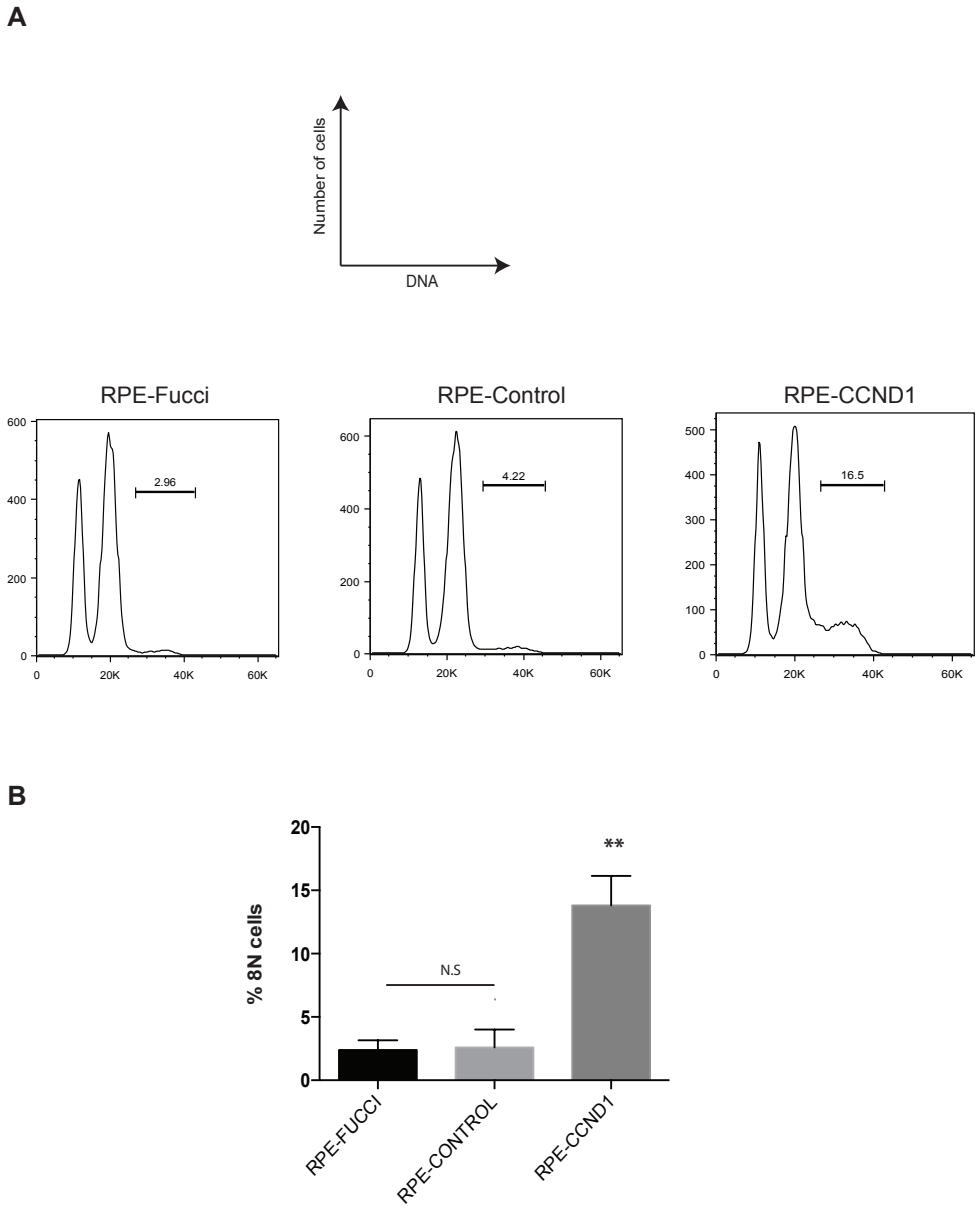

Figure 5.10 RPE 8N population quantification 16hrs post-DCB treatment

(A) DNA ploidy plots showing the percentage of 8N cells post DCB treatment and a comparative quantification. (B) Quantification of average percentage of 8N cells from three independent experiments P= <0.01. Error bars representative of SD.

5.3.3 Cyclin D1 overexpression provides tetraploid tolerance

The previous experiment quantified the number of tetraploid G2/M cells after a relatively short period of 16h hours. To investigate if cyclin D1-overexpressing RPE cells could propagate and tolerate the tetraploid phenotype over longer periods of time, cells from each condition were sorted by selecting G1 mCherry-positive cells, in order to specifically isolate G1 tetraploids from the 4N peak (Figure 5.8D). Cells were then seeded into multi-well plates before fixation and quantification of the green fluorescent G2/M cells. As p21 and p53 are key components of the tetraploidy checkpoint, they were silenced by siRNA after plating to act as positive to control, given that depletion of either protein would abrogate the checkpoint and allow G1 tetraploid cells to proliferate (Ganem et al., 2014).

The G2/M fraction of the RPE-Fucci and RPE-control tetraploid cells under untransfected, mock and control siRNA conditions was between 2-4% of cells (Figure 5.11A). TP53 and CDKN1A knockdown resulted in an increase of G2/M cells, consistent with the involvement of p53 and p21 in the tetraploidy checkpoint, although a high level of variability between experiments was observed in the untransfected and control conditions. CCND1-overexpressing cells displayed a G2/M population ranging between 9-12% across the untransfected, mock and control siRNA conditions, representing an average increase of 4-fold compared to RPE-Fucci cells (Figure 5.11B). The vector control displayed a slight increase of 1.5-fold relative to RPE-Fucci, however the fold change between RPE-CCND1 cells and RPE-control was highly significant under all conditions (2.6-fold on average). These data suggest that overexpression of cyclin D1 can override the tetraploidy checkpoint in RPE cells and sustain tetraploidy tolerance for at least 72 hours. Images obtained for the G2/M microscopy analysis (Figure 5.11C), clearly showed more G2/M cells in the CCND1 overexpressing cells.

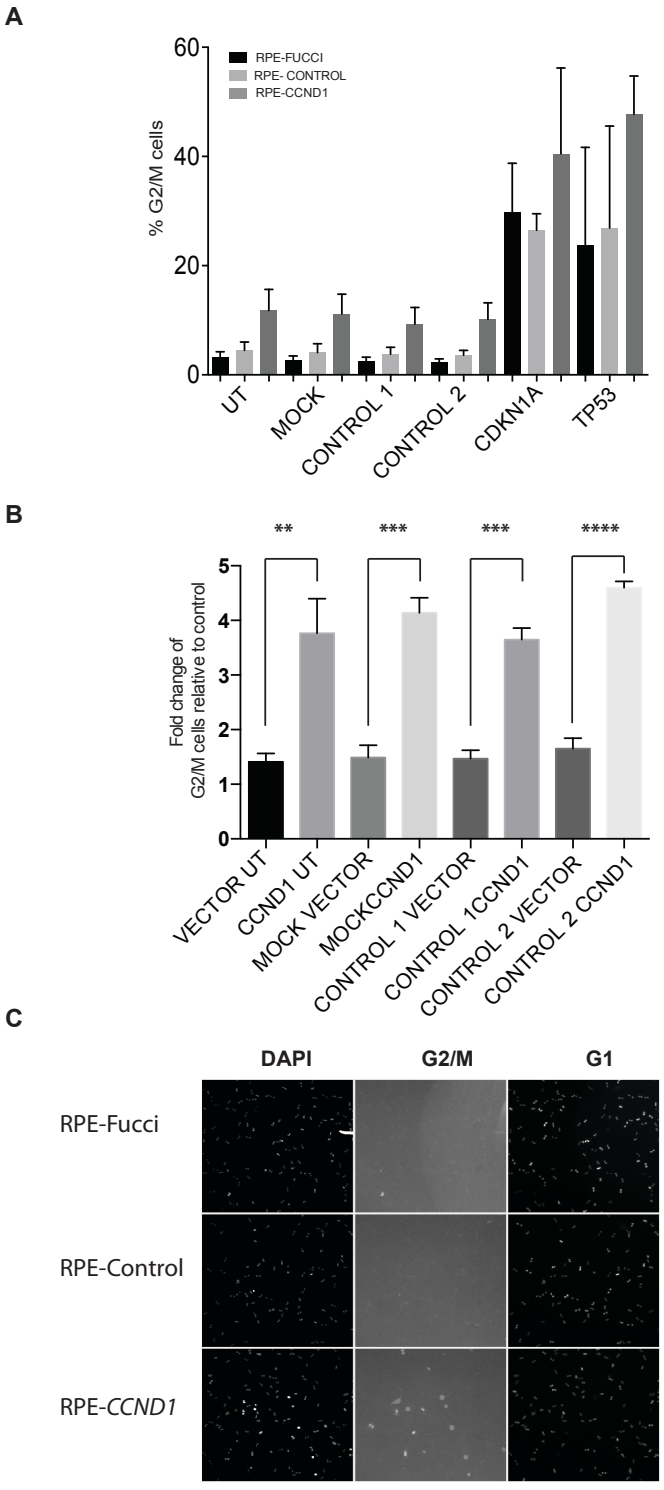

Figure 5.11 G2/M cells 72 hours post-DCB treatment

(A) Percentage of cyclin D1 cells 72 hours post-DCB treatment and TP53 and CDKN1A controls. Cells were plated after sorting and reverse transfected with the indicated siRNAs. (B) Fold change of control vector and CCND1 overexpressing G2/M cells relative to RPE-control. Error bars representive of SD. Unpaired stsudents t-test **, ***, ****p = ≤ 0.01, 0.01, 0.0001 respectively. (C) Microscopy images of fixed cells in G1 and G2/M phases of the cell cycle.

5.3.4 p53 and p21 are induced in RPE cells after tetraploidization by DCB treatment

TP53 and CDKN1A knockdown produced average fold changes in G2/M cells of 10-fold and 7.5-fold respectively, highlighting their importance in the response to tetraploidization (Figure 5.11A). To highlight this further and to investigate their expression dynamics, p53 and p21 were analysed by western blot after DCB-induced tetraploidization. In the RPE-Fucci and control cells there was no detection of p53 or p21 in diploid untreated cells, however after DCB treatment there was a time-dependent increase in both proteins (Figure 5.12A). In the RPE-CCND1 cells the basal levels of p53 and p21 were greater but also increased in time-dependent manner. In Figure 5.11, Cyclin D1 expression was reduced below normal RPE-Control cell line levels, shown in Figure 5.8A, which is consistent with a G1 arrest in the RPE-Fucci and control lines. The increase in cyclin D1 expression after 72 hours in the RPE-CCND1 cells could be a direct effect of p21 increase and, thus, stabilisation (Figure 5.12A).

In order to investigate if the same regulatory mechanisms were in place in the RPE cells as in the HCT-116 cells and specifically if there were any p21-CDK4-Cyclin D1 complexes forming, p21 was immunoprecipitated 72 hours after DCB treatment (Figure 5.12B). In the RPE-CCND1 cells there were more CDK4-Cyclin D1-p21 complexes, whereas in the RPE-Fucci and control cells there was p21 bound to cyclin D1 but less bound to CDK4. This may suggest a more catalytically active CDK4 in the RPE-CCND1 cells contributing to the enhanced survival and proliferation, which is consistent with observations in the HCT-116 system.

5.3.5 Cyclin D1 overexpression provides long-term tetraploid tolerance in RPE cells

To test if the CCND1 overexpression could provide an advantage to the tetraploid cells in a long-term clonogenic assay, DCB generated tetraploids were seeded at low density and allowed to form colonies over a 12-day period (Figure 5.12C). Untreated diploids were also analysed to obtain the plating efficiency (PE) for each condition. The diploid PE was similar between all conditions with RPE-Fucci, RPE-

control and RPE-Cyclin D1 displaying efficiencies of 25%, 19% and 18% respectively (Figure 5.12D). The tetraploid PE was calculated for each condition, 12 days post-DCB treatment, revealing an increase in colony formation in the RPE-CCND1 cells (D). The RPE-Fucci and control cells had plating efficiencies of 1.6% and 1.06% respectively, compared to 7.8% of RPE-CCND1 cells, representative of a 7.3-fold change relative to RPE-Control ($p \leq 0.01$). These data support the notion that tetraploidy is poorly tolerated and provides strong evidence that cyclin D1 overexpression can significantly enhance tolerance to tetraploidy over a prolonged period of time.

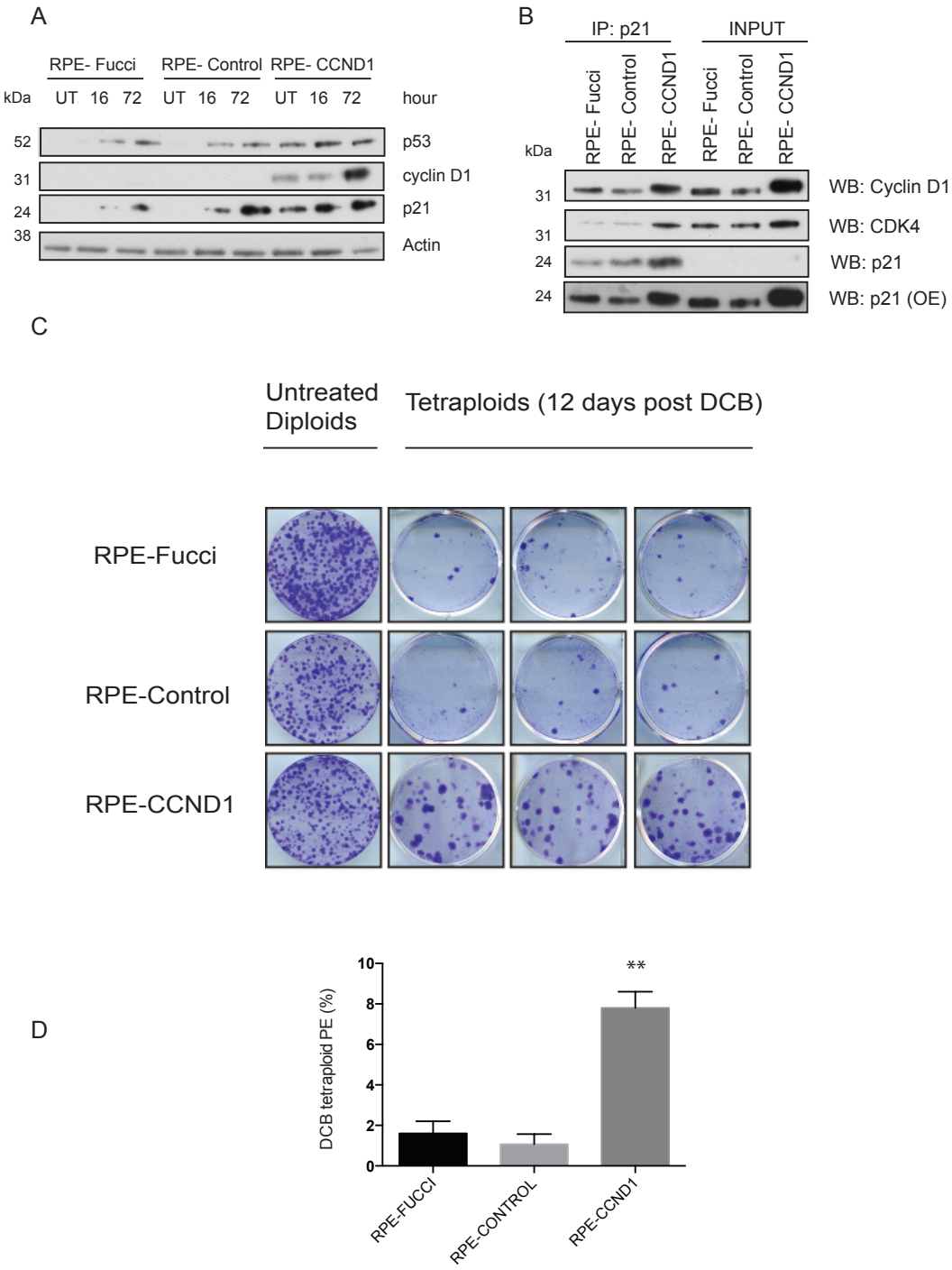

Figure 5.12 Molecular characterisation and survival benefit of the RPE system

(A) p53, p21 and cyclin D1 status at 0, 16 and 72 hour time points. Representative of two independent experiments. (B) p21 IP 72 hours post-DCB treatment showing complex formation with CDK4 and cyclin D1. Representative of two independent experiments. (C) DCB sorted tetraploid cells were plated in a long term clonogenicity assay for 12 days. Colonies were stained, counted and the surviving fraction was calculated. Error bars represent SD. Representative of two independent experiments.

5.4 D-type cyclin overexpression and tetraploid tolerance in human TGCTs

As discussed in section 3.5, 65% of genome-doubled tumours are *TP53* wild-type and understanding how tolerance is provided in this molecular setting is of great interest. One tumour group that show frequent genome-doubling and the absence of *TP53* mutations are Testicular Germ Cell Tumours (TGCTs). TGCTs affect young male adults and are the most frequent solid cancers in Caucasian males. TGCT consist of two major histological subtypes comprising of seminoma and non-seminomatous lesions. The two subtypes show marked differences in morphology but share many pathogenic genetic aberrations including hypertriploid karyotypes and gain of chromosome 12p (Gilbert et al., 2011). Gain of 12p occurs in approximately 80% of clinical cases and contains the *CCND2* locus.

All three D-type cyclins (*CCND1, CCND1* and *CCND3*) are closely related and 62% identical to each other. The greatest homology between the thee proteins is in the cyclin box domain which is required for CDK and CDK inhibitor binding (p21, p27 and p57), suggesting the G1/S and p21 sequestration functions of these three cyclins are highly conserved (Gilbert et al., 2011). Early stage TGCTs have been shown to be tetraploid and can become hypertriploid or hexaploid in later disease, providing evidence for tetraploidy as intermediate that precedes aneuploidy (Ottesen et al., 2004, Dewhurst et al., 2014). *TP53* mutations are rare in TGCTs (approximately 7%), and therefore, I hypothesised that the tetraploidy checkpoint is likely to be overridden by an alternative mechanism.

5.4.1 Genome doubled p53 wild-type TGCTs display elevated D-type cyclin copy number and expression

The previous data in this chapter provided evidence that CCND1 overexpression can mediate tetraploid tolerance in a *TP53* wild-type background. Due to the sequence homology and protein functions of *CCND1* and *CCND2,* it was hypothesised that CCND2 overexpression would also provide tolerance in the presence of wild-type p53 wild-type and might permit tetraploidization tolerance in TGCTs. Due time constraints, the involvement of CCND2 was not investigated in our experimental systems, however the clinical samples were analysed bioinformatically.

To explore whether D-type cyclins were associated with genome-doubled *TP53 wild-type* tumours, 117 testicular TCGA data based tumours were analysed (42 seminomas, 62 non-seminomas and 13 uncharacterised samples) for copy number and expression of *CCND1, CCND2* and *CCND3.* Genome-doubling was calculated by applying a modified version of the ABSOLUTE algorithm (Carter et al., 2012).

Genome-doubling occurred in all but one tumour, however there was only one tumour with a *TP53* or *CDKN2A* non-synonymous mutation and none with *RB1*, while all three genes were expressed in the remaining tumours. No tumours displayed *CDKN1A* mutations, suggesting a functional p21 pathway. Five out of 117 (4.2%) tumours displayed *MDM2* copy number gains, possibly suggesting p53 could be reduced by enhanced ubiquitination in this small fraction of tumours (Abdel-Fattah et al., 2000). Taken together, these results suggest that most of the analysed tumours are tetraploid with wild-type tetraploidy checkpoint components and imply that another tetraploidy tolerance mechanism exists.

Copy number analysis revealed copy number gains in *CCND2* (98%) and *CCND3* in a smaller proportion of tumours (4.2%), while *CCND1* gains were not observed (Figure 5.13A-C). CCND2 mRNA expression correlated with gene copy number and showed a positive correlation in the seminoma subtype. The non-seminomas did not correlate as strongly, with some tumours displaying lower CCND2 expression relative to copy number (Figure 5.14A). CCND1 expression correlated

with CCND2 in both subtypes and revealed the non-seminomas had greater CCND1 expression than the seminoma (Figure 5.14B). The CCND2 low tumours were also CCND1 low, demonstrating CCND1 is not compensating for low CCND2 expression. Interestingly, when CCND3 expression correlated with CCND2, an inverse relationship was observed with CCND3 high cells expressing lower levels of CCND2 (Figure 5.14C). This finding may suggest that in non-seminoma tumours with lower CCND2 expression, despite elevated CCND2 copy number, CCND3 expression may serve to compensate for CCND activity. These data, combined with the observation that cyclin D1 overexpression can provide tolerance to tetraploidy *in vitro,* strongly suggests that the D-type cyclins might contribute to tetraploidy tolerance in TGCTs.

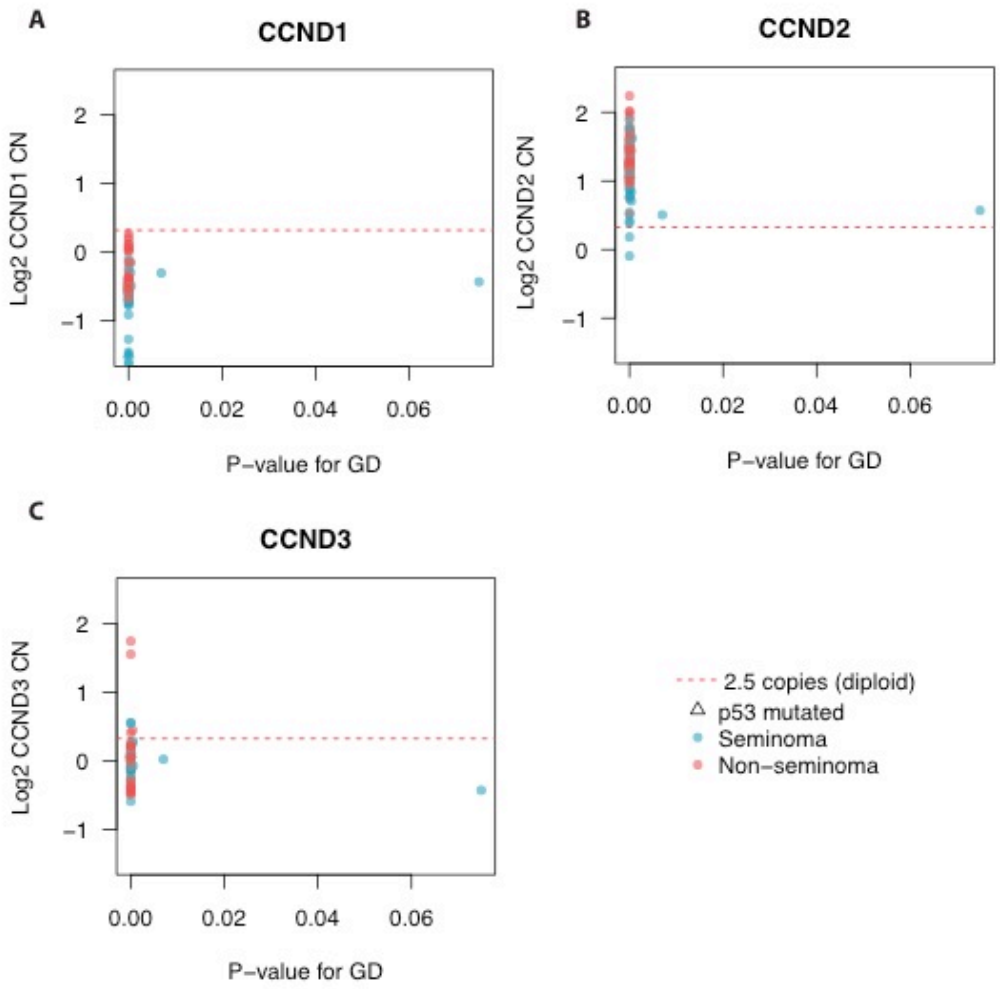

Figure 5.13 CCND1, CCND2 and CCND3 copy number in TGCT

(A-B) Copy number analysis of *CCND1*, *CCND2* and *CCND3* in 117 seminoma and non-seminoma TGCTs. TGCT SNP data and matched normal samples were downloaded from the TCGA database and processed as described in Materials and Methods.

Interestingly, correlation of CDKN1A and CCND1 mRNA expression revealed a significant positive correlation ($p \leq 0.0001$) and was evident in both seminoma and non-seminoma TGCT subtypes (Figure 5.15A). A correlation between CDKN1B and CCND1 was observed in seminoma tumours but not non-seminoma, suggesting the effects seen are not a general function of CCND1 overexpression (Figure 5.15B). Analysis of CCND2 and CDKN1A showed no significant correlation, although here was strong positive correlation when compared to CDKN1B (Figure 5.15C and D). These findings further support the hypothesis that cyclin D1 overexpression can circumvent high p21 expression and possibly provide tetraploidy tolerance.

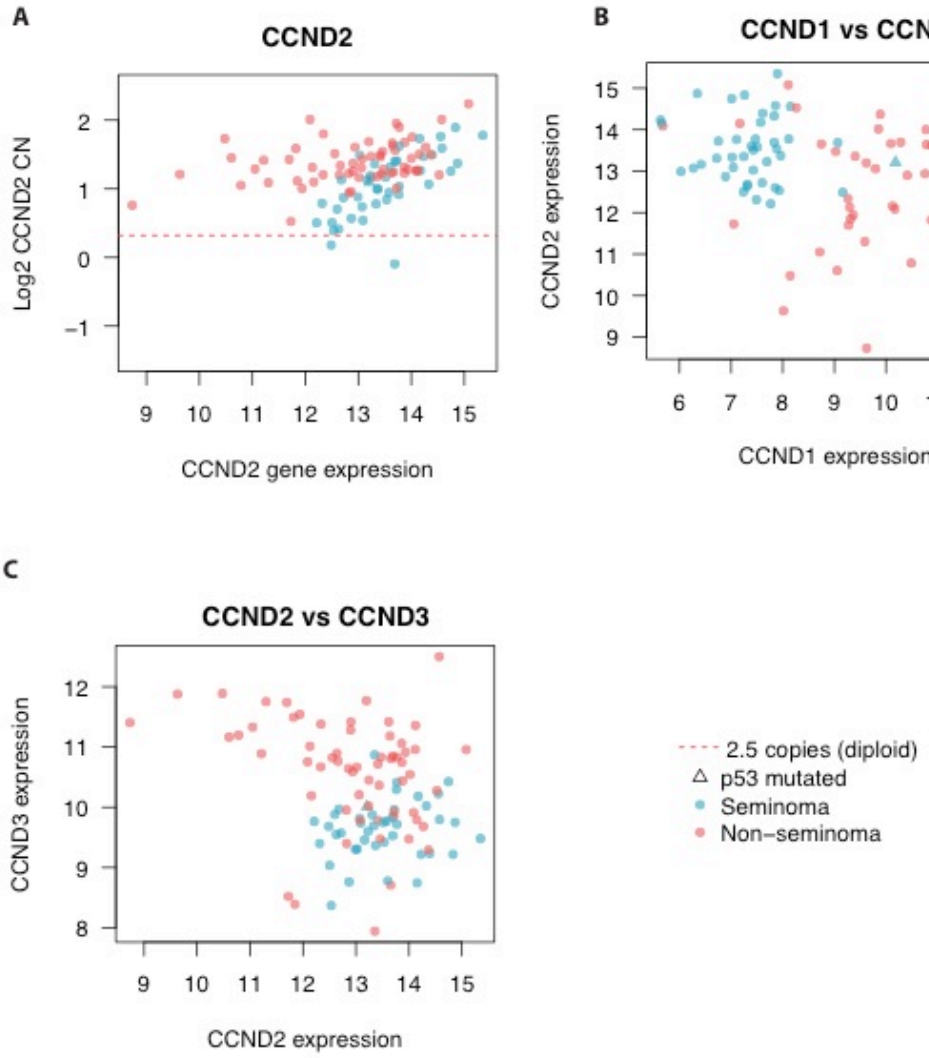

Figure 5.14 CCND1, CCND2 and CCND3 mRNA expression in TGCT

(A) CCND2 mRNA expression correlated with copy number for seminoma and non-seminoma sub-types. (B) CCND1 and CCND2 mRNA expression correlations for seminoma and non-seminoma sub-types. (C) CCND2 and CCND3 mRNA expression correlations for seminoma and non-seminoma subtypes.

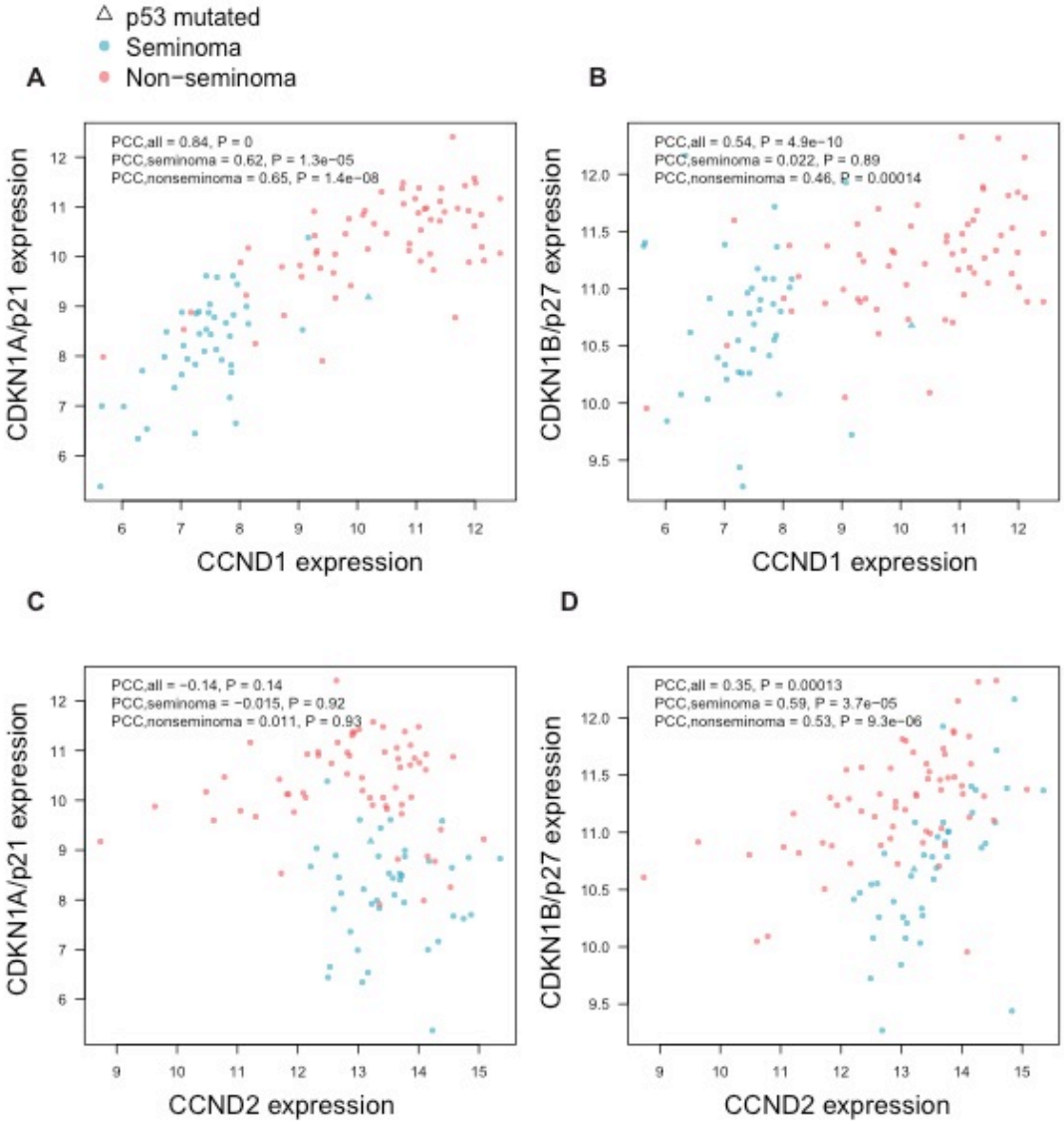

Figure 5.15 CDKN1A, CDKN1B and CCND1 expression

mRNA expression correlation analysis of 117 TGCTs; seminoma and non-seminoma histological subtypes. (A) CCND1 and CDKN1A (B) CCND1 and CDKN1B (C) CCND2 and CDKN1A (D) CCND2 and CDKN1B.

5.5 Discussion and Conclusions

Quantitative proteomics (*see* Chapter 4) showed an elevation in cyclin D1, which validated in four out of six independently-derived tetraploid clones. The primary aim of this chapter was to investigate cyclin D1 as a mediator of tetraploid tolerance. The principle finding suggests that cyclin D1 overexpression can provide tolerance to pharmacologically-induced tetraploidy *in vitro* and overexpression of D-type cyclins are found in genome-doubled *TP53*$^{+/+}$, *CDKN1A*$^{+/+}$ and *RB1*$^{+/+}$ human testicular tumours. Although not unequivocally proven, this notion is at minimum supported in the HCT116 system. These data suggest that D-type cyclins can override the activated tetraploidy checkpoint and constitute a possible mechanism used to tolerate tetraploidy in genome-doubled testicular germ cell tumours.

Overexpression of cyclin D1 was specific to the tetraploid clones, as analysis of the other major cyclins showed no up-regulation at the protein level. Silencing of TP53, resulting in complete p53 and p21 loss, reduced the amount of cyclin D1 in the diploids and tetraploids by the same extent. However, after knockdown there was still more cyclin D1 in all tetraploid clones, suggesting that elevated and p53 and p21 levels were not solely responsible for elevated cyclin D1. In this experiment, DC8 cyclin D1 levels did not fall as dramatically after knockdown, indicative of less stabilisation by p21 or p53. This may suggest abnormal cyclin D1 regulation in DC8, which is the parental clone for the second-generation clones with high cyclin D1. Abnormal regulation of cyclin D1 in this clone may result in subclones with higher protein expression that could provide tetraploidy tolerance if a genome-doubling event occurs.

After confirming protein overexpression of cyclin D1, we set out to investigate the reasons behind this event and looked at the most prominent mechanisms of cyclin regulation. *CCND1* mRNA levels were consistently elevated in the tetraploid clones although no copy number gains were detected (Dewhurst et al., 2014). A possible reason for CCND1 mRNA elevation was enhanced ERK pathway signalling, which is implicated in *CCND1* gene transcription. All but one of the tetraploid clones had more heightened signalling after 24 hours of serum starvation and showed prolonged activation up serum re-addition. Another mechanism resulting in cyclin

D1 overexpression was enhanced protein stability, as CHX experiments showed that cyclin D1 was more stable in the tetraploid clones. This finding suggests that the overall increase in cyclin D1 protein observed is a combination of increased mRNA expression and enhanced stability. An intriguing extension of this part of the study would involve knocking down p21 and repeating the experiment under these conditions. As p21 is required for complex formation, this experiment could show if the unbound cyclin D1 fraction was stabilised or if stability is specifically provided when the protein is a p21-bound complex.

Cyclin D1 levels are high in G1 and G2 phases of the cell cycle and the protein helps drive proliferation by activating CDK4. However during S phase, cyclin D1 levels are rapidly reduced by Thr286 phosphorylation and subsequent cytoplasmic degradation by the PCF4 complex to very low levels (Guo et al., 2005, Alao, 2007, Yang et al., 2006b, Gong et al., 2014). An elevation in cyclin D1-Thr286 was observed in the tetraploid clones, which may be caused by an increased S phase due to a doubled genome. Indeed, there were nearly 2-fold more tetraploid p21-expressing S phase cells and as result may have even lower S phase cyclin D1 compared to diploids. When cyclin D1 levels were quantified in different phases of the cell cycle, there was a reduction in S phase relative to G1 and G2 phases but surprisingly levels did not fall extensively in either diploids or tetraploids as reported by others (Yang et al., 2006b, Okabe et al., 2006). In fact, tetraploid cyclin D1 levels were found to be greater in all cell cycle phases. Thus, despite a longer S phase and elevated phosphorylation, cyclin D1 levels were still higher in the tetraploids. In addition, the level of S phase degradation was significantly less in the tetraploids. These findings suggest that cyclin D1 is elevated in every cell cycle stage and, therefore, could provide protection from the inhibitory effects of p21. The high levels in S phase are surprising, however this could allow heightened tetraploid cyclin D1 to sequester elevated p21 during this phase, as if cyclin D1 was exported and degraded in the presence of high S phase p21, it could result in arrest (Zhu et al., 2004). It cannot be excluded that the cyclin D1 levels in the diploids and tetraploids are cytoplasmic during S phase and, therefore, unable to sequester nuclear p21. However, if cyclin D1 was cytoplasmic, it would likely be rapidly degraded by the proteasome, suggesting a proportion of the levels observed would be nuclear during S phase and could inhibit p21.

In support of these findings, subcellular fractionation experiments revealed that nuclear cyclin D1 was higher in the tetraploids compared to diploids. There was no tetraploid cytoplasmic enrichment, suggesting that the increased S phase and cyclin D1-Thr286 was not enhancing tetraploid cyclin D1 nuclear export. This experiment suggests that although tetraploids have elevated nuclear p21, this is counteracted by increased cyclin D1. As cyclin D1 levels are high in every phase it is possible that nuclear p21 is sequestered in every cell cycle phase by nuclear cyclin D1. As the subcellular fractionation experiment do not measure co-localisation directly or separate distribution relative cell cycle phases, it cannot be formally excluded that p21 and cyclin D1 are in different cellular compartments at different phases of the cell cycle. Alternatively, if the two proteins are in complex they may be co-localised but may not be distributed in both the nucleus and cytoplasm at given cell cycle phase. However, it is likely that if cyclin D1 is expressed then it will be equally distributed, which is why it is rapidly degraded if not required.

Taken together, the above experiments provide evidence that cyclin D1 is high in all cell cycle phases and could therefore sequester the observed elevated p21. One possible issue with this hypothesis is that high cyclin D1 during S phase is inhibitory, acting as a backup mechanism if cells aberrantly overexpress the G1 cyclin (Guo et al., 2005). Therefore, there must be mechanism in place to tolerate high S phase cyclin D1 levels in the tetraploid clones. In order to progress through S phase with high cyclin D1 it is likely that cancer cells with cyclin D1 overexpression adapt the molecular mechanics S phase to accommodate high cyclin D1 and resist arrest (Guo et al., 2005). Parental HCT-116 cells do not have a *CCND1* amplification but have elevated β-catenin levels, through loss of the APC tumour suppressor, leading to heightened cyclin D1 expression (Tetsu and McCormick, 1999). Therefore, it is possible that HCT-116 cells have evolved a mechanism to replicate DNA with elevated cyclin D1. This molecular phenotype may have influenced why cyclin D1 was selected as a tolerance mechanism in tetraploid clones. Elevated cyclin D1 could have sequestered p21 and permitted progression past the G1/S checkpoint. As HCT-116 cells overexpress cyclin D1, they may have been inherently resistant to further cyclin D1 overexpression in S

phase, permitting progression of cyclin D1 high tetraploids though the cell cycle. Therefore, cyclin D1 can sequester p21 in all cell cycle phases and provide tetraploidy tolerance.

The CDK2 IP showed that there was still p21 binding to the kinase. Previous studies have shown that most CDK2 is p21 bound and only a minor fraction of p21-free CDK2 is sufficient for catalytic activity (Planas-Silva and Weinberg, 1997). Therefore, it is tempting to speculate that although more p21 is bound to CDK2 in the tetraploid clones, p21 binding to CDK4-cyclin D1, possibly as result of elevated cyclin D1, ensures enough p21 is sequestered to maintain a p21/CDK2-free fraction capable of S phase initiation. In support of this hypothesis, CDK2 kinases assays showed that tetraploid clones could phosphorylate RB at greater levels compared to DC14 and DC25, suggesting increased CDK2 catalytic activity.

It was expected that a greater number of cyclin D1 in complex with CDK4 and p21 would be present in tetraploid clones. However, the level of cyclin D1 binding was highly variable between all clones, as was cyclin E association with CDK2. It is generally accepted that the cyclin D is required for p21 binding to CDKs. Therefore, in order to have elevated p21-containing complexes in the tetraploid clones, cyclin D1-CDK4 association would also have to be elevated. This discrepancy may be of technical nature, through the dissociation of cyclin D1 from CDK4 during the immunoprecipitation process. Another explanation could be that there are more than one molecule of p21 is binding per CDK4-Cyclin D1 complex. The CDK4 kinase assay supports the first possibility, as although activity is variable, activity is observed in all the tetraploid clones. However, more activity in the kinase assay could also be explained by the presence of more complexes.

An important question that has not been answered from this work is that, although cyclin D1 is elevated in tetraploids, it has not been determined whether the cyclin is in excess, relative to p21. In order to explore this, a sequential IP strategy would need to be employed, as used by Quintanilla-Martinez *et al* (Quintanilla-Martinez et al., 2003). Confirming that cyclin D1 is in excess if of great importance, and if proved, would greatly strengthen the argument for the role of cyclin D1 in providing tetraploidy tolerance.

In order to investigate the functional significance of cyclin D1 in tetraploid survival, cyclin D1 knockdown could be performed. Complete knockdown of cyclin D1 is problematic, as loss of CDK4 activity and displacement of p21 to CDK2 would cause arrest in diploids and tetraploids. This strategy would, therefore, not reveal if the specific loss of elevated tetraploid cyclin D1 fraction could cause arrest and was responsible for tetraploid tolerance. Instead, the tetraploid arrest would result from the total loss of p21 sequestration. Cyclin D1 knockdown to diploid expression levels would demonstrate the function of the elevated cyclin D1 fraction. If at this level there were reduced tetraploid kinase activity and cell cycle arrest, this would suggest that the elevated levels of p21 are being sequestered by the enhanced cyclin D1 fraction, permitting Cyclin E/CDK2 activity for passage through the G1/S checkpoint. As titrating siRNA to achieve a defined and reproducible level of knockdown is technically challenging, instead cyclin D1 was overexpressed in HCT-116 cells to test whether cyclin D1 could provide survival benefit. Overexpression did not increase the basal tetraploid fraction. The fraction of tetraploid cells in the HCT-116 population is approximately 0.5% and cyclin D1 is likely to provide a survival benefit to only a fraction of this subpopulation, thus making detection by flow cytometry very difficult and thus creating a need for a more sensitive assay. This approach could be improved by sorting the tetraploid cells before single cell cloning and quantification of cloning efficiency and comparison to the normal HCT-116 rate of 6%.

Equally important, p21 should be over-expressed in diploid HCT-116 cells to the levels of detected in tetraploids, in an attempt to prove that that level of p21 is growth inhibitory and a mechanism such as cyclin D1 is required to counteract it. In combination with titrated cyclin D1 knockdown experiments, as outlined above, this would provide further evidence that elevated cyclin D1 is essential for tetraploid proliferation and that diploid levels of cyclin D1 are insufficient to sequester tetraploid p21 levels. It has been previously shown that HCT-116 cells arrest in G1 after DNA damage or after pharmacologically-induced cytokinesis failure, demonstrating that elevated p21 can cause G1 arrest in HCT-116 cells (Waldman et al., 1995, Stewart et al., 1999). Furthermore, 5-FU causes a G1 arrest through the induction of DNA and RNA damage (Sun et al., 2007). 5-FU-treated diploid clones showed similar p21 levels to untreated tetraploid p21. Therefore, since the

levels of 5-FU-induced p21 in diploid clones are comparable to untreated tetraploid levels, which are cycling under these conditions, it is logical to speculate that tetraploid p21 levels would also be inhibitory in the absence of a tolerance mechanism.

The aforementioned cyclin D1 knockdown experiments are challenging. Even if they could be achieved technically, they may fail to detect the role of cyclin D1 due to characteristics of the HCT-116 cell line. HCT-116 cells are highly mutagenic through genetic loss of mis-match repair enzymes, leading to microsatellite instability (de las Alas et al., 1997). Therefore, after the tetraploidization event the system could have equilibrated, masking the tolerance effects of cyclin D1. Specifically, it is possible that cyclin D1 may have provided the initial tolerance but soon after a more efficient genetic aberration was gained (e.g. through copy number alterations or non-convergent somatic mutations). Therefore, loss of cyclin D1 in this hypothetical scenario would have no effect on viability, even though cyclin D1 would have been the initial tetraploidy tolerance mechanism. In support of this hypothesis, Dewhurst *et al* performed CGH analysis of the tetraploid clones and showed copy number alterations at the earliest passage analysed (p5). Therefore, tetraploid clones can undergo genomic rearrangement soon after tetraploidization, which may lead to acquisition and selection of a more efficient tolerance mechanism.

Due to the technical restraints presented by the HCT-116 system, the RPE-Fucci cell line was adopted to investigate whether cyclin D1 could provide a functional role in tetraploidy tolerance. There are multiple advantages of using this system over the HCT-116 cell line. Firstly, RPE cells have fully active cell cycle checkpoints and are known to arrest after induction of tetraploidy. Secondly, the RPE cell line has clean genetic background, in contrast to the MIN HCT-116 cell line. Cyclin D1 may have provided the initial tolerance to tetraploidy, however a complex array of mutations may have been selected soon after genome-doubling, masking the tolerance effect of cyclin D1 expression. The RPE cells paired with the Fucci system, which allows determination of cell cycle phase, made for a very powerful experimental system to investigate the role of cyclin D1 and tetraploidy in tolerance in greater detail.

In light of these advantages, *CCND1* was overexpressed in the RPE-Fucci system before sorting of DCB-induced tetraploid cells. This strategy allowed the comparison of newly formed *CCND1*-overexpressing tetraploid cells with *CCND1*-normal cells, which enabled the direct effects of cyclin D1 overexpression on tetraploidy tolerance to be monitored. Of note, overexpression of cyclin D1 alone did not cause an increase in >6N the basal faction. The percentage of >6N cells was more than 10-fold lower than HCT-116s at 0.015%, equating to an actual number of three cells in a population of $2x10^4$. Therefore, as with HCT-116s, low tetraploid numbers and diploid competition may supress the outgrowth tetraploids and mask the tolerance effect of cyclin D1.

The short-term assays showed 5.7-fold more CCND1 cells could start to cycle and enter G2/M within 16 hours of DCB treatment. A reproducible survival benefit of around 2.5-fold, compared to vector control, 72 hours post-tetraploid induction was observed, with western blotting providing evidence of p53 and p21 activation. A limitation of this medium-term survival assay is that the different lag phases observed between the cell lines could have affected the result. The growth curve analysis predicted an approximately 1.7-fold increase in cell numbers after 60 hours, compared to the RPE-Fucci. Therefore, it is likely that at 72 hours there are 1.7-fold *CCND1*-overexpressing cells and this is just a function of a decreased lag phase. If there are more cells because of differential cell cycle kinetics, this could affect the result, as there would be more G2/M cells purely through enhanced growth. However, the fold change in survival was 2.5-fold. This implies the lag effect cannot fully account for the observed increase, implying cyclin D1 can specifically override the G1 arrest.

More strikingly, the difference was 7.3-fold in a long-term clonogenic assay. This assay overcomes the problem of differential lag phases between cell lines. The previous short-term assay counts the number of G2/M cells as the endpoint, therefore, if more cells existed due to proliferation, this could mask the result and resemble an escape from G1 arrest. In the clonogenic assay, cells are seeded at low-density and colonies from single cells were allowed to form, which were counted at the end of the experiment. This means that the number colonies were

directly proportional to the number of cells that can escape the G1 arrest. The difference in lag time would only affect the size of colony. It could be argued that smaller diploids colonies would be below a counting threshold and therefore underestimated, however, given the experiment is long term and after the initial lag dip lids and tetraploids grow at the same rate, this effect is likely to be minimal as most colonies will breach the lower detection limit. Therefore this assay represents a cleaner and more precise method to measure survival.

The clonogenic potential was similar between the *CCND1* cells and controls, suggesting overexpression of *CCND1* in the diploid state does not provide a significant advantage for colony formation. Therefore, the increased survival after tetraploidy induction is not due to a mechanism present in the diploids (e.g. CDK4-cyclinD1 catalytic activity and enhanced proliferation rate) but specific to the tetraploid karyotype. This finding suggests that the effect seen in the *CCND1*-overexpressing tetraploids is selected for when the cell enters a tetraploid state of high p53 and p21, as the overexpression provides a selective advantage.

Finally, D-type cyclin expression was specifically investigated in genome-doubled human tumours by analysing the TCGA data set using a genome-doubling algorithm, as discussed in Sections 5.5, 2.2.20.3 and (Carter et al., 2012). Genome-doubled TGCTs showed *CCND2* copy number and overexpression through chromosome 12p gain. Importantly, nearly all tumours were *TP53*, *MDM2*, *CDKN1A* and *RB1* wild type, suggestive of a functional tetraploidy checkpoint. These findings, combined with the ability of *CCND1* to bypass the p53/p21 tetraploidy checkpoint *in vitro,* provide evidence that that D-type cyclins may mediate tolerance to genome-doubling events in human tumours. In addition to these findings, CCND1 expression strongly correlated with CDKN1A transcript levels in TGCTs, recapitulating the previous *in vitro* data obtained. Therefore this observation further supports the hypotheses that D-type cyclin and p21 expression is functionally related in p53/p21/RB wild-type tetraploid cells and tumours. Although the *in vitro* data strongly suggest that D-type cyclins are likely to provide tolerance in TGCTs, other genetic events cannot be excluded such as K-RAS gain on chr12p (Sheikine et al., 2012)

As discussed in section 1.5.2.2, tetraploidy is an intermediate of CIN and aneuploidy. Therefore, it is important to determine if chromosome 12p gain in TGCTs has preceded genome-doubling and could have therefore provided tolerance to the initial tetraploidization event. Most evidence presented in this thesis would suggest that copy number alterations occur after genome-doubling, as a result of CIN and therefore challenges the idea of 12p gain before genome-doubling in TGCTs. Two major theories have been proposed regarding the origin of seminoma (Houldsworth et al., 1997, Skakkebaek et al., 1998). Based on genetic evidence, Chaganti and Houldsworth hypothesised that the 4N zygotene-pachytene spermatocyte is the TGCT cell of origin (Houldsworth et al., 1997). This is the meiotic stage, where chromosome cross-over by homologous recombination is subject to a p53-dependent recombination checkpoint (Roeder, 1997). The authors propose that, during this stage of cellular development, aberrant chromatid exchange can lead to 12p copy number gain and CCND2 overexpression. The overexpression of CCND2 allows the cell to bypass the recombination checkpoint and also induces cell cycle re-entry with a 4N genome. Based on the data presented in the present study, it is possible that the newly formed tetraploid cell can also resist p53/p21-mediated arrest as result of CCND2 overexpression. In this context, the tetraploid cell could then undergo CIN, eventually resulting in the hypertriploid seminoma or hypotriploid non-seminoma tumours.

A second theory, proposed by Skakkebaek and colleagues, argues that the cell of origin is the primordial germ cell (PGC), which undergoes abnormal cell division as result of *in utero* environmental factors, leading to carcinoma *in situ* (Skakkebaek et al., 1998). Importantly, this theory states that tetraploidization precedes 12p gain and therefore challenges the role of cyclin D2-mediated tetraploidy tolerance. PGCs migrate into the developing gonad after 5 weeks of gestation and differentiate into gonocytes. Mitchell *et al* recently showed that the most common subpopulation of germ cell neoplasia show a gonocyte expression profile, supporting the hypothesis that TGCTs arise from early germ cells *in utero* (Mitchell et al., 2014).

PGCs and gonocytes possess a functional DNA damage-dependent p53 pathway that can be activated by DNA damage (Forand and Bernardino-Sgherri, 2009, Luo

et al., 2014). Therefore, it is likely that a genome-doubling event could induce a p53 dependent arrest and, thus, a mechanism must be in place to tolerate such a situation. One explanation could be that, although CCND2 copy number may be diploid, D-type cyclin expression may be elevated during this developmental stage, which could in turn result in a greater chance of polyploid cells overriding the tetraploidy checkpoint (Gilbert et al., 2011, Beumer et al., 2000). There is clearly a debate as to whether cyclin D2 is expressed prior to tetraploidization.

An important extension of this work would be to determine the timing of CCND2 copy number gains. This is not possible, bioinformatically, due to the inherent genetic characteristics of TGCTs. In order to use the copy number data to determine whether or not the gain of 12p is early or late, the arm level event has to fall into categories that match the expected: pre-genome-doubling, 2 -> 3 copies, which following genome-doubling becomes 6 copies, or post-genome-doubling, 4 -> 5 copies. However in the TCGA data, the amplification on 12p rarely falls into one of these categories. An alternative is to investigate if the copy number mutations on 12p may follow a pattern that indicates early genome-doubling. Mutations generally showing 1 copy suggests early genome-doubling, as mutations occur later and are therefore present on only one gene copy. Mutations generally occurring on two copies would suggest they were present prior to genome-doubling and, therefore, doubled with the genome. But unfortunately, in TGCT the total mutation numbers are so low that we cannot use this as an estimate.

Taken together, these data suggest that D-type cyclins can provide tolerance to tetraploidy in a p53-independent manner both *in vitro* and in human tumours. In tumours, such as TGCTs, where there is relatively low frequency for p53/p21/RB inactivation, D-type cyclin overexpression may provide a mechanism of tetraploidy tolerance. This can promote the formation and subsequent selection of aneuploid subclones that may promote tumour evolution in the clinical setting.

Chapter 6. Discussion

6.1 Molecular model

The work in this thesis reinforces the central role for a p53 and p21 dependent arrest after a genome-doubling event. Furthermore, the data obtained in this work provides evidence that cyclin D1 overexpression can override the tetraploidy checkpoint and provide tetraploid tolerance, and is central in the proposed molecular model (Figure 6.1 and Figure 6.2)

6.1.1 Tetraploidization results in p53 and p21 elevation

The steady state levels of p53 and p21 were elevated and functional in the HCT116 tetraploids, whilst in the RPE system a graded response was observed after genome doubling, resulting in G1 arrest. Therefore, this functional p53 response further supports the hypothesis that tetraploid cells activate the p53/p21 pathway to supress the outgrowth of pathogenic tetraploid clones.

Previous studies also support the notion of p53 dependent response after a tetraploidization event. A heightened level of p53 in tetraploid cells has been reported in early work by Andreassen *et al* and others (Andreassen et al., 2001b, Di Leonardo et al., 1997). These groups showed p53 is induced in tetraploid cells resulting in p21 dependent G1 arrest, consistent with the findings in this thesis. A problem with earlier studies was the use of pharmacological agents to induce tetraploidy. Indeed, some studies suggested that the p53 and p21-dependent arrest observed by Andreassen *et al* was a result of off-target effects (as discussed in section 1.4.1). However, a more recent study disputed this and proposed that discrepancies between studies were due to differences in G1 length and graded p53 response (Ganem et al., 2014). Specifically, newly formed tetraploid cells cultured on fibronectin have a shorter G1 and thus p53 levels could not reach the required inhibitory threshold and ceased to arrest. Therefore, this important study provided some clarification as to how tetraploid cells elicit a p53 response after cytokinesis failure. These findings, together with the observed tetraploid p53 and

p21 kinetics described in this thesis, support the concept of a p53 and p21 response after spontaneous or pharmacological tetraploidization.

A model outlining the p53 and p21 dependent response to a tetraploidization event is presented in Figure 6.1. Accordingly, after a tetraploidization event, high p21 levels through p53 signalling will bind and inhibit CDK4 and CDK2, resulting in cell cycle arrest through RB-E2F stabilisation (Massague, 2004). The stoichiometric model dictates that if one p21 molecule is bound to CDK4, the kinase is active. This is the molecular state apparent in a cycling G1 cell, as cyclin D1 is equimolar or in excess relative to p21. In addition, CDK2 in this context will be active, as p21 will be sequestered into CDK4-CyclinD1-p21 complexes. However, if p21 levels are raised above a threshold, then more than one molecule can bind CDK4 resulting in kinase inhibition (Figure 6.1) (LaBaer et al., 1997). In addition, when CDK4-CyclinD1 complexes are saturated with p21, a single p21 molecule is sufficient to inhibit CDK2 (Hengst et al., 1998). Therefore, when p21 is induced by a p53 dependent stress mechanism (e.g. tetraploidization) both G1 kinases are inactive, and the cell is arrested.

Alternatively, the phosphorylation model predicts the posttranslational state of p21 may be important in switching the CKI from a kinase inhibitor to an activator during G1, and states only one p21 molecule can bind CDK4 (James et al., 2008, Hukkelhoven et al., 2012). During G1, phosphorylation of p21 *via* mitogenic signalling can result in a conformational change, switching the CKI from a CDK2 inhibitor to a CDK4 activator, promoting cell cycle progression. However, during periods of high p21 levels (i.e. stress), the system can become saturated and most p21 is in an inactive un-phosphorylated confirmation, and thus will inhibit CDK4 and CDK2. Regardless the model applied, CDK4 and CDK2 will be inhibited when p21 is elevated after a tetraploidization event (Figure 6.1).

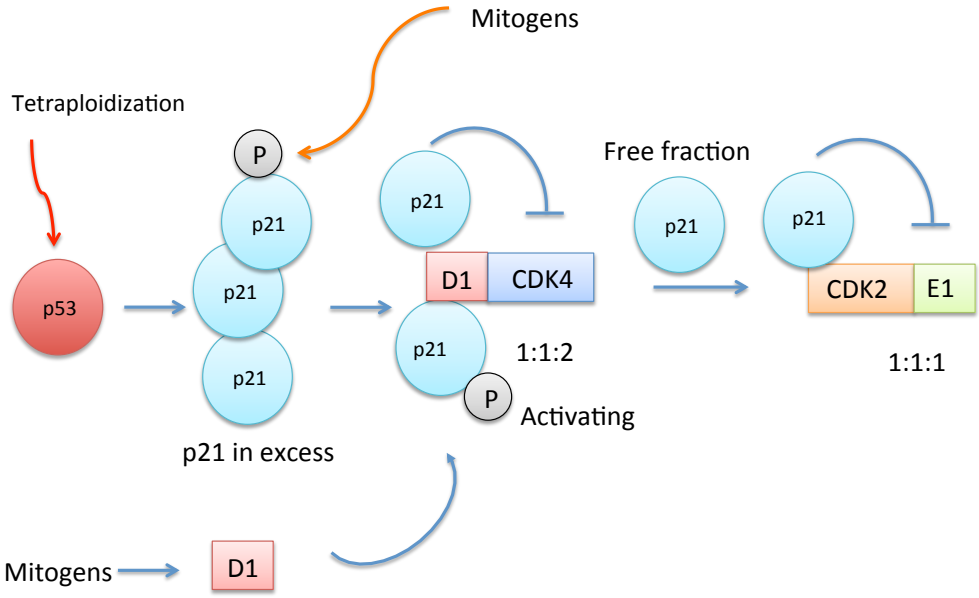

Figure 6.1 Intracellular mechanism indicating a p53 dependent tetraploid arrest. A tetraploid cell with low cyclin D1 expression enters G1 and arrests.

6.1.2 Cyclin D1 overexpression can sequester p21 and permit proliferation of tetraploid cells in the presence of a functional p53/21 axis

Inactivating the p53/p21 response as previously described in section 6.1.1 is an efficient way for a newly formed tetraploid cell to resist a G1 cell cycle arrest and acquire tetraploid tolerance. However, 65% of genome-doubled tumours are p53 wild type, as was the tetraploid HCT-116 system studied in this thesis (McGranahan et al., 2015). In the HCT-116 system, tetraploid cells possessed high p21 and showed no indication of G1 arrest, suggesting a mechanism was inhibiting the CKI, permitting CDK2-Cyclin E activity, cell cycle progression and tetraploid tolerance. Taken together, these observations suggest alternative tetraploid tolerance mechanisms exist in human tumours, and may act thorough disruption of p21 function.

The work presented in this thesis proposes cyclin D1 overexpression can provide such a tolerance mechanism. Quantitative proteomics revealed the cyclin was significantly elevated in the HCT-116 tetraploids and provided long-term tolerance after pharmacological induction of tetraploidy in the RPE system, despite a simultaneous p53/21 response. Furthermore, D-type cyclin overexpression was identified in p53, p21 and RB wild-type genome doubled testicular germ cell tumours (TGCTs), providing evidence the mechanism may exist in human tumours. Studies by LeBaer and Planas-silva *et al* support the hypothesis that cyclin D1 overexpression could inhibit p21 and provide tetraploid tolerance. The two investigations demonstrated that cyclin D1 could bind and sequester p21, inactivating the cyclin kinase inhibitor (CKI) and allow progression from G1 to S phase (Planas-Silva and Weinberg, 1997, LaBaer et al., 1997). Quintanilla-Martinez *et al* have shown that cyclin D1 overexpression in Mantal cell Lymphomas (MCL) may sequester the inhibitory effects of p27, resulting in aggressive tumours in the presence of CKIs (Quintanilla-Martinez et al., 2003).

A more recent study directly supports the argument of cyclin D1 mediated tetraploid tolerance. Ganem *et al* showed that enhanced growth factor signalling, through activation of the AKT and ERK pathways, could override the tetraploidy checkpoint after DCB-induced cytokinesis failure. ERK and AKT signalling transcriptionally

induce cyclin D1 expression (Musgrove et al., 2011, Diehl et al., 1998). Therefore, the mechanistic basis of Ganem *et al's* observations could involve ERK/AKT-dependent cyclin D1 overexpression, resulting in p21 sequestration. Interestingly, in the present study, ERK signalling was shown to be enriched in the tetraploid clones and was possibly contributing to cyclin D1 overexpression.

Based on the findings from the current investigation and others, D-type cyclin overexpression can be integrated into the classical tetraploid checkpoint model, providing an elegant mechanism that can override the p53/p21 dependent tetraploidy checkpoint (Figure 6.2).

With regard to the stoichiometric model, If a newly formed tetraploid cell possessed equimolar or excessive cyclin D1, high p21 levels could be sequestered from CDK2 by unbound or complexed cyclin D1 resulting in active CDK4-CyclinD1-p21 complexes, as a result correct stoichiometry (Figure 6.2) (Planas-Silva and Weinberg, 1997, Sherr and Roberts, 1999, Quintanilla-Martinez et al., 2003). Therefore, under these molecular conditions, CDK4 and CDK2 will be catalytically active, cell cycle progression can occur and the tetraploidy checkpoint is overridden (Figure 6.2). This mechanism can also protect the cell from future insults, such as elevations of p21 from enhanced rates of segregation errors and, thus, the mechanism can provide continuous tolerance and facilitate CIN and aneuploidy.

The impact of p21 phosphorylation on this model remains to be discovered. If phosphorylation of p21 bound to CDK4 is required for kinase activation, high cyclin D1 levels will still sequester excess p21 from CDK2, but a fraction may be inactive, as the phosphorylation mechanism is saturated (Hukkelhoven et al., 2012). However, a proportion of CDK4-CyclinD1-p21 complexes may still be phosphorylated and active resulting in a p21 high cell with active CDK4 and CDK2. Even supposing CDK4 was inhibited in this situation through lack of p21 phosphorylation, it has been shown that CDK2 can compensate for the loss of CDK4 (Wang et al., 2007). Therefore as long as cyclin D1 overexpression can shield CDK2 from p21 inhibition, tolerance can be provided.

On the other hand, Stewart *et al* showed p21 elevations in newly formed tetraploid cells specifically inhibited CKD2-Cyclin E complexes (Stewart et al., 1999). Although p21 bound CDK4-Cyclin D1 complexes, their catalytic activity was not affected, suggesting phosphorylation status is redundant. Therefore, this study implies that after tetraploidization, the elevation in p21 is only inhibitory to CDK2. Applying these finding to the current model implies that in a high cyclin D1 scenario, there will be an elevation in active CDK4-Cyclin D1-p21 complexes, while CDK2 will be sheltered from p21 inhibition, activating both kinases.

Therefore, crucially, regardless of whether the stoichiometric or phosphorylation model is applied, in a high cyclin D1 environment, CDK2 would always remain active, in contrast to a cyclin D1 low background where the kinase would be inhibited (Figure 6.2).

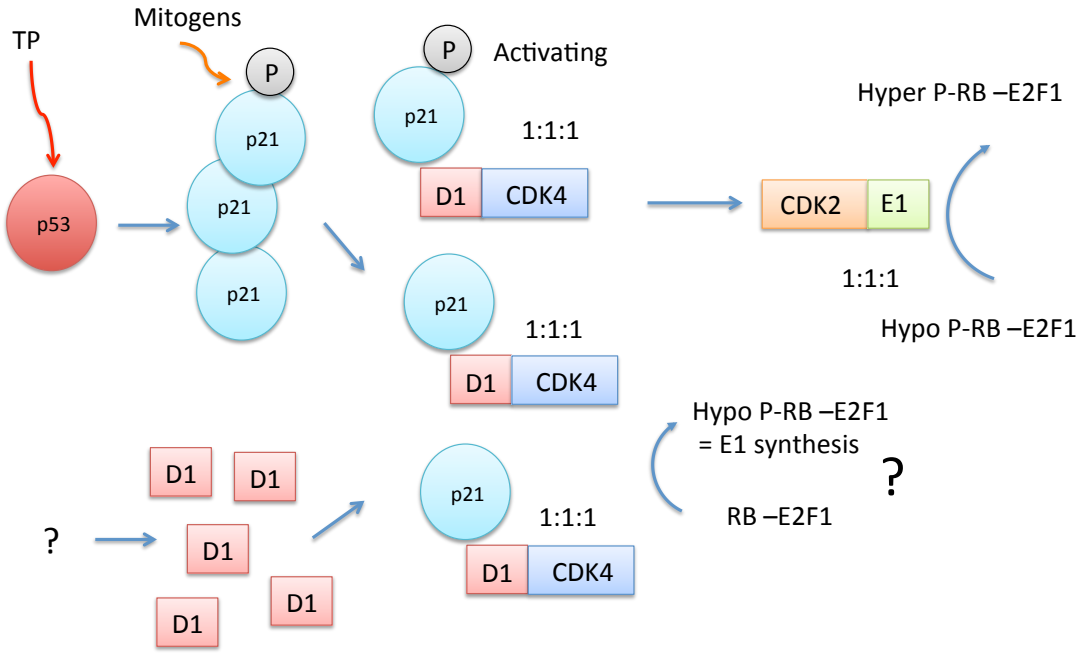

Figure 6.2 Mechanism describing cyclin D1 mediated tetraploid tolerance

A tetraploid cell with high cyclin D1 overexpression enters G1 and bypasses G1 arrest.

6.1.3 A cyclin D1-derived tetraploid cell could the tumour cell of origin.

The previously described molecular model could contribute the development of a cancerous lesion from a normal diploid precursor, such as a diploid epithelial cell (Figure 6.3). The first step would require a cycling diploid cell to exhibit elevation in D-type cyclin expression. This could be a result of abnormal stochastic fluctuations in growth factor signalling, such as ERK or AKT, leading to pathway activation and cyclin D overexpression. Alternatively, subtle genetic lesions could result in cyclin D overexpression. Subsequently, when a cyclin D1-overexpressing cell undergoes a genome-doubling event, such as a failed cytokinesis, the normal p53/p21-dependent G1 arrest could be overridden by elevated cyclin D-dependent inhibition of p21 by sequestration. This would permit CDK2-Cyclin E-dependent phosphorylation of RB, freeing E2F to induce S phase initiation genes. The tetraploid cells would then enter mitosis, where supernumerary centrosomes could lead to increased merotelic and syntelic attachment and, thus, resulting in generation of segregation errors and DNA damage. As the response to segregation errors is p21-driven, the elevated cyclin D1 levels can also permit proliferation of cells with elevated segregation errors, resulting in CIN and aneuploidy. The resulting CIN provides a mechanism for proliferating tetraploid cells to acquire additional genetic aberrations such as *TP53*, *RB1* and *CDKN1A* loss, facilitating molecular evolution and progression towards a heterogeneous malignancy.

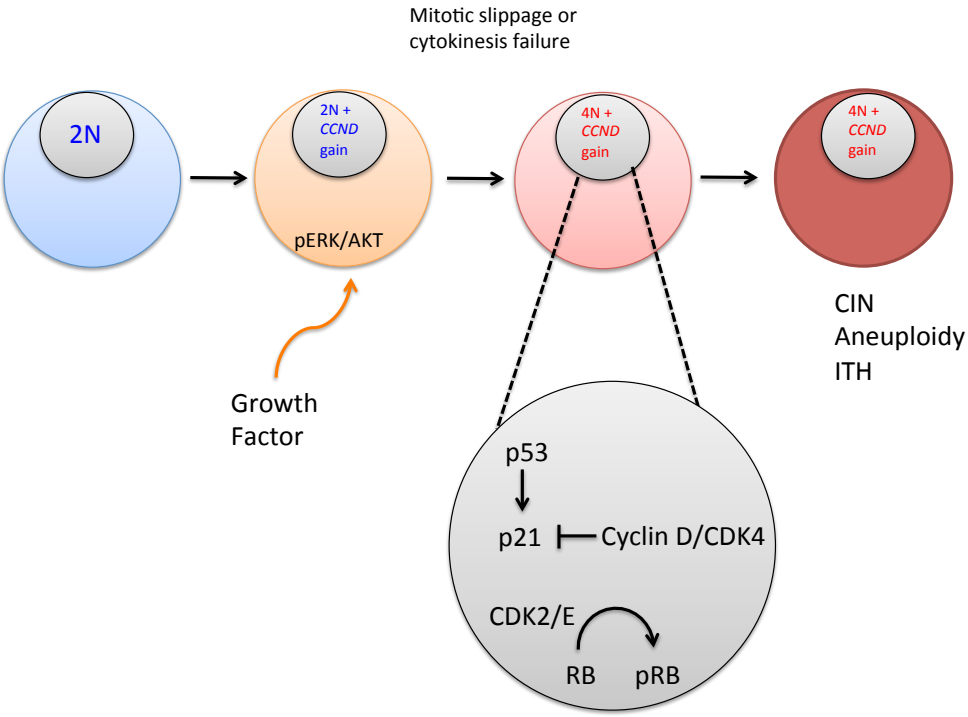

Figure 6.3 A route to tumorigenesis

Model depicting how D-type cyclin overexpression can result in tetraploid tolerance, and thus facilitate CIN, aneuploidy and tumorigenesis

6.2 Concluding remarks

This thesis has sought to advance our understanding and knowledge regarding tetraploidy tolerance independent of mutations of the p53/p21 pathway. HCT-116 tetraploid clones with elevated p53 and p21 were analysed by SILAC that revealed overexpression of cyclin D1, a protein known to sequester and inhibit the function of p21 (Sherr and Roberts, 1999). Overexpression of cyclin D1 provided a significant survival benefit for newly formed tetraploid clones, indicating that deregulation of cyclin D can override the p53-dependent tetraploidy checkpoint and provide tolerance. Furthermore, analysis of genome-doubled *TP53* wild-type TGCTs showed elevations of all three D-type cyclins, providing evidence that their overexpression may provide tetraploidy tolerance in these tumours.

Chapter 7. Appendix

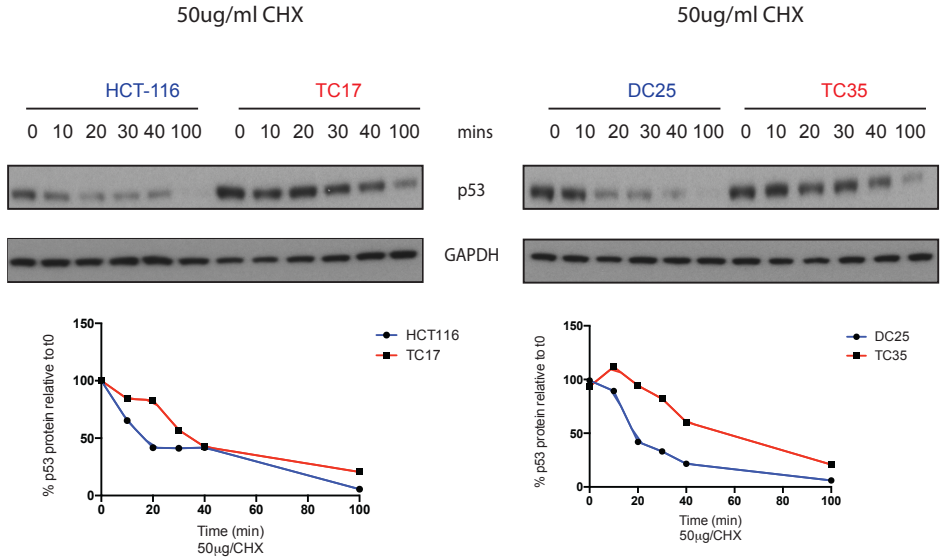

Figure 7.1 p53 protein stability

A comparison of p53 protein stability between diploid and tetraploid clones. Cells were treated with 50µg/ml cycloheximide and incubated at 37°C for the indicated times. Cells were lysed before immunoblotting and western blotting for p53. For quantification, p53 protein was normalised to GADPH before expression as percentage relative to 0 minutes.

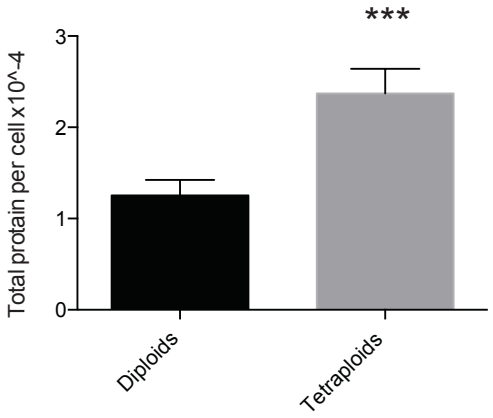

Figure 7.2 Total protein levels

Diploid and tetraploid clones were counted before lysis in equal volumes 8M urea buffer. Total protein amounts were determined by Bradford assay and dived by the cell number to gain an approximate protein per cell value.

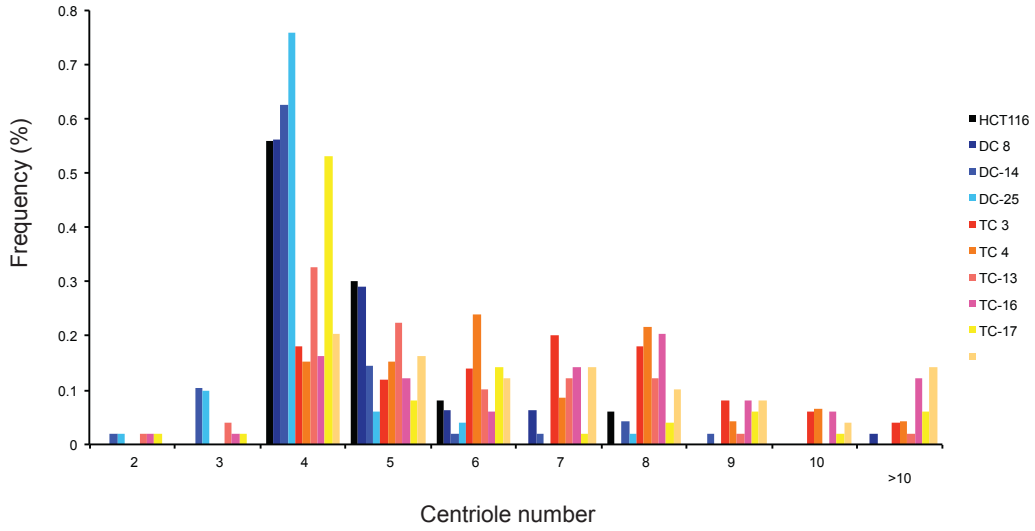

Figure 7.3 Quantification of HCT-116 isogenic cell system centriole number
Analysis performed by Sally Dewhurst.

7.1 Small molecule modulation of G6PD

7.1.1 Introduction

The pentose phosphate pathway (PPP) is responsible for around 20% of cellular glucose oxidation (Wamelink et al., 2008). Like glycolysis, the PPP is oxygen-independent, however in contrast, it does not require adenosine triphosphate (ATP). The primary products of this biosynthetic pathway are nicotinamide adenine dinucleotide phosphate (NADPH) and ribose-5-phosphate (R5-P). The oxidative branch of the pathway contains the rate-limiting enzyme, glucose-6-phospahe dehydrogenase (G6PD), which is mainly responsible for NADPH production and approximately 30% of ribose production; the non-oxidative branch produces the majority of the remaining ribose. NADPH is utilised for lipid synthesis and redox control, whereas R5-P is a precursor for nucleotide production (Wamelink et al., 2008).

A recent study has implicated G6PD and the oxidative PPP in the maintenance of genome stability after IR (Cosentino et al., 2011). The ataxia telangiectasia mutated kinase (ATM) senses DNA double strand breaks (DSBs) though chromatin disruption (Kastan, 2008). DSB-induced autophosphorylation activates the kinase, which then phosphorylates downstream targets such as p53-Ser15 and BRCA1 to induce arrest and DNA repair (Kastan, 2008). Aside from the classical function of ATM, the kinase has been shown to interact with the PPP. Due to subnormal NADPH levels in *ATM*$^{-/-}$ neuronal cells, Cosentino *et al* investigated the possibility that ATM may interact with the PPP (Cosentino et al., 2011). Activation of ATM by DSBs resulted in G6PD activation, via allosteric binding of hsp27 to G6PD, and heightened levels of NADPH and R5-P (Figure 7.4) (Cosentino et al., 2011). As the PPP provides R5-P, it was hypothesised that the activation of G6PD assists DNA repair by providing nucleotide precursors. These findings suggest treatment of cancer cells with a G6PD inhibitor prior to IR, could reduce their DNA repair capacity, increase DSBs and CIN, resulting in cell death through extreme genetic instability (Kops et al., 2004).

Studies by Varshney *at al* demonstrated the effects of PPP inhibition *in vitro* and *in vivo*. BMG-1 glioma cells were treated with either 2-deoxy-glucose (2-DG), an inhibitor of glycolysis or 6-aminonicotinamide (6-AN), a G6PD competitive inhibitor, and both result in decreased PPP flux (Varshney et al., 2005). Single-agent or combined treatment before and during IR enhanced sensitivity. PPP-inhibited cells showed a significant decrease in survival factions, depleted GSH levels, elevated S phase arrest and increased micronuclei formation (inactive of S phase segregation errors). Furthermore, the group showed treatment of mice bearing Ehrlich ascites tumours with 6-AN and IR, resulted in complete regression in 80% of animals, whereas IR alone resulted in stable disease followed by progression (Varshney et al., 2004).

Taken together, these studies show that classical DNA damage pathways interact with central glucose metabolism pathways to facilitate DNA repair and maintain genomic integrity. Inhibition of these pathways after DNA damage can lead to further genomic instability through saturation of repair pathways, resulting in lethal DNA damage and enhanced sensitivity. Therefore inhibition of the PPP in tumour cells prior to radiotherapy may improve efficacy.

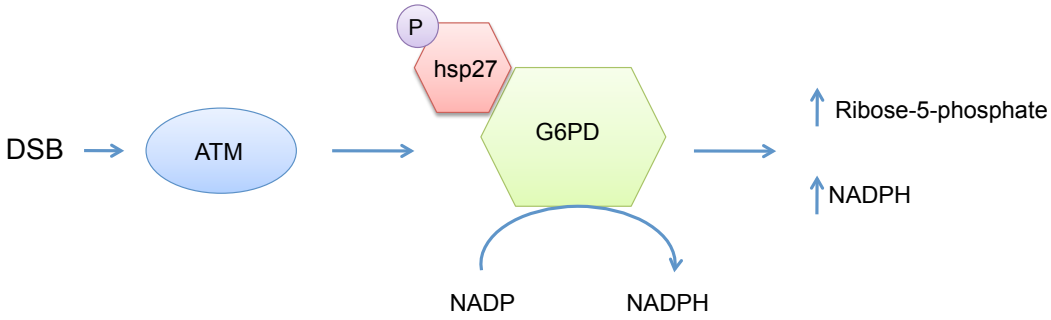

Figure 7.4 ATM regulates the pentose phosphate pathway

After DSB induction by a genotoxic agent of IR, ATM senses DNA damage and is activated. ATM phosphorylates hsp27, possibly via p38. Phosphorylated hsp27 can allosterically bind G6PD and activate the PPP rate-limiting enzyme. The activated PPP provides ribose-5-phosphate for nucleotide synthesis and DNA repair, reducing the extent of DNA damage. Elevated NADPH levels also reduce the extent damage caused by ROS after IR treatment.

7.1.2 G6PD compound screen

High throughput screening (HTS) is a common drug discovery approach, used to identify novel bioactive molecules. A collaboration with the HTS screening facility was formed in order to discover inhibitors of G6PD. The enzyme was produced and purified, before estimation of its oligomeric species by size exclusion chromatography (SEC). The purified G6PD was used in an isolated molecular target (IMT) assay, optimised for HTS. Screen hits were validated in a secondary screen, before specific validation and testing.

7.1.2.1 Recombinant G6PD purification

The first step of the process was to produce stocks of catalytically active human recombinant G6PD. A collaboration was formed with Cancer Research Technology and they provided human G6PD expression vectors and assay design information.

A human His-tagged G6PD (pHis:hG6PD) bacterial expression plasmid was freshly transformed into JM109DE3 *E.coli* cells. Protein expression was induced by autoinduction, as this produced a greater soluble protein fraction than IPTG-induction based methods. His:hG6PD expression is controlled by the *lac operon* and the autoinduction method uses carefully formulated media to control recombinant expression. The autoinduction media contains carbon sources of energy, such as glucose and lactose. After glucose stocks are depleted and the bacterial population is near saturation, lactose is transported into the bacterial cell and production of its isomer allolactose inhibits the *lac* repressor initiating gene transcription of His:hG6PD (Blommel et al., 2007). By utilising endogenous metabolism to induce recombinant protein expression, a greater yield and soluble fraction was obtained. The soluble fraction was incubated with nickel beads, which have affinity for His-binding, and tagged proteins were bound and eluted with imidazole. Elution fractions were separated by SDS-PAGE to confirm G6PD expression and purification (Figure 7.5A). SDS-PAGE analysis showed clear protein expression within the region expected for a protein with molecular weight of 59kD. Western blot analysis of fraction 3, using an anti-histidine antibody, confirmed the presence of purified recombinant G6PD (Figure 7.5B).

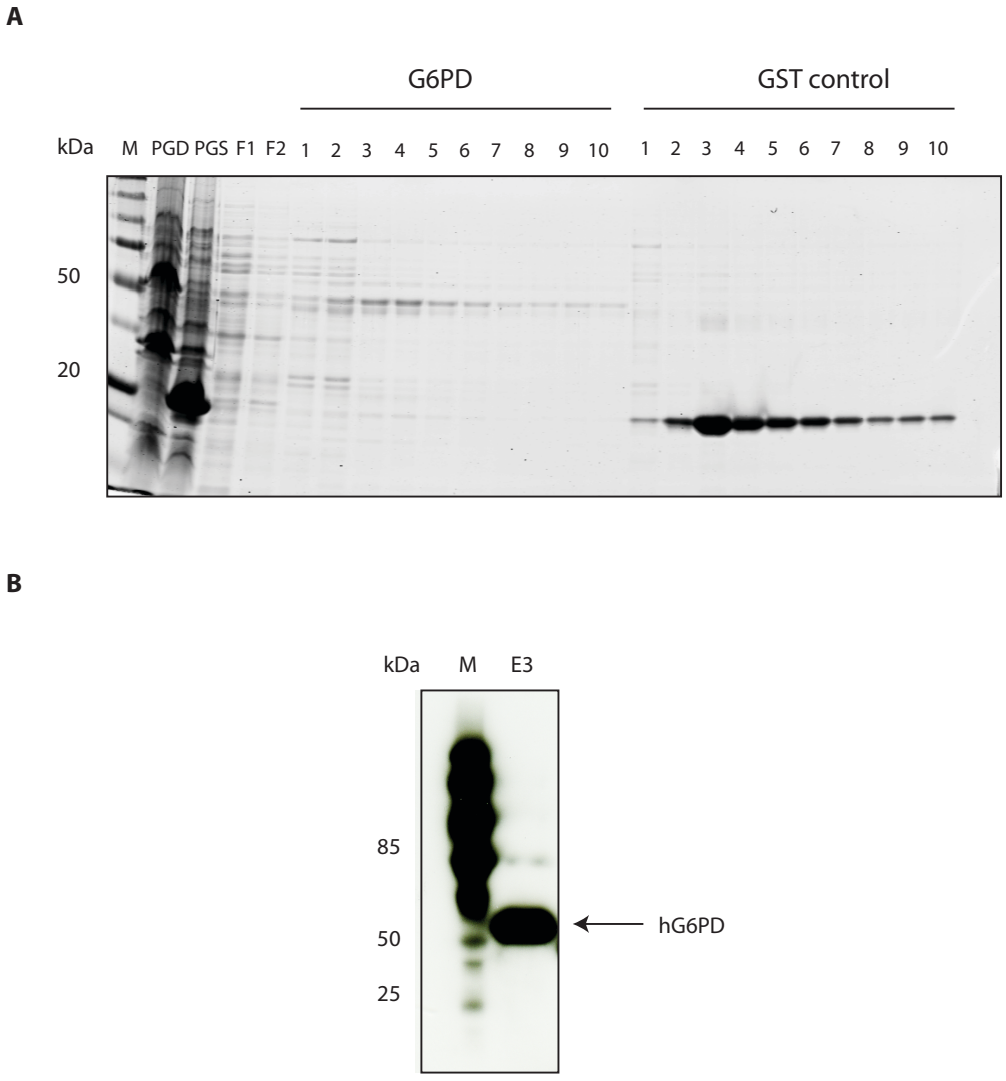

Figure 7.5 Nickel bead purification of His-G6PD

(A) SDS-PAGE of His-G6PD imidazole elution fractions and His-tagged GST control. Proteins were expressed in *E. coli* JM109DE3 cells, via the autoinduction method. His-tagged G6PD was purified using nickel beads. PGS and PGD bacterial pellet samples. F1: flow wash one, F2: flow wash two. KDa, kilodalton. (B) Protein purification was confirmed by Western blot analysis. Proteins were probed using an anti-His antibody. M (marker); E3 (G6PD eluate).

7.1.2.2 Size-exclusion chromatography and oligomeric species identification

G6PD can exist in an active multimeric complex or an inactive/semi-activity monomer. SEC analysis was performed in order to determine purity and confirm the presence of catalytic higher order enzyme species.

Gel filtration analysis of purified His:hG6PD resulted in a single well-defined elution profile, indicating a predominant oligomeric species with high purity and low contaminants (Figure 7.6A). Fractions were collected and samples were separated by SDS-PAGE to further check purity and perform protein quantification, using a BSA standard curve (Figure 7.6B). The most prevalent protein bands were present at 59kDa, which is the region where monomeric G6PD is expected to migrate based on its amino acid sequence. Fraction eight displayed the greatest concentration of 169µg/ml and correlated with the centre of the chromatogram peak.

Gel filtration analysis was also used to estimate the molecular weight of the purified proteins. A protein standard was loaded and eluted from the gel filtration column, and elution times were recorded. Purified His:hG6PD underwent the same procedure and the elution profiles were overlaid. The overlay showed that G6PD was eluted slightly earlier than the 158kDa standard, suggesting the possible presence of a tetrameric G6PD (Figure 7.7A). Using the standard curve to calculate an approximate value, by plotting it against the ratio of the void volume (V_o) and elution volume (Ve) (Figure 7.7B), resulted in an estimated molecular mass of 198kD, which is indicative of a tetramer. The calculated molecular mass did not precisely equate to the actual mass of a G6PD tetramer, as in the SEC process, proteins are separated by shape and size, which is not directly proportional to weight, and therefore the predictive value of this assay is limited. However, the predicted molecular weight of 198kD is closest to the actual weight (236kD) of the tetramer, providing satisfactory evidence for the production of a higher order tetrameric species.

A

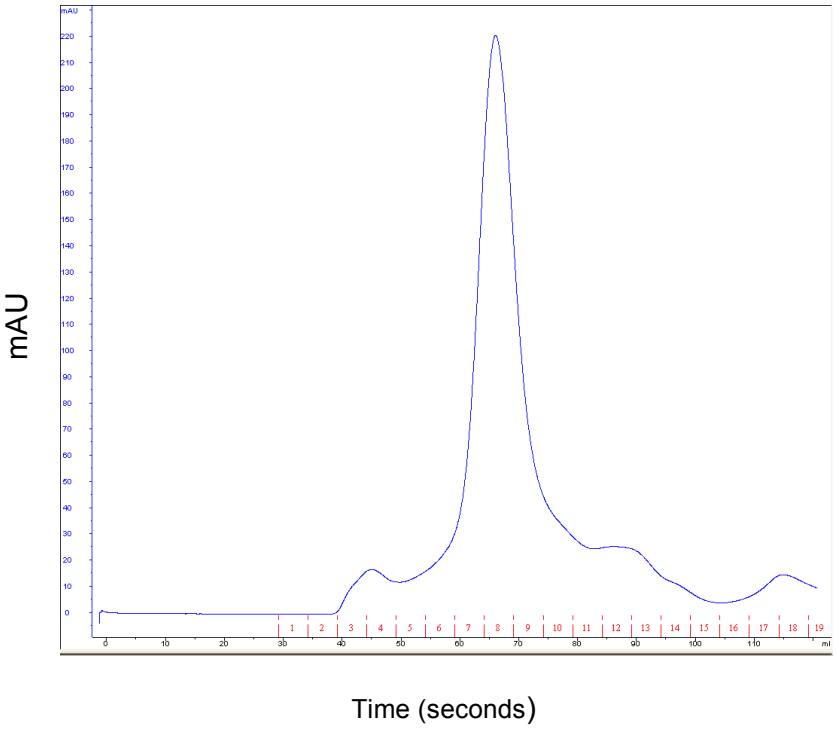

B

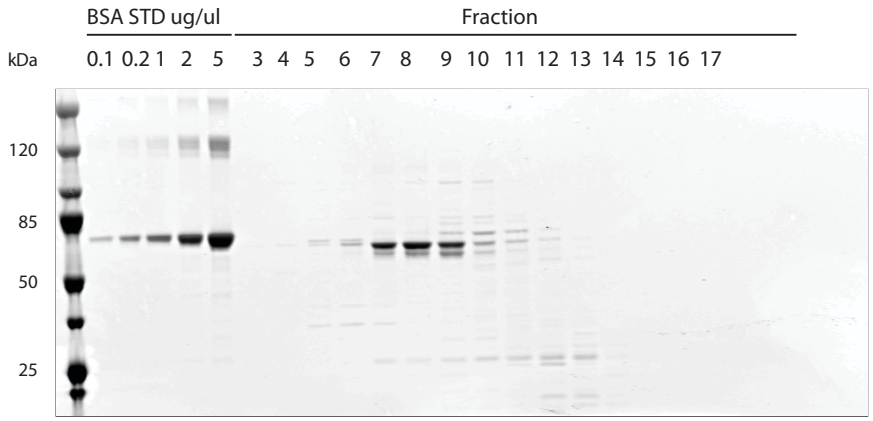

Figure 7.6 Size exclusion chromatography of purified G6PD

(A) Chromatogram displaying purified His:hG6PD expressed in JM109DE3 *E.coli* cells. Nickel bead-separated fractions were pooled before separation by gel filtration. mAU; milli absorbance units (B) SEC fraction separated on a SDS-PAGE gel, alongside a BSA quantification curve and stained with coomassie blue.

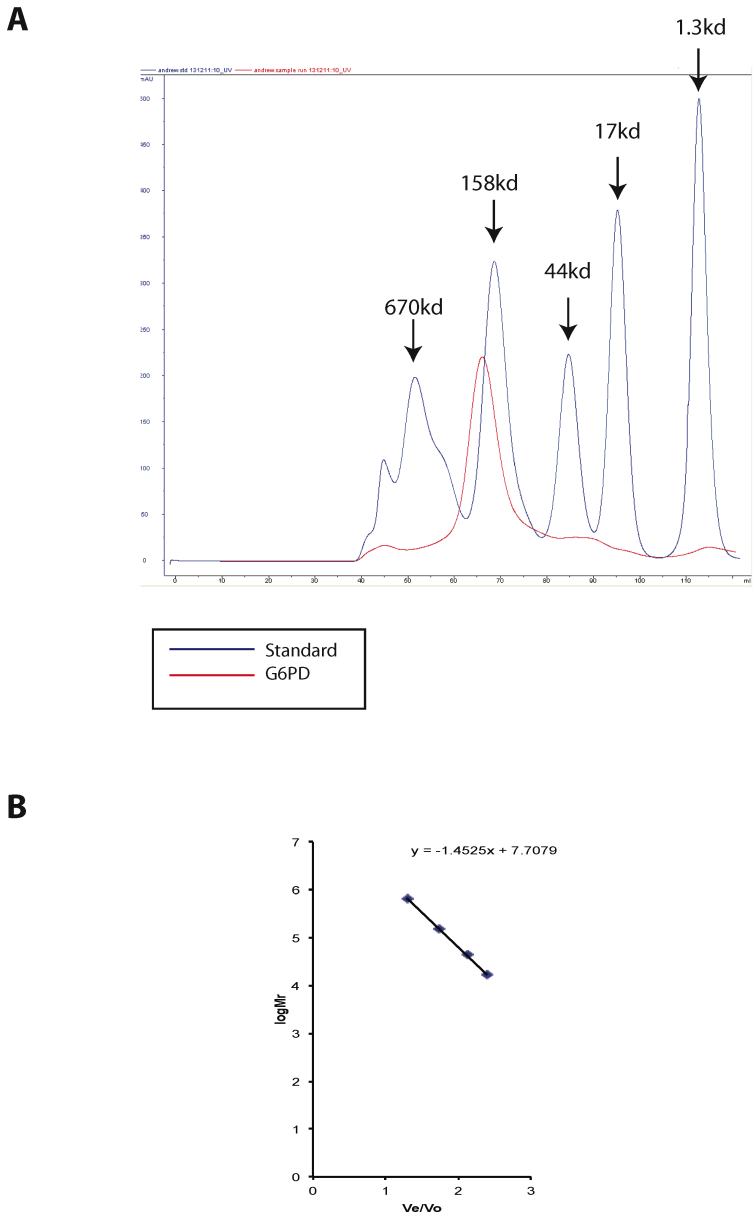

Figure 7.7 SEC standard curve and G6PD molecular weight estimation

(A) Overlay of protein standards (blue) and His:hG6PDH (red) purified from JM109DE3 cells on after gel filtration column (B) Standard curve and equation used to estimate molecular weight/oligomer species.

7.1.3 Enzyme assay development

In order to assess the ability of small molecules to modulate G6PD activity, an isolated molecular target assay was designed (Figure 7.8A). The reduction of NADP to NADPH was measured by fluorescence intensity, which is directly proportional to the rate of G6PD activity. Molecules that affected NADPH production could, therefore, be considered as 'hits'. An array of test experiments was required to optimise the conditions for a large HTS compound screen; the basic assay procedure is outlined in Figure 7.8B.

The specific reaction mixture conditions were first determined using purified recombinant His:hG6PD. Next, the SEC purified fractions were tested for activity and inhibition potential, to ensure the optimal factions was selected for the HTS procedure. All fractions could be inhibited with the known G6PD inhibitor, 5-Dehydroepiandrosterone (DHEA), and factions six, seven and eight displayed the greatest activity (Figure 7.8C). Given that fraction eight displayed the greatest concentration, activity and showed good purity, it was selected for use in the primary screen and for further assay optimisation. This characterisation provided evidence for a physiologically relevant and catalytically active enzyme that would give the greatest possible chance of discovering small chemical molecules that could modulate G6PD activity.

Enzyme inhibition was tested over a dose range to ensure the enzyme could be inhibited in a dose-dependent manner. Figure 7.9 demonstrates that the enzyme could be inhibited with DHEA, producing an IC_{50} of 10.02μM. Importantly, there was very little difference between 96 and 384-well format, confirming 384-well plates could be used to assay the 20,000 compounds. As DHEA could inhibit G6PD *in vitro*, the compound was chosen to act a positive control and any compounds that inhibited G6PD to similar level would be considered 'hits', given that the sample compounds were 5-fold less concentrated.

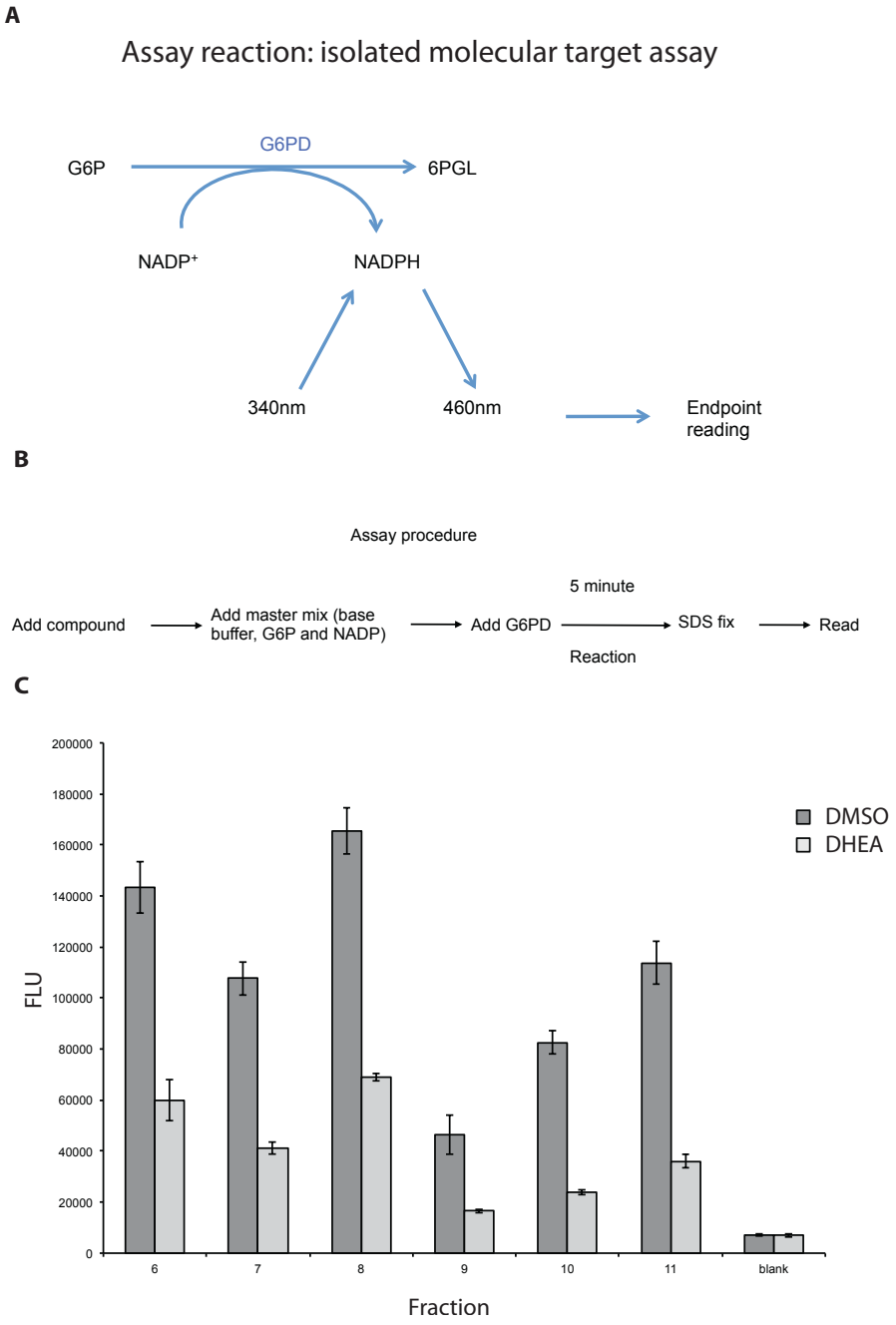

Figure 7.8 Assay reaction scheme

A) Assay reaction outline. G6PD catalyses the irreversible oxidation of glucose-6-phosphate (G6P) to 6-phosphoglucono-δ-lactone, resulting in the subsequent reduction of $NADP^+$. (B) Outline of reaction strategy. Compounds were used at a 20μM final concentration. NADPH is excited at 340nm and gives a 460nm emission (C) Fraction activity of 1ng SEC-purified His:hG6PD, in the presence of DMSO and DHEA, using the above assay conditions. Error bars represent SD, N=3.

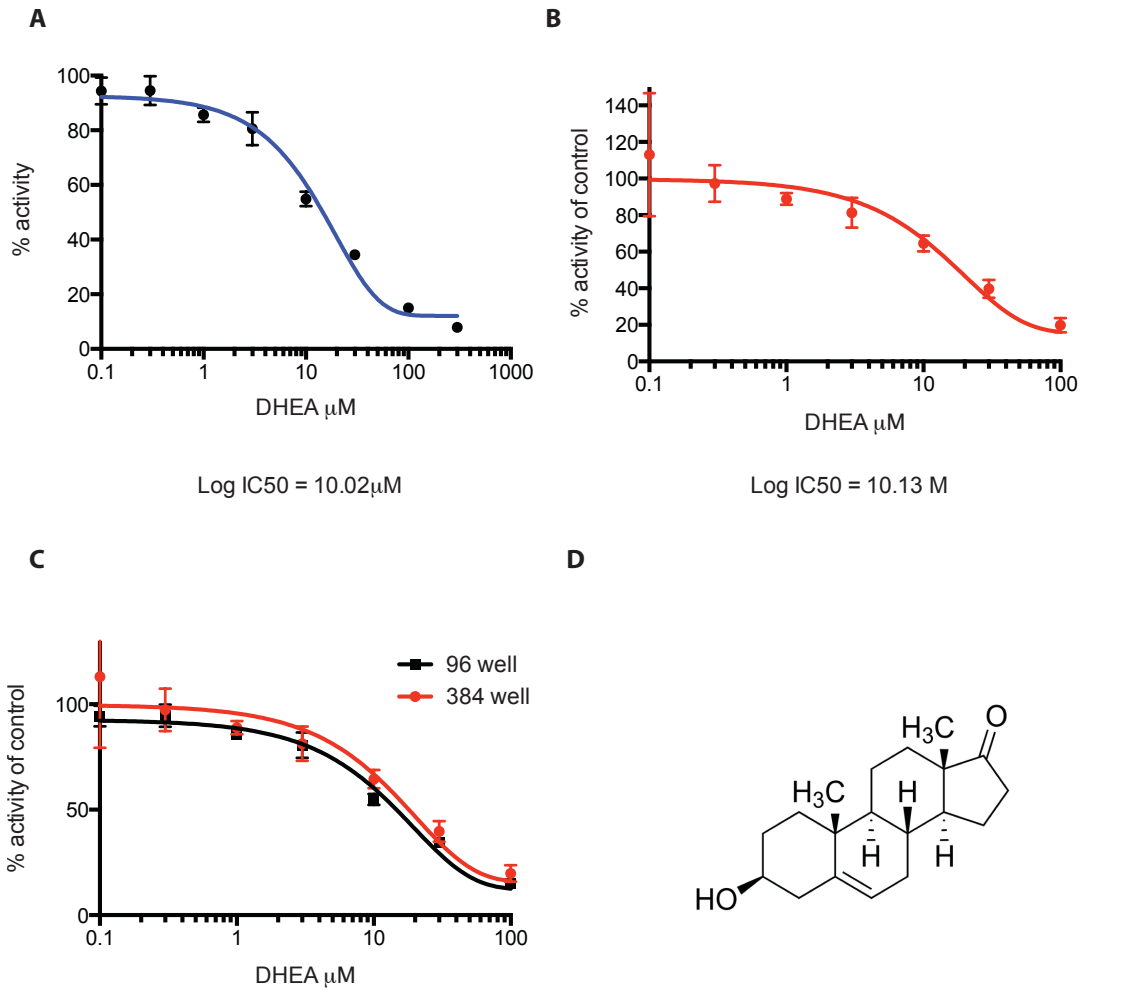

Figure 7.9 Inhibition of purified enzyme

(A,B,C) Dose response curves and IC_{50} values of His:hG6PD. A range of DHEA doses were used in the assay to ensure a dose-dependent inhibition. Activity is expressed relative to control. (D) Chemical structure of DHEA. Error bars represent SD, N=3.

In order to assess whether the enzyme functioned as expected, without chemical modulation, and to determine an acceptable concentration for the primary screen, various enzyme concentrations were assayed (Figure 7.10A). Varying amounts of G6PD, ranging from 1-0.0625ng, were analysed and a dose-dependent relationship was observed, in the presence or absence of DHEA. The control/inhibition ratio remained constant at 2.5-fold for all enzyme amounts, except for the lowest concentration of 0.0625ng, where the ratio was reduced to 1.7-fold.

The upper range limit of detection was 250,000 Fluorescence intensity (FI) units. In order to identify inhibitors of G6PD, the reaction baseline for a fixed incubation period was required to be approximately 125,000 FI units, allowing detection of a sufficient dynamic range of enzymatic activity. From the data, it was clear that 0.5ng of G6PD per reaction provides this, giving a fluorescence value of 115,000 FI units, which provided the greatest dynamic range between DMSO control and inhibitor.

Rapid reaction termination was required to achieve an endpoint value, ensuring that all values could be compared and normalised to the DMSO control. As well as efficient termination of the NADPH produced by the reaction over the selected incubation period, NADPH was required to remain stable over time to ensure accurate read-out values were obtained, as the experimental process inevitably resulted in over two-hour periods between reading the first and last plates. Fluctuations in signal during this time would otherwise be problematic resulting in poor accuracy. The reaction was terminated using SDS, as this detergent denatured the protein and ceased NADPH production (Hamilton et al., 2012). A final concentration of 0.083% SDS was sufficient for reaction fixation and termination (Figure 7.10B) There was a small decay of NADPH signal over a four-hour period, however this was minimal and still allowed effective normalisation of plates.

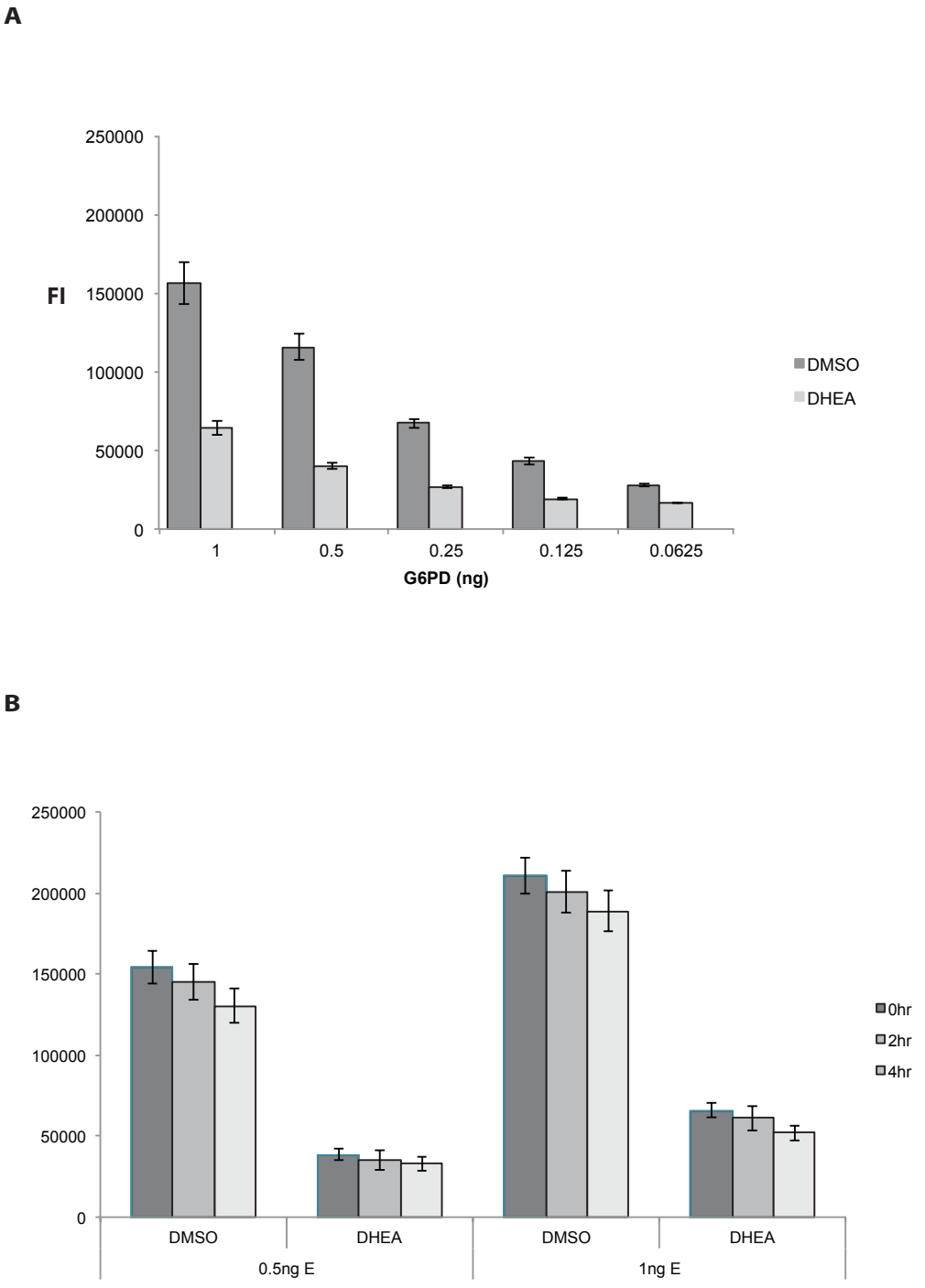

Figure 7.10 Enzyme dose and SDS termination

(A) Enzymatic activity relative to amount of enzyme added to reaction (1 - 0.625ng) -/+ DHEA. (B) SDS fixation of assay reaction with 0.083% SDS; 0.5 and 1ng of enzyme were tested. Error bars represent SD, N=3.

It was essential that the screen was carried out at the optimal reaction temperature to ensure accurate valid results, as enzyme reactions are sensitive to temperature (Daniel and Danson, 2013). To investigate the effect of temperature on the assay, reactions were performed at room temperature (RT), 25^{o}C and 37^{o}C and data demonstrated an inverse correlation between temperature and catalytic activity (Figure 7.11A). From the data, it was decided that the screen would be performed at RT due to optimal activity and practical advantages.

The inhibitor library used for the screen was the Chembridge DriverSet™, which contains 20,000 compounds dissolved in 100% DMSO. Therefore, the assay was tested for DMSO tolerance, by applying 1% and 10% DMSO to the assay reaction (Figure 7.11B). From the data, it was clear there was little difference in activity at either DMSO concentration, when compared to non-DMSO treated control. These data suggested that the reaction could be performed at 10% DMSO without compromising enzymatic activity and this concentration could be used to minimise the risk of compounds becoming insoluble in the reaction buffer.

7.1.4 The screen

In order to test assay quality, the *z*-factor was calculated (Figure 7.12A) (the value obtained was 0.67, which is regarded as an excellent assay). The *z*-factor takes into account the dynamic range (range between highest and lowest value) and the degree of separation between variability of controls. There was no overlap between positive control (inhibitor) and negative control (DMSO) variation, suggesting any effect comparable to the positive control in the screen was valid and not a result of noise.

With a fully optimised, robust and reproducible assay a pilot screen was first performed with a small kinase inhibitor library. Figure 7.12B shows a heat map of the kinase library replicated four times in a single 384-well plate, with the last lane containing DHEA as a positive control. The result clearly demonstrates that many compounds auto-fluoresced, which is a limitation of the wavelength used for this assay. In light of these findings, it was decided for the primary screen that an

enzyme-deficient screen would be performed to determine the intrinsic compound fluorescence and this could be subtracted from the screen endpoint value.

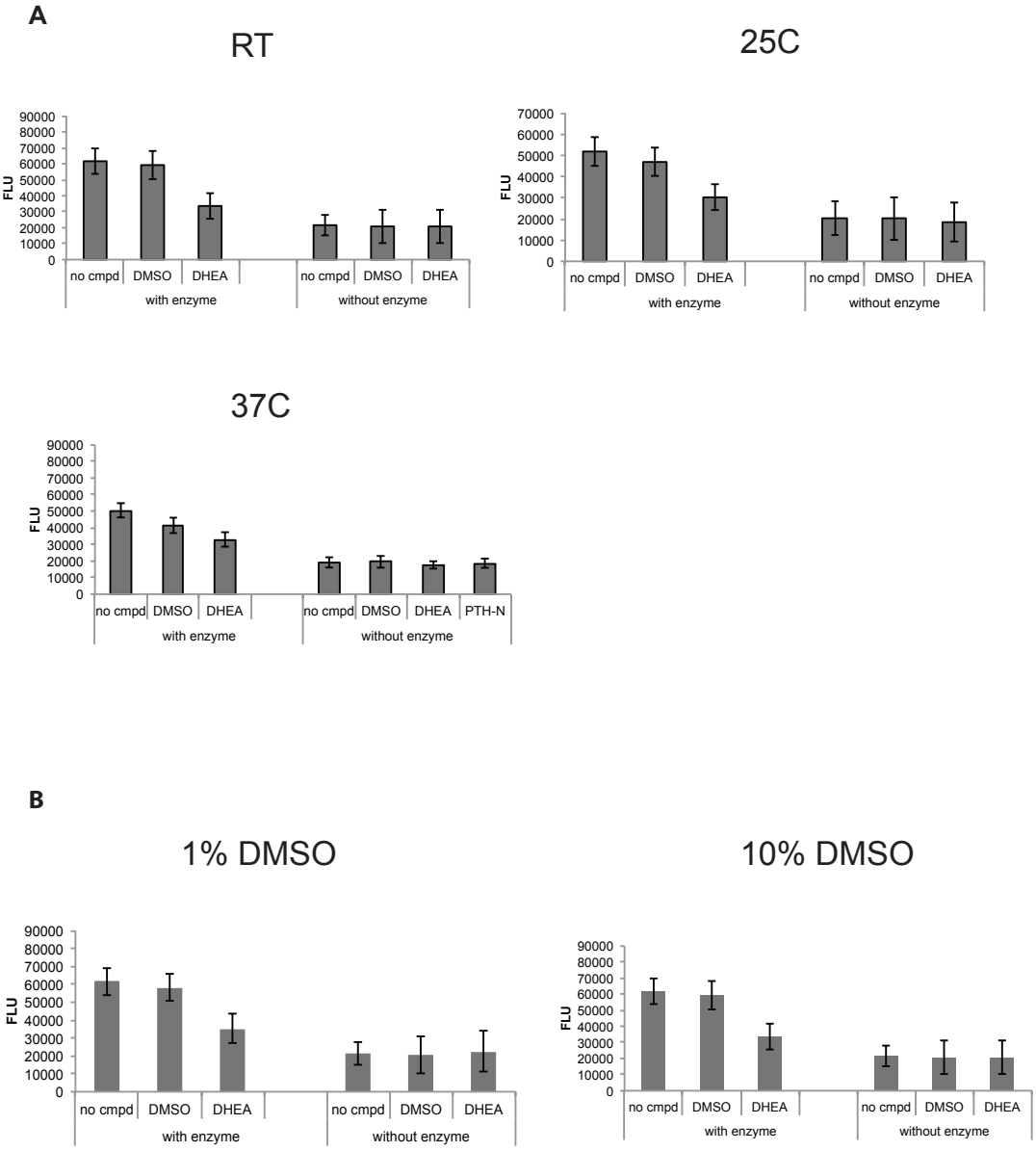

Figure 7.11 Temperature and DMSO tolerance

(A) Reactions were performed at room temperature, 25^{o}C and 37^{o}C in order to find the optimal temperature for the assay. (B) 1% or 10% DMSO was incubated in the reaction to test for tolerance to the solvent. Error bars represent SD, N=3.

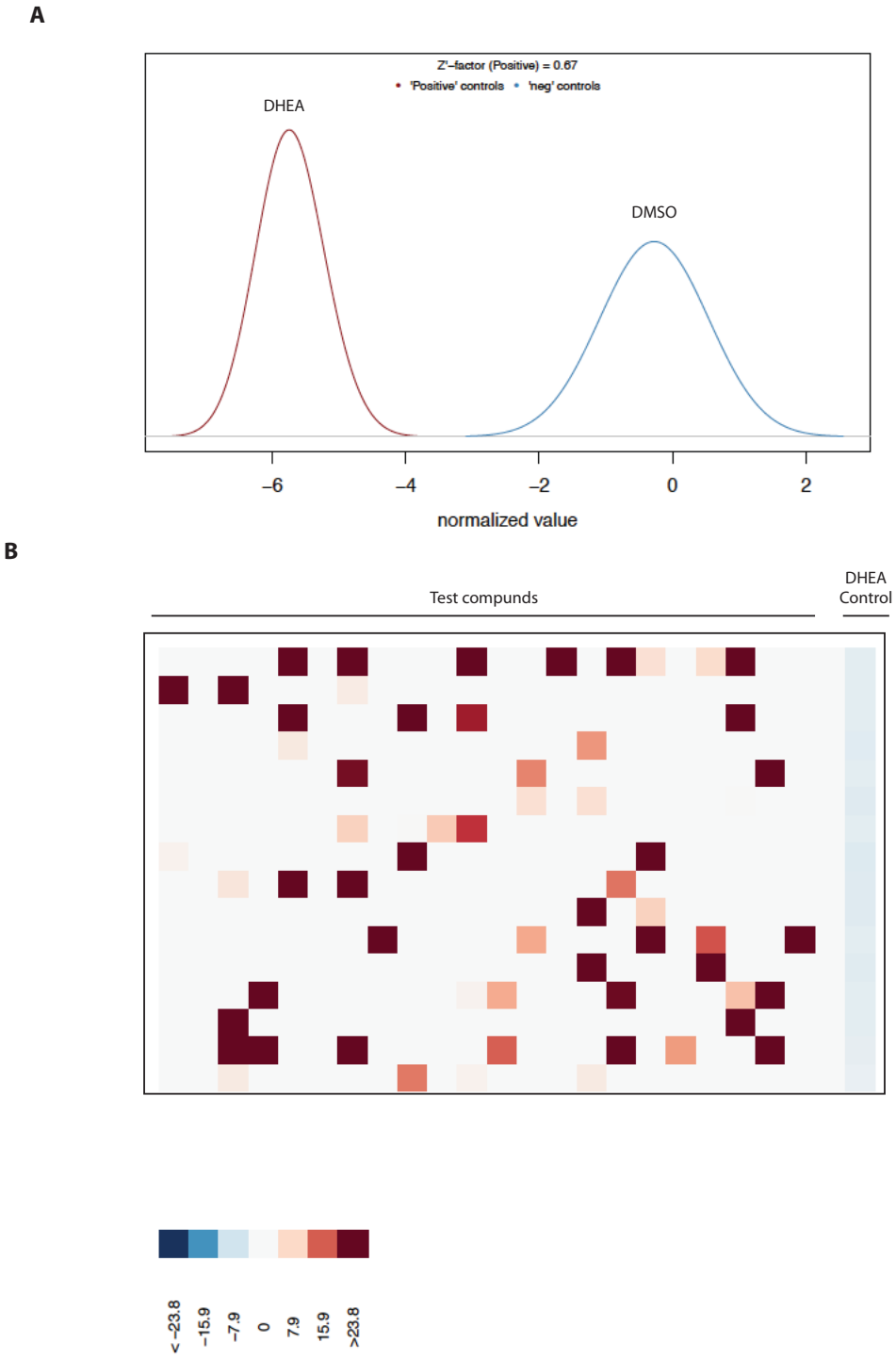

Figure 7.12 Pilot screen and z-factor

A) Assay *Z*-factor shows satisfactory distance between DMSO control and DHEA inhibitor control. (B) Heat map representing a kinase inhibitor library replicated four times in one 384-well plate. Blue represents low signal fluorescence and red high, which is relative to enzymatic activity. Many of the compounds showed auto fluorescence (orange-red squares).

7.1.5 Primary screen results

The primary screen was performed in triplicate with or without enzyme. The non-enzyme control screen provided autofluorescence data that was used to reduce the number of false positives. The library was screened in two parts, screening 10,000 compounds per experiment. Figure 7.13A shows the variation across all sixty-two 384-well plates. From the raw data, it is clear that four plates were incubated for an incorrect amount of time before fixation, however this error was corrected upon data normalisation.

Analysis for potential inhibitors was performed on all compounds that had low autofluorescence values, with the data expressed as a percentage of DMSO control. Inhibitors were defined as compounds that reduced signal by ≥25%, relative to control. Using this rule, eleven inhibitors were discovered in the primary screen and were re-ordered to repeat in a secondary screen (Figure 7.13B).

A

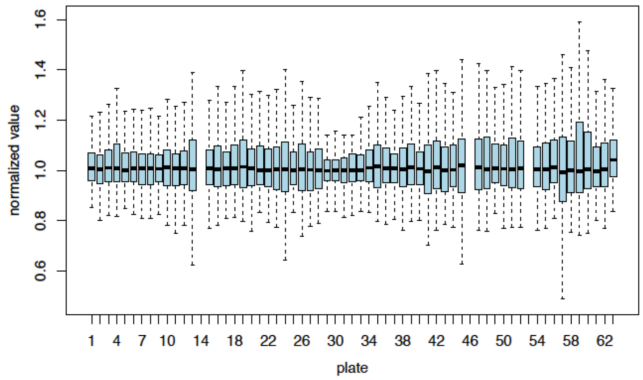

B

Mol Weight	Mol Formula	Mol Name	cLogP	LogSW	RB	tPSA	hDon	hAcc	Signal relative to DMSO control
260.3	$C_{13}H_{12}N_2O_2S$	(2-methyl-5-nitrophenyl)[(5-methyl-2-thienyl)methylene]amine	3.6	-4.173	2	55.5	0	3	0.73909
370.5	$C_{17}H_{26}N_2O_5S$	1-[(2,5-dimethoxyphenyl)sulfonyl]-4-(3-methylbutanoyl)piperazine	2.063	-3.663	2	76.15	0	6	0.73869
394.2	$C_{16}H_9Cl_2N_3O_3S$	5-(2-chloro-5-nitrobenzylidene)-2-[(2-chlorophenyl)imino]-1,3-thiazolidin-4-one	5.18	-6.888	2	84.6	1	4	0.73667
336.3	$C_{15}H_{17}F_5N_2O$	2,3,4,5,6-pentafluoro-N-(1-isopropyl-4-piperidinyl)benzamide	1.891	-3.267	2	32.34	1	2	0.73435
303.4	$C_{17}H_{21}NO_2S$	N-(2,4-dimethylphenyl)-2,4,6-trimethylbenzenesulfonamide	4.51	-5.264	2	46.17	1	2	0.73214
258.3	$C_{15}H_{15}FN_2O$	2-(2-fluorophenyl)-N-[1-(4-pyridinyl)ethyl]acetamide	1.673	-1.213	4	41.99	1	2	0.73002
285.4	$C_{18}H_{23}NO_2$	5,5-dimethyl-2-{[(2-phenylpropyl)amino]methylene}-1,3-cyclohexanedione	3.49	-3.254	4	46.17	1	2	0.72975
358.4	$C_{21}H_{18}N_4O_2$	1-(3-methoxyphenyl)-5-methyl-N-1-naphthyl-1H-1,2,3-triazole-4-carboxamide	3.781	-5.042	3	69.04	1	4	0.71843
387.5	$C_{20}H_{25}N_3O_3S$	1-[(4-sec-butylphenyl)sulfonyl]-4-(3-pyridinylcarbonyl)piperazine	3.304	-4.847	3	70.58	0	5	0.70806
203.2	$C_{11}H_9NO_3$	4-(4-hydroxybenzylidene)-3-methyl-5(4H)-isoxazolone	2.31	-2.076	1	58.89	1	4	0.70343
387.2	$C_{15}H_{12}Cl_2N_2O_4S$	4-[(2,3-dichloro-4-methoxyphenyl)sulfonyl]-3,4-dihydro-2(1H)-quinoxalinone	2.921	-4.63	1	75.71	1	4	0.56594

Figure 7.13 Primary screen results

(A) Normalised values representing the signal variation across all plates. (B) Table of inhibitors identified from the primary screen, displaying chemical formula, physiochemical properties and normalised signal. cLogP; Lipid solubility. LogSW; Water solubility. RB; Rotatable bonds. hDon; Hydrogen donor. hAcc; Hydrogen acceptor.

7.1.6 Secondary screen and hit validation

The secondary screen employed the same methods as the primary and was carried out over a dose range of 0.01-60μM for each compound. Only 9126408 ($C_{15}H_{12}CL_2N_2O_4S$) validated in the secondary screen, displaying a dose-dependent relationship and was confirmed as a G6PD inhibitor (Figure 7.14A).

The physiochemical properties presented provide evidence that the compound is soluble and has low toxicity odds. A LogSW (water solubility) value of 4.63 is suggestive of good solubility in water, while a CLogP value of 2.9 is indicative of good lipid solubility, suggesting that the compound could pass through lipid membranes (Sangester, 1989) (Figure 7.14A). Analogues of 9126408 were obtained (6731786 [$C_{16}H_{16}N_2O_4S$) and 9121326 [$C_{15}H_{13}CLNO_4S$]) to investigate if they also showed activity (Figure 7.14B). Chemical analogues have similar molecular structures but differ by certain components (e.g. different functional groups) and are often used in drug discovery in order to investigate how a molecule interacts with its target, as well as to increase potency (McKinney et al., 2000). The two analogues tested did show activity against G6PD, suggesting a relationship between this class of compound and G6PD inhibition. A greater number of number of chloride atoms on each molecule correlated positively with potency suggesting these groups are important in the mechanism of inhibition. However, neither was as potent as the screen 'hit' and, therefore, were not taken forward and 9126408 remained as the lead compound.

Drugs designed to target a specific enzyme can have off-target effects, especially with proteins that share a similar structure and function. As G6PD is a dehydrogenase that oxidises glucose-6-phoshate permitting reduction of NADP→NADPH, isocitrate dehydrogenase (IDH1) was chosen as a means to investigate target specificity. IDH1 catalyses the production of α-ketoglutarate from isocitrate and also uses NADP as a co-factor in a dehydrogenation reaction, similar to the G6PD-mediated reaction (Smolkova and Jezek, 2012). Compound 9126408 showed no activity against IDH1, providing preliminary evidence of target specificity Figure 7.14C. In order to investigate if the compound demonstrated activity against endogenous G6PD, human breast adenocarcinoma cells (MCF-7) were lysed by

sonication to obtain a native extract with an intact and active G6PD. Native cell lysates were supplemented with NADP, glucose-6-phosphate and 9126408 or DHEA (Figure 7.14D). It was clear that endogenous G6PD could also be inhibited effectively, suggesting the compound may show efficacy in cell line systems.

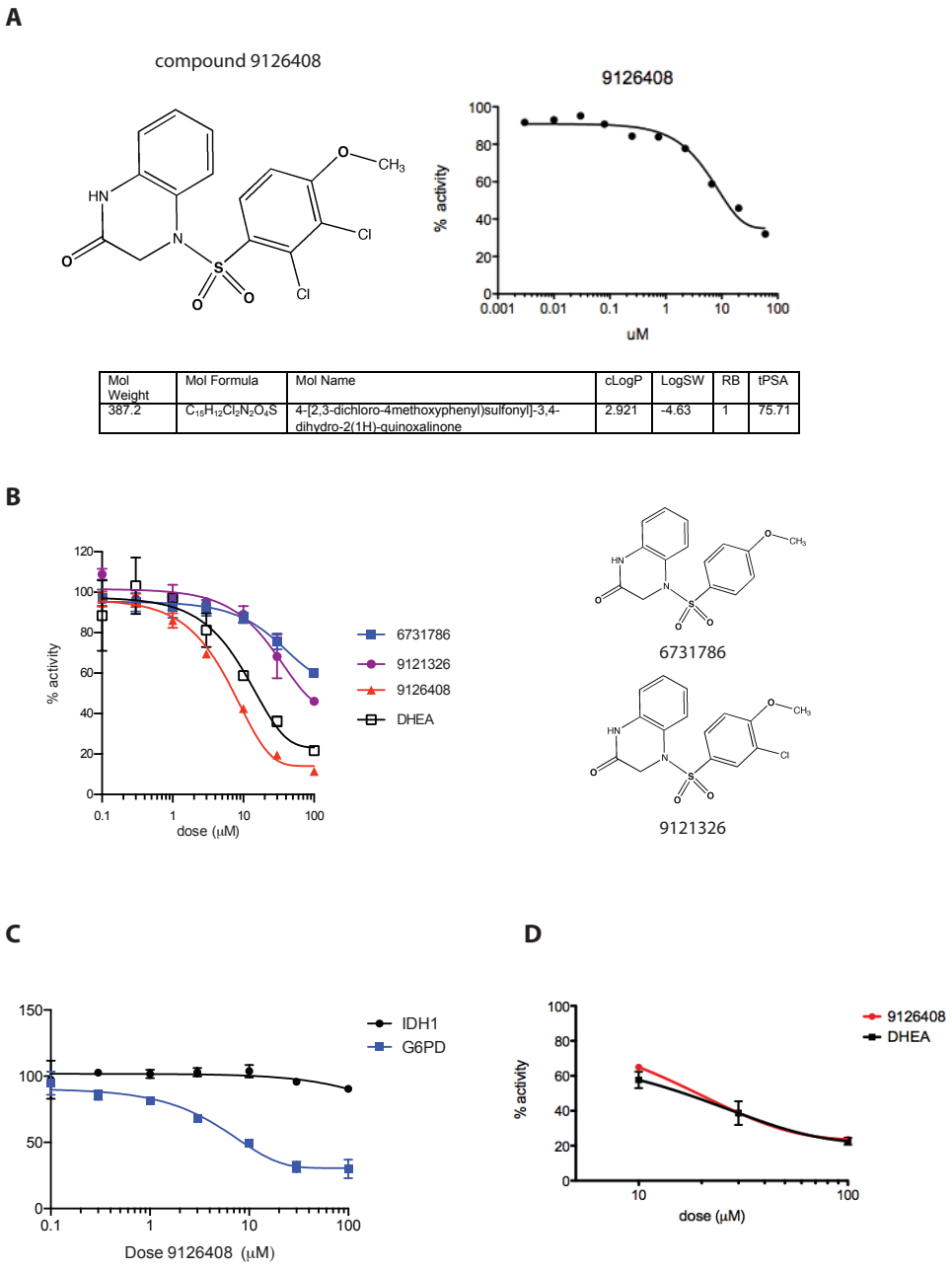

Mol Weight	Mol Formula	Mol Name	cLogP	LogSW	RB	tPSA
387.2	$C_{15}H_{12}Cl_2N_2O_4S$	4-[2,3-dichloro-4methoxyphenyl)sulfonyl]-3,4-dihydro-2(1H)-quinoxalinone	2.921	-4.63	1	75.71

Figure 7.14 Hit validation of compound 9126408

(A) Compound 9126408 structure, secondary screen result and physiochemical properties. Compound 9126408 was assayed with all primary hits in the secondary screen. (B) Analysis of 9126408 analogues in the G6PD assay. (C) IDH1 was incubated with a range of 9126408 to investigate compound specificity to G6PD. (D) MCF-7 native lysates were prepared by sonication to investigate if 9126408 could inhibit endogenous G6PD. Error bars represent the SD (N=3) for all experiments.

7.1.7 Discussion and Conclusions

The aim of this chapter was to discover inhibitors of G6PD, as they may provide therapeutic benefit, and it was anticipated that the 'hit' compounds could be used for research in cell lines, in an attempt to improve the effect of radiotherapy. Recombinant tetrameric G6PD was successfully purified and its function assessed in an enzymatic assay. The assay was designed to be as robust as possible, in order to reproducibly screen 20,000 compounds. A number of inhibitors were identified in the primary screen and one inhibitor was validated. The validated inhibitor displayed a dose-dependent relationship with the enzyme and was more potent than its commercially available analogues. The compound showed no activity against an enzyme of similar catalytic function as G6PD (IDH1), suggesting a degree of specificity and showed activity against endogenous G6PD in cells.

The primary screen used the Chembridge DriverSet™ consisting of 20,000 compounds picked to provide high coverage of chemical space, covering all possible stoichiometric configurations in all possible topological isomers. Using a library such as this, increases the probability of discovering 'hits', as many classes of compounds are represented. The compounds in the library have been selected to ensure favourable physicochemical properties, such as solubility and lipophilicity, while undesirable chemical groups that may cause toxicity have been omitted.

The primary screen identified a potential inhibitor of G6PD. The compound (no. 9126408) displayed IC_{50} values comparable to the standard inhibitor DHEA (~10μM), providing a starting point for development. Analogues of the compound were commercially available and were obtained and tested in the assay, however showed inferior potency compared to 9126408. The physiochemical properties of the molecule were also promising, suggesting water and lipid solubility. A relationship between topological polar surface area and CLogP has been reported and can be used to predict potential compound toxicity. Compounds with a CLogP >3 and TPSA <75A^2 appear to be 25x more likely to have off-target effects and cause toxicity (Allen et al., 2010). Compound 9126408 does not fall into this category, as both parameters were within the aforementioned limits, implying that the compound is less likely to have toxic off-target effects.

A clear issue with 9126048 is a high IC_{50} of 10μM. This was expected, as HTS screening intends to find molecules that can be used as a foundation for further chemical optimisation. However, when used in the cell lysate system, the inhibition potential of the compound was reduced and in cell lines this is expected to fall even further. Therefore, the next stage of the process is to collaborate with medicinal chemists in order to perform structural activity relationship (SAR) analysis that can increase potency and further improve solubility. Increased efficacy and potency will also reduce the likelihood of cellular toxicity, as lower doses would suffice for activity.

Future work on the compound would also involve determination of Michaelis-Menten kinetics to understand whether the inhibition is competitive or allosteric (Strelow et al., 2004). As the assay was performed at V^{max}, where enzyme substrate is in excess and not rate-limiting, this favours the discovery of allosteric inhibitors. In contrast to competitive inhibitors that bind active sites, allosteric inhibitors interact with sites that are less evolutionary conserved and therefore can display grater selectivity (May et al., 2007). This is demonstrated by the specific inhibition of G6PD by compound 9126048, by comparison to IDH1. In order to further increase confidence in the specificity of the compound to G6PD, a panel of oxidoreductases should be screened. This assay would best be performed after the SAR process, as a more potent molecule is less likely to interact with other enzymes (Hughes et al., 2011). After compound optimisation *in vitro,* cell lines should be treated to investigate whether the compound can reach its target and potentiate the effect of IR.

The degree of compound autofluorescence was a major limitation in the presented assay. The primary screen was performed with and without enzyme in order to assess the level of background fluorescence. Background fluorescence could be subtracted from medium-to-low fluorescing compounds, however, highly fluorescent compounds that saturated the detection threshold were problematic, as the enzyme reaction combined with autofluorescence pushed the signal beyond the detection range and subtraction would result in incorrect results. Even with the removal of fluorescent compounds from the analysis, the secondary screen

activators did not validate. It is likely that these compounds autofluoresced in the primary and not in the secondary screen. This may be due to bond rotations within the molecule leading to false positives results.

In order to overcome this problem, the screen should be repeated using a different wavelength for excitation and emission, or using a non-fluorescence based approach. Large fractions of screening libraries contain heterocyclic molecules and compounds with conjugated bonds that are responsible for autofluorescence at short wavelengths (Thorne et al., 2010). Data has shown that screens performed in the blue spectral region (340/460nm) are likely to have a greater proportion of autofluorescent compounds; approximately 2-5% of the library (Thorne et al., 2010). Conversely, excitation in the red/orange (e.g. 540ex/590em) spectrum ensures background fluorescence is reduced to approximately 0.004-0.01% (Thorne et al., 2010).

During the course of this investigation, Hamilton *et al* synthesised a novel uncompetitive inhibitor of G6PD (Hamilton et al., 2012). The steroid based compound was a 10-fold more potent derivative of DHEA. In addition to good physiochemical properties, the DHEA derivatives could inhibit cellular G6PD in the low μM range. It will be interesting to see if these compounds can potentiate the effects of DNA damage and CIN after IR treatment, and if their potency can be further increased into the nM range.

In conclusion, this chapter aimed to find novel inhibitors of G6PD that could be used in cell line systems to inhibit the function of the PPP. An inhibitor was discovered and preliminary experiments warrant further optimisation of the molecule by medicinal chemistry techniques. Compound autofluorescence may have masked a number of positive ‘hits’. A repeat screen exciting within the red spectrum would provide a greater chance of increasing the ‘hit’ rate.

7.1.8 Methods

7.1.8.1 G6PD assay and screen

The G6PD plasmid was kindly provided by Dr Dominic James (CRUK Patterson Institute). Protein purification, assay development and guidance were provided by Dr Ed McKenzie (Manchester University).

7.1.8.2 Protein purification

pHis: hG6PDH (Figure 7.15) plasmid was freshly transformed into JM109DE3 cells and plated into LB amp selection plate. A single colony was used to inoculate 5 ml LB amp and was incubated for 8 hours at 37^{o}C. The 5ml starter culture was then used to inoculate a 500ml auto-induction broth (for 1L; 6g phosphate buffer pH 7.2 6g Na_2HPO_4/3g KH_2PO_4, 20g trypton, 5g yeast extract, 5g NaCl, 60 % v/v Glycerol, 10 % w/v Glucose, 8 % w/v Lactose) and left overnight at 37^{o}C with shaking (220rpm). Cells were harvested by centrifugation (4000rpm for 10mins) and resuspended in 20mL lysis buffer (50mM NaP, 0.3M NaCl, pH 8.0 and 1% Triton X-100 supplemented with proteinase inhibitors).

Samples were sonicated for six 30 second bursts on ice (setting 20%) and spun at 20,000rpm for 30 minutes at 4^{o}C. Lysates were incubated in batch to nickel-sepharose beads (Qiagen) in the presence of 10mM imidazole for 2 hours at 4^{o}C (on roller). Beads were pelleted and washed with increasing stringency buffers containing 10mM-50mM imidazole in lysis buffer-free detergent. Protein was eluted in 250mM imidazole and fractions 1-3 pooled. Proteins were further purified and analysed by gel filtration on a superdex200 (120ml column volume) column at 4^{o}C. BioRad protein standards were used to determine molecular species of glucose-6-phosphaste dehydrogenase (G6PD). Eluted sample was stored in 50mM NaP, 0.3M NaCl, pH8.0, 10% glycerol buffer at -80^{o}C.

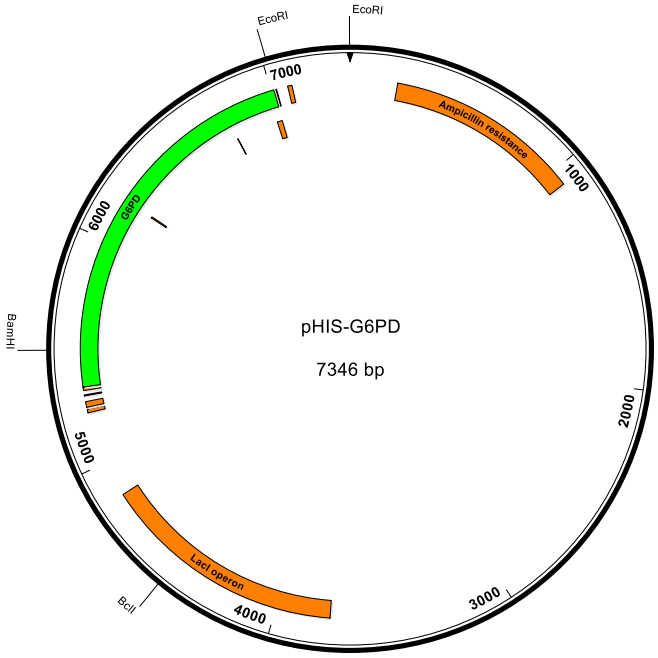

Figure 7.15 pHis-G6PD plasmid map

7.1.8.3 Enzyme reaction assay

The following methods were adjusted for one assay reaction in a 96-well format, whereas ¼ of the indicted volume was used for 384-well format. 10µl of test compound or dimethyl sulfoxide (DMSO) (control) was dispensed into corresponding wells. Then, 50µl of G6PD assay base buffer 2.5x (50mM Tris pH 8.0, $MgCl_2$ 25mM, BSA 0.0075% [w/v]), 10µl of 10x glucose-6-phosphate (500µM final concentration; Sigma-Aldrich) and 10µl of 10x G6PD recombinant enzyme were mixed to create a master mix and dispensed in wells. Finally, 20µl of 5x nicotinamide adenine dinucleotide phosphate (NADP) (50µM final concentration; Sigma-Aldrich) was added to start the reaction. After five minutes at room temperature the reaction was inhibited with sodium dodecyl sulfate (SDS) (Sigma-

Aldrich) at 0.083% final concentration. Endpoint fluorescence was analysed on a Pherastar (BMG Labtech) plate reader at Ex340/Em440nm.

7.1.8.4 Screening procedure

2.5µl of compound dissolved in DMSO (1µM final concentration) was dispended using a Biomek® FXP Laboratory Automation Workstation and stored at -80^{o}C until screening. Compound plates were thawed for 20 minutes at room RT. Plates were centrifuged at 1,200rpm to ensure compounds were equally distributed in wells. Next, 17.5µl/well NAPD master-mix was applied to each well using WellMate liquid handlers. 5µl/well G6PDH (10X) enzyme was then added to start the reaction. Plates were incubated at room temperature for five minutes. To inhibit the reaction, 5µl of SDS was applied to each well (final concentration 0.5%). Fluorescence intensity signal was immediately measured on the Pherastar Plate reader (Ex340/Em440nm).

7.1.8.5 Isocitrate dehydrogenase assay

1µg of human recombinant isocitrate dehydrogenase (Sigma-Aldrich) was incubated with NADP 5.2mM isocitrate (Sigma-Aldrich) in assay base buffer. Reactions were carried out a room temperature for five minutes before SDS fixing. Endpoint fluorescence was analysed on a Pherastar (BMG Labtech) plate reader at Ex340/Em440nm.

7.1.8.6 Native extract assay

MCF-7 cells were trypsinised and washed in cold PBS 4^{o}C. Cells were sonicated six times for 10 seconds and cooled on ice. Lysates were centrifuged at 13,000rpm for 15 minutes (4^{o}C). Protein concentrations were determined by Bradford assay and 25µg of lysate was incubated with 0.5mM NADP, 5mM G6P, 10mM Tris pH 7.5 and 3mM $MgCl_2$. Fluorescence was analysed on a Pherastar (BMG Labtech) plate reader at Ex340/Em440nm over a five minute period.

Reference List

ABBAS, T. & DUTTA, A. 2009. p21 in cancer: intricate networks and multiple activities. *Nat Rev Cancer,* 9**,** 400-14.

ABDEL-FATTAH, G., YOFFE, B., KRISHNAN, B., KHAOUSTOV, V. & ITANI, K. 2000. MDM2/p53 protein expression in the development of colorectal adenocarcinoma. *J Gastrointest Surg,* 4**,** 109-14.

AHUJA, D., SAENZ-ROBLES, M. T. & PIPAS, J. M. 2005. SV40 large T antigen targets multiple cellular pathways to elicit cellular transformation. *Oncogene,* 24**,** 7729-45.

ALAO, J. P. 2007. The regulation of cyclin D1 degradation: roles in cancer development and the potential for therapeutic invention. *Mol Cancer,* 6**,** 24.

ALLEN, J., JEFFREY, P., WILLIAMS, R. & RATCLIFFE, A. J. 2010. Approaches to assessing drug safety in the discovery phase. *Drugs of the future,* 35 (1)**,** 67-75.

ANDREASSEN, P. R., LACROIX, F. B., LOHEZ, O. D. & MARGOLIS, R. L. 2001a. Neither p21WAF1 nor 14-3-3sigma prevents G2 progression to mitotic catastrophe in human colon carcinoma cells after DNA damage, but p21WAF1 induces stable G1 arrest in resulting tetraploid cells. *Cancer Res,* 61**,** 7660-8.

ANDREASSEN, P. R., LOHEZ, O. D., LACROIX, F. B. & MARGOLIS, R. L. 2001b. Tetraploid state induces p53-dependent arrest of nontransformed mammalian cells in G1. *Mol Biol Cell,* 12**,** 1315-28.

AYLON, Y., MICHAEL, D., SHMUELI, A., YABUTA, N., NOJIMA, H. & OREN, M. 2006. A positive feedback loop between the p53 and Lats2 tumor suppressors prevents tetraploidization. *Genes Dev,* 20**,** 2687-700.

AYLON, Y. & OREN, M. 2011. p53: Guardian of ploidy. *Molecular Oncology,* 5**,** 315-323.

BAE, D. H., JANSSON, P. J., HUANG, M. L., KOVACEVIC, Z., KALINOWSKI, D., LEE, C. S., SAHNI, S. & RICHARDSON, D. R. 2013. The role of NDRG1 in the pathology and potential treatment of human cancers. *J Clin Pathol,* 66**,** 911-7.

BAGUI, T. K., MOHAPATRA, S., HAURA, E. & PLEDGER, W. J. 2003. P27Kip1 and p21Cip1 are not required for the formation of active D cyclin-cdk4 complexes. *Mol Cell Biol,* 23**,** 7285-90.

BALSAS, P., GALAN-MALO, P., MARZO, I. & NAVAL, J. 2012. Bortezomib resistance in a myeloma cell line is associated to PSMbeta5 overexpression and polyploidy. *Leuk Res,* 36**,** 212-8.

BARTEK, J. & HODNY, Z. 2014. PARK2 orchestrates cyclins to avoid cancer. *Nat Genet,* 46**,** 527-8.

BARTKOVA, J., HOREJSI, Z., KOED, K., KRAMER, A., TORT, F., ZIEGER, K., GULDBERG, P., SEHESTED, M., NESLAND, J. M., LUKAS, C., ORNTOFT, T., LUKAS, J. & BARTEK, J. 2005. DNA damage response as a candidate anti-cancer barrier in early human tumorigenesis. *Nature,* 434**,** 864-70.

BENDALL, S. C., HUGHES, C., STEWART, M. H., DOBLE, B., BHATIA, M. & LAJOIE, G. A. 2008. Prevention of amino acid conversion in SILAC experiments with embryonic stem cells. *Mol Cell Proteomics,* 7**,** 1587-97.

BENGTSSON, H., NEUVIAL, P. & SPEED, T. P. 2010. TumorBoost: normalization of allele-specific tumor copy numbers from a single pair of tumor-normal genotyping microarrays. *BMC Bioinformatics,* 11**,** 245.

BENGTSSON, H., RAY, A., SPELLMAN, P. & SPEED, T. P. 2009. A single-sample method for normalizing and combining full-resolution copy numbers from multiple platforms, labs and analysis methods. *Bioinformatics,* 25**,** 861-7.

BEUMER, T. L., ROEPERS-GAJADIEN, H. L., GADEMAN, I. S., KAL, H. B. & DE ROOIJ, D. G. 2000. Involvement of the D-type cyclins in germ cell proliferation and differentiation in the mouse. *Biol Reprod,* 63**,** 1893-8.

BIRKBAK, N. J., EKLUND, A. C., LI, Q., MCCLELLAND, S. E., ENDESFELDER, D., TAN, P., TAN, I. B., RICHARDSON, A. L., SZALLASI, Z. & SWANTON, C. 2011. Paradoxical relationship between chromosomal instability and survival outcome in cancer. *Cancer Res,* 71**,** 3447-52.

BIRKBAK, N. J., WANG, Z. C., KIM, J. Y., EKLUND, A. C., LI, Q., TIAN, R., BOWMAN-COLIN, C., LI, Y., GREENE-COLOZZI, A., IGLEHART, J. D., TUNG, N., RYAN, P. D., GARBER, J. E., SILVER, D. P., SZALLASI, Z. & RICHARDSON, A. L. 2012. Telomeric allelic imbalance indicates defective DNA repair and sensitivity to DNA-damaging agents. *Cancer Discov,* 2**,** 366-75.

BLAGOEV, B., KRATCHMAROVA, I., ONG, S. E., NIELSEN, M., FOSTER, L. J. & MANN, M. 2003. A proteomics strategy to elucidate functional protein-protein interactions applied to EGF signaling. *Nat Biotechnol,* 21**,** 315-8.

BLAGOSKLONNY, M. V. 2007. Mitotic arrest and cell fate: why and how mitotic inhibition of transcription drives mutually exclusive events. *Cell Cycle,* 6**,** 70-4.

BLOMMEL, P. G., BECKER, K. J., DUVNJAK, P. & FOX, B. G. 2007. Enhanced bacterial protein expression during auto-induction obtained by alteration of lac repressor dosage and medium composition. *Biotechnol Prog,* 23**,** 585-98.

BOCKSTAELE, L., COULONVAL, K., KOOKEN, H., PATERNOT, S. & ROGER, P. P. 2006a. Regulation of CDK4. *Cell Div,* 1**,** 25.

BOCKSTAELE, L., KOOKEN, H., LIBERT, F., PATERNOT, S., DUMONT, J. E., DE LAUNOIT, Y., ROGER, P. P. & COULONVAL, K. 2006b. Regulated activating Thr172 phosphorylation of cyclin-dependent kinase 4(CDK4): its relationship with cyclins and CDK "inhibitors". *Mol Cell Biol,* 26**,** 5070-85.

BOUTROS, R., LOBJOIS, V. & DUCOMMUN, B. 2007. CDC25 phosphatases in cancer cells: key players? Good targets? *Nat Rev Cancer,* 7**,** 495-507.

BRADFORD, M. M. 1976. A rapid and sensitive method for the quantitation of microgram quantities of protein utilizing the principle of protein-dye binding. *Anal Biochem,* 72**,** 248-54.

BRAGADO, P., ARMESILLA, A., SILVA, A. & PORRAS, A. 2007. Apoptosis by cisplatin requires p53 mediated p38alpha MAPK activation through ROS generation. *Apoptosis,* 12**,** 1733-42.

BROWN, E. J. & BALTIMORE, D. 2000. ATR disruption leads to chromosomal fragmentation and early embryonic lethality. *Genes Dev,* 14**,** 397-402.

BRUZZANITI, A. & BARON, R. 2006. Molecular regulation of osteoclast activity. *Rev Endocr Metab Disord,* 7**,** 123-39.

BUIS, J., WU, Y., DENG, Y., LEDDON, J., WESTFIELD, G., ECKERSDORFF, M., SEKIGUCHI, J. M., CHANG, S. & FERGUSON, D. O. 2008. Mre11 nuclease activity has essential roles in DNA repair and genomic stability distinct from ATM activation. *Cell,* 135**,** 85-96.

BURRELL, R. A., MCCLELLAND, S. E., ENDESFELDER, D., GROTH, P., WELLER, M. C., SHAIKH, N., DOMINGO, E., KANU, N., DEWHURST, S. M., GRONROOS, E., CHEW, S. K., ROWAN, A. J., SCHENK, A., SHEFFER, M., HOWELL, M., KSCHISCHO, M., BEHRENS, A., HELLEDAY, T., BARTEK, J., TOMLINSON, I. P. & SWANTON, C. 2013a. Replication stress links structural and numerical cancer chromosomal instability. *Nature,* 494**,** 492-6.

BURRELL, R. A., MCGRANAHAN, N., BARTEK, J. & SWANTON, C. 2013b. The causes and consequences of genetic heterogeneity in cancer evolution. *Nature,* 501**,** 338-45.

CANCER GENOME ATLAS RESEARCH, N. 2008. Comprehensive genomic characterization defines human glioblastoma genes and core pathways. *Nature,* 455**,** 1061-8.

CANEPA, E. T., SCASSA, M. E., CERUTI, J. M., MARAZITA, M. C., CARCAGNO, A. L., SIRKIN, P. F. & OGARA, M. F. 2007. INK4 proteins, a family of mammalian CDK inhibitors with novel biological functions. *IUBMB Life,* 59**,** 419-26.

CARTER, S. L., CIBULSKIS, K., HELMAN, E., MCKENNA, A., SHEN, H., ZACK, T., LAIRD, P. W., ONOFRIO, R. C., WINCKLER, W., WEIR, B. A., BEROUKHIM, R., PELLMAN, D., LEVINE, D. A., LANDER, E. S., MEYERSON, M. & GETZ, G. 2012. Absolute quantification of somatic DNA alterations in human cancer. *Nat Biotechnol,* 30**,** 413-21.

CASIMIRO, M. C., CROSARIOL, M., LORO, E., ERTEL, A., YU, Z., DAMPIER, W., SARIA, E. A., PAPANIKOLAOU, A., STANEK, T. J., LI, Z., WANG, C., FORTINA, P., ADDYA, S., TOZEREN, A., KNUDSEN, E. S., ARNOLD, A. & PESTELL, R. G. 2012. ChIP sequencing of cyclin D1 reveals a transcriptional role in chromosomal instability in mice. *J Clin Invest,* 122**,** 833-43.

CASTEDO, M., COQUELLE, A., VITALE, I., VIVET, S., MOUHAMAD, S., VIAUD, S., ZITVOGEL, L. & KROEMER, G. 2006a. Selective resistance of tetraploid cancer cells against DNA damage-induced apoptosis. *Ann N Y Acad Sci,* 1090**,** 35-49.

CASTEDO, M., COQUELLE, A., VIVET, S., VITALE, I., KAUFFMANN, A., DESSEN, P., PEQUIGNOT, M. O., CASARES, N., VALENT, A., MOUHAMAD, S., SCHMITT, E., MODJTAHEDI, N., VAINCHENKER, W., ZITVOGEL, L., LAZAR, V., GARRIDO, C. & KROEMER, G. 2006b. Apoptosis regulation in tetraploid cancer cells. *EMBO J,* 25**,** 2584-95.

CHEN, J., SAHA, P., KORNBLUTH, S., DYNLACHT, B. D. & DUTTA, A. 1996. Cyclin-binding motifs are essential for the function of p21CIP1. *Mol Cell Biol,* 16**,** 4673-82.

CHENG, M., OLIVIER, P., DIEHL, J. A., FERO, M., ROUSSEL, M. F., ROBERTS, J. M. & SHERR, C. J. 1999. The p21(Cip1) and p27(Kip1) CDK 'inhibitors' are essential activators of cyclin D-dependent kinases in murine fibroblasts. *EMBO J,* 18**,** 1571-83.

CHIN, K., DE SOLORZANO, C. O., KNOWLES, D., JONES, A., CHOU, W., RODRIGUEZ, E. G., KUO, W. L., LJUNG, B. M., CHEW, K., MYAMBO, K., MIRANDA, M., KRIG, S., GARBE, J., STAMPFER, M., YASWEN, P., GRAY, J. W. & LOCKETT, S. J. 2004. In situ analyses of genome instability in breast cancer. *Nat Genet,* 36**,** 984-8.

CHUAIRE-NOACK, L., RONDON-LAGOS, S., RAMIREZ-CORREDOR, A., IBANEZ-PINILLA, M. & RAMIREZ-CLAVIJO, S. 2010. Cytogenetic aberrations in primary cell cultures of the ovarian surface epithelium. *Invest Clin,* 51**,** 541-51.

CIARALLO, S., SUBRAMANIAM, V., HUNG, W., LEE, J. H., KOTCHETKOV, R., SANDHU, C., MILIC, A. & SLINGERLAND, J. M. 2002. Altered p27(Kip1) phosphorylation, localization, and function in human epithelial cells resistant to transforming growth factor beta-mediated G(1) arrest. *Mol Cell Biol,* 22**,** 2993-3002.

COSENTINO, C., GRIECO, D. & COSTANZO, V. 2011. ATM activates the pentose phosphate pathway promoting anti-oxidant defence and DNA repair. *EMBO J,* 30**,** 546-55.

COX, J., MATIC, I., HILGER, M., NAGARAJ, N., SELBACH, M., OLSEN, J. V. & MANN, M. 2009. A practical guide to the MaxQuant computational platform for SILAC-based quantitative proteomics. *Nat Protoc,* 4**,** 698-705.

CRASTA, K., GANEM, N. J., DAGHER, R., LANTERMANN, A. B., IVANOVA, E. V., PAN, Y., NEZI, L., PROTOPOPOV, A., CHOWDHURY, D. & PELLMAN, D. 2012. DNA breaks and chromosome pulverization from errors in mitosis. *Nature*.

DAI, C. & GU, W. 2010. p53 post-translational modification: deregulated in tumorigenesis. *Trends Mol Med,* 16**,** 528-36.

DANIEL, R. M. & DANSON, M. J. 2013. Temperature and the catalytic activity of enzymes: a fresh understanding. *FEBS Lett,* 587**,** 2738-43.

DAVOLI, T. & DE LANGE, T. 2011a. The Causes and Consequences of Polyploidy in Normal Development and Cancer. *Annual Review of Cell and Developmental Biology,* 27**,** 585-610.

DAVOLI, T. & DE LANGE, T. 2011b. The causes and consequences of polyploidy in normal development and cancer. *Annu Rev Cell Dev Biol,* 27**,** 585-610.

DAVOLI, T. & DE LANGE, T. 2012. Telomere-driven tetraploidization occurs in human cells undergoing crisis and promotes transformation of mouse cells. *Cancer Cell,* 21**,** 765-76.

DAVOLI, T., DENCHI, E. L. & DE LANGE, T. 2010. Persistent Telomere Damage Induces Bypass of Mitosis and Tetraploidy. *Cell,* 141**,** 81-93.

DE BRUIN, E. C., TAYLOR, T. B. & SWANTON, C. 2013. Intra-tumor heterogeneity: lessons from microbial evolution and clinical implications. *Genome Med,* 5**,** 101.

DE LAS ALAS, M. M., AEBI, S., FINK, D., HOWELL, S. B. & LOS, G. 1997. Loss of DNA mismatch repair: effects on the rate of mutation to drug resistance. *J Natl Cancer Inst,* 89**,** 1537-41.

DECKBAR, D., BIRRAUX, J., KREMPLER, A., TCHOUANDONG, L., BEUCHER, A., WALKER, S., STIFF, T., JEGGO, P. & LOBRICH, M. 2007. Chromosome breakage after G2 checkpoint release. *J Cell Biol,* 176**,** 749-55.

DENICOURT, C. & DOWDY, S. F. 2004. Cip/Kip proteins: more than just CDKs inhibitors. *Genes Dev,* 18**,** 851-5.

DEPRISTO, M. A., BANKS, E., POPLIN, R., GARIMELLA, K. V., MAGUIRE, J. R., HARTL, C., PHILIPPAKIS, A. A., DEL ANGEL, G., RIVAS, M. A., HANNA, M., MCKENNA, A., FENNELL, T. J., KERNYTSKY, A. M., SIVACHENKO, A. Y., CIBULSKIS, K., GABRIEL, S. B., ALTSHULER, D. & DALY, M. J. 2011. A framework for variation discovery and genotyping using next-generation DNA sequencing data. *Nat Genet,* 43**,** 491-8.

DEWHURST, S. M., MCGRANAHAN, N., BURRELL, R. A., ROWAN, A. J., GRONROOS, E., ENDESFELDER, D., JOSHI, T., MOURADOV, D., GIBBS, P., WARD, R. L., HAWKINS, N. J., SZALLASI, Z., SIEBER, O. M. & SWANTON, C. 2014. Tolerance of whole-genome doubling propagates chromosomal instability and accelerates cancer genome evolution. *Cancer Discov,* 4**,** 175-85.

DI LEONARDO, A., KHAN, S. H., LINKE, S. P., GRECO, V., SEIDITA, G. & WAHL, G. M. 1997. DNA rereplication in the presence of mitotic spindle inhibitors in human and mouse fibroblasts lacking either p53 or pRb function. *Cancer Res,* 57**,** 1013-9.

DI MICCO, R., FUMAGALLI, M., CICALESE, A., PICCININ, S., GASPARINI, P., LUISE, C., SCHURRA, C., GARRE, M., NUCIFORO, P. G., BENSIMON, A., MAESTRO, R., PELICCI, P. G. & D'ADDA DI FAGAGNA, F. 2006. Oncogene-induced senescence is a DNA damage response triggered by DNA hyper-replication. *Nature,* 444**,** 638-42.

DIEHL, J. A., CHENG, M., ROUSSEL, M. F. & SHERR, C. J. 1998. Glycogen synthase kinase-3beta regulates cyclin D1 proteolysis and subcellular localization. *Genes Dev,* 12**,** 3499-511.

DIEHL, J. A., ZINDY, F. & SHERR, C. J. 1997. Inhibition of cyclin D1 phosphorylation on threonine-286 prevents its rapid degradation via the ubiquitin-proteasome pathway. *Genes Dev,* 11**,** 957-72.

DIKOVSKAYA, D., SCHIFFMANN, D., NEWTON, I. P., OAKLEY, A., KROBOTH, K., SANSOM, O., JAMIESON, T. J., MENIEL, V., CLARKE, A. & NATHKE, I. S. 2007. Loss of APC induces polyploidy as a result of a combination of defects in mitosis and apoptosis. *J Cell Biol,* 176**,** 183-95.

DING, L., LEY, T. J., LARSON, D. E., MILLER, C. A., KOBOLDT, D. C., WELCH, J. S., RITCHEY, J. K., YOUNG, M. A., LAMPRECHT, T., MCLELLAN, M. D., MCMICHAEL, J. F., WALLIS, J. W., LU, C., SHEN, D., HARRIS, C. C., DOOLING, D. J., FULTON, R. S., FULTON, L. L., CHEN, K., SCHMIDT, H., KALICKI-VEIZER, J., MAGRINI, V. J., COOK, L., MCGRATH, S. D., VICKERY, T. L., WENDL, M. C., HEATH, S., WATSON, M. A., LINK, D. C., TOMASSON, M. H., SHANNON, W. D., PAYTON, J. E., KULKARNI, S., WESTERVELT, P., WALTER, M. J., GRAUBERT, T. A., MARDIS, E. R., WILSON, R. K. & DIPERSIO, J. F. 2012. Clonal evolution in relapsed acute myeloid leukaemia revealed by whole-genome sequencing. *Nature,* 481**,** 506-10.

DUELLI, D. & LAZEBNIK, Y. 2007. Cell-to-cell fusion as a link between viruses and cancer. *Nat Rev Cancer,* 7**,** 968-76.

DUELLI, D. M., PADILLA-NASH, H. M., BERMAN, D., MURPHY, K. M., RIED, T. & LAZEBNIK, Y. 2007. A Virus Causes Cancer by Inducing Massive Chromosomal Instability through Cell Fusion. *Current Biology,* 17**,** 431-437.

DUNCAN, A. W., TAYLOR, M. H., HICKEY, R. D., HANLON NEWELL, A. E., LENZI, M. L., OLSON, S. B., FINEGOLD, M. J. & GROMPE, M. 2010. The ploidy conveyor of mature hepatocytes as a source of genetic variation. *Nature,* 467**,** 707-710.

DURRBAUM, M., KUZNETSOVA, A. Y., PASSERINI, V., STINGELE, S., STOEHR, G. & STORCHOVA, Z. 2014. Unique features of the transcriptional response to model aneuploidy in human cells. *BMC Genomics,* 15**,** 139.

ELANGOVAN, S., HSIEH, T. C. & WU, J. M. 2008. Growth inhibition of human MDA-mB-231 breast cancer cells by delta-tocotrienol is associated with loss of cyclin D1/CDK4 expression and accompanying changes in the state of phosphorylation of the retinoblastoma tumor suppressor gene product. *Anticancer Res,* 28**,** 2641-7.

ELHAJOUJI, A., CUNHA, M. & KIRSCH-VOLDERS, M. 1998. Spindle poisons can induce polyploidy by mitotic slippage and micronucleate mononucleates in the cytokinesis-block assay. *Mutagenesis,* 13**,** 193-8.

ENSERINK, J. M. & KOLODNER, R. D. 2010. An overview of Cdk1-controlled targets and processes. *Cell Div,* 5**,** 11.

FOIJER, F. & TE RIELE, H. 2006. Restriction beyond the restriction point: mitogen requirement for G2 passage. *Cell Div,* 1**,** 8.

FORAND, A. & BERNARDINO-SGHERRI, J. 2009. A critical role of PUMA in maintenance of genomic integrity of murine spermatogonial stem cell precursors after genotoxic stress. *Cell Res,* 19**,** 1018-30.

FOX, D. T. & DURONIO, R. J. 2013. Endoreplication and polyploidy: insights into development and disease. *Development,* 140**,** 3-12.

FRANKEN, N. A., RODERMOND, H. M., STAP, J., HAVEMAN, J. & VAN BREE, C. 2006. Clonogenic assay of cells in vitro. *Nat Protoc,* 1**,** 2315-9.

FUJIWARA, T., BANDI, M., NITTA, M., IVANOVA, E. V., BRONSON, R. T. & PELLMAN, D. 2005. Cytokinesis failure generating tetraploids promotes tumorigenesis in p53-null cells. *Nature,* 437**,** 1043-7.

FUKAMI-KOBAYASHI, J. & MITSUI, Y. 1999. Cyclin D1 inhibits cell proliferation through binding to PCNA and cdk2. *Exp Cell Res,* 246**,** 338-47.

FUNG, T. K. & POON, R. Y. 2005. A roller coaster ride with the mitotic cyclins. *Semin Cell Dev Biol,* 16**,** 335-42.

GABEN, A. M., SAUCIER, C., BEDIN, M., BARBU, V. & MESTER, J. 2004. Rapamycin inhibits cdk4 activation, p 21(WAF1/CIP1) expression and G1-phase progression in transformed mouse fibroblasts. *Int J Cancer,* 108**,** 200-6.

GALIPEAU, P. C., COWAN, D. S., SANCHEZ, C. A., BARRETT, M. T., EMOND, M. J., LEVINE, D. S., RABINOVITCH, P. S. & REID, B. J. 1996. 17p (p53) allelic losses, 4N (G2/tetraploid) populations, and progression to aneuploidy in Barrett's esophagus. *Proc Natl Acad Sci U S A,* 93**,** 7081-4.

GANEM, N. J., CORNILS, H., CHIU, S. Y., O'ROURKE, K. P., ARNAUD, J., YIMLAMAI, D., THERY, M., CAMARGO, F. D. & PELLMAN, D. 2014. Cytokinesis failure triggers hippo tumor suppressor pathway activation. *Cell,* 158**,** 833-48.

GANEM, N. J., GODINHO, S. A. & PELLMAN, D. 2009. A mechanism linking extra centrosomes to chromosomal instability. *Nature,* 460**,** 278-82.

GANEM, N. J. & PELLMAN, D. 2007. Limiting the proliferation of polyploid cells. *Cell,* 131**,** 437-40.

GENG, Y., YU, Q., SICINSKA, E., DAS, M., SCHNEIDER, J. E., BHATTACHARYA, S., RIDEOUT, W. M., BRONSON, R. T., GARDNER, H. & SICINSKI, P. 2003. Cyclin E ablation in the mouse. *Cell,* 114**,** 431-43.

GERLINGER, M., HORSWELL, S., LARKIN, J., ROWAN, A. J., SALM, M. P., VARELA, I., FISHER, R., MCGRANAHAN, N., MATTHEWS, N., SANTOS, C. R., MARTINEZ, P., PHILLIMORE, B., BEGUM, S., RABINOWITZ, A., SPENCER-DENE, B., GULATI, S., BATES, P. A., STAMP, G., PICKERING, L., GORE, M., NICOL, D. L., HAZELL, S., FUTREAL, P. A., STEWART, A. & SWANTON, C. 2014. Genomic architecture and evolution of clear cell renal cell carcinomas defined by multiregion sequencing. *Nat Genet,* 46**,** 225-33.

GERLINGER, M., ROWAN, A. J., HORSWELL, S., LARKIN, J., ENDESFELDER, D., GRONROOS, E., MARTINEZ, P., MATTHEWS, N., STEWART, A., TARPEY, P., VARELA, I., PHILLIMORE, B., BEGUM, S., MCDONALD, N. Q., BUTLER, A., JONES, D., RAINE, K., LATIMER, C., SANTOS, C. R., NOHADANI, M., EKLUND, A. C., SPENCER-DENE, B., CLARK, G., PICKERING, L., STAMP, G., GORE, M., SZALLASI, Z., DOWNWARD, J., FUTREAL, P. A. & SWANTON, C. 2012. Intratumor heterogeneity and branched evolution revealed by multiregion sequencing. *N Engl J Med,* 366**,** 883-92.

GERSTUNG, M., BEISEL, C., RECHSTEINER, M., WILD, P., SCHRAML, P., MOCH, H. & BEERENWINKEL, N. 2012. Reliable detection of subclonal single-nucleotide variants in tumour cell populations. *Nat Commun,* 3**,** 811.

GILBERT, D., RAPLEY, E. & SHIPLEY, J. 2011. Testicular germ cell tumours: predisposition genes and the male germ cell niche. *Nat Rev Cancer,* 11**,** 278-88.

GOLDSTONE, S., PAVEY, S., FORREST, A., SINNAMON, J. & GABRIELLI, B. 2001. Cdc25-dependent activation of cyclin A/cdk2 is blocked in G2 phase arrested cells independently of ATM/ATR. *Oncogene,* 20**,** 921-32.

GONG, Y., ZACK, T. I., MORRIS, L. G., LIN, K., HUKKELHOVEN, E., RAHEJA, R., TAN, I. L., TURCAN, S., VEERIAH, S., MENG, S., VIALE, A., SCHUMACHER, S. E., PALMEDO, P., BEROUKHIM, R. & CHAN, T. A. 2014. Pan-cancer genetic analysis identifies PARK2 as a master regulator of G1/S cyclins. *Nat Genet,* 46**,** 588-94.

GORDON, D. J., RESIO, B. & PELLMAN, D. 2012. Causes and consequences of aneuploidy in cancer. *Nat Rev Genet,* 13**,** 189-203.

GRAHAM, J., MUSHIN, M. & KIRKPATRICK, P. 2004. Oxaliplatin. *Nat Rev Drug Discov,* 3**,** 11-2.

GREAVES, M. 2009. Darwin and evolutionary tales in leukemia. The Ham-Wasserman Lecture. *Hematology Am Soc Hematol Educ Program***,** 3-12.

GREGAN, J., POLAKOVA, S., ZHANG, L., TOLIC-NORRELYKKE, I. M. & CIMINI, D. 2011. Merotelic kinetochore attachment: causes and effects. *Trends Cell Biol,* 21**,** 374-81.

GRETARSDOTTIR, S., THORLACIUS, S., VALGARDSDOTTIR, R., GUDLAUGSDOTTIR, S., SIGURDSSON, S., STEINARSDOTTIR, M., JONASSON, J. G., ANAMTHAWAT-JONSSON, K. & EYFJORD, J. E. 1998. BRCA2 and p53 mutations in primary breast cancer in relation to genetic instability. *Cancer Res,* 58**,** 859-62.

GUO, Y., YANG, K., HARWALKAR, J., NYE, J. M., MASON, D. R., GARRETT, M. D., HITOMI, M. & STACEY, D. W. 2005. Phosphorylation of cyclin D1 at Thr 286 during S phase leads to its proteasomal degradation and allows efficient DNA synthesis. *Oncogene,* 24**,** 2599-612.

HALL, M., BATES, S. & PETERS, G. 1995. Evidence for different modes of action of cyclin-dependent kinase inhibitors: p15 and p16 bind to kinases, p21 and p27 bind to cyclins. *Oncogene,* 11**,** 1581-8.

HAMILTON, N. M., DAWSON, M., FAIRWEATHER, E. E., HAMILTON, N. S., HITCHIN, J. R., JAMES, D. I., JONES, S. D., JORDAN, A. M., LYONS, A. J., SMALL, H. F., THOMSON, G. J., WADDELL, I. D. & OGILVIE, D. J. 2012. Novel steroid inhibitors of glucose 6-phosphate dehydrogenase. *J Med Chem,* 55**,** 4431-45.

HAYASHI, M. T. & KARLSEDER, J. 2013. DNA damage associated with mitosis and cytokinesis failure. *Oncogene,* 32**,** 4593-601.

HENGST, L., GOPFERT, U., LASHUEL, H. A. & REED, S. I. 1998. Complete inhibition of Cdk/cyclin by one molecule of p21(Cip1). *Genes Dev,* 12**,** 3882-8.

HORSLEY, V. & PAVLATH, G. K. 2004. Forming a multinucleated cell: molecules that regulate myoblast fusion. *Cells Tissues Organs,* 176**,** 67-78.

HOULDSWORTH, J., REUTER, V., BOSL, G. J. & CHAGANTI, R. S. 1997. Aberrant expression of cyclin D2 is an early event in human male germ cell tumorigenesis. *Cell Growth Differ,* 8**,** 293-9.

HU, L., PLAFKER, K., VOROZHKO, V., ZUNA, R. E., HANIGAN, M. H., GORBSKY, G. J., PLAFKER, S. M., ANGELETTI, P. C. & CERESA, B. P. 2009. Human papillomavirus 16 E5 induces bi-nucleated cell formation by cell-cell fusion. *Virology,* 384**,** 125-34.

HUGHES, J. P., REES, S., KALINDJIAN, S. B. & PHILPOTT, K. L. 2011. Principles of early drug discovery. *Br J Pharmacol,* 162**,** 1239-49.

HUKKELHOVEN, E., LIU, Y., YEH, N., CIZNADIJA, D., BLAIN, S. W. & KOFF, A. 2012. Tyrosine phosphorylation of the p21 cyclin-dependent kinase inhibitor facilitates the development of proneural glioma. *J Biol Chem,* 287**,** 38523-30.

JAMES, M. K., RAY, A., LEZNOVA, D. & BLAIN, S. W. 2008. Differential modification of p27Kip1 controls its cyclin D-cdk4 inhibitory activity. *Mol Cell Biol,* 28**,** 498-510.

JANSSEN, A., KOPS, G. J. & MEDEMA, R. H. 2009. Elevating the frequency of chromosome mis-segregation as a strategy to kill tumor cells. *Proc Natl Acad Sci U S A,* 106**,** 19108-13.

JANSSEN, A., VAN DER BURG, M., SZUHAI, K., KOPS, G. J. & MEDEMA, R. H. 2011. Chromosome segregation errors as a cause of DNA damage and structural chromosome aberrations. *Science,* 333**,** 1895-8.

JONKERS, Y. M., CLAESSEN, S. M., PERREN, A., SCHMID, S., KOMMINOTH, P., VERHOFSTAD, A. A., HOFLAND, L. J., DE KRIJGER, R. R., SLOOTWEG, P.

J., RAMAEKERS, F. C. & SPEEL, E. J. 2005. Chromosomal instability predicts metastatic disease in patients with insulinomas. *Endocr Relat Cancer,* 12**,** 435-47.

KAESER, M. D., PEBERNARD, S. & IGGO, R. D. 2004. Regulation of p53 stability and function in HCT116 colon cancer cells. *J Biol Chem,* 279**,** 7598-605.

KALLAS, A., POOK, M., MAIMETS, M., ZIMMERMANN, K. & MAIMETS, T. 2011. Nocodazole treatment decreases expression of pluripotency markers Nanog and Oct4 in human embryonic stem cells. *PLoS One,* 6**,** e19114.

KANDA, T., SULLIVAN, K. F. & WAHL, G. M. 1998. Histone-GFP fusion protein enables sensitive analysis of chromosome dynamics in living mammalian cells. *Curr Biol,* 8**,** 377-85.

KANEKO, Y. & KNUDSON, A. G. 2000. Mechanism and relevance of ploidy in neuroblastoma. *Genes Chromosomes Cancer,* 29**,** 89-95.

KAPOOR, T. M., MAYER, T. U., COUGHLIN, M. L. & MITCHISON, T. J. 2000. Probing spindle assembly mechanisms with monastrol, a small molecule inhibitor of the mitotic kinesin, Eg5. *J Cell Biol,* 150**,** 975-88.

KARDINAL, C., DANGERS, M., KARDINAL, A., KOCH, A., BRANDT, D. T., TAMURA, T. & WELTE, K. 2006. Tyrosine phosphorylation modulates binding preference to cyclin-dependent kinases and subcellular localization of p27Kip1 in the acute promyelocytic leukemia cell line NB4. *Blood,* 107**,** 1133-40.

KASTAN, M. B. 2008. DNA damage responses: mechanisms and roles in human disease: 2007 G.H.A. Clowes Memorial Award Lecture. *Mol Cancer Res,* 6**,** 517-24.

KEHN, K., DENG, L., DE LA FUENTE, C., STROUSS, K., WU, K., MADDUKURI, A., BAYLOR, S., RUFNER, R., PUMFERY, A., BOTTAZZI, M. E. & KASHANCHI, F. 2004. The role of cyclin D2 and p21/waf1 in human T-cell leukemia virus type 1 infected cells. *Retrovirology,* 1**,** 6.

KHAN, S. H. & WAHL, G. M. 1998. p53 and pRb prevent rereplication in response to microtubule inhibitors by mediating a reversible G1 arrest. *Cancer Res,* 58**,** 396-401.

KOPS, G. J., FOLTZ, D. R. & CLEVELAND, D. W. 2004. Lethality to human cancer cells through massive chromosome loss by inhibition of the mitotic checkpoint. *Proc Natl Acad Sci U S A,* 101**,** 8699-704.

KOPS, G. J., WEAVER, B. A. & CLEVELAND, D. W. 2005. On the road to cancer: aneuploidy and the mitotic checkpoint. *Nat Rev Cancer,* 5**,** 773-85.

KUZNETSOVA, A. Y., SEGET, K., MOELLER, G. K., DE PAGTER, M. S., DE ROOS, J. A., DURRBAUM, M., KUFFER, C., MULLER, S., ZAMAN, G. J., KLOOSTERMAN, W. P. & STORCHOVA, Z. 2015. Chromosomal instability, tolerance of mitotic errors and multidrug resistance are promoted by tetraploidization in human cells. *Cell Cycle,* 14**,** 2810-20.

KWON, M., GODINHO, S. A., CHANDHOK, N. S., GANEM, N. J., AZIOUNE, A., THERY, M. & PELLMAN, D. 2008. Mechanisms to suppress multipolar divisions in cancer cells with extra centrosomes. *Genes Dev,* 22**,** 2189-203.

LABAER, J., GARRETT, M. D., STEVENSON, L. F., SLINGERLAND, J. M., SANDHU, C., CHOU, H. S., FATTAEY, A. & HARLOW, E. 1997. New functional activities for the p21 family of CDK inhibitors. *Genes Dev,* 11**,** 847-62.

LAN, W. & CLEVELAND, D. W. 2010. A chemical tool box defines mitotic and interphase roles for Mps1 kinase. *J Cell Biol,* 190**,** 21-4.

LARREA, M. D., LIANG, J., DA SILVA, T., HONG, F., SHAO, S. H., HAN, K., DUMONT, D. & SLINGERLAND, J. M. 2008. Phosphorylation of p27Kip1 regulates assembly and activation of cyclin D1-Cdk4. *Mol Cell Biol,* 28**,** 6462-72.

LEE, A. J., ENDESFELDER, D., ROWAN, A. J., WALTHER, A., BIRKBAK, N. J., FUTREAL, P. A., DOWNWARD, J., SZALLASI, Z., TOMLINSON, I. P.,

HOWELL, M., KSCHISCHO, M. & SWANTON, C. 2011. Chromosomal instability confers intrinsic multidrug resistance. *Cancer Res,* 71**,** 1858-70.

LEHMAN, N. L., VERSCHUREN, E. W., HSU, J. Y., CHERRY, A. M. & JACKSON, P. K. 2006. Overexpression of the anaphase promoting complex/cyclosome inhibitor Emi1 leads to tetraploidy and genomic instability of p53-deficient cells. *Cell Cycle,* 5**,** 1569-73.

LI, H. & DURBIN, R. 2009. Fast and accurate short read alignment with Burrows-Wheeler transform. *Bioinformatics,* 25**,** 1754-60.

LI, R., HEHLMAN, R., SACHS, R. & DUESBERG, P. 2005. Chromosomal alterations cause the high rates and wide ranges of drug resistance in cancer cells. *Cancer Genet Cytogenet,* 163**,** 44-56.

LIN, D. I., BARBASH, O., KUMAR, K. G., WEBER, J. D., HARPER, J. W., KLEIN-SZANTO, A. J., RUSTGI, A., FUCHS, S. Y. & DIEHL, J. A. 2006. Phosphorylation-dependent ubiquitination of cyclin D1 by the SCF(FBX4-alphaB crystallin) complex. *Mol Cell,* 24**,** 355-66.

LOHEZ, O. D., REYNAUD, C., BOREL, F., ANDREASSEN, P. R. & MARGOLIS, R. L. 2003. Arrest of mammalian fibroblasts in G1 in response to actin inhibition is dependent on retinoblastoma pocket proteins but not on p53. *J Cell Biol,* 161**,** 67-77.

LONGLEY, D. B., HARKIN, D. P. & JOHNSTON, P. G. 2003a. 5-fluorouracil: mechanisms of action and clinical strategies. *Nat Rev Cancer,* 3**,** 330-8.

LONGLEY, D. B., MCDERMOTT, U. & JOHNSTON, P. G. 2003b. Predictive markers for colorectal cancer: current status and future prospects. *Clin Colorectal Cancer,* 2**,** 223-30.

LUO, Y., HARTFORD, S. A., ZENG, R., SOUTHARD, T. L., SHIMA, N. & SCHIMENTI, J. C. 2014. Hypersensitivity of primordial germ cells to compromised replication-associated DNA repair involves ATM-p53-p21 signaling. *PLoS Genet,* 10**,** e1004471.

LV, L., ZHANG, T., YI, Q., HUANG, Y., WANG, Z., HOU, H., ZHANG, H., ZHANG, W., HAO, Q., GUO, Z., COOKE, H. J. & SHI, Q. 2012. Tetraploid cells from cytokinesis failure induce aneuploidy and spontaneous transformation of mouse ovarian surface epithelial cells. *Cell Cycle,* 11**,** 2864-2875.

MACEK, B., MANN, M. & OLSEN, J. V. 2009. Global and site-specific quantitative phosphoproteomics: principles and applications. *Annu Rev Pharmacol Toxicol,* 49**,** 199-221.

MALEY, C. C., GALIPEAU, P. C., FINLEY, J. C., WONGSURAWAT, V. J., LI, X., SANCHEZ, C. A., PAULSON, T. G., BLOUNT, P. L., RISQUES, R. A., RABINOVITCH, P. S. & REID, B. J. 2006. Genetic clonal diversity predicts progression to esophageal adenocarcinoma. *Nat Genet,* 38**,** 468-73.

MANN, M. 2006. Functional and quantitative proteomics using SILAC. *Nat Rev Mol Cell Biol,* 7**,** 952-8.

MAPELLI, M., MASSIMILIANO, L., SANTAGUIDA, S. & MUSACCHIO, A. 2007. The Mad2 conformational dimer: structure and implications for the spindle assembly checkpoint. *Cell,* 131**,** 730-43.

MARGOTTIN-GOGUET, F., HSU, J. Y., LOKTEV, A., HSIEH, H. M., REIMANN, J. D. & JACKSON, P. K. 2003. Prophase destruction of Emi1 by the SCF(betaTrCP/Slimb) ubiquitin ligase activates the anaphase promoting complex to allow progression beyond prometaphase. *Dev Cell,* 4**,** 813-26.

MASSAGUE, J. 2004. G1 cell-cycle control and cancer. *Nature,* 432**,** 298-306.

MATSON, D. R. & STUKENBERG, P. T. 2011. Spindle poisons and cell fate: a tale of two pathways. *Mol Interv,* 11**,** 141-50.

MAY, L. T., LEACH, K., SEXTON, P. M. & CHRISTOPOULOS, A. 2007. Allosteric modulation of G protein-coupled receptors. *Annu Rev Pharmacol Toxicol,* 47**,** 1-51.

MCCALL, M. N., BOLSTAD, B. M. & IRIZARRY, R. A. 2010. Frozen robust multiarray analysis (fRMA). *Biostatistics,* 11**,** 242-253.

MCGRANAHAN, N., FAVERO, F., DE BRUIN, E. C., BIRKBAK, N. J., SZALLASI, Z. & SWANTON, C. 2015. Clonal status of actionable driver events and the timing of mutational processes in cancer evolution. *Sci Transl Med,* 7**,** 283ra54.

MCKINNEY, J. D., RICHARD, A., WALLER, C., NEWMAN, M. C. & GERBERICK, F. 2000. The practice of structure activity relationships (SAR) in toxicology. *Toxicol Sci,* 56**,** 8-17.

MERALDI, P., HONDA, R. & NIGG, E. A. 2002. Aurora-A overexpression reveals tetraploidization as a major route to centrosome amplification in p53-/- cells. *EMBO J,* 21**,** 483-92.

MIRZA, A., WU, Q., WANG, L., MCCLANAHAN, T., BISHOP, W. R., GHEYAS, F., DING, W., HUTCHINS, B., HOCKENBERRY, T., KIRSCHMEIER, P., GREENE, J. R. & LIU, S. 2003. Global transcriptional program of p53 target genes during the process of apoptosis and cell cycle progression. *Oncogene,* 22**,** 3645-54.

MITCHELL, R. T., M, E. C.-M., MACDONALD, J., ANDERSON, R. A., KELNAR, C. J., O'DONNELL, M., SHARPE, R. M., SMITH, L. B., GRIGOR, K. M., WALLACE, W. H., STOOP, H., WOLFFENBUTTEL, K. P., DONAT, R., SAUNDERS, P. T. & LOOIJENGA, L. H. 2014. Intratubular germ cell neoplasia of the human testis: heterogeneous protein expression and relation to invasive potential. *Mod Pathol,* 27**,** 1255-66.

MULLINS, J. M. & BIESELE, J. J. 1977. Terminal phase of cytokinesis in D-98s cells. *J Cell Biol,* 73**,** 672-84.

MUNDT, K. E., GOLSTEYN, R. M., LANE, H. A. & NIGG, E. A. 1997. On the regulation and function of human polo-like kinase 1 (PLK1): effects of overexpression on cell cycle progression. *Biochem Biophys Res Commun,* 239**,** 377-85.

MUSACCHIO, A. & SALMON, E. D. 2007. The spindle-assembly checkpoint in space and time. *Nat Rev Mol Cell Biol,* 8**,** 379-93.

MUSGROVE, E. A., CALDON, C. E., BARRACLOUGH, J., STONE, A. & SUTHERLAND, R. L. 2011. Cyclin D as a therapeutic target in cancer. *Nat Rev Cancer,* 11**,** 558-72.

NEWMAN, R. H. & ZHANG, J. 2008. Fucci: street lights on the road to mitosis. *Chem Biol,* 15**,** 97-8.

NIGG, E. A. 2001. Mitotic kinases as regulators of cell division and its checkpoints. *Nat Rev Mol Cell Biol,* 2**,** 21-32.

NILSSON, I. & HOFFMANN, I. 2000. Cell cycle regulation by the Cdc25 phosphatase family. *Prog Cell Cycle Res,* 4**,** 107-14.

NORDEN, C., MENDOZA, M., DOBBELAERE, J., KOTWALIWALE, C. V., BIGGINS, S. & BARRAL, Y. 2006. The NoCut pathway links completion of cytokinesis to spindle midzone function to prevent chromosome breakage. *Cell,* 125**,** 85-98.

NORMAND, G. & KING, R. W. 2010. Understanding cytokinesis failure. *Adv Exp Med Biol,* 676**,** 27-55.

NOWELL, P. C. 1976. The clonal evolution of tumor cell populations. *Science,* 194**,** 23-8.

ODORIZZI, G. 2006. The multiple personalities of Alix. *J Cell Sci,* 119**,** 3025-32.

OKABE, H., LEE, S. H., PHUCHAREON, J., ALBERTSON, D. G., MCCORMICK, F. & TETSU, O. 2006. A critical role for FBXW8 and MAPK in cyclin D1 degradation and cancer cell proliferation. *PLoS One,* 1**,** e128.

OLAHARSKI, A. J. 2006. Tetraploidy and chromosomal instability are early events during cervical carcinogenesis. *Carcinogenesis,* 27**,** 337-343.

ONG, S. E., BLAGOEV, B., KRATCHMAROVA, I., KRISTENSEN, D. B., STEEN, H., PANDEY, A. & MANN, M. 2002. Stable isotope labeling by amino acids in cell culture, SILAC, as a simple and accurate approach to expression proteomics. *Mol Cell Proteomics,* 1**,** 376-86.

ORTIZ-ESTEVEZ, M., ARAMBURU, A., BENGTSSON, H., NEUVIAL, P. & RUBIO, A. 2012. CalMaTe: a method and software to improve allele-specific copy number of SNP arrays for downstream segmentation. *Bioinformatics,* 28**,** 1793-4.

OTTESEN, A. M., LARSEN, J., GERDES, T., LARSEN, J. K., LUNDSTEEN, C., SKAKKEBAEK, N. E. & RAJPERT-DE MEYTS, E. 2004. Cytogenetic investigation of testicular carcinoma in situ and early seminoma by high-resolution comparative genomic hybridization analysis of subpopulations flow sorted according to DNA content. *Cancer Genet Cytogenet,* 149**,** 89-97.

OTTO, S. P. 2007. The evolutionary consequences of polyploidy. *Cell,* 131**,** 452-62.

PAVELKA, N., RANCATI, G., ZHU, J., BRADFORD, W. D., SARAF, A., FLORENS, L., SANDERSON, B. W., HATTEM, G. L. & LI, R. 2010. Aneuploidy confers quantitative proteome changes and phenotypic variation in budding yeast. *Nature,* 468**,** 321-5.

PICARD, B. 2012. http://broadinstitute.github.io/picard/ [Online]. Available: http://broadinstitute.github.io/picard/.

PLANAS-SILVA, M. D. & WEINBERG, R. A. 1997. Estrogen-dependent cyclin E-cdk2 activation through p21 redistribution. *Mol Cell Biol,* 17**,** 4059-69.

POTAPOVA, T. A., DAUM, J. R., BYRD, K. S. & GORBSKY, G. J. 2009. Fine tuning the cell cycle: activation of the Cdk1 inhibitory phosphorylation pathway during mitotic exit. *Mol Biol Cell,* 20**,** 1737-48.

QUINTANILLA-MARTINEZ, L., DAVIES-HILL, T., FEND, F., CALZADA-WACK, J., SORBARA, L., CAMPO, E., JAFFE, E. S. & RAFFELD, M. 2003. Sequestration of p27Kip1 protein by cyclin D1 in typical and blastic variants of mantle cell lymphoma (MCL): implications for pathogenesis. *Blood,* 101**,** 3181-7.

RAMEL, S., SANCHEZ, C. A., SCHIMKE, M. K., NESHAT, K., CROSS, S. M., RASKIND, W. H. & REID, B. J. 1995. Inactivation of p53 and the development of tetraploidy in the elastase-SV40 T antigen transgenic mouse pancreas. *Pancreas,* 11**,** 213-22.

RAPPSILBER, J., MANN, M. & ISHIHAMA, Y. 2007. Protocol for micro-purification, enrichment, pre-fractionation and storage of peptides for proteomics using StageTips. *Nat Protoc,* 2**,** 1896-906.

RAVID, K., LU, J., ZIMMET, J. M. & JONES, M. R. 2002. Roads to polyploidy: the megakaryocyte example. *J Cell Physiol,* 190**,** 7-20.

REINA-SAN-MARTIN, B., NUSSENZWEIG, M. C., NUSSENZWEIG, A. & DIFILIPPANTONIO, S. 2005. Genomic instability, endoreduplication, and diminished Ig class-switch recombination in B cells lacking Nbs1. *Proc Natl Acad Sci U S A,* 102**,** 1590-5.

ROEDER, G. S. 1997. Meiotic chromosomes: it takes two to tango. *Genes Dev,* 11**,** 2600-21.

ROSSIO, V., GALATI, E., FERRARI, M., PELLICIOLI, A., SUTANI, T., SHIRAHIGE, K., LUCCHINI, G. & PIATTI, S. 2010. The RSC chromatin-remodeling complex influences mitotic exit and adaptation to the spindle assembly checkpoint by controlling the Cdc14 phosphatase. *J Cell Biol,* 191**,** 981-97.

RUBIN, S. M. 2013. Deciphering the retinoblastoma protein phosphorylation code. *Trends Biochem Sci,* 38**,** 12-9.

SANGESTER, J. 1989. Octanol-Water Partition Coefficients of Simple Organic Compounds. *Journal of Physical Chemistry Reference Data,* 18**,** 1111-1227.

SANTAGUIDA, S., TIGHE, A., D'ALISE, A. M., TAYLOR, S. S. & MUSACCHIO, A. 2010. Dissecting the role of MPS1 in chromosome biorientation and the spindle

checkpoint through the small molecule inhibitor reversine. *J Cell Biol,* 190**,** 73-87.

SANTARIUS, T., SHIPLEY, J., BREWER, D., STRATTON, M. R. & COOPER, C. S. 2010. A census of amplified and overexpressed human cancer genes. *Nat Rev Cancer,* 10**,** 59-64.

SCHUH, A., BECQ, J., HUMPHRAY, S., ALEXA, A., BURNS, A., CLIFFORD, R., FELLER, S. M., GROCOCK, R., HENDERSON, S., KHREBTUKOVA, I., KINGSBURY, Z., LUO, S., MCBRIDE, D., MURRAY, L., MENJU, T., TIMBS, A., ROSS, M., TAYLOR, J. & BENTLEY, D. 2012. Monitoring chronic lymphocytic leukemia progression by whole genome sequencing reveals heterogeneous clonal evolution patterns. *Blood,* 120**,** 4191-6.

SHARMA, S., ZENG, J. Y., ZHUANG, C. M., ZHOU, Y. Q., YAO, H. P., HU, X., ZHANG, R. & WANG, M. H. 2013. Small-molecule inhibitor BMS-777607 induces breast cancer cell polyploidy with increased resistance to cytotoxic chemotherapy agents. *Mol Cancer Ther,* 12**,** 725-36.

SHEIKINE, Y., GENEGA, E., MELAMED, J., LEE, P., REUTER, V. E. & YE, H. 2012. Molecular genetics of testicular germ cell tumors. *Am J Cancer Res,* 2**,** 153-67.

SHERR, C. J. & ROBERTS, J. M. 1999. CDK inhibitors: positive and negative regulators of G1-phase progression. *Genes Dev,* 13**,** 1501-12.

SHI, Q. & KING, R. W. 2005. Chromosome nondisjunction yields tetraploid rather than aneuploid cells in human cell lines. *Nature,* 437**,** 1038-1042.

SKAKKEBAEK, N. E., RAJPERT-DE MEYTS, E., JORGENSEN, N., CARLSEN, E., PETERSEN, P. M., GIWERCMAN, A., ANDERSEN, A. G., JENSEN, T. K., ANDERSSON, A. M. & MULLER, J. 1998. Germ cell cancer and disorders of spermatogenesis: an environmental connection? *APMIS,* 106**,** 3-11; discussion 12.

SKOUFIAS, D. A., DEBONIS, S., SAOUDI, Y., LEBEAU, L., CREVEL, I., CROSS, R., WADE, R. H., HACKNEY, D. & KOZIELSKI, F. 2006. S-trityl-L-cysteine is a reversible, tight binding inhibitor of the human kinesin Eg5 that specifically blocks mitotic progression. *J Biol Chem,* 281**,** 17559-69.

SMITH, G. F., RIDLER, M. A. & FAUNCH, J. A. 1967. Action of cytochalasin B on cultured human lymphocytes. *Nature,* 216**,** 1134-5.

SMOLKOVA, K. & JEZEK, P. 2012. The Role of Mitochondrial NADPH-Dependent Isocitrate Dehydrogenase in Cancer Cells. *Int J Cell Biol,* 2012**,** 273947.

SOTILLO, R., HERNANDO, E., DÍAZ-RODRÍGUEZ, E., TERUYA-FELDSTEIN, J., CORDÓN-CARDO, C., LOWE, S. W. & BENEZRA, R. 2007. Mad2 Overexpression Promotes Aneuploidy and Tumorigenesis in Mice. *Cancer Cell,* 11**,** 9-23.

STEEN, H. & MANN, M. 2004. The ABC's (and XYZ's) of peptide sequencing. *Nat Rev Mol Cell Biol,* 5**,** 699-711.

STEWART, Z. A., LEACH, S. D. & PIETENPOL, J. A. 1999. p21(Waf1/Cip1) inhibition of cyclin E/Cdk2 activity prevents endoreduplication after mitotic spindle disruption. *Mol Cell Biol,* 19**,** 205-15.

STINGELE, S., STOEHR, G., PEPLOWSKA, K., COX, J. U. R., MANN, M. & STORCHOVA, Z. 2012. Global analysis of genome, transcriptome and proteome reveals the response to aneuploidy in human cells. *Molecular Systems Biology,* 8**,** 1-12.

STORCHOVA, Z. & PELLMAN, D. 2004. From polyploidy to aneuploidy, genome instability and cancer. *Nat Rev Mol Cell Biol,* 5**,** 45-54.

STRELOW, J., DEWE, W., IVERSEN, P. W., BROOKS, H. B., RADDING, J. A., MCGEE, J. & WEIDNER, J. 2004. Mechanism of Action assays for Enzymes. *In:* SITTAMPALAM, G. S., COUSSENS, N. P., NELSON, H., ARKIN, M., AULD, D., AUSTIN, C., BEJCEK, B., GLICKSMAN, M., INGLESE, J., IVERSEN, P. W.,

LI, Z., MCGEE, J., MCMANUS, O., MINOR, L., NAPPER, A., PELTIER, J. M., RISS, T., TRASK, O. J., JR. & WEIDNER, J. (eds.) *Assay Guidance Manual.* Bethesda (MD).

SUN, X. X., DAI, M. S. & LU, H. 2007. 5-fluorouracil activation of p53 involves an MDM2-ribosomal protein interaction. *J Biol Chem,* 282**,** 8052-9.

TAYLOR, R. C., CULLEN, S. P. & MARTIN, S. J. 2008. Apoptosis: controlled demolition at the cellular level. *Nat Rev Mol Cell Biol,* 9**,** 231-41.

TETSU, O. & MCCORMICK, F. 1999. Beta-catenin regulates expression of cyclin D1 in colon carcinoma cells. *Nature,* 398**,** 422-6.

THOMPSON, S. L. & COMPTON, D. A. 2010a. Proliferation of aneuploid human cells is limited by a p53-dependent mechanism. *J Cell Biol,* 188**,** 369-81.

THOMPSON, S. L. & COMPTON, D. A. 2010b. Proliferation of aneuploid human cells is limited by a p53-dependent mechanism. *The Journal of Cell Biology,* 188**,** 369-381.

THOMPSON, S. L. & COMPTON, D. A. 2011. Chromosomes and cancer cells. *Chromosome Res,* 19**,** 433-44.

THORNE, N., AULD, D. S. & INGLESE, J. 2010. Apparent activity in high-throughput screening: origins of compound-dependent assay interference. *Curr Opin Chem Biol,* 14**,** 315-24.

UETAKE, Y. & SLUDER, G. 2004. Cell cycle progression after cleavage failure: mammalian somatic cells do not possess a "tetraploidy checkpoint". *J Cell Biol,* 165**,** 609-15.

UHLMANN, F. 2001. Secured cutting: controlling separase at the metaphase to anaphase transition. *EMBO Rep,* 2**,** 487-92.

ULLAH, Z., KOHN, M. J., YAGI, R., VASSILEV, L. T. & DEPAMPHILIS, M. L. 2008. Differentiation of trophoblast stem cells into giant cells is triggered by p57/Kip2 inhibition of CDK1 activity. *Genes Dev,* 22**,** 3024-36.

VAN HOOF, D., PINKSE, M. W., OOSTWAARD, D. W., MUMMERY, C. L., HECK, A. J. & KRIJGSVELD, J. 2007. An experimental correction for arginine-to-proline conversion artifacts in SILAC-based quantitative proteomics. *Nat Methods,* 4**,** 677-8.

VAN LOO, P., NORDGARD, S. H., LINGJAERDE, O. C., RUSSNES, H. G., RYE, I. H., SUN, W., WEIGMAN, V. J., MARYNEN, P., ZETTERBERG, A., NAUME, B., PEROU, C. M., BORRESEN-DALE, A. L. & KRISTENSEN, V. N. 2010. Allele-specific copy number analysis of tumors. *Proc Natl Acad Sci U S A,* 107**,** 16910-5.

VARSHNEY, R., DWARAKANATH, B. & JAIN, V. 2005. Radiosensitization by 6-aminonicotinamide and 2-deoxy-D-glucose in human cancer cells. *Int J Radiat Biol,* 81**,** 397-408.

VARSHNEY, R., GUPTA, S. & DWARAKANATH, B. S. 2004. Radiosensitization of murine Ehrlich ascites tumor by a combination of 2-deoxy-D-glucose and 6-aminonicotinamide. *Technol Cancer Res Treat,* 3**,** 659-63.

VERMEULEN, K., VAN BOCKSTAELE, D. R. & BERNEMAN, Z. N. 2003. The cell cycle: a review of regulation, deregulation and therapeutic targets in cancer. *Cell Prolif,* 36**,** 131-49.

WALDMAN, T., KINZLER, K. W. & VOGELSTEIN, B. 1995. p21 is necessary for the p53-mediated G1 arrest in human cancer cells. *Cancer Res,* 55**,** 5187-90.

WAMELINK, M. M., STRUYS, E. A. & JAKOBS, C. 2008. The biochemistry, metabolism and inherited defects of the pentose phosphate pathway: a review. *J Inherit Metab Dis,* 31**,** 703-17.

WANG, K., LI, M. & HAKONARSON, H. 2010. ANNOVAR: functional annotation of genetic variants from high-throughput sequencing data. *Nucleic Acids Res,* 38**,** e164.

WANG, L., WANG, J., BLASER, B. W., DUCHEMIN, A. M., KUSEWITT, D. F., LIU, T., CALIGIURI, M. A. & BRIESEWITZ, R. 2007. Pharmacologic inhibition of CDK4/6: mechanistic evidence for selective activity or acquired resistance in acute myeloid leukemia. *Blood,* 110**,** 2075-83.

WANG, X., ZOU, L., ZHENG, H., WEI, Q., ELLEDGE, S. J. & LI, L. 2003. Genomic instability and endoreduplication triggered by RAD17 deletion. *Genes Dev,* 17**,** 965-70.

WANG, Z., ZHANG, Y., KAMEN, D., LEES, E. & RAVID, K. 1995. Cyclin D3 is essential for megakaryocytopoiesis. *Blood,* 86**,** 3783-8.

WEAVER, B. A., SILK, A. D. & CLEVELAND, D. W. 2006. Cell biology: nondisjunction, aneuploidy and tetraploidy. *Nature,* 442**,** E9-10; discussion E10.

WHEATLEY, S. P., HINCHCLIFFE, E. H., GLOTZER, M., HYMAN, A. A., SLUDER, G. & WANG, Y. 1997. CDK1 inactivation regulates anaphase spindle dynamics and cytokinesis in vivo. *J Cell Biol,* 138**,** 385-93.

WONG, C. & STEARNS, T. 2005. Mammalian cells lack checkpoints for tetraploidy, aberrant centrosome number, and cytokinesis failure. *BMC Cell Biol,* 6**,** 6.

WRIGHT, W. E. & HAYFLICK, L. 1972. Formation of anucleate and multinucleate cells in normal and SV 40 transformed WI-38 by cytochalasin B. *Exp Cell Res,* 74**,** 187-94.

YANG, K., GUO, Y., STACEY, W. C., HARWALKAR, J., FRETTHOLD, J., HITOMI, M. & STACEY, D. W. 2006a. Glycogen synthase kinase 3 has a limited role in cell cycle regulation of cyclin D1 levels. *BMC Cell Biol,* 7**,** 33.

YANG, K., HITOMI, M. & STACEY, D. W. 2006b. Variations in cyclin D1 levels through the cell cycle determine the proliferative fate of a cell. *Cell Div,* 1**,** 32.

YAP, T. A., GERLINGER, M., FUTREAL, P. A., PUSZTAI, L. & SWANTON, C. 2012. Intratumor heterogeneity: seeing the wood for the trees. *Sci Transl Med,* 4**,** 127ps10.

YE, J., COULOURIS, G., ZARETSKAYA, I., CUTCUTACHE, I., ROZEN, S. & MADDEN, T. L. 2012. Primer-BLAST: a tool to design target-specific primers for polymerase chain reaction. *BMC Bioinformatics,* 13**,** 134.

YOSHIHARA, T., ISHIDA, M., KINOMURA, A., KATSURA, M., TSURUGA, T., TASHIRO, S., ASAHARA, T. & MIYAGAWA, K. 2004. XRCC3 deficiency results in a defect in recombination and increased endoreduplication in human cells. *EMBO J,* 23**,** 670-80.

YU, H. 2006. Structural activation of Mad2 in the mitotic spindle checkpoint: the two-state Mad2 model versus the Mad2 template model. *J Cell Biol,* 173**,** 153-7.

ZHU, H., ZHANG, L., WU, S., TERAISHI, F., DAVIS, J. J., JACOB, D. & FANG, B. 2004. Induction of S-phase arrest and p21 overexpression by a small molecule 2[[3-(2,3-dichlorophenoxy)propyl] amino]ethanol in correlation with activation of ERK. *Oncogene,* 23**,** 4984-92.